AGARD-R-795

AGARD
ADVISORY GROUP FOR AEROSPACE RESEARCH & DEVELOPMENT
7 RUE ANCELLE 92200 NEUILLY SUR SEINE FRANCE

AGARD REPORT 795

Introduction of Ceramics into Aerospace Structural Composites

(L'Introduction des Céramiques
dans les Composites Utilisés
dans les Structures des Systèmes Aérospatiaux)

Papers presented at a Workshop held by the AGARD Structures and Materials Panel, in Antalya, Turkey, 21st—22nd April 1993.

NORTH ATLANTIC TREATY ORGANIZATION

Published November 1993

Distribution and Availability on Back Cover

AGARD-R-795

AGARD
ADVISORY GROUP FOR AEROSPACE RESEARCH & DEVELOPMENT
7 RUE ANCELLE 92200 NEUILLY SUR SEINE FRANCE

AGARD REPORT 795

Introduction of Ceramics into Aerospace Structural Composites

(L'Introduction des Céramiques
dans les Composites Utilisés
dans les Structures des Systèmes Aérospatiaux)

Papers presented at a Workshop held by the AGARD Structures and Materials Panel, in Antalya, Turkey, 21st—22nd April 1993.

North Atlantic Treaty Organization
Organisation du Traité de l'Atlantique Nord

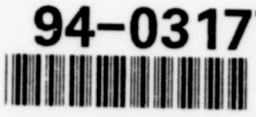

The Mission of AGARD

According to its Charter, the mission of AGARD is to bring together the leading personalities of the NATO nations in the fields of science and technology relating to aerospace for the following purposes:

- Recommending effective ways for the member nations to use their research and development capabilities for the common benefit of the NATO community;
- Providing scientific and technical advice and assistance to the Military Committee in the field of aerospace research and development (with particular regard to its military application);
- Continuously stimulating advances in the aerospace sciences relevant to strengthening the common defence posture;
- Improving the co-operation among member nations in aerospace research and development;
- Exchange of scientific and technical information;
- Providing assistance to member nations for the purpose of increasing their scientific and technical potential;
- Rendering scientific and technical assistance, as requested, to other NATO bodies and to member nations in connection with research and development problems in the aerospace field.

The highest authority within AGARD is the National Delegates Board consisting of officially appointed senior representatives from each member nation. The mission of AGARD is carried out through the Panels which are composed of experts appointed by the National Delegates, the Consultant and Exchange Programme and the Aerospace Applications Studies Programme. The results of AGARD work are reported to the member nations and the NATO Authorities through the AGARD series of publications of which this is one.

Participation in AGARD activities is by invitation only and is normally limited to citizens of the NATO nations.

Published November 1993

ISBN 92-835-0728-2

Printed by Specialised Printing Services Limited
40 Chigwell Lane, Loughton, Essex IG10 3TZ

Preface

Ceramics have been considered over the last two decades as a possible alternative to refractory metals and alloys to be used as structural materials in hot parts of engines or for space or missile applications. A specialist meeting has already been held in 1979 by AGARD SMP on this topic. There is some disappointment however among users and producers due to the fact that it has not been possible yet to overcome the main disadvantage of these materials, i.e. their brittleness and the very low value of the critical size of defects leading to fracture.

It has been recognized that one of the ways, and probably the best, to escape this difficulty is to use the concept of ceramic matrix composites. If the adhesion or the friction force between fibre and matrix is not too high, it has been proved that cracks do not propagate catastrophically, as for monolithic ceramics, across both fibres and matrix, but rather deviate when they reach a fibre and run along the fibre-matrix interface. Moreover, when general fracture of the specimen (or the part) is reached, energy must be dissipated to extract broken fibres out of the surrounding matrix.

Extensive work has already been performed to better identify these mechanisms for unidirectional composites, laminates or other fabrics, including the understanding of long term response: creep and fatigue effects or environmental degradation.

A lot still remains to be done in the field of modelling and defining specific concepts for design using these materials.

The Workshop which has been held by AGARD SMP at Antalya (Turkey), April 1993, aimed at reviewing the present knowledge on all these aspects.

Préface

Beaucoup de travaux ont été accomplis au cours des vingt dernières années sur les céramiques qui apparaissaient comme une alternative éventuelle aux métaux et aux alliages réfractaires pour réaliser certaines pièces de moteurs ou encore certains éléments structuraux pour des applications spatiales ou des engins. Une réunion de spécialistes s'est déjà tenue dans le cadre de l'AGARD (SMP) en 1979 sur ce sujet. Un certain désenchantement est toutefois perceptible chez les utilisateurs et les producteurs, car il n'a pas été possible, au fil des années de surmonter le principal inconvénient de ces matériaux: leur fragilité et la très faible valeur de la taille critique des défauts conduisant à la rupture.

Une voie a toutefois été identifiée — probablement la meilleure — qui permet d'échapper à cette difficulté, c'est la voie composite à matrice céramique. Si les forces d'adhésion ou de friction entre fibre et matrice ne sont pas trop élevées, il est établi qui les fissures, au lieu de se propager selon un mode catastrophique igonorant le détail de la structure, analogue aux céramiques monolithiques, sont arrêtées à l'aplomb des fibres et déviées suivant l'interface fibre/matrice. De plus, lorsque la rupture généralisée de l'échantillon se produit, elle s'accompagne d'une dissipation notable d'énergie, utilisée à extraire les fibres rompues de la matrice environnante.

De nombreux travaux ont déjà été accomplis pour caractériser les mécanismes pour des composites uni-ou multidirectionnels, ou pour des matériaux obtenus à partir de tissages, portant notamment sur le comportement à long terme de ces matériaux: effets liés au fluage, à la fatigue ou encore à la dégradation physico-chimique causée par les interactions avec l'environnement.

Il reste par contre beaucoup à faire pour la modélisation, ou pour définir des concepts spécifiques à l'usage des bureaux d'étude.

Le séminaire qui s'est tenu lors de la réunion du SMP de l'AGARD à Antalya (Turquie) en avril 1993 avait pour but de passer en revue les connaissances relevant de ces divers aspects.

Paul Costa
Chairman,
SMP Subcommittee on Composite Ceramics

Structures and Materials Panel

Chairman: Mr Roger Labourdette
Directeur Scientifique des Structures
ONERA
29 ave de la Division Leclerc
92322 Châtillon Cedex
France

Deputy Chairman: Dipl.Ing. O. Sensburg
Deutsche Aerospace Structures
Militärflugzeuge LME 202
Postfach 80 11 60
8000 Munich 80
Germany

SUB-COMMITTEE

Chairman: Dr P. Costa
Directeur Scientifique des Matériaux
ONERA
29, ave de la Division Leclerc
92322 Châtillon Cedex
France

Members

Dr Ing. E. Campo	IT	Dr Ing. P. Marchese	IT
Dr Ing. H.J.G. Carvalhinhos	PO	Prof. S. Paipetis	GR
Mr D. Chaumette	FR	Dr B.F. Peters	CA
Prof. M. Doruk	TU	Mr R. Potter	UK
Prof. G. Duvaut	FR	Dr T. Ronald	US
Mr C.R. Gostelow	UK	Dr Ing. M. Scolaris	IT
Dr L. Grabowski	UK	Mr S.L. Venneri	US
Prof. A. Guemes	SP	Dr J. Waldman	US
Mr L. Kompotiatis	GR	Dipl.Ing. H. Zocher	GE

PANEL EXECUTIVE

Dr Jose M. Carballal, Spain

Mail from Europe:
AGARD—OTAN
Attn: SMP Executive
7, rue Ancelle
92200 Neuilly-sur-Seine
France

Mail from US and Canada:
AGARD—NATO
Attn: SMP Executive
Unit 21551
APO AE 09777

Tel: 33(1)47 38 57 90 & 57 92
Telex: 610176 (France)
Telefax: 33 (1) 47 38 57 99

Contents

An overview on the main available ceramic composites and their processing routes

J.F. Stohr
ONERA, BP 72
F92322 Châtillon, France

ABSTRACT

During the last decade, Ceramic Matrix Composites (CMC) have undergone a rapid development, so that quite a number of composites are available today. The best known SiC/SiC and C/SiC processed by the Chemical Vapour Infiltration technique are now produced on an industrial scale. C/SiC composite currently operates at temperature above 1600°C for propulsion application on launchers and missiles ; other composites with oxide or silicon-nitride matrices are under development.

The processing routes are moving from CVI to more cost-effective processes such as sol-gel and polymer precursor. These routes appear very promising since they currently use the technologies already developed for Organic Matrix Composites and carbon-carbon. The real challenge for these materials today refers to both the working temperature, which must overpass 1600°C and the environmental behaviour. To meet these requirements, new fibres with an increased thermal stability are under development.

INTRODUCTION

Since the very first research work performed in the early 80's, Ceramic Matrix Composites (CMC's) have experienced an exceptional development throughout the last decade. The reported increase of CMC's use mainly for the manufacture of missile and rocket-engine hot components has been driven by the constant need to reduce their weight and to increase their working temperatures.

Today, the question of using CMC's on turbojet engines is raised, with the double aim of reducing the weight and increasing the thrust to improve the thrust over weight ratio. It is worth mentionning that actually, the cooling of the blades requires to remove up to 12 % of the engine total airflow, thus reducing the thrust by the same amount. The replacement of heavily cooled metallic components by solid ceramic parts appears as one of the ways of improving the engine efficiency without increasing the hot stages working temperature and therefore the NOx release.

However, to achieve this aim, the reliability of CMC's relative to the requirements of their use on civilian or military engines has to be proved. That means that CMC's able to work at temperature higher than 1400°C for long terms (>10.000 hours) within an oxydizing and corrosive environment must be available. The purpose of this paper is to review briefly the existing materials and processing technologies, so as to highlight their limitations and to present the future needs for CMC's development.

1. MAIN CERAMIC COMPOSITES AVAILABLE TODAY

Up to now, the ceramic composites to be used for aircraft structures or engine components have been designed with continuous fibres, due to the ability of these materials to undergo matrix damaging under the form of cracking without a simultaneous failure of the part. This very specific behaviour of ceramic-ceramic composites with a continuous reinforcement is always observed provided that a weak bond is achieved between the fibre and the matrix [1]. Therefore, CMC's development has been driven by that of ceramic fibres. Only three types of fibres have been used, due to high temperature requirements, (table 1) :

- carbon fibres which can work up to 2200°C but may undergo oxydation, as soon as 500°C,
- silicon carbide and nitride yarn fibres, which are limited in temperature at 1400°C, for the new grades developed in Japan,
- large diameter CVD SiC fibres, and alumina single crystal fibres which are not weavable due to their fairly large diameter (100 µm).

As far as matrices are concerned, four types are considered today, glass-ceramics, oxides, silicon-carbide or nitride and carbon as illustrated on fig. 1 as a function of the potential working temperature.

The second point to be taken into account is the component itself. Most of the components that have been used today in engines or hypersonic vehicles have been designed starting from the fibre preform. Therefore, except for unidirectionnal or eventually cross-ply stackings, processing of these composites cannot rely on the sintering techniques in use for monolithic ceramics or short fibres or particulate reinforced composites for the two following reasons :

- the limited thermal stability of ceramic fibres does not allow their hold at the temperature level

Presented at an AGARD Workshop entitled 'Introduction of Ceramics into Aerospace Structural Composites', April, 1993.

required for sintering cycles (1500 - 2100°C),

- the constraining of shrinkage due to the presence of fibres will lead to a wholly cracked matrix.

These are the reasons why CMC's processing relies mainly on techniques based on the infiltration of the fibre preform. The matrix is then obtained by the decomposition of a gas phase, the pyrolysis of an infiltrated and transformed liquid phase or the infiltration by a glassy phase.

2. PROCESSING ROUTES IN USE FOR CERAMIC COMPOSITES MANUFACTURE

The various processing routes, which can be classified in three main families i.e. gas infiltration, liquid phase infiltration and hot pressing or prepreg technology, solid state hot pressing, each of these technologies applying generally to specific types of matrices as shown in table 2 [2].

Among all those techniques, Chemical Vapour Infiltration appears to be the most flexible one, since it allows the deposit of quite a variety of matrices. It has been mainly applied to carbon and silicon carbide so as the polymeric precursors route ; this last technique has been derived from the polymer used for the manufacture of nicalon [3] and Tonen [4] fibres. On the opposite, the sol-gel route has been exclusively used for oxide or glass-ceramic composite processing. The Viscous phase hot pressing is used for glass and glass ceramic, while the gas phase reaction route has been extended from the lanxide process first used for alumina matrices. Finally, the solid state hot pressing is restricted to the manufacture of composites with large diameter fibres, such as SiC Textron fibres, using either silicon carbide or nitride as a matrix.

2.1. The Chemical Vapour Infiltration (CVI) route

The CVI technique allows the processing of any complex shape starting from the fibre preform with a 2D stacking sequence or a n D weaving (n = 3,4,5) generally held in a tooling (fig. 2). In the CVI furnace, the ceramic matrix is obtained by the decomposition of the gaseous species within the open porosity of the preform. Therefore two different phenomena may control the matrix growth rate within the depth of the preform :

- the mass transfer of the reacting species and that of the products of reaction along the porosity which occurs only by diffusion in an isothermal process
- the kinetics of the chemical reactions

In order to get a good in depth infiltration of the matrix, it is necessary to operate under both a low pressure and a low temperature condition under which the matrix growth rate is controlled by the chemical reaction kinetics [5].

This processing route leads to good quality components at the expense of long processing times, which remains acceptable for the aerospace industry. Three primary approaches have been developed on an industrial basis :

- isothermal CVD for carbon and silicon-carbide matrices by SEP in France, mainly for the manufacture of C/C and C/SiC composites in use for ramjet and liquid or solid propellant boosters.
- thermal and pressure gradients CVI developed by ORNL [6] in the United States which allows a fifty fold increase of the deposit rate and offers the promise of thick section densification ability,
- "cyclic" CVI developed by Kawasaki Heavy Industries in Japan ; this processed based on very quick and short cycles (a few seconds each) allows an accurate control of the deposit morphology through a monitoring of the crystals growth from the gaseous phase [7]. CVI allows the deposit of a large number of matrices, carbon, carbides, borides, oxides as illustrated in table 3 [5].

Besides the quality of the composites processed by CVI, one of the major advantages of this manufacturing route is that it allows a control of the fibre-matrix interphase nature. As an example, C/SiC and SiC/SiC composites processed that way are first given a short carbon deposit cycle to monitor the fibre-matrix bond strength.

2.2. The liquid processing route starting from a matrix precursor

The idea of using polymeric precursors for the consolidation of ceramic matrix composites originates from the processing route used for carbon-carbon composites, thus allowing the manufacture of quite large components. However, a large difference in ceramic yields exists between a carbon-precursor and ceramic or oxides precursors. In other words, the difference of density between the polymer precursor and the matrix is much larger for a silicon-carbide or oxide (1:2.5) matrix than it is for a carbon one (1:1.8) ; therefore the shrinkage of the matrix will be much more important 75 % instead of 35 %. To obtain a carbide or oxide-matrix with a sufficient density, i.e. a residual porosity ranging between 8 and 20 %, quite a number of successive cycles of infiltration followed by pyrolysis are required, which of course is not cost effective. However, a lot of composites with either an oxide, or a carbide-matrix have been processed that way and given correct strength [8,9].

To overcome the formerly stated difficulty of the ceramic yield, a two step infiltration technique has been developed and patented by ONERA in France (fig. 3) [10] :

- the first step consists in an infiltration of the fibre preform by fine submicronic ceramic particles of the wanted matrix, achieved uring a slurry technique, which allows to fill 50 % of the remaining free volume within the fibre preform.

- the second step consists in an injection of this green body by either a polymeric precursor for covalent matrices or an alkoxide for oxide matrices. These cycles are followed by curing for the resin precursor, hydrolysis and drying for the alkoxyde. In both cases a final pyrolysis cycle is given to achieve the CMC. Using that technique with a single injection cycle allows to reach a porosity ranging between 10 and 15 % for polymeric precursors.

2.2.1. *The sol-gel route for oxide matrix composites processing*

The sol-gel route has been known for a long time in the ceramic industry due to its ability to produce both ceramic powders and monoliths with a high purity and a great homogeneity [11]. Sol-gel route is thus a versatile technique since it allows the production of a large variety of solid oxides under the form of a gel, starting from a metallic or non metallic alkoxide, by the following hydrolysis polycondensation reactions :

$M(OR)_n + nH_2O \rightarrow M(OH)_n + nR - OH$ (hydrolysis)

$M(OH)_n \rightarrow MOn/2 + n/2H_2O$ (polycondensation)

The chemistry for the achievement of quite a number of single and mixed oxides is given in table 4 [12]. After drying, the gels are converted into oxides or ceramed-glasses by pyrolysis and/or hot pressing at temperatures above 800°C (fig. 3). These processing temperatures are fairly low compared to those necessary to process glass-matrix composites by hot pressing in the viscous state (> 1300°C).

Two other examples can be given relative to sol-gel processing, the first-one deals with the achievement of C-Al_2O_3 composite and the second with the use of a gel-phase as a compaction aid through viscous flow.

Concerning the C-Al_2O_3 composite it has been shown that shrinkage during the matrix-sintering might be controlled by the nature of the precursor chosen for infiltration. As already stated the carbon-fibre preform is first infiltrated by fine submicronic Al_2O_3 powders ; after a single infiltration followed by a natural sintering below 1200°C, the composite exhibits a high level of porosity and a poor tensile strength (40 MPa). The use of a precursor conveniently chosen to reduce the matrix shrinkage relative to a pure alumina alkoxyde both allows to limit the number of post-infiltrations to 6-8 instead of 15 usually and to provide a two fold increase in the tensile rupture stress (80 MPa), together with a porosity restricted to 20 % [13].

The second point worth to be mentioned is the ability to control the fibre-matrix bond-strength through the composition of the alkoxyde used for infiltration. This has been demonstrated in the case of SiC nicalon/mullite composites where the reduction of the Al_2O_3/SiO_2 ratio permits a drop of the interfacial shear-strength from 60 to 20 MPa [14].

2.2.2. *The polymeric precursor infiltration processing route*

The use of polymer precursor to achieve the densification of a carbide or nitride-matrix ceramic-composite is a growing research and development area since it appears as a convenient way to take advantage of existing technologies for organic or carbon-matrix composites processing. The component is first processed by a double infiltration of powder and polymer followed by curing which leads to an organic-matrix part ; the ceramic is then simply obtained by a pyrolysis without tooling. This allows to obtain sound materials with a limited porosity of 15 % [15]. Different kinds of polymers have been used : polycarbosilanes, the Tonen perhydro-polysilazane, vinylmethylsilane by UTRC [9]. A nicalon SiC fibre/SiC matrix composite has been developed by Nippon Carbon using a polycarbosilane precursor and trade-marked nicaloceram [16].

2.3. The prepreg processing route

As the formerly mentioned infiltration of a fibre preform by a liquid precursor, the prepreg technique applies to both covalent (carbide, nitride) and oxide matrices. In the two cases, the main problem of the prepreg processing is to achieve a correct monitoring of the viscous flow of a diphasic matrix (powder ceramic particles + precursor) during the densification stage.

2.3.1. *Oxide matrix composites*

Processing of the composite is performed in two steps :

- firstly an impregnation of the 2D Woven fabric by a gel precursor formed in situ,

- secondly, the deposit of fine ceramic submicronic powders on the tissue.

The composite is then obtained by hot pressing within the temperature range where a viscous flow of the gel may occur, i.e. below 1400°C, temperature at which the SiC fibres remain stable. This has been applied to different matrices such as NASICON [17], mullite [18] and the Ba A.S. ceramic glass [19].

2.3.2. *Covalent matrix composites*
The prepreg technique has also been extended to SiC matrices using a cost-effective technology of filament winding [20]. The prepreg is prepared by impregnation of a fibre tow in a slurry made of a dispersion of SiC powder in a Si-containing polymer. Composites are then processed by the lay-up technique and pressed in a tooling. All samples use 2D laminates (0/90) stack-up. Fig. 4 gives an example of C/SiC shingle for an hypersonic-vehicule thermal protection system. These composites are proned to be used up to 1200°C.

Composites have also been performed, using a similar technology, by the Tonen company. The only difference with the former technique is that the polymer used to realize the matrix, the perhydropolysilazane does not contain ceramic powders. Eight infiltration and curing (under pressure) cycles are necessary to obtain a sound composite with a very low residual porosity [21].

2.4. The Viscous phase hot pressing
This technique which applies to glass and glass-ceramic matrices was first developed in the United Kingdom and the United States in mid 60's. Fibre preforms were first made of stacking of U.D. layers obtained by pre-impregnation and winding. The hot pressing is performed in the temperature range 1000-1400°C using pressures comprised between 3.5 and 15 MPa, depending upon the matrix. This process leads to a fully dense matrix with a residual porosity of about 2 to 3%. Quite a large variety of matrices have been used for composite processing :

- firstly borosilicate matrices with a carbon reinforcement [22, 23],

- secondly alumino-silicate containing lithium oxide-matrices with nicalon-SiC fibres as a reinforcement [24] ; these matrices have been optimized by Corning glass and UTRC thus leading to the well-known LAS III [24]. Matrices for a use at higher temperatures have been defined such as MAS-L [25], MAS Y [26], and more recently BAS [27] and CAS [28]. With these new matrices, operating-temperatures over 1100°C may be reached as will be seen in section 3.

2.5. Liquid metal infiltration
This process has been mainly used to process silicon carbide matrices by a reaction between a carbon porous matrix and liquid silicon. The very first work in that area was performed by General Electric in the 70's with the infiltration of a carbon-fibre preform with liquid silicon. The silicon-carbide/silicon composite obtained, which exhibits mechanical properties up to 1200°C was trade-marked under the name SILCOMP.

Then carbon/silicon-carbide composites, with non-transformed carbon fibres, were obtained by T*Fitzger and Gadow [29] by infiltrating carbon-carbon composites with a high level of porosity by liquid silicon. These composites exhibit similar strength to that of monolithic ceramics with a somewhat improved elongation to rupture.

2.6. Gas-metal reaction
This process has been first developed in the 80's by the Lanxide company to process alumina matrix composites and further trade-marked. In the Lanxide process, the alumina-matrix is grown by the reaction between the molten metal and a reactant gas. This process has been applied to composites by allowing the alumina formed to grow outward through a fibrous preform. The first work done at Lanxide on composites was achieved with relatively low volume fractions of both coated nicalon and SCS6 silicon-carbide fibres in an alumina matrix formed by oxidation [31]. The process has still been improved to remove the residual metal from the matrix. This processing route allows the manufacture of complex shapes. First used with an oxidizing atmosphere the process has been extended to the formation of nitrides.

2.7. Solid sate hot pressing
Processing of ceramic composites using this route proceeds from laminates of alternate layers of fibre plies and matrix- powder containing the sintering aids ; hot pressing is performed within the temperature range 1800°C-2100°C for silicon-carbide or nitride matrices. Up to now, only composites processed from the large diameter Textron SCS6 fibres do exhibit some non brittle behaviour. Both UD and 0/90 cross-plies composites have been manufactured by the AVCO specialty metals division. These composites do exhibit a non brittle failure related to the presence of a carbon- interphase between the fibre and the matrix [32]. The same kind of materials has been manufactured by NASA using the well-known RBSN technique, silicon infiltration and subsequent nitridation. These composites exhibit lower resistance than the AVCO ones, due to a higher porosity. With the advent of weavable small diameter (Si,C) or (Si, N) fibres from Japan, the processing of composites using these reinforcements was achieved by UBE through hot pressing of fibres

UD lay-up or cross-ply stacking with or without the addition of powder obtained from the polymer pyrolysis [33]. Hot pressing achieved around 1400°C leads to hexagonal-shaped fibres, which apparently keep their properties, and to an improvement of the rupture behaviour in three points bending relative to monolithic matrix.
More recently, the Tonen company [21] has been proceeding to the manufacture of composites starting from prepregs, as has been described formerly in section 232.

3. MECHANICAL AND ENVIRONMENTAL BEHAVIOUR OF SOME CERAMIC MATRIX COMPOSITES

In this section mainly materials with a 2D reinforcement under the from of either a woven-fabrics or cross-plies will be considered. However, for some very particular composites, comparisons will also be made on 1D reinforced materials.

3.1. Glass and glass ceramic composites

The main available glass ceramic composites available today are collected in Table 5. At room temperature and for similarly resistant fibres i.e. nicalon NLM 202 or CG, and tyranno LoxM reinforced composites, no significant difference in rupture strength arises from the matrix. When tested in temperature (fig. 5) the situation appears quite different since SiC/LAS and SiC/MLAS processed by the sol-gel route show strength loss as soon as 700°C. On the opposite, the SiC/UTRC 200 modified glass-ceramic composite exhibits a maximum strength at 900°C, while the BMAS- matrix composite shows a potential in strength up to 1200°C [34].

Nevertheless, in all these composites, the non brittle behaviour observed on the failure surfaces originates from the presence of a few hundred nanometers thick a carbon-layer at the fibre-matrix interface. This carbon interphase is of course prone to oxidation, which will lead to a rupture-strength decrease when these materials are submitted to long-term holds in an oxidizing environment. An example of the strength loss after high temperature holds in air is given in table 6 for different materials. Degradation of the composite rupture-strength is closely related to the oxidation of the fibre-matrix carbon interphase as has been observed in the SiC/LAS materials [35], the degradation in that case being linked to the existence of a NbC diffusion layer formed next to the carbon interphase. On the opposite the MLAS matrix composite seems to exhibit a much better behaviour with only a 10 % drop in strength after a 100 hours hold in temperature. The best composite relative to oxidation sensitivity is the SiC/UTRC 200 in which the interfacial carbon layer is protected against oxidation by boron oxide [34].
The last point to be mentioned concerning these composites is the fatigue behaviour which appears to be very similar for every material. So, an illustration will be given in the case of the SiC nicalon/1723 glass composite studied by AFWAL and Dayton University [36]. For a U.D material, the fatigue limit appears to be very close to the elastic proportional limit of the composite, and about twice the stress at which the matrix first crack initiates. The same behaviour has been observed for 0/90 cross-ply laminates (fig. 6).

As far as thermal fatigue is concerned, work performed at AFWAL Wright Patterson [37] base highlights a sharp drop in the flexural strength of SiC/1723 glass composite after 500 cycles between 250°C and a maximum temperature ranging between 650°C and 800°C ; by the way, the more deleterious effect was observed for a maximum temperature cycle of 650°C with a sixfold reduction in rupture stress.

3.2. Covalent matrix composites

The best known silicon-carbide matrix composites are the materials processed by CVI by SEP. The mechanical properties of both SiC nicalon/SiC carbon (T300)/SiC composites are given in table 7 and 8 [38]. With tensile strength of respectively 200 MPa and 350 MPa at 1000°C these materials, which are processed under the form of components, appear as a reference. Table 9 compares the mechanical tensile strength of composites processed both by CVI and the polymer-precursor route. Two main conclusions may be drawn :

- at least three polymer post-infiltration and pyrolysis cycles seem to be necessary to achieve a residual porosity of 10 % i.e. similar to that obtained by C.V.I.

- rupture-strength as high as those achieved by the CVI processing route may be obtained by the polymer infiltration technique. Moreover, if the prepreg route is to be used, the component manufacture can rely on CMO technologies.

And now if some attention is paid to the environmental behaviour of these composites, some recent work performed on uncoated SiC/SiC composites do highlight a strength loss (fig. 7) together with some structural modifications of the fibre-matrix interface after long term holds (more than 100 hours) in air at temperatures ranging between 800°C and 1300°C. The observations performed in TEM show a progressive consuming of the carbon interphase layer by oxidation and its replacement by a silica- layer. From a mechanical point of view, a decrease of the Youngs modulus is first observed, which corresponds to the removal of

the carbon-layer followed by a sharp increase corresponding to the formation of the silica layer which achieves a strong fibre-matrix bond [39]. In parallel, a strong increase of the fibre matrix shear-strength measured by microindentation has been observed [40] ; then the composite exhibits a brittle failure.

As far as fatigue is concerned, tests performed in tension-tension on 2D SiC/SiC processed by CVI illustrates that the fatigue limit of the material appears to be quite high, 140 MPa as compared to the elastic proportional limit of about 160 MPa (fig. 8) [41]. A model has been proposed which takes into account the evolution of the fibre-matrix load-transfer shear-stress with the wearing of the interface during fatigue.

Silicon nitride composites need also to be mentioned ; most of the results available today refer to 1D reinforced materials. Rupture tensile strength over 600 MPa have been reported for materials with 30 vol.% of SCS6 Textron fibres [42]. However, ageing of these composites at temperatures ranging between 1260 and 1370 °C for one hundred hours leads to a twofold decrease of their rupture strength, so that the aged matrix and composite exhibit the same residual strength [43]. In fatigue at high temperatures (1000°C) the behaviour of these materials resembles that of glass-ceramic matrix composites : the fatigue limit of the composite is nearly equal to the elastic proportional limit i.e. 200 MPa for a rupture strength of 400 MPa [33].
To end with covalent-matrix composites, it is worth mentioning some recent results obtained in Japan with 1D carbon-SiC and carbon-Si_3N_4 composites. Work performed by Tonen company [21] shows the possibility of obtaining flexural rupture stresses of 480 MPa at room temperature and still 430 MPa at 1200°C while with a SiC matrix derived from polycarbosilane precursors, NAGOYA GIRI's reports flexural rupture strength of 400 MPa at R.T. and 600 MPa in the temperature range 1400-1600°C [44].

4. DISCUSSION : LIMITS AND PERSPECTIVES FOR CERAMIC-CERAMIC COMPOSITES

As shown formaly, quite a number of CMC's are available today, which have been demonstrated as operating components. Nevertheless, two limitations appear today since one thinks of using those materials for long term in oxidizing or corrosive environments :

- the first limitation comes from the fibres : if carbon fibres undergo no temperature limit as far as strength is concerned, they are sensitive to oxidation at very low temperatures (500°C). Ceramic fibres available today, even the last oxygen free SiC fibres developed in Japan seem to be limited to 1400°C [45, 46]. Large diameter silicon-carbide fibres like SCS6 loses their properties beyond 1100°C. The newly developed SiC fibres by Textron [47] do exhibit a much higher thermal stability, probably due to the existence of a carbon-interphase between the silicon-carbide grains, interphase which acts as a grain-growth inhibitor. The two other fibres that have to be mentioned is the sintered SiC fibre from Carborandum [48] and the polycrystalline SiC fibre derived from an organic precursor from Dow Corning [49]. For the Dow Corning near stoechiometric SiC fibre, the limit in temperature again seems to be just below 1400°C while the carborandum fibres only exhibit a tensile strength of 1 GPa, but keep their strength up to 1600°C, at least for short time exposures.

- the second limitation originates from the nature of the fibre-matrix interphase which has to be built to give the composite a non brittle, energy dissipative failure. Up to now, almost all composites have relied upon a carbon- interphase due to the ability of either pyro-carbon or in situ grown carbon-interphases to achieve a weak fibre-matrix bond strength. As shown in section 3, most of the interphases undergo oxidation after a 100 hours hold in temperature. Fig. 9 gives an example of the limits of the silicon carbide composites.

The alternative ways that appear today, are :

- either to change the nature of the composite constituents and work, performed at Santa Barbara university has shown that an oxide interphase may allow a crack deflection to occur

- or to protect the carbon interphase by an adequate addivive, and the way shown by UTRC seems to be promising.

However, to be of some interest for turbo engine components, the limit put forward by engine designers seems to be around 1600°C. At that temperature no fibre is today available even if some development work is on the way on single-crystal fibres of alumina or garnett [50]. These developments appear as the only ones able to reach the above temperature limits, which is a real challenge.

CONCLUSIONS

The R and D work performed in the area of ceramic-ceramic composites has lead to the emergence of four classes of materials :
- ceramic-glass matrix composites for use at temperatures up to 1200°C,
- oxide matrix composites for temperatures up to 1600°C,
- covalent matrices composites up to 1700°C,

- finally coated C/C that can be used up to 2000°C.

If carbon-carbon composites are kept aside two families have been produced under the form of components carbon or silicon carbide fibres/silicon carbide matrix and silicon carbide/glass-ceramic composites.

The second family has given the way to materials than can be operated up to 1200°C in air.

The first family has been produced for rocket engines and ramjet components mainly and demonstrated for hypersonic vehicule components in France essentially.

CMC's composites produced today appear nevertheless to be limited in working time due to the presence of oxidation sensitive constituents, mainly a carbon fibre-matrix interphase. To overcome this drawback, new materials based on oxide have been proved to be good candidates up to 1600°C.

Further development of CMC's mainly rely on the designing of new ceramic-fibres with stability in temperature up to 2000°C, able to operate in an oxidizing environment for 2000 hours.

Literature

1. Evans A.G., paper N° 2 "Ceramic Composites opportunities and challenges", this workshop.

2. Strife J.R., Brennan J.J. and Prewo K.M., Ceram.Eng.Sci.Proc. 11 [7, 8] pp 871-919, (1990).

3. Yajima S., Hayashi J. and Okamura K., "Development of a SiC fibre with high tensile strength", Nature, 261, pp 683-685, (1976).

4. Tonen Corp. 1-1-1 Hitotsubashi, Chiyoda-Ku Tokyo 100, Japan, Commercial documentation.

5. Naslain R. and Langlais F., "CVD processing of ceramic-ceramic composite materials", Tayloring multiphase and composite ceramics, Mat.Sci.Res., Vol.20, Plenum Press New-York 1985, pp 145-164.

6. Stinton D.P., Caputo A.J., Lowden R.A., "Synthesis of fibre-reinforced SiC composites by CVI", Ceram.Bull., Vol.165, N° 2, (1986).

7. Stohr J.F. and Remy L., rapports de mission au Japon, "Les matériaux pour l'hypersonique", Min. Aff. Etr. (1991).

8. Fitzger E., "Fiber reinforced ceramics", wihiskers and fiber toughened ceramics Conference Proceedings, ASM int., (1988).

9. Strife J.R., Wesson J.P. and Streckert H.H., "Study of critical factors controlling the synthesis of CMC's from preceramic polymer", AFOSR contrat N° F49620-87-C-0093, annual report, (1989), (op. cit, ref 2).

10. French patent 91 012 37, 4 Feb. 1991, "Matériaux composites céramiques fibre-matrice multi-couche et procédé pour son élaboration".

11. Colomban P., "Gel technology in ceramics, glass ceramics and ceramic-ceramic composites", Ceramic International 0272-8842, 503-20, Elsevier Science, (1989).

12. Fitzger E. and Gadow G., "Fiber reinforced composites via the sol-gel route", ibid [5], pp 571-608.

13. Wey M., PhD Thesis, to be published.

14. Parlier M., Grenier T., Renevey S., Passilly B., "Mullite and SiC matrix SiC fibre composites for high temperature application", 4th Int. Symposium on Cer. Mat. and components for engines", Göteborg, Sweden, June 10-12, 1991.

15. Parlier M., Stohr J.F. and Costa P., "High strength ceramic-ceramic composites for high temperature applications", 1st Int. Cong. on future high technology materials, Praha, Tchecoslovakia, 20-25 mars 1991.

16. Ichikawa H., Mitsuno S., Imai Y. and Ishikawa T., "Mechanical and electrical properties of SiC fibres and their composites, Proceedings of the first Japan Int. SAMPE Symposium, 1989.

17. Mouchon E., Lagrange J.L. and Colomban Ph., "SiC nicalon fibre-Nasicon matrix composite : the influence of alkaline ions on the sliding interface, in Proc. 8èmes Journées nationales sur les composites, nov. 16-18, 1992, Palaiseau. Allix O., Favre J.P. and Ladeveze P. Eds, AMAC, Paris (1993).

18. Mouchon E. and Colomban Ph., Zirconia precipitates and zirconia interphase in mullite SiC Woven fabrics composites prepared through a sol-gel route. EACM - High Temperature Ceramic matrix composites, Bordeaux, France, 20-24 sept. 1993 (to be published).

19. Chen M., Lee W.E. and James P.F., "Crystallisation of CELSIAN (Ba $Al_2Si_2O_8$) glass derived from alkoxyde precursors", 2nd European Conference on Materials and Processes, Cambridge, U.K., 9 July, 1991.

20. Ostertag R. and Trabandt U., "Fibre-reinforced ceramic components by filament winding for intermediate temperature applications", Proc. Int. Symp. on Advanced materials for light weight structures, ESTEC Noordwijk, the Netherlands, 25-27 March 1992 (ESA SP336, October 92).

21. Sato K., Susuki T., Funayama O. and Isodo T., "Fabrication of Silicon-nitride based composites by impregnation with perhydropolysilazane". Jal of the Ceramc. Soc. of Japan, Vol. 100, N° 4, pp. 444-447, (1992).

22. Nardone V.C. and Prewo K.M., "Tensile performance of carbon fibre-reinforced glass", Jal Mat. Sci. 23, 168-80, (1988).

23. Prewo K.M., "Carbon fibre reinforced glass matrix composite tension and flexure properties", Jal Mat. Sci. 23, 2745-52, (1982).

24. Prewo K.M., Johnson B. and Starett S., "Silicon-carbide reinforced glass ceramic composites tensile behaviour at elevated temperatures", Jal Mat. Sci., 24, 1373-79, (1989).

25. Brevet Français n° 8915987 du 4 décembre 1989. "Composition vitrocéramique Li-Al-Si-O et son procédé de fabrication".

26. Montardi Y., Menessier E., Nussbaum H., Drouet C., "Microstructure and thermomechanical properties of SiC fibres reinforced glass-ceramic matrix composite : influence of the matrix precursor", ECCM 5, Bordeaux, France 7-10 April, (1992).

27. Colomban Ph., "Multilevel Ceramic Composites : the advantages of the sol-gel route", Proc. 8èmes Journées nationales sur les composites, 16-18 novembre 1992, Palaiseau, Allix O., Favre J.P. and Ladeveze P., edts AMAC, Paris (1993).

28. Bleay S.P., Scott V.D., Harris B., Cooke R.G. and Habib F.A., "Interface characterization and fracture of calcium alumino-silicate glass-ceramics reinforced with nicalon fibres", J. Mat. Sci. 27, pp. 2811-22, (1992).

29. Fitzger E. and Gadow R., "Fibre reinforced silicon-carbide", Am. Ceram. Soc. Bull, 65, pp. 326-35, (1986).

30. Andersson A.C., Barron-Antolin P., Fareed A.S. and Shirocky G., "Properties of fibre-reinforced Lamxide aluminium-matrix composites" pp. 209-16, Op. Cit. ref. 8.

31. Fareed A.S., Sonuparlak S., Lee C.T., Fortini A.J. and Shiroky G., "Mechanical properties of 2D nicalon-fibres reinforced Al_2O_3 and AlN matrix composites". Ceram. Eng. Sci. proc. 11, [7,8], (1990).

32. Fould W., Lecostaouec J.F., Landry C., Di Pietro S. and Vasilos T., "Tough nitride matrix composites using Textron silicon-carbide monofilaments", Ceram. Eng. Sci. Proc. 10 (9-10), pp. 1083-99, (1989).

33. Yamamura T., Ishikawa T., Shiouya M., Nagasawa T. and Okamura K., "An approach to manufacture a new type of ceramic composites", pp. 1084-89, Proc. 1st, Japan Int. Sampe Symposium, (1989).

34. Brennan J.J., "Interfacial studies of refractory glass-ceramic matrix/advanced SiC fibres reinforced composites", UTRC annual report (1991), contract n° 00014-87-C-0699 for Navy Dpt, ONR, Arlington, VA 22217.

35. Parlier M. and Sudre O., "Composites céramiques à matrice oxyde", Journées Thématiques DRET sur "les matériaux composites structuraux", Paris 4-5 mars 1993.

36. Larry P., Zawada P., Butkus L.M. and Hartman G.A., "Room temperature and fatigue properties of Silicon Carbide fibre-reinforced aluminosilicate glass", Ceram. Eng. Sci. Proc. 11, [9-10], pp. 1592-06, (1990).

37. Zawada L.P. and Wetherhold R.C., "The effect of thermal fatigue on a SiC fibre/aluminosilicate glass composite".

38. Cavalier J.C., Lacombe A. and Rouges J.P., "Ceramic-matrix composites, new materials with very high performances", ECCM 3, Bunsell A.R., Lamicq P. and Massian A. edts, appl. Sci. p. 99-110, (1989).

39. Cuttard T., Fargeot D. and Gault C., U.S. Evolution of SiC/SiC and SiC/MASL mechanical properties in relation with the interface structure. To be published in "Revue des composites et des matériaux avancés".

40. Passilly B., Sudre O. and Parlier M., "Caractérisation mécanique des interfaces dans les composites céramiques. ibid. (ref. 39).

41. Reynaud P., Rouby D. and Fantozzi G., "A model describing the changes in ceramic-fibre composite under cyclic loading", ECCM 5, 5th

European Conf. Comp. Mat., Bordeaux, France, 7-10 avril, (1992).

42. Bhatt R.T. and Kiser J.D., "Matrix density effects on the mechanical properties of SiC-fibre reinforced silicon-carbide matrix properties", Ceram. Eng. Sci. Proc. 11 [7-8], pp. 974-94, (1989).

43. Holmes J.W., Kotil T. and Foulds W.T., "High temperature fatigue of SiC fibre reinforced Si_3N_4 ceramic composites", Symp. High Temp. Comp., Am. Soc. for comp., (1989).

44. Yoshida H., Miyata N., Sagawa M., Ishikawa S., Naito K., Enomoto N. and Yamagishi C., "Preparation of U.D. reinforced C/SiC composites by repeated infiltration of polycarbosilane", Jal. Ceram. Soc. Japan, Vol. 100 n° 4, pp. 454-58, 1992.

45. Takeda M., Imai Y., Ichikawa H. and Ishikawa T., "Properties of low oxygen content SiC fibres on high temperature heat treatments", Ceram. Eng. Sci. Proc. 12 [7-8], pp. 1007-18, (1991).

46. Takeda M., Imai Y., Ishikawa T., Kasai N., Suguchi N. and Okamura K., "Thermal stability of the low oxygen silicon-carbide fibres derived from polycarbosilanes". Ceram. Eng. Sci. Past. 13 [9-10], pp. 209-17, (1992).

47. Schoenberg T., "New CVD SiC fibres : High temperature properties", Textron Internal document, April 1992.

48. Frechette F., Dover B., Venkateswaron V. and Kim J., "High temperature continuous sintered SiC fibres for composites applications". Ceram. Eng. Sci. Proc. 12 [7-8], pp. 992-1006, (1991).

49. Lipowitz J., Rabe J.A. and Zank G.A., "Polycrystalline SiC fibres from organosilicon polymers", Ceram. Eng. Sci. 12 [9-10], pp. 1819-1931, (1991).

50. Saphikon Inc. Ltd. Commercial literature.

Table 1 : Main continuous ceramic fibres available for ceramic-matrix composites processing

TYPE	GRADE	COMPANY	PROPERTY					COMMENTS
			Composition	d/(g/cm3)	R (MPa)	E (GPa)	e (%)	
SiC, Si, C, N	HPZ	Dow Corning	Si, N, C, O	2,35	2100 à 2450	140 à 175	-	Tu < 1000°C
			SiC stoechio	-	-	-	-	Tu ≥ 1000°C in development
	NLM 202	Nippon Carbon	Si, C, O	2,55	2800	175	1,6	Tu ≤ 1200°C depending upon atmosphere
	NL 300	Nippon Carbon	Si, C	2,74	2900	190	1,5	
	Tyranno	UBE	Si, C, Ti, O	2,4	2800	175	1,6	Tu ≤ 1000°C
Si_3N_4	Fibre SiN Tonen	Tonen	Si, N, O, C	2,5	2500	250	1	Tu ≤ 1000°C
	•	Toshiba ceramics	-	-	-	-	-	in development
SiC	SCS 6	Textron	SiC stoechio	3	3920	400	0,95	non wovable
Al_2O_3	Saphikon fibre	Saphikon Inc.	Al_2O_3 stoechio	3,97	2100 à 3400	414	0,5 à 0,85	1600°C ? non development

Table 2 : Main processing routes for CMC's

PROCESSING ROUTE	MATRICES	POROSITY
Chemical Vapour Infiltration	carbides, nitride carbon, oxides, borides	10 - 20 %
Viscous phase hot pressing (2D preforms)	glasses, ceramic-glasses	2 %
Sol-gel route 2D, 3D preform	oxides	10 - 20 %
Polymer precursor route (3D preform)	SiC, Si_xN_y $Si_xC_yN_z$	10 - 20 %
Liquid Metal Infiltration	(Si) -> SiC	2 %
Gas-metal reaction	oxide (Al) nitrides (Al, Zn, Ti)	< 5 %
Solid state Hot pressing	SiC, Si_3N_4	< 2 %
Prepeg curing and pyrolysis	SiC, Si_3N_4	10 - 20 %
Hot pressing (2D preforms)	oxides	< 10 %

Table 3 : Ceramics processed by CVI and usual precursors (after 5)

Refractory Materials	Gaseous precursors
Carbon	CH_4 ; C_3H_8 ; C_2H_2 ; C_6H_6
Boron	BCl_3-H_2 ; BBr_3-H_2
SiC	CH_3SiCl_3-H_2 ; $(CH_3)_2SiCl_2$-H_2 ; $SiCl_4$-CH_4-H_2
Si_3N_4	$SiCl_4$-NH_3 ; SiF_4-NH_3
B_4	BCl_3-CH_4-H_2 ; BBr_3-CH_4-H_2
TiC, ZrC	MCl_4-CH_4-H_2 (M = Ti, Zr)
TiB_2, ZrB_2C	MCl_4-BCl_3-H_2 (M = Ti, Zr)
BN	BCl_3-NH_3-H_2 ; BF_3-NH_3
Al_2O_3, ZrO_2	$AlCl_3$-H_2-CO_2 ; $ZrCl_4$-H_2-CO_2

Table 4 : Chemistries for forming single and mixed oxides (after 12)

Matrix	Used Precursor	Gel-Formation Process
SiO_2	Tetraethoxysilane (TEOS)	HCl catalysis in ethanolic solution
TiO_2-SiO_2	TEOS + $Ti(OC_2H_5)_4$	Simultaneous hydrolysis HCl catalyzed in ethanolic solution
	TEOS + $Ti(iso\text{-}OC_3H_7)_4$	
GeO_2-SiO_2	TEOS + tetraethoxy-germane (TEOG)	HCl catalysis in ethanolic solution
	TEOS + $GeCl_4$	Ethanolic solution without additional catalyst
B_2O_3-SiO_2	TEOS + B_2O_3hydr	HCl catalyst in ethanolic solution
Al_2O_3-SiO_2	TEOS + Al (sec-OC_4H_9)	Aqueous ethanolic solution
Al_2O_3	Al (iso-C_3H_7)$_3$	HCl catalysis in ethanolic solution
	Al (sec-OC_4H_9)$_3$	2-step (NH_4OH/HCl) catalysis
ZrO_2-SiO_2	TEOS + $ZrCl_4$	Ethanolic solution without catalyst

Table 5 : Compared mechanical strength of different glass-ceramic matrix composites with a 2D reinforcement

Composite	Matrix	Reinforcement	Flexural strength	Tensile strength
SiC/LAS III	LAS	Nicalon NLM 202 0/90	480	216
SiC/ITRC 200	LAS (Boror doped)	Tyranno LOXM 0/90	480	
SiC/LAS (ONERA/SGR)	LAS	Nicalon NLM 202 Woven-fabric	350	200
SiC/MAS-L	MAS-L	" 0/90	460	290
SiC/BMAS	BaMAS	Tyranno LOXM 0/90	476	
SiC/BMAS	BaMAS	Nicalon CG 0/90	428	
SiC/CAS	CAS	Nicalon NLM 202 0/90		200

Table 6 : Loss in rupture stress of some glass-ceramic composites with a 2D reinforcement after an exposure at temperature in air

FLEXURAL STRENGTH AFTER EXPOSURE IN AIR					
Composite	Room Temp.	550 70 h	700 70 h	800 100 h	900 70 h
SiC/LAS	350	-	-	10 %	-
	200 (tensile)			20 (T)	
SiC/MASL	460	-	-	420	-
SiC/LAS 200 Tyranno	460	496	434	-	462
SiC/BMAS Nicalon	480	152*	242*	-	310*
SiC/BMAS Tyranno	480	248	242	-	165

Table 7 : Mechanical properties od 2D SiC/SiC composites (after 38)

Properties	Units	Temperature		
		23°C	1000°C	1400°C
Fibre volume fraction	%	40		
Density		2.5		
Open porosity	%	10		
Tensile strength	MPa	200	200	150
Elongation to rupture	%	0.3	0.4	0,5
Tensile Young's modulus	GPa	230	200	170
Flexural strength	MPa	300	400	280
Compressive strength //	MPa	580	480	300
Compressive strength ⊥	MPa	420	380	250
Interlaminar shear strength	MPa	40	35	25
"Toughness" K_{1R}	MPa$\sqrt{m}$	30	30	30

Table 8 : Mechanical properties of 2D C/SiC composites (after 38)

Properties	Units	Temperature		
		23°C	1000°C	1400°C
Fibre volume fraction	%	45		
Density		2.1		
Open porosity	%	10		
Tensile strength	MPa	350	350	350
Elongation to rupture	%	0.9	0.9	
Tensile Young's modulus	GPa	90	100	100
Flexural strength	MPa	500	700	700
Compressive strength //	MPa	580	600	700
Compressive strength ⊥	MPa	420	450	500
Interlaminar shear strength	MPa	35	35	35
"Toughness" K_{1R}	MPa$\sqrt{m}$	32	32	32

Table 9 : Comparison of 2D SiC/SiC and C/SiC composites processe by different routes

Composite / Characteristics	2D SiC/SiC			2D C/SiC			
processing route	S.E.P CVI	Dornior expolysilazane prepeg + 3 polymeric injections	ONERA ex-PVS SiC powder + 2 polymer injections	ONERA ex-PVS SiC powder		Nippon Carbon	Dow Corning ex(Si, N, C)
reinforcement Type	Skinex	0/90°	Skinex			2D woven-fabric	2D woven-fabric
Vf	45%	45%	45%	30%	35%	40%	-
Porosity	8-12%	10-15%	17%	17%	20%	-	-
rupture strength (MPa) fl	400	200-400	250	200	250	110	350-420
tens	260	200-350	-	-	-	-	210-245

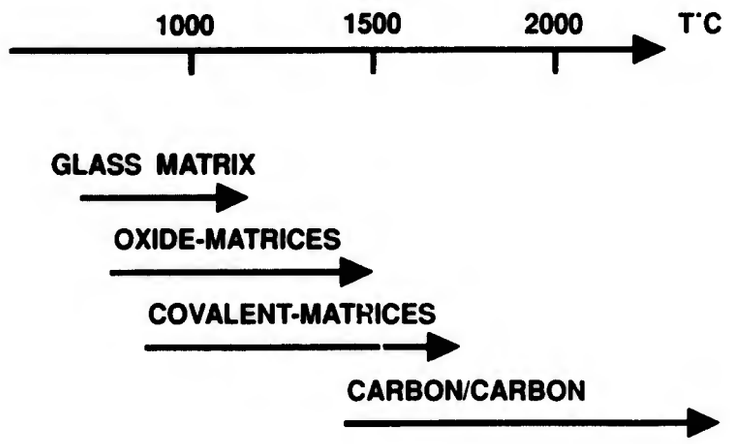

Fig. 1 : Main CMC's available today according to their matrix ultimate working temperature.

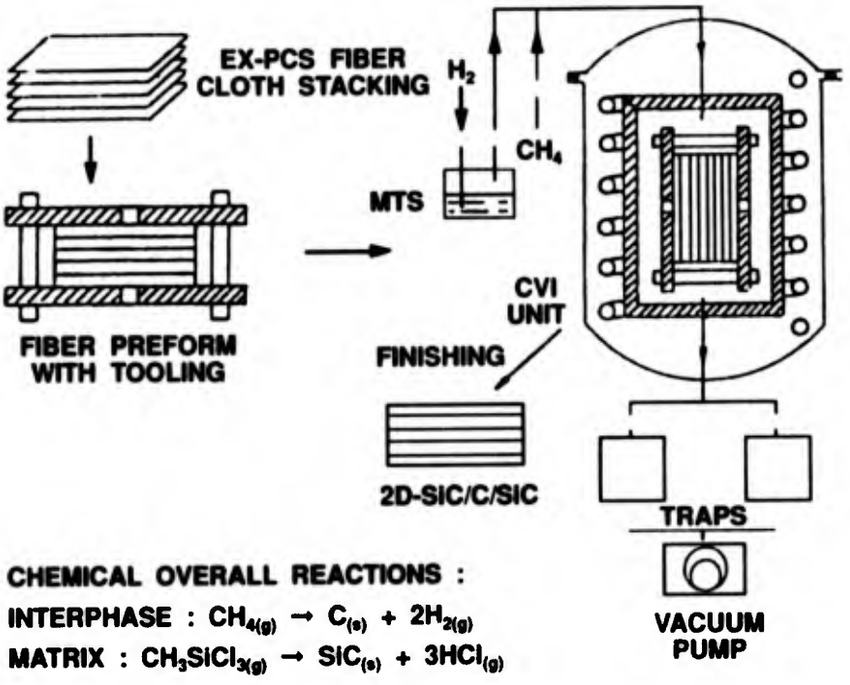

Fig. 2 : Chemical Vapor Infiltration processing route for CMC's.

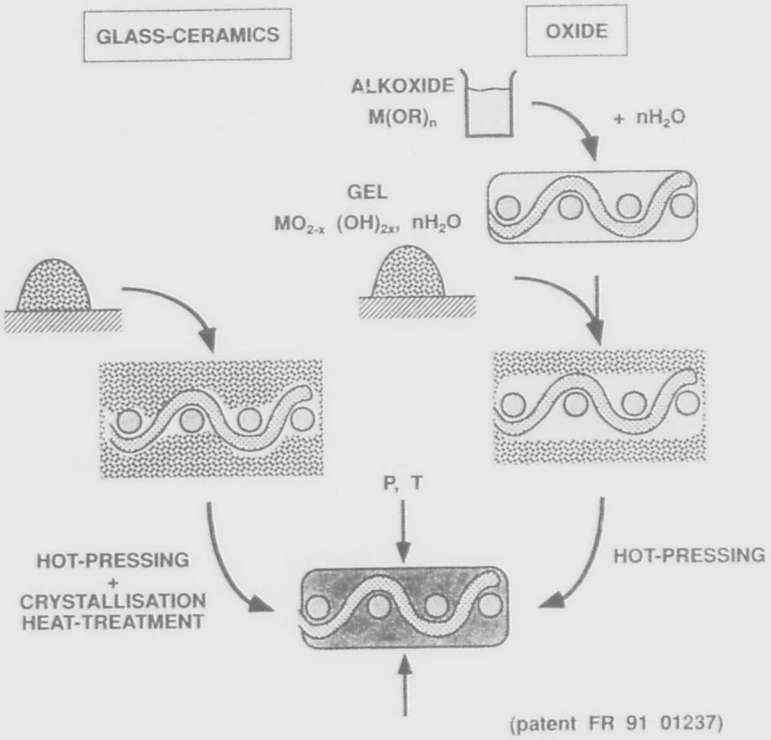

Fig. 3 : Processing of oxide composites : the sol-gel and the viscous phase infiltration routes.

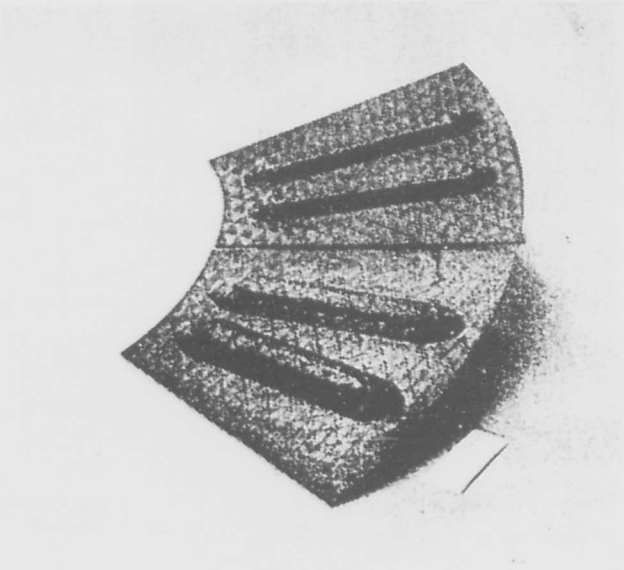

Fig. 4 : C/SiC shingles for a thermal protection system of a re-entry vehicule (after 20).

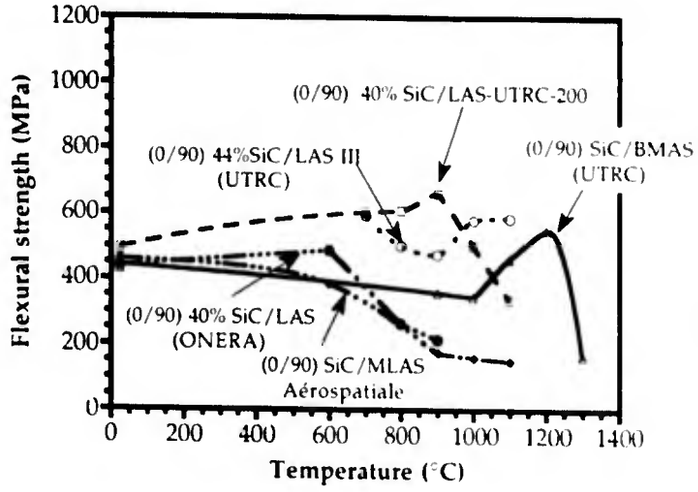

Fig. 5 :

Rupture stress as a function of temperature for the main available glass-ceramic matrix composites.

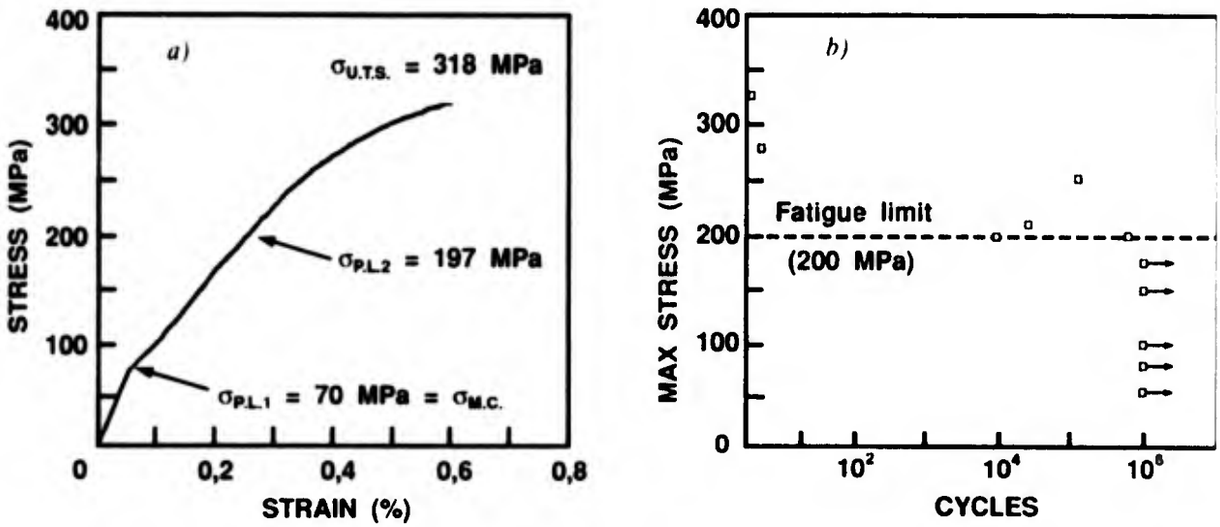

Fig. 6 : Fatigue behaviour of a 2D SiC reinforced/glass composite
a) monotonic tensile cure
b) fatigue limit

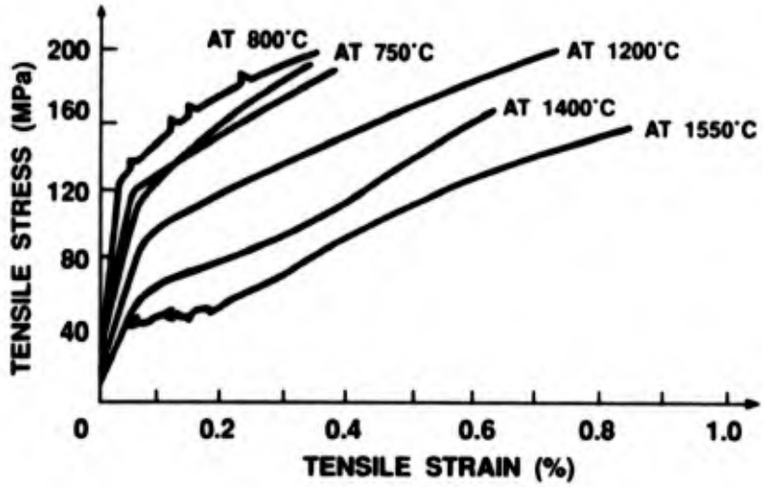

Fig. 7 :

Evolution of SiC/SiC mechanical properties after ageing in air

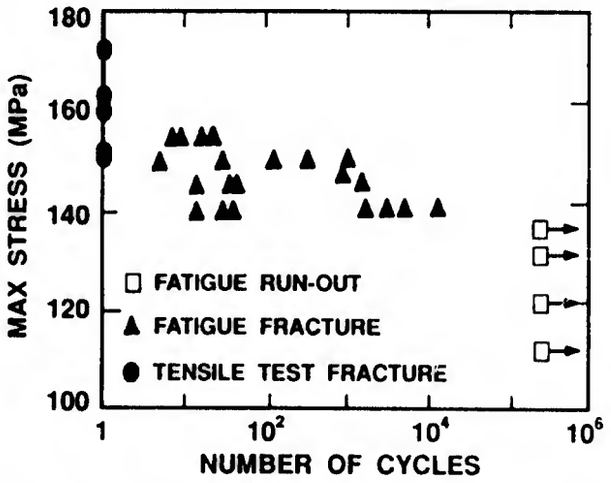

Fig. 8 : Fatigue limit of a 2D SiC/SiC composite under tension-tension loading (R = 0,1).

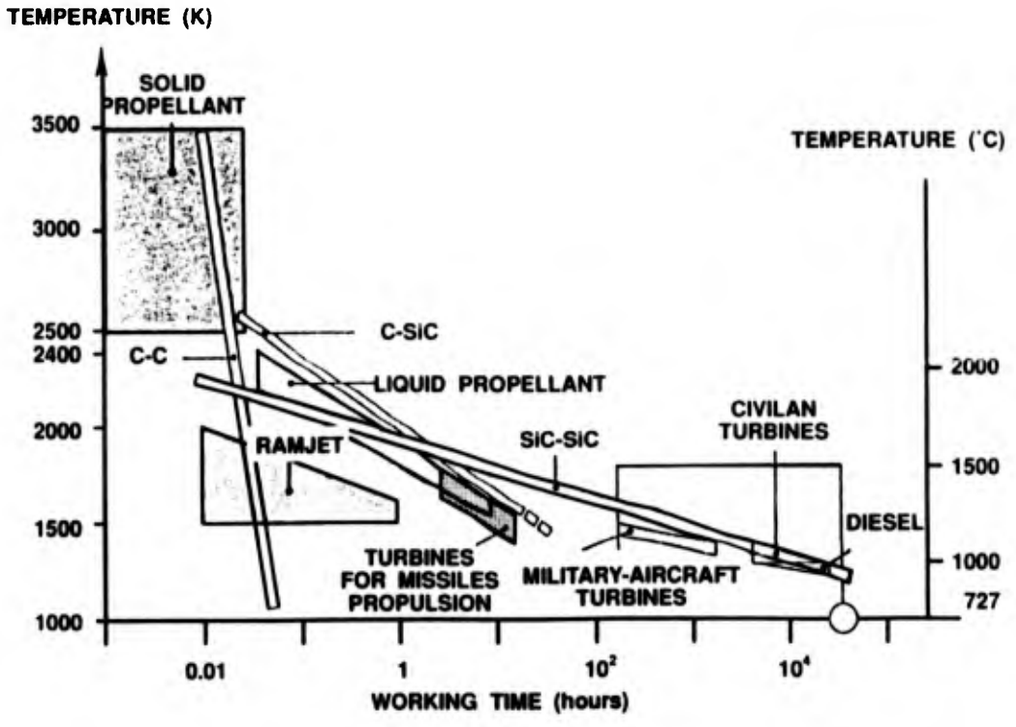

Fig. 9 : Potential use of CMC's as a function of temperature and time.

CERAMIC MATRIX COMPOSITES: CHALLENGES AND OPPORTUNITIES

by

A.G. Evans
Materials Department
College of Engineering
University of California
Santa Barbara, California 93106-5050
United States

LIST OF SYMBOLS

T	shear strength
α	compliance coefficient
β	residual stress coefficient
γ	shear strain
δ	displacement
δ_c	characteristic length
$\delta\varepsilon$	hysteresis loop width
ε	strain
ε_e	elastic strain
ε_p	permanent strain
ε^*	contribution to permanent strain caused by matrix cracks
ν	Poisson's ratio (assumed to be the same for fiber and matrix)
λ	pull-out coefficient
σ	stress
σ_R	residual stress in 0/90 material along fiber axis
σ_t	lower bound stress for tunnel cracking
$\tilde{\sigma}_i$	debond stress
$\tilde{\sigma}_{mc}$	matrix cracking stress
$\tilde{\sigma}_o$	stress acting on 0° plies in a 2-D material
$\tilde{\sigma}_p$	peak stress
$\tilde{\sigma}_s$	saturation stress
$\tilde{\sigma}_T$	misfit stress
τ	interface sliding resistance
χ	matrix cracking coefficient
Γ	fracture energy
Γ_i	interface debond energy
Γ_o	dissipation associated with traction law
Γ_m	matrix fracture energy
Ω	misfit strain

SUMMARY

A methodology for the straightforward and consistent evaluation of the constituent properties of CMCs is summarized, based on analyses from the literature. The results provide a constitutive law capable of simulating the stress/strain behavior of these materials. The approach is illustrated using data for two CMCs: SiC/CAS and SiC/SiC. The constituent properties are also used as input to mechanics procedures that characterize stress redistribution and predict the effect of strain concentrations on macroscopic performance.

1. INTRODUCTION

For the structural application of ceramic matrix composites (CMCs), it is necessary to have a methodology that prescribes the influence of strain concentrations, such as notches, on tensile properties. Ideally, this methodology should have explicit connections to the constituent properties (fibers, matrix, interface), such that efficient design procedures can be implemented. This article contributes toward this objective by surveying the tensile properties of CMCs and the mechanisms that govern their properties, in a manner that leads to a methodology for relating macroscopic behavior to constituent properties. A mechanics approach that addresses the influence of strain concentrations is then summarized and compared with preliminary experimental results.

CMCs usually have substantially lower notch sensitivity than monolithic brittle materials[1-4] and, in several cases, exhibit notch insensitive behavior.[5-7] This desirable characteristic of CMCs arises because the material may *redistribute stresses* around strain concentration sites. There are two fundamental mechanisms of stress redistribution:[8-12] (i) distributed *matrix cracking* and (ii) fiber failure involving *pull-out*. An understanding of these effects provides a basis for devising a methodology to characterize and predict properties. In most CMCs, the Linear Elastic Fracture Mechanics (LEFM) methodology successfully devised for metals cannot be used,[2,8,12-14] because failure does not occur by the propagation of a dominant mode I crack. Alternative mechanics are needed, based on the actual mechanisms of failure. A more relevant mechanics is that based on the Large-Scale Bridging of matrix cracks by fibers[8,13-15] (LSBM). However, even LSBM is inadequate. It must be augmented by Continuum Damage Mechanics (CDM)[16] in order to establish a rigorous methodology.

The basic approach has the following features. An informed background needed for progress is provided by experimental results used in conjunction with models of matrix cracking and fiber failure. The matrix cracking and fiber failure observations are conducted on 2-D materials in tension and shear. Large-Scale Bridging Mechanics are used to rationalize the observed damage mechanisms. The tensile properties measured in the presence of holes and notches, when combined with damage observations, establish the mechanics approach needed to rationalize the influence of strain concentrations.

The strategy is facilitated by devising *mechanism maps* that use *non-dimensional parameters*, which combine the basic constituent properties listed on Table I in mechanistically relevant ways. A list of these parameters is presented in Table II. The most successful methodology will be that using the *minimum* number of constituent properties needed to repre-

Presented at an AGARD Workshop entitled 'Introduction of Ceramics into Aerospace Structural Composites', April, 1993.

sent the constitutive behavior. At mechanism transitions, the mechanics needed to characterize composite behavior often change.[12,17]

2. BASIC RESULTS FOR 1-D MATERIALS

2.1 Phenomenology

Models for a range of damage phenomena found in 1-D CMCs, have been established and validated by experiment.[18-40] These models provide the basis upon which the behavior of 2-D and 3-D CMCs can be addressed. The underlying phenomenology involves matrix cracking and fiber failure. *Matrix cracks* form first and interact with predominantly intact fibers,[2,18-24] subject to interfaces that debond, at energy Γ_i, and then slide at a constant shear stress, τ. ‡ This process commences at an energy bound stress, $\bar{\sigma}_{mc}$. The crack density increases with increase in stress above $\bar{\sigma}_{mc}$ and may eventually attain a saturation spacing, $\bar{\ell}_s$. The details of crack evolution are governed by the distribution of matrix flaws. The matrix cracks reduce the elastic modulus, $\bar{E}$, cause hysteresis in the presence of sliding interfaces, and also induce a permanent strain, ε_p. These matrix cracking effects are schematically illustrated in Figure 1. The intent is to relate these quantities to the constituent properties (Table I) through non-dimensional parameters (Table II).

The matrix cracks may enhance the stress of the fibers and encourage fiber failure.[8,15] However, when a fiber fails, the stress does not reduce to zero everywhere along that fiber. Load transfer can still occur through the sliding stress, τ, even though the matrix has many cracks.[25-27] As a result, the ultimate tensile strength (UTS) may exceed the value expected for a 'dry bundle' (fibers with no matrix). Two bounds appear to be involved. When failed fibers and matrix cracks do not induce a significant *stress concentration* within *intact* fibers, global load sharing (GLS) applies.[25] Then, the effective gauge length relevant to fiber failure is governed by the load transfer length. Consequently, the UTS becomes independent of the actual gauge length. Conversely, when an unbridged segment of matrix crack exists (because of processing flaws, etc.), the stress concentration induced within the fibers reduces the UTS.[8,15] In this case, fiber pull-out appears to control the UTS.[41] Constituent properties that lead to this transition in behavior wil be discussed below.

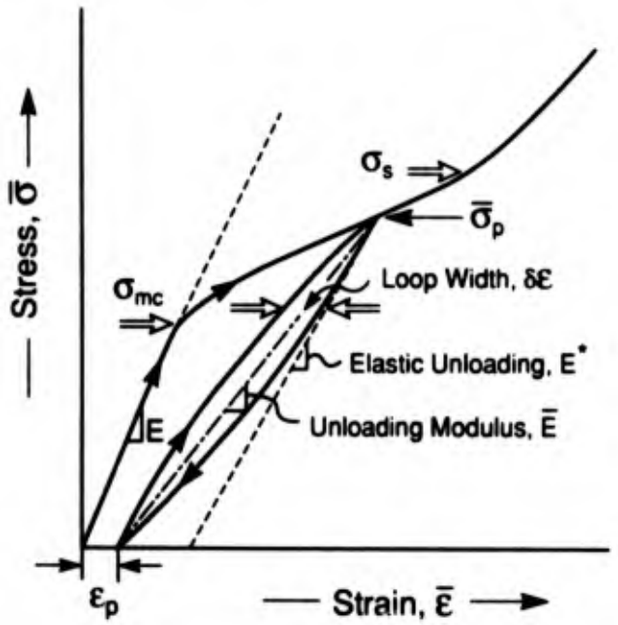

Fig. 1. A schematic indicating the consequence of matrix cracking in CMCs on the stress/strain behavior.

‡ More rigorous debonding and sliding behaviors have been analyzed,[21] but have not yet been found necessary for the derivation of useful constitutive laws.

Table I
Measurement methods

CONSTITUENT PROPERTY	MEASUREMENT
Sliding Stress, τ	• Pull-Out Length, h[25,36] • Saturation Crack Spacing, $\bar{\ell}_s$[20,22] • Hysteresis Loop, $\delta\bar{\varepsilon}_{1/2}$[23,24] • Unloading Modulus, E_I[23,24]
Characteristic Strength, S_c, m	• Fracture Mirrors[38,39] • Ultimate Strength, S[25]
Misfit Strain, Ω	• Bilayer Distortion[9] • Permanent Strain, ε_p[23,24] • Residual Crack Opening[32]
Matrix Fracture Energy, Γ_m	• Monolithic Material • Saturation Crack Spacing, $\bar{\ell}_s$[22] • Matrix Cracking Stress, $\bar{\sigma}_{mc}$[19]
Debond Energy, Γ_i	• Permanent Strain, ε_p[21,24] • Residual Crack Opening[21,24]

Table II
Summary of non-dimensional coefficients

$$\Sigma_T \equiv \frac{\bar{\sigma}_T}{\bar{\sigma}_p} = (c_T/c_i)E_m\Omega/\bar{\sigma}_p, \quad \text{Misfit Index}^{21,24,32}$$

$$\Sigma_i \equiv \frac{\bar{\sigma}_i}{\bar{\sigma}_p} = (1/c_i)\sqrt{E_m\Gamma_i/R\bar{\sigma}_p^2} - \Sigma_T, \quad \text{Debond Index}^{21,24}$$

$$\mathcal{H} = b_i(1-a_i f)^2 R\bar{\sigma}_p^2/4\bar{\ell}\tau E_m f^2, \quad \text{Hysteresis Index}^{24,32}$$

$$\mathcal{L} = \Gamma_m(1-f)^2 E_f E_m/f\tau^2 E_L R, \quad \text{Crack Spacing Index}^{22}$$

$$\mathcal{M} = 6\tau\Gamma_m f^2 E_f/(1-f)E_m^2 R E_L, \quad \text{Matrix Cracking Index}^{2,18,19}$$

$$Q = E_f f\Omega/E_L(1-\nu), \quad \text{Residual Stress Index}^{19,24}$$

$$\mathcal{A} = a_o S^2/E_L\Gamma, \quad \text{Flaw Index}^{8}$$

$$\mathcal{A}_b = \left[f/(1-f)\right]^2(E_f E_L/E_m^2)(a_o\tau/RS_u), \quad \text{Flaw Index for Bridging}^{8,15}$$

$$\mathcal{A}_p = (a_o/\bar{h})(S_p/E_L), \quad \text{Flaw Index for Pull-Out}^{37,41}$$

2.2 Matrix Cracks

A summary of the matrix cracking results is presented, which apply to materials with relatively small debond energies (SDE). More complete results are presented elsewhere.[21,24] *Long* matrix cracks interacting with fibers are subject to a steady-state condition, which leads to a *lower bound* cracking stress, given by [2,18,19]

$$\frac{\bar{\sigma}_{mc}}{E_L} = \left[\frac{6\tau\Gamma_m f^2 E_f}{(1-f)E_m^2 R E_L}\right]^{1/3} - q/E_m \tag{1a}$$

where q is the residual axial stress in the matrix, which is related to the misfit strain, Ω^*, by;[19]

$$q/E_m = \beta\left[E_f/E_L(1-\nu)\right]f\Omega \tag{1b}$$

with $\beta \approx 1$. The first important non-dimensional relationship is thus (Table II),

$$\bar{\sigma}_{mc}/E_L = M^{1/3} - \beta Q \tag{1c}$$

As multiple matrix cracking develops, the slip zones from neighboring cracks overlap and produce a *shielding* effect.[20,22] When the shielding proceeds to completion, a *saturation* crack density results. This occurs at stress $\bar{\sigma}_s$, with an associated spacing, $\bar{\ell}_s$, given by[20]

$$\bar{\ell}_s/R = \chi\left[\Gamma_m(1-f)^2 E_f E_m/f\tau^2 E_L R\right]^{1/3} \tag{2a}$$

The coefficient χ depends on crack evolution: periodic, random, etc. Recent estimates[22] indicate that, $\chi \approx 1.6$. The second important non-dimensional formula is thus (Table II),

$$\bar{\ell}_s/R = \chi\mathcal{L}^{1/3} \tag{2b}$$

The actual *evolution of matrix cracks* at stresses above σ_{mc} is governed by the size and spatial distribution of matrix flaws. If this distribution is known, the evolution can be simulated[20] (Fig. 2).‡ A simple formula that can be used to approximate crack evolution is [9]

$$\bar{\ell} \approx \bar{\ell}_s\frac{\left[\bar{\sigma}_s/\bar{\sigma}_{mc} - 1\right]}{\left[\bar{\sigma}/\bar{\sigma}_{mc} - 1\right]} \tag{3}$$

Direct application of Equations 1 to 3 requires that the elastic properties be known and, moreover, that the constituent properties (τ, Γ_m and Ω) be independently measured.[9,30] However, it would be more convenient if a methodology existed that related the constituent properties to *readily measured macroscopic features*. With this objective, a series of formulae have been derived from basic solutions for debonding and sliding at interfaces, as matrix cracks evolve.[21,24,31]

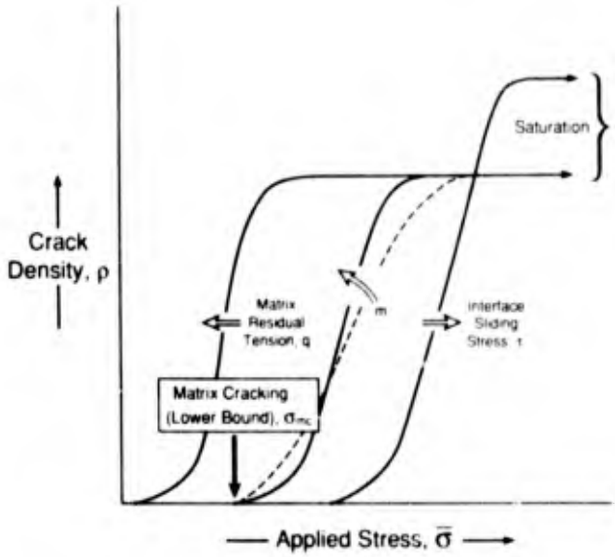

Fig. 2. A schematic indicating the parameters that influence the evolution of matrix cracks in 1-D CMCs.[30]

Matrix cracks *increase* the elastic compliance. Numerical calculations indicate that the *unloading elastic modulus*, E^*, is given by[31]

$$E_L/E^* - 1 = (R/\bar{\ell})\alpha\left[f, E_f/E_m\right] \tag{4}$$

where α is another non-dimensional function (Fig. 3). Initial unloading occurs with modulus, E^*. However, the displacements caused by reverse sliding soon dominate.[32,33] These lead to an effective unloading/reloading modulus, $\bar{E}_L$ and generate a hysteresis loop, width $\delta\varepsilon$. When the stress $\bar{\sigma}_p$ is below $\bar{\sigma}_s$, such that limited slip zone overlap occurs, the unloading modulus and the loop width (Fig. 1) are independent of the misfit strain, Ω, but relate to the sliding stress, τ. They are also independent of Γ_i, for SDE.[24,32] The unloading modulus is given by[23,24,31,32]

$$E^*/\bar{E}_L = 1 + \mathcal{H}E^*/\bar{\sigma}_p \tag{5}$$

where $\mathcal{H}$ is the third important non-dimensional parameter (Table II), given by

$$\mathcal{H} = b_2(1-a_1 f)^2 R\bar{\sigma}_p^2/4\bar{\ell}\tau E_m f^2 \tag{6}$$

The width of the hysterisis loop $\delta\varepsilon$ is[24,32]

$$\delta\varepsilon = 2\mathcal{H}\left(\bar{\sigma}/\bar{\sigma}_p\right)\left[1 - \bar{\sigma}/\bar{\sigma}_p\right] \tag{7a}$$

such that the loop width at half maximum, $\delta\varepsilon_{1/2}$ (at $\bar{\sigma} = \bar{\sigma}_p/2$), is

$$\delta\varepsilon_{1/2} = \mathcal{H}/2 \tag{7b}$$

---

* Ω may be related to the thermal expansion coefficients of fiber α_f and matrix α_m, by, $\Omega = (\alpha_m - \alpha_f)\Delta T$, where ΔT is the cooling range, taken as a positive quantity. However, in some cases, there are additional contributions from phase transformation, 'intrinsic' stress, etc.

‡ In some cases, *small* matrix cracks can form at stresses below $\bar{\sigma}_{mc}$.[28,29] These occur either within matrix-rich regions or around processing flaws. However, the non-linear composite properties are usually dominated by fully-developed matrix cracks that form at stresses above $\bar{\sigma}_{mc}$ (Fig. 1).

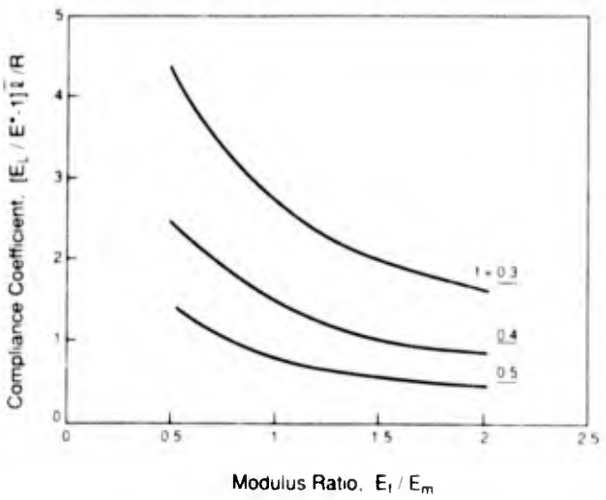

Fig. 3. Effects of matrix crack density on the elastic compliance of 1-D CMCs.[31]

The *permanent strain*, ε_p, is sensitive to the sliding stress and the misfit, as well as the debond energy. It is given by:[21,24,32]

$$\varepsilon_p = 2\mathcal{H}\left[1 - \Sigma_t\right]\left[1 - \Sigma_t + 2\Sigma_T\right] + \varepsilon^* \tag{8}$$

where Σ_t and Σ_T are two non-dimensional parameters (Table II) that introduce the influence of the debond energy Γ_i and the misfit strain Ω given by[21,24,32]

$$\Sigma_T \equiv \frac{\bar{\sigma}_T}{\bar{\sigma}_p} = (c_2/c_1)E_m\,\Omega/\bar{\sigma}_p$$

$$\Sigma_t \equiv \frac{\bar{\sigma}_t}{\bar{\sigma}_p} = (1/c_1)\sqrt{E_m\Gamma_i/R\,\bar{\sigma}_p^2} - \Sigma_T \tag{9}$$

and ε^* is the extension associated with relief of the residual stress caused by matrix cracks, in the absence of interface sliding,[31]

$$\varepsilon^* = (E_m\,\Omega/E)\left[f a_2/(1 - a_1 f)\right]\left[E/E_c - 1\right] \tag{10}$$

The above results can be combined to give an expression for the secant modulus, $\bar{E}_s$.[24] The resulting constitutive law may be used to simulate stress/strain curves.[24] The results may also be used to evaluate τ, Γ_i and Ω, provided that ℓ_c has been measured, as elaborated below.

At stresses above $\bar{\sigma}_t$, the behavior is less well-documented. It has generally been assumed that the tangent modulus $\bar{E}_t$ is that associated exclusively with the fibers,[18]

$$\bar{E}_t = f E_f \tag{11}$$

However, deviations from Equation 11 often arise.[22]

Finally, it is noted that certain matrices (especially oxides) are susceptible to stress corrosion cracking.[25] This phenomenon leads to time-dependent matrix cracking, which can occur at stresses below $\bar{\sigma}_{mc}$.

2.3 Fiber Failure

Several factors are important concerning fiber failures within a composite matrix. (i) Fibers begin to fail prior to the UTS.[25-27] At the UTS, the fraction of failed fibers within the characteristic length, δ_c, is sufficient that the remaining intact fibers are unable to support the load. (ii) The stochastic nature of fiber failure dictates that the fiber failure sites have a *spatial* distribution around the fracture plane. Consequently, a frictional *pull-out resistance* exists. This resistance allows the material to sustain load, beyond the UTS. The associated pull-out strength S_p is an important property of the composite. (iii) When unbridged flaws exist in the material, the matrix cracks introduce stress concentrations within intact fibers. This effect may lead to a reduced UTS.[8,15]

The basic stochastics of fiber failure have identified two non-dimensional parameters: a characteristic strength[25,36]

$$S_c = S_o\left[\tau L_o/R S_o\right]^{\gamma_{(m+1)}} \tag{12a}$$

and a characteristic length

$$\delta_c = L_o\left[S_o R/\tau L_o\right]^{\gamma_{(m+1)}} \tag{12b}$$

related by

$$S_c = \tau\delta_c/R \tag{12c}$$

When multiple matrix cracking precedes composite failure, and when GLS applies, the UTS is gauge length independent at large lengths ($L_g \geq \delta_c$). The UTS is given by[25]

$$S_u = f S_c F(m) \tag{13}$$

where

$$F(m) = \left[2/(m+2)\right]^{\gamma_{(m+1)}}\left[(m+1)/(m+2)\right]$$

At shorter gauge lengths ($L_g < \delta_c$), the UTS increases as L_g decreases[26] (Fig. 4).

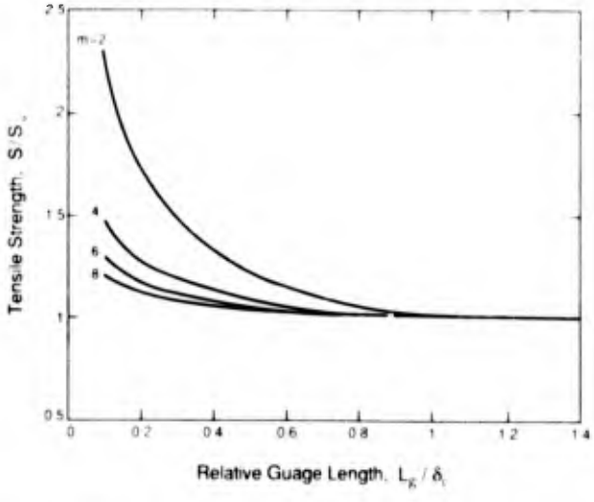

Fig. 4. Effects of gauge length on the ultimate tensile strength predicted by global load sharing analysis.[27]

In principle, it is possible for composite failure to be preceded by relatively few matrix cracks, with GLS still applicable. Then, because the average stress on the fibers is lower, the UTS is predicted to be higher than S_u. In the limit wherein only *one* matrix crack has formed, the UTS (subject to GLS) is

$$S_u^* = f S_c G(m) \tag{14}$$

where

$$G(m) = \left[(5m+1)/5m\right]\exp\left[-1/(m+1)\right]$$

The spatial distribution of the fiber failures that occur upon loading results in fiber pull-out on the matrix fracture plane. The mean pull-out length, $\bar{h}$ (for $L_g > \delta_c$), has the non-dimensional form[25,36]

$$\bar{h}\,\tau/RS_c = \lambda(m) \tag{15}$$

There are two bounding solutions for the function λ (Fig. 5). Composite failure subject to *multiple matrix cracking* gives the *upper bound*. Failure in the presence of *a single crack* gives the *lower bound*.

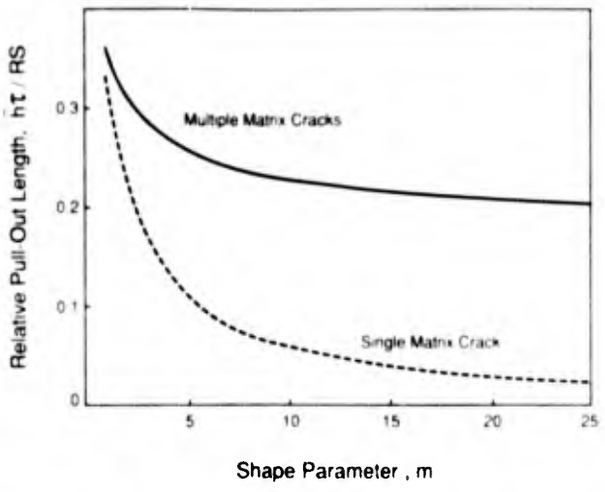

Fig. 5. Bounding solutions for the non-dimensional fiber pull-out length.[25]

Because of pull-out, the system has a *residual* strength, S_p, (Fig. 6a) given by

$$S_p = 2\tau f \bar{h}/R \equiv 2 f S_c \lambda(m) \tag{16}$$

The preceding results are applicable provided that there are no unbridged segments along the matrix crack. Unbridged regions concentrate the stress in the adjacent fibers and weaken the composite. The effect can be addressed using Large-Scale Bridging Mechanics (LSBM). Simple linear scaling considerations require that the strength S^* depend on a non-dimensional *flaw index*[8,15] (Table II),

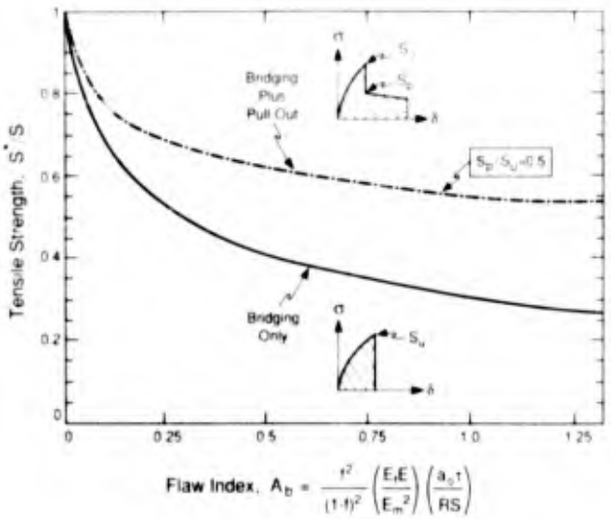

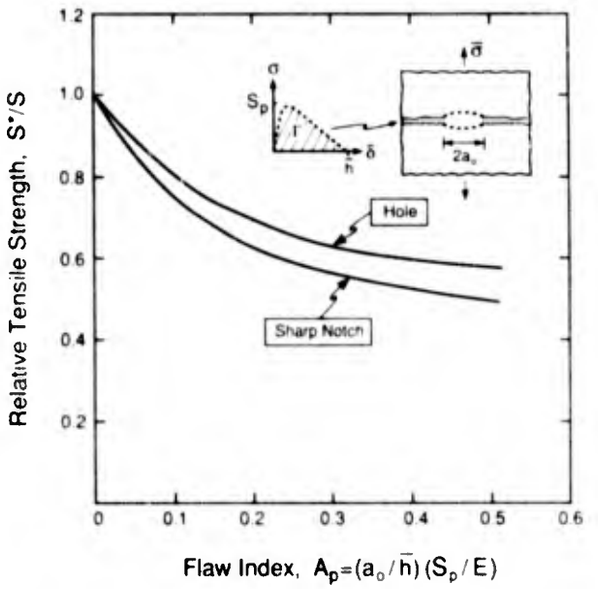

Fig. 6. Strength degradation in elastically isotropic CMCs subject to unbridged segments (length $2a_o$) a) combined bridging and pull-out; b) pull-out.[8,37]

$$\mathcal{A} = a_o S^2/E_1 \Gamma_o \tag{17}$$

where Γ_o is the area under the stress/displacement curve for the bridging fibers, S is the fully-bridged UTS and $2a_O$ is the length of the unbridged segment. The flaw index $\mathcal{A}$ must be specified for each bridging law, based on Γ_o. The functional dependence of strength S^* on $\mathcal{A}$ has been determined by numerical analysis for two limiting cases.[37] A *lower bound* arises in the presence of bridging without pull-out ($S = S_u$, $S_p = 0$), with flaw index,[8,15] (Table II),

$$\mathcal{A}_b = 3\left[f/(1-f)\right]^2\left(E_f E_L/E_m^2\right)\left(a_o\tau/RS\right) \tag{18a}$$

The dependence of the UTS on $\mathcal{A}_b$ is plotted on Figure 6a. An *upper bound* obtains when the UTS is pull-out dominated ($S = S_p$), with flaw index[8,37,41] (Table II),

$$\mathcal{A}_p = 2(a_o/\bar{h})(S_p/E_L) \tag{18b}$$

The degradation is plotted on Figure 6b. The behavior between the bounds has not been well-established. It involves coupled bridging and pull-out. One result[37] (plotted on Fig. 6a) suggests that the lower bound is more relevant when $\mathcal{A}_b \lesssim 0.3$, whereas the upper bound is a reasonable approximation when $\mathcal{A}_b > 1.5$.

Experimental validation of the above results requires independent measurement of S_c, and m. Tests conducted on pristine fibers are *not relevant*, because fiber degradation usually occurs upon composite processing.[10,38,42] Two approaches have been used. One approach entails removal of the matrix, by dissolution,[1] which is only feasible if further fiber degradation does not occur. The second approach involves *fracture mirror* measurements on failed fibers, after tensile testing of the composite.[10,38,39,42]

3. CHARACTERISTICS OF 2-D MATERIALS

3.1 Matrix Cracking

General comparison between the stress/strain, $\sigma(\varepsilon)$, curves measured for 1-D and 2-D materials[41] (Figs. 7 and 8) provides important perspective. It is found that $\sigma(\varepsilon)$ for 2-D materials is quite closely matched by simply scaling down the 1-D curve from S to S/2. The behavior of 2-D materials must, therefore, be *dominated* by the 0° plies,‡ which provide a fiber volume fraction in the loading direction about half that present in 1-D material.

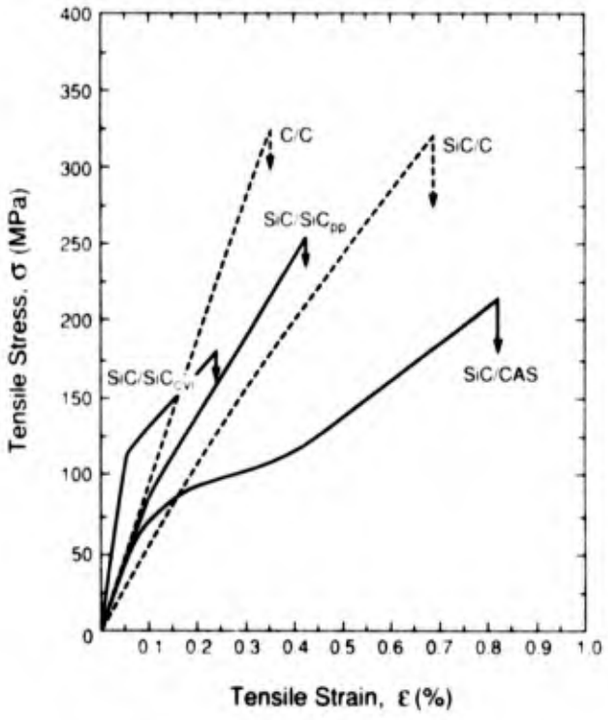

Fig. 7. A comparison of stress/strain curves for 2-D CMCs all reinforced with Nicalon fibers (with $f \approx 0.4$). The SiC/CAS is a laminate, the SiC/SiC$_{CVI}$ has a plain weave: the other materials have a 8-harness satin weave.[41]

‡ Furthermore, since some of the 2-D materials are woven, the S/2 scaling infers that the curvatures introduced by weaving have minimal effect on the stress/strain behaviors.

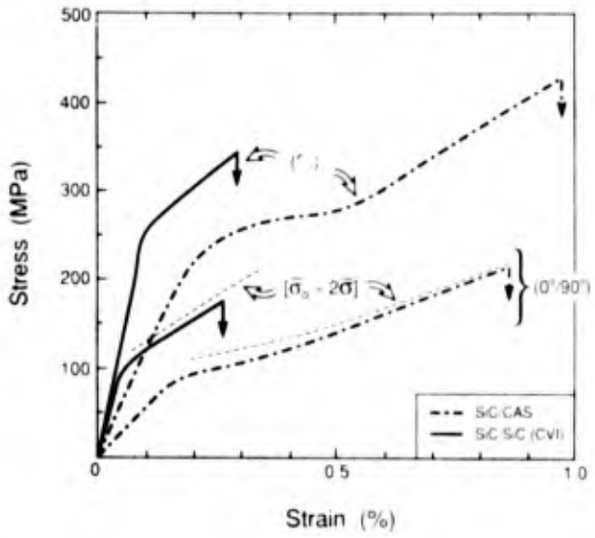

Fig. 8. A comparison of 1-D and 2-D CMC tensile properties obtained for SiC/CAS and SiC/SiC$_{CIV}$. The lines marked (1/2)1-D are the results for 1-D material reduced in scale by (1/2).[41]

The only significant 2-D effects occur at the initial deviation from linearity. At this stage, matrix cracks that form either in matrix-rich regions or in 90° plies evolve at somewhat lower stresses than cracks in 1-D materials.[29,30] However, the associated non-linearities are usually slight and do not normally contribute in an important manner to the overall non-linear response of the material. For example, matrix cracking in the 90° plies often proceeds by a tunneling mechanism[9,43,44] (Fig. 9). Tunnel cracking occurs subject to a lower bound stress[11,43,44]

$$\sigma_t = \left[\Gamma_m E/gt\right]^{\frac{1}{2}} - \sigma_R(E_L + E_T)/2E_T \tag{19}$$

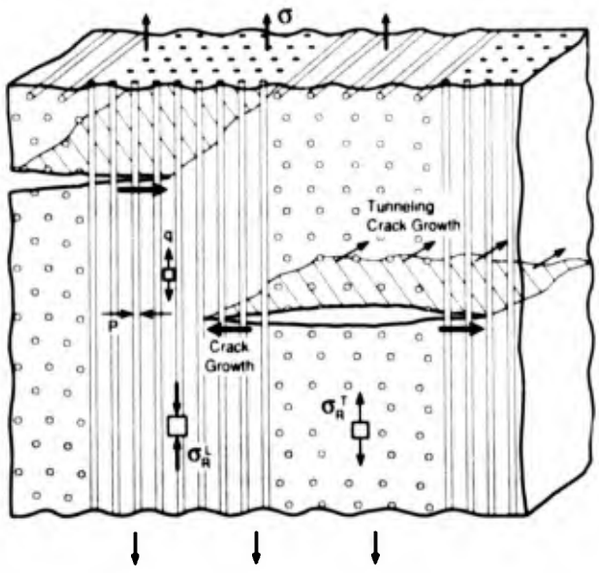

Fig. 9. A typical matrix cracking mode in 2-D CMCs.[9]

where g is a function that ranges between 1/3 and 2/3.[44] The unloading modulus associated with tunnel cracks is[44]

$$\bar{E}/E = h\left(E_f/E_m, f, t/\bar{L}\right) \tag{20}$$

with $\bar{L}$ being the mean crack spacing in the 90° plies. The function h varies between 1 and ~ 0.6 as $t/\bar{L}$ changes from ~ 0 to > 1. The corresponding permanent strain is[44]

$$\varepsilon_p = \left(1 - E_T \nu^2/E_L\right)\sigma_R/E_L \tag{21}$$

The actual evolution of cracks at stresses above σ_r depends on the availability of flaws in the 90° plies.

Extension of these tunnel cracks into the matrix of the 0° plies results in behavior similar to that found in 1-D material. Moreover, if the stress $\tilde{\sigma}_0$ acting on the 0° plies is known, the 1-D solutions may be used directly. Otherwise, this stress must be estimated. For a typical 0/90 system, $\tilde{\sigma}_0$ ranges between $\tilde{\sigma}$ and $2\tilde{\sigma}$, depending upon the extent of matrix cracking in the 90° plies and upon E_T/E_L.[44] Preliminary analysis has been conducted below using, $\tilde{\sigma}_0 = 2\tilde{\sigma}$, as implied by the comparison between 1-D and 2-D stress/strain curves (Fig. 8). Additional modelling is required on this topic.

3.2 Fiber Failure

The matrix cracks that originate in the 90° plies and extend through the 0° plies must induce a stress concentration in the fibers. The phenomenon is analogous to that considered above for 1-D material containing unbridged segments. When the stress concentration is small, the UTS should be given by Equation 13, but with f replaced by f_t. In a typical case ($f_t/f = 1/2$), the UTS would be $S_u/2$, consistent with experimental findings on several CMCs (Fig. 8). In other cases, the stress concentration is important and the UTS is significantly smaller than $S_u/2$.

Major factors governing the stress concentration are the modulus ratio, E_T/E_L, the crack spacing, $\bar{L}$, and τ. That is, small values of E_T/E_L, $\bar{L}$ and τ alleviate the stress concentration.[41]

3.3 Shear Damage

When loaded in shear, 2-D CMCs are subject to non-linear deformation.[45] The deformations are governed primarily by matrix cracks. Typical shear stress/strain, $T(\gamma)$ curves (Fig. 10) indicate that CMCs can normally sustain larger shear strains than tensile strains prior to failure. The matrix damage often consists of cracks oriented at 45° to the fiber axis. Since fiber sliding is inhibited in shear loading, the elastic compliance of the composite with matrix cracks may be a useful upper bound for the shear strength. Consequently, when normalized by the shear modulus of the composite (Fig. 10), the $T(\gamma)$ curves found a range of CMCs tend to converge into a band.

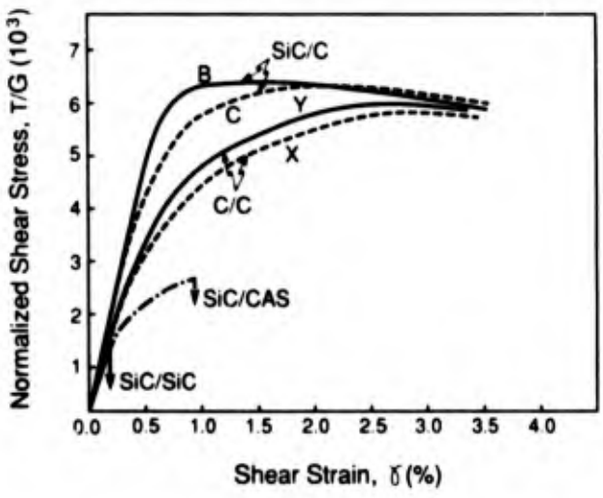

Fig. 10. The shear strength of various CMCs normalized by the composite shear modulus.[45]

4. TEST METHODOLOGY

The preceding characteristics suggest a methodology that can be used to efficiently evaluate constituent properties, which may then be used to make predictions about composite performance. The basic philosophy is that straightforward procedures be used, with consistency demonstrated between independent measurement approaches. The measurements that are experimentally convenient include: the fiber pull-out length, $\bar{h}$, the matrix crack spacing at saturation, $\bar{\ell}_s$, the stress/strain (σ, ε) behavior, the fracture mirror dimensions and the bending deformation of a bilayer (Table I).

The steps are as follows. Generally, the fiber modulus is known, whereupon E_m can be evaluated from the measured initial composite modulus. Both S_c and m are known, provided that fracture mirror measurements have been made. Curvature measurements made on bilayer provide Ω. At this stage, measurements of pull-out, saturation crack spacing and unloading/reloading hysteresis are used to determine τ, Γ_i and Γ_m, as well as to provide checks on the magnitudes of S_c and Ω.[24,34] Specifically, the magnitude of τ is obtained from the hysteresis loop width at half maximum, $\delta\varepsilon_{1/2}$, measured as a function of $\tilde{\sigma}_p$ (Eqn. 7b) and checked using the unloading modulus, $\bar{E}$ (Eqn. 5). Typical results are shown in Figures 11 and 12. Then, the misfit strain, Ω, and the debond energy, Γ_i, are evaluated from the permanent strain ε_p (Fig. 13) by using Equation 8. Additional procedures have been devised to determine Ω.[24] The misfit is compared with the bilayer measurements. Thereafter, the fiber pull-out lengths are used to provide consistency checks on τ and S_c, by using Equation 15, with the appropriate bound for λ.

When the preceding measurements provide consistent information, two other results can be used. The saturation crack spacing $\bar{\ell}_s$, allows estimation of Γ_m (Eqn. 2), which may be compared with values found for the monolithic matrix material. The same value of Γ_m can be used to calculate the matrix cracking stress, $\tilde{\sigma}_{mc}$ (Eqn. 1), which can be compared with the onset of linearity found in the stress/strain curves.

Finally, with S_c and m known, the UTS may be compared with the strengths predicted from global load sharing analysis (Eqn. 13) and fiber pull-out analysis (Eqn. 16). This comparison gives insight about the influence of matrix flaws on stress concentrations expected in the fibers.

The procedure is briefly illustrated by referring to a comprehensive set of results obtained on both SiC/CAS[6,9,24,30] and SiC/SiC[29,34,46] (see Figs. 11-13). The constituent properties for these two CMC systems obtained using the above methodology are summarized in Table III. More complete assessments are provided elsewhere.[24,34] The comparison between these two systems is interesting, because the constituent properties are very different. (i) In the SiC/SiC system, the fibers have clearly been degraded during processing. (ii)

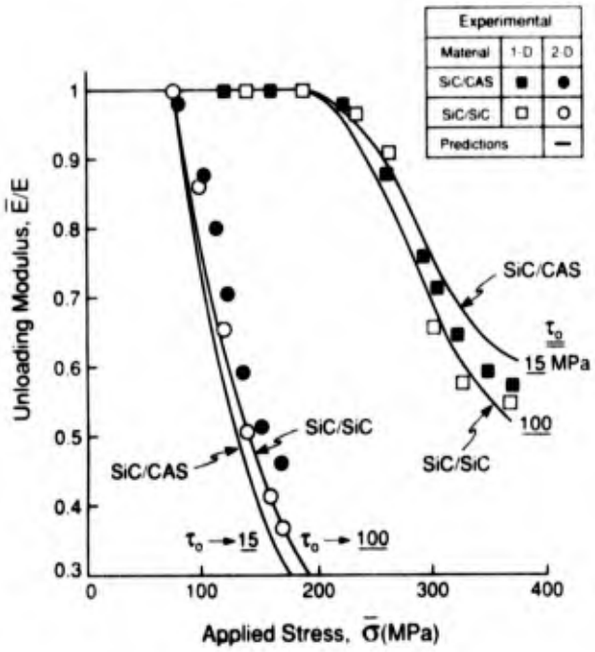

Fig. 11. The unloading modulus measured for 1-D and 2-D SiC/CAS and SiC/SiC_{CVI} showing comparisons with the model (Eqn. 5) for various sliding stresses.[24,34]

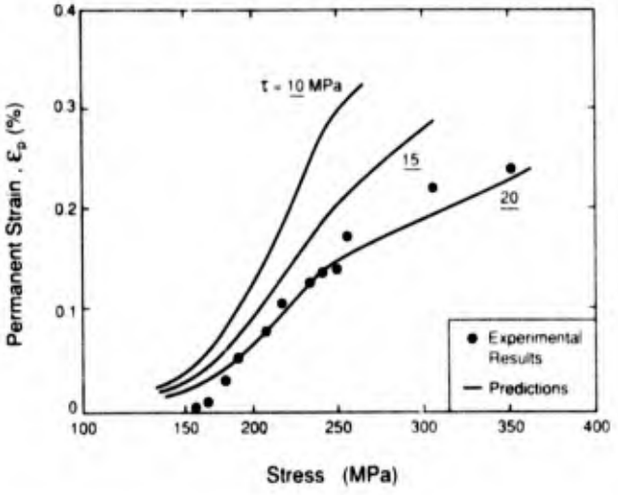

Fig. 13. Variation in permanent strain for a 1-D SiC/CAS material showing comparisons with the model (Eqn. 8) for various values of the sliding stress, using an independently determined value for the misfit strain, with ($\Gamma_i \approx 0$).[30]

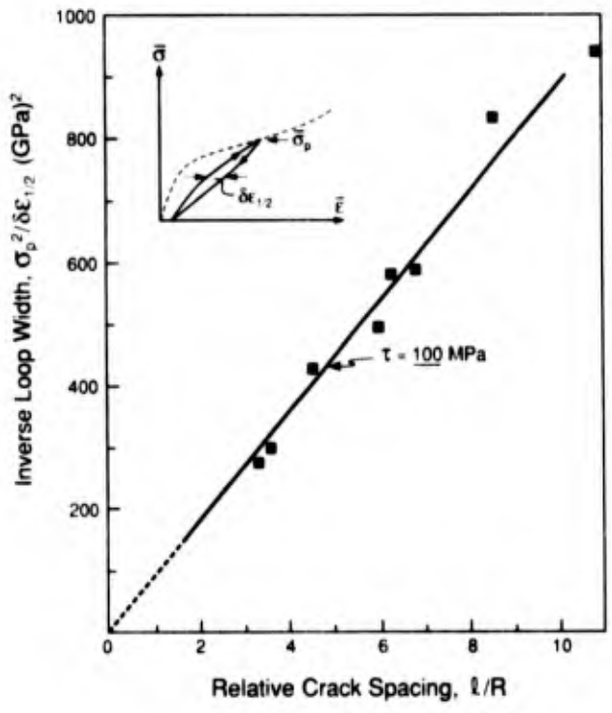

Fig. 12. Variations in the relative hysteresis loop width with crack density obtained for 2-D SiC/SiC_{CVI} showing comparisons with the model (Eqn. 7) for various sliding stresses.[24]

Table III
Important constituent properties for CMCs: comparison between SiC/SiC and SiC/CAS

PROPERTY		MATERIAL	
		SiC/CAS	SiC/SiC
CONSTITUENTS	Matrix Modulus, E_m (GPa)	100	400
	Fiber Modulus, E_f (GPa)	200	200
	Sliding Stress, τ (MPa)	15–20	100–150
	Residual Stress, q (MPa)	80–100	50–100
	Fiber Strength, S_c (GPa)	2.0–2.2	1.3–1.6
	Shape Parameter, m	3.3–3.8	4.2–4.7
	Matrix Fracture Energy, Γ_m (Jm^{-2})	20–25	5–10
	Debond Energy, Γ_i (Jm^{-2})	~0.1	~2
DEPENDENT PROPERTIES	Matrix Cracking Stress, σ_{mc} (MPa)	140–160	200–220
	Saturation Crack Spacing, $\bar{d}_s$ (μm)	110–130	15–20
	Pull-out Length h (μm)	250–350	25–40

The large difference in τ indicates that the C coating placed on the fibers in the SiC/SiC material (by vapor deposition) has very different properties than the C interphase in the CAS system, which is governed by reaction during processing. The high stiffness of the SiC matrix may also have an important influence on τ. (iii) The SiC/SiC system has a substantially larger debond energy, Γ_i, which is the origin of the relatively small permanent strain.

5. SIMULATIONS

When the constituent properties have been evaluated in a consistent manner, the stress/strain curves, for SDE materials, at stresses prior to saturation may be simulated by using Equations 1 to 10.[24,34] The procedure is straightforward for 1-D material, provided that Equation 3 is a reasonable representation of matrix crack evolution. Some examples are presented in Figure 14a.[24] Further work is needed to predict the behavior above $\bar{\sigma}_s$. The simulation capability for 2-D material depends on the assumption made about the stress $\bar{\sigma}_o$ acting on the 0° plies. If this stress is considered to be, $\bar{\sigma}_o = 2\bar{\sigma}$, the simulations for SDE materials, based on SiC/CAS (Fig. 14b), agree quite well with experiments except at small plastic strain.[34] Further research is needed to understand the behaviors at small plastic strains.

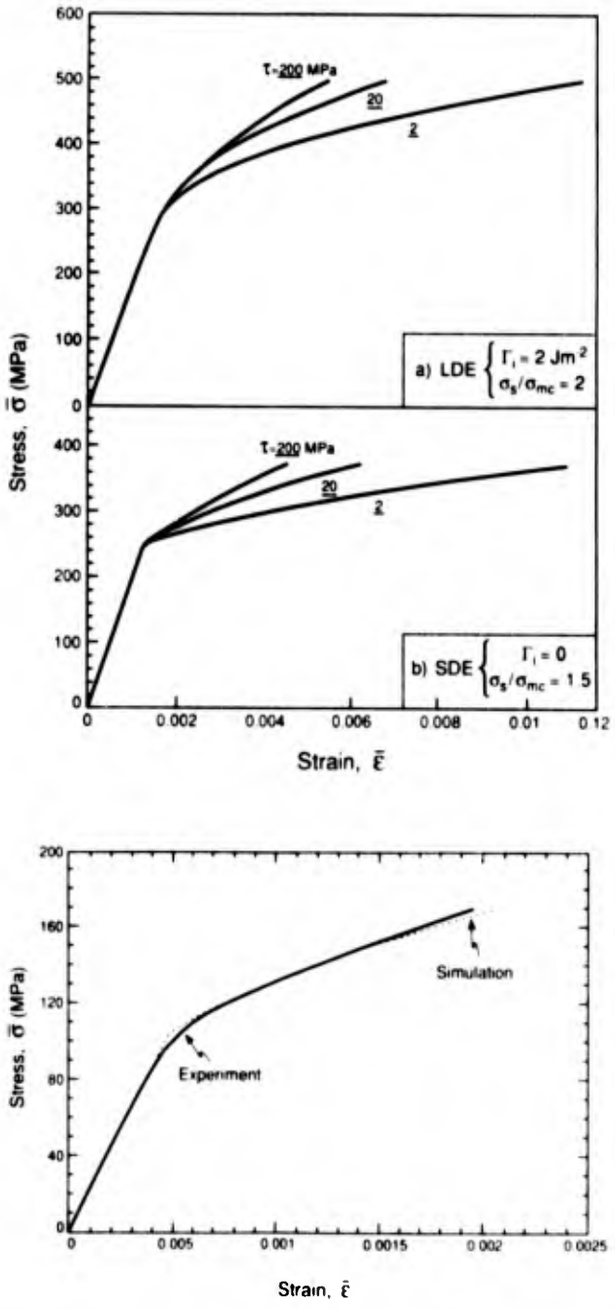

Fig. 14. Simulated stress, strain curves for SDE material a) 1-D material with notational constituent properties. b) 2-D material simulation obtained by assuming $\bar{\sigma}_o$ $2\bar{\sigma}$, compared with experimental measurements (constituent properties relevant to SiC/CAS)

6. EFFECTS OF STRAIN CONCENTRATIONS

6.1 General Considerations

When either holes or notches (or other strain concentrating sites) are introduced, experimental results have indicated that CMCs can exhibit (at least) three classes of behavior,[12,40] as sketched in Figure 15. Class I materials exhibit a dominant (mode I) crack emanating from the notch, with fiber failures occurring as the crack extends across the material. Class II materials experience multiple (mode I) matrix cracking from the notch. These cracks usually extend across the net section prior to fiber failure. In class III materials, shear damage occurs from the notch and extends normal to the notch plane prior to composite failure. In all three cases, *stresses are redistributed* by matrix cracking as well as by fiber pull-out.

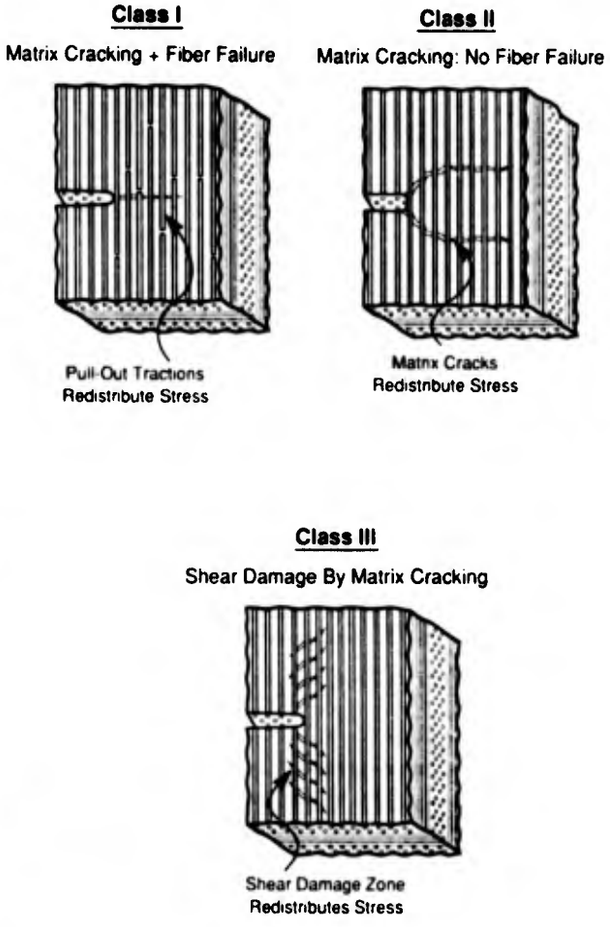

Fig. 15. The three classes of behavior found in CMCs and the associated mechanisms of stress redistribution.[40,41]

The characterization of notch effects for CMCs exhibiting these three classes of behavior appears to require different *mechanics,* because the stress redistribution mechanism within each class operates over different physical scales. Class I behavior involves stress redistribution by fiber bridging/ pull-out, which occurs along the crack plane. Large-Scale Bridging Mechanics (LSBM) is preferred for such materials.[8,13-15] Class II behavior allows stress redistribution by large-scale matrix cracking. Consequently, mechanism-based, Continuum Damage Mechanics (CDM) is regarded as most appropriate.[16] Class III behavior involves material responses similar to those found in metals,[12,40,41] and a comparable mechanics might be used: either LEFM for small-scale yielding or non-linear fracture mechanics for large-scale yielding. Since a unified mechanics has not yet been identified, it is necessary to devise *mechanism maps* that distinguish the various classes, through constituent properties. Initial attempts are elaborated below.

6.2 Mechanism Transitions

The transition between class I and class II behaviors involves considerations of both matrix crack growth and fiber failure. One hypothesis for the transition may be analyzed using LSBM. Such analysis allows the condition for fiber failure at the end of an unbridged crack segment to be solved simultaneously with the energy release rate of the matrix front. The latter is equated to the matrix fracture energy.[15] By using this solution to specify that fiber failure occurs *before the matrix crack extends into steady-state,* class I behavior is presumed to ensue. Conversely, class II behavior is assigned when the steady-state matrix cracking condition is achieved prior to fiber failure. The resulting mechanism map involves two indices:[15]

$$S = \left(RS/a_o\tau\right)\left(E_m^2/E_L E_f\right)\left[(1-f)/f\right]^2 \equiv 3/\mathcal{A}_b \qquad (22a)$$

and

$$C_m = \sigma_{mc}/S \qquad (22b)$$

With S and C_m as coordinates, a mechanism map may be constructed that distinguishes class I and class II behavior (Fig. 16). While this map has qualitative features consistent with experience, the experiments required for validation have not been completed. In practice, the mechanism transition in CMCs must involve additional considerations.

The incidence of class III behavior is found at relatively small magnitudes of the ratio of shear strength, T, to tensile strength S. When T/S is small, a shear band develops at the notch front and extends normal to the notch plane.[10,40] Furthermore, since T is related to G (Fig. 10), the parameter G/S is selected as the ordinate of a mechanism map.[12,41] Experimental results suggest that class III behavior arises when G/S ≥50 (Fig. 17).

6.3 Mechanics Methodology

i) Class I Materials

The class I mechanism, when dominant, has features compatible with LSBM. These mechanics may be used to characterize effects of notches, holes and manufacturing flaws on tensile properties, whenever a single matrix crack is prevalent. For cases wherein the flaw or notch is small compared with specimen dimensions, the tensile strength may be plotted as functions of *both* flaw indices: $\mathcal{A}_b$ and $\mathcal{A}_p$ (Fig. 6). For the

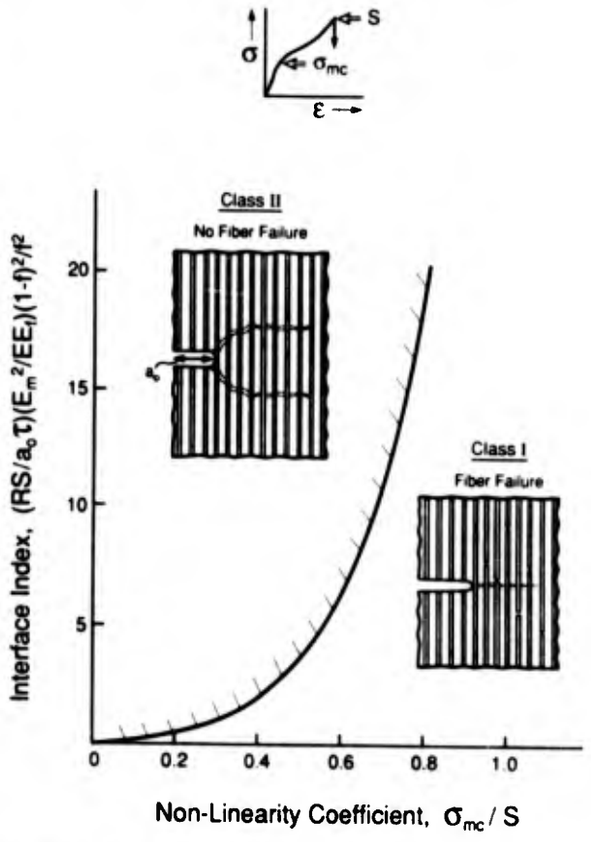

Fig. 16. A proposed mechanism map for the transition between class I and class II behaviors.[15,41]

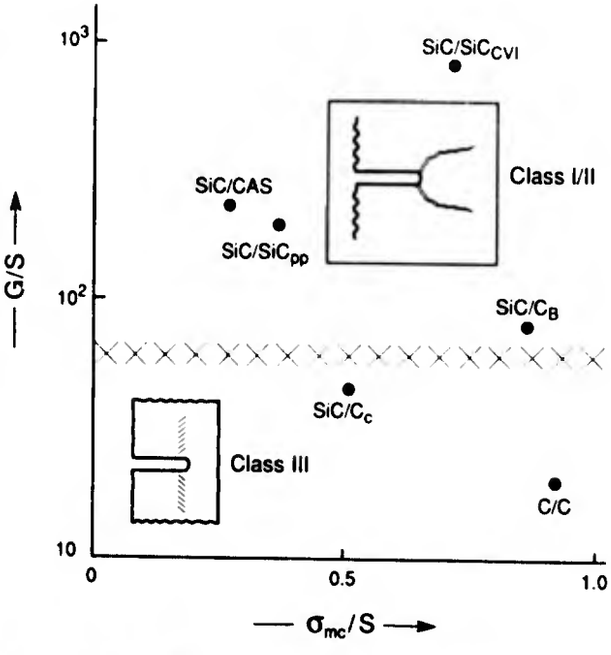

Fig. 17. A proposed mechanism map for the transition to class III behavior.[45]

former, the results are sensitive to the ratio of the pull-out strength S_p to the UTS. These results should be used whenever the unnotched tensile properties are compatible with global load sharing. Conversely, $\mathcal{A}_p$ should be used as the notch index when the unnotched properties appear to be pull-out dominated.

When the notch and hole have dimensions that are significant fraction of the plate width ($a_o/w > 0$), *net section* effects must be included.[8,37] Some results (Fig. 18) illustrate the behavior.

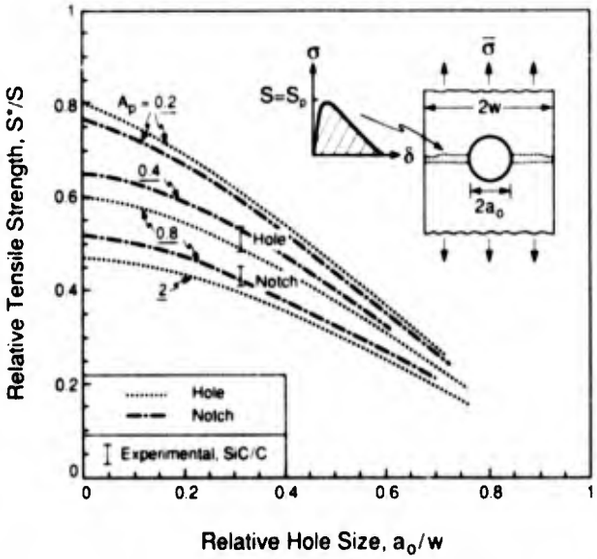

Fig. 18. Effects of holes and notches on the tensile strength predicted using LSBM. Also included are results obtained for SiC/C_B.[12]

Complete experimental validation of LSBM for class I materials has not been undertaken. Partial results for the material, SiC/C_B, are compatible with LSBM, as shown for data obtained with center notches and center holes[12] (Fig. 17), with $\mathcal{A} \approx 0.8$. For this material, the unnotched properties appear to be pull-out controlled,[10,12] and the constituent properties give a pull-out notch index, $\mathcal{A}_p \approx 0.76$.

ii) Class II Materials

The non-linear stress/strain behavior governed by matrix cracking, expressed through $\bar{E}$ (Eqn. 5) and ε_p (Eqn. 8) provide a basis for a Damage Mechanics approach that may be used to predict the effects of notches and holes. Such developments are in progress. An important factor that dictates whether continuum or discrete methods are used concerns the ratio of the matrix crack spacing to the radius of curvature of the notch.

In practice, several class II CMCs have been shown to exhibit notch insensitive behavior for holes and notches in the size range: 1-5mm (Fig. 19). These materials include: SiC/CAS[6] and SiC/glass (1070).[7] The non-linearity provided by the matrix cracks thus appears to allow stress redistribution to an extent that essentially *eliminates* the stress concentration.[7,47] The elimination of the stress concentration has been established both by notch strength measurement[6,7] and by thermoelastic emission tests.[46]

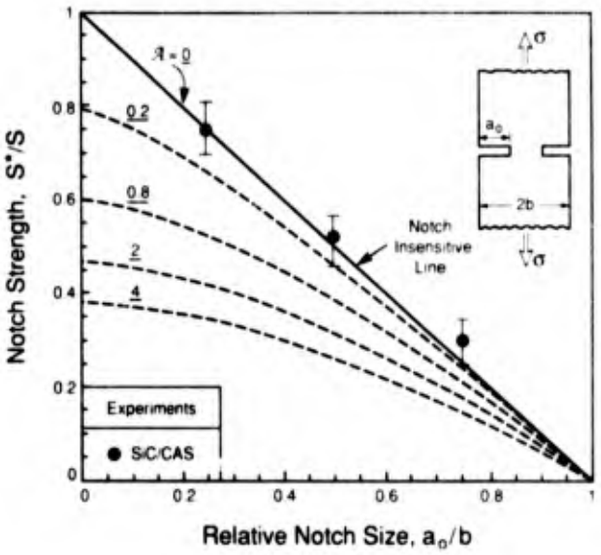

Fig. 19. The notch strength of a 2-D SiC/CAS composite revealing that this is a notch insensitive material.[6]

iii) Class III Materials

Class III behavior has been found in several C matrix composites[10,12] (Fig. 16). In these materials, the extent of the shear deformation zone ℓ_p is found to be predictable from measured shear strengths, T, in approximate accordance with [12]

$$\ell_p/a_o \approx \sigma/T \tag{23}$$

Calculations have indicated that this shear zone diminishes the stress ahead of the notch,[12] analogous to the *effect of a plastic zone in metals*, and provides good notch properties. For several C/C materials, it has been found that the shear band lengths are small enough that LEFM characterizes the

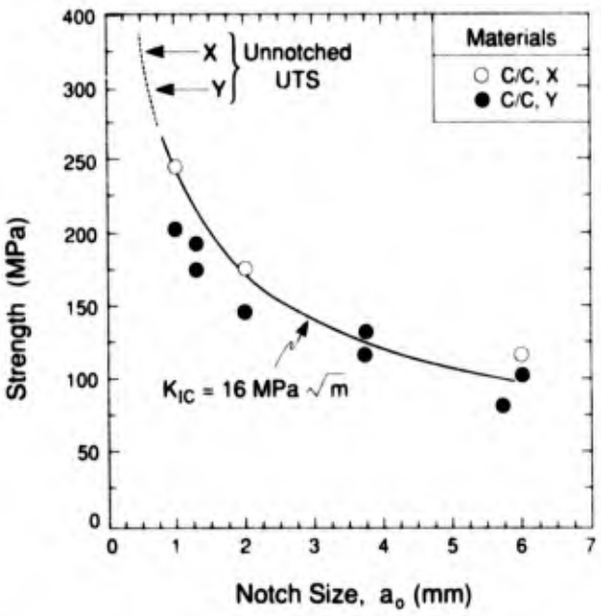

Fig. 20. Use of LEFM to characterize the notch strength of C/C composites.[12]

experimental data over a range of notch lengths. For edge notched specimens, it is found that,[12] $K_{IC} \approx 16$ MPa$\sqrt{m}$ (Fig. 20). However, conditions must exist where LEFM is violated. For example, when $\ell_p/a_o \lesssim 4$, the stress concentration is essentially eliminated and the material must then become notch insensitive.[12] Further work is needed to identify parameters that bound the applicability of LEFM, as well as establish the requirements for notch insensitivity.

7. CONCLUSION

Test methods have been described that relate constituent properties to macroscopic behaviors in a consistent manner. The approach has been illustrated for two CMC systems. It is expected that the methodology will be used to predict stress/strain curves and examine their sensitivity to constituent properties. These properties may be used to delineate mechanism maps that represent transitions in macroscopic performance, especially in the presence of strain concentrations. Mechanics procedures for each mechanism have been described in a preliminary manner. A concerted effort is needed to further develop and validate the mechanics, which should have applicability to a wide range of technologically important CMCs.

ACKNOWLEDGEMENTS

This work was supported by the Defense Advanced Research Projects Agency through the University Research Initiative under Office of Naval Research Contract No. N-00014-86-K-0753.

REFERENCES

1. Prewo KM and Brennan JJ
J. Mater. Sci., 17, 1201-06, 1982.
2. Marshall DB, Cox BN and Evans AG
Acta Metall., 33, 2013. 1985.
3. Brennan JJ and Prewo KM
J. Mater. Sci., 17, 2371-83, 1982.
4. Bouquet M, Birbis J-M, Quenisset J-M and Naslain R
ICCM-VI, Elsevier, London, Vol. 2, p. 248-49, 1987.
5. Domergue JM, Cao HC, Evans AG and Petrak D
J. Am. Ceram. Soc., to be published.
6. Cady C and Evans AG
J. Am. Ceram. Soc., to be published.
7. Mall S, Bullock DE and Pernot JJ
To be published.
8. Bao G and Suo Z
ASME Book No. AMR118, *Appl. Mech. Rev.*, 45, 355-66, 1992.
9. Beyerle D, Spearing SM and Evans AG
J. Am. Ceram. Soc., 75, 3321-30, 1992.
10. Heredia FE, Spearing SM, Mosher P, Evans AG and Curtin WA
J. Am. Ceram. Soc., 75, 3017-25, 1992.
11. Laws N and Dvorak G
Jnl. Composite Mtls., 22, 900, 1980.
12. Heredia FE, Spearing SM, He MY, Mackin TJ, Brøndsted PA, Evans AG and Mosher P
J. Am. Ceram. Soc., to be published.
13. Cox BN and Marshall DB
Fatigue and Fracture of Eng. Mtls., 14, 847, 1991.
14. Cox BN and Lo CS
Acta Metall. Mater., 40, 69, 1992.
15. Cui L and Budiansky B
To be published.
16. Hayhurst D, Leckie FA and Evans AG
Proc. Roy. Soc., London, A434, 369, 1991.
17. Evans AG and Zok FW
Topics In Fracture and Fatigue (ed. A.S. Argon), pp. 271-308, 1992.
18. Aveston J, Cooper GA and Kelly A
In *The Properties of Fiber Composites*, NPL Conf. Proc., pp. 15-26.
19. Budiansky B, Hutchinson JW and Evans AG
J. Mech. Phys. Solids, 34, 167, 1986.
20. Zok FW and Spearing SM
Acta Metall. Mater., 40, 2033, 1992.
21. Hutchinson JW and Jensen H
Mech. of Mtls., 9, 139, 1990.
22. Spearing SM and Zok FW
Jnl. Eng. Mtls. Tech., in press.
23. Pryce AW and Smith P
J. Mater. Sci., 27, 2695-2704, 1992.
24. Vagaggini E, Domergue JM and Evans AG
J. Am. Ceram. Soc., to be published.
25. Curtin WA
J. Am. Ceram. Soc., 74, 2837-45, 1991.
26. Phoenix L and Raj R
Acta Metall. Mater., 40, 2813-28, 1992.
27. Hild F, Domergue JM, Leckie FA and Evans AG
Intl. Jnl. Solids Structures, to be published.
28. Kim BY and Pagano N
J. Am. Ceram. Soc., 74, 1082-90, 1991.
29. Aubart X
Thèse de Doctorat de L'Université de Paris, *Modélisation et Identification du Comportement de Composites à Matrice Céramique*, Nov. 1991.
30. Beyerle D, Spearing SM, Zok FW and Evans AG
J. Am. Ceram. Soc., 75, 7519, 1992.
31. He MY, Wu B-X, Evans AG and Hutchinson JW
Mech. of Mtls., to be published.
32. Marshall DB
Acta Metall. Mater., 40, 427-41, 1992.
33. Kotil TJ, Holmes JW and Cominou M
J. Am. Ceram. Soc., 73, 1879, 1990.
34. Domergue JM, Vagaggini E, Evans AG and Roach D
J. Am. Ceram. Soc., to be published.
35. Spearing SM, Zok FW and Evans AG
J. Am. Ceram. Soc., in press.
36. Thouless MD and Evans AG
Acta Metall., 36, 517, 1988.

37. Suo Z, Ho S and Gong X
J. Matl. Engr. Tech., in press.

38. Eckel AJ and Bradt RC
J. Am. Ceram. Soc., 72, 435, 1989.

39. Jamet JF, Lewis D and Luh EY
Ceram. Eng. Sci. Proc., 5, 625, 1984.

40. Evans AG
Mat. Sci. Eng., A143, 63, 1991.

41. Evans AG, Zok FW and Mackin TJ
To be published.

42. Cao HC, Bischoff E, Rühle M, Evans AG, Marshall DB and Brennan JJ
J. Am. Ceram. Soc., 73, 1691, 1990.

43. Hutchinson JW and Suo Z
Appl. Mech. Rev., 28, 1991.

44. Xia C, Carr RR and Hutchinson JW
Harvard Univ. Report Mech-202, to be published, 1992.

45. Brøndsted PA, Heredia FE and Evans AG
J. Am. Ceram. Soc., to be published.

46. Mackin TJ, Evans AG and Purcell TE
To be published.

INTERFACE EVALUATION IN CERAMIC COMPOSITES

by

Paul D. Jero, Triplicane A. Parthasarathy and **Ronald J. Kerans**
USAF, WRDC/MLLM, Bld 655
Wright-Patterson Air Force Base
2230 Tenth St STE1
OH 45433-7817
United States

ABSTRACT

The results of pushout tests on two ceramic matrix composites are presented and discussed. Emphasis is placed on the effect of interface roughness on the interfacial properties. Toward that end, techniques used to characterize fiber and interface topography are described and results presented. An advanced analysis, which takes account of the roughness contribution to the radial stress during debonding, is used to calculate interfacial properties. It is observed that the fiber fabrication technique has a profound effect on the nature of the interfacial topography.

1. INTRODUCTION

The fiber pushout test has become one of the more popular techniques used to examine interfacial phenomena in both ceramic and metal matrix composites. There has been significant progress made in both experimental technique and in analysis of the data, such that it is now possible to derive useful interface properties (e.g. friction coefficient, toughness, etc.) from the test. In addition, both experimental [1-2] and theoretical [3-4] works have begun to examine the effects of a previously unappreciated parameter, the interfacial topography or roughness. Since the energy dissipation associated with frictional sliding is a major contributor to the increased toughness of composites, understanding the role of interface topography is important to the continued development of these materials. Control of this parameter presents both a challenge and an opportunity, the latter being the ability to engineer interfacial roughness for optimization of composite behavior.

Recently, Jero et al. [1-2] described an extension of pushout testing in which a fiber which has been pushed partially out, is subsequently pushed back in. This is done in order to examine the reseating of the fiber within the matrix. The momentary decrease in sliding friction which is observed, referred to as the seating drop, results from the re-mating of the corresponding fiber and matrix irregularities. The parameters of the seating drop (period and magnitude) are related to the spatial extent and amplitude of the interfacial roughness, respectively, and give an indication of the overall contribution of roughness to the sliding friction. Other investigators have confirmed the observations and begun to examine roughness effects [5-7].

Of the more advanced analyses of the pushout test, only that of Kerans and Parthasarathy [3] explicitly accounts for interface topography. They assume that

Presented at an AGARD Workshop entitled 'Introduction of Ceramics into Aerospace Structural Composites', April, 1993.

the effect of displacing the fiber and matrix asperities can be modeled as an increased radial clamping stress,

$$\sigma_{rough} = \Lambda\left(\frac{A}{r}\right), \tag{1}$$

where $$\Lambda = k\left(\frac{E_f}{\nu_f}\right), \quad k = \frac{E_m \nu_f}{E_f\left(1+\nu_m\right) + E_m\left(1-\nu_f\right)}$$

A is the effective roughness amplitude, r is the fiber radius, and E_f, E_m, ν_f, and ν_m are the elastic modulus and Poisson's ratio of the fiber and matrix, respectively. The approach only applies when the relative fiber/matrix displacement is large compared to half the period of the roughness, $\lambda/2$, typically after complete debonding of the fiber. It would be expected, however, that the roughness would play a role even when the displacements are smaller than λ, although the relative importance should decrease. Recently, Parthasarathy & Kerans [4] extended their treatment to include a roughness contribution during the debonding phase of fiber pushout. The treatment assumes a simplified linear dependence of the radial displacement (of the fiber and matrix), $\delta_r(x)$, on the axial displacement, $\delta(x)$, for displacements less than $\lambda/2$.

$$\delta_r(x) = A\left(\frac{\delta(x)}{\lambda/2}\right) \tag{2}$$

For displacements greater than $\lambda/2$, $\delta_r(x)=A$. The inclusion of the roughness significantly complicates the equations, which were fairly transparent in the previous model. However, the salient features remain unchanged. The basic load-displacement relationship is of the form

$$\delta = \frac{(1-2\nu_f k)}{\pi r^2 E_f}\left(\frac{a}{b_1}\left(e^{-b_1 l_d} - 1\right) - \frac{c}{b_2}\left(e^{+b_2 l_d} - 1\right)\right) \tag{3}$$

where $$a = \frac{P_a - P_r + \frac{c_2 b_2}{c_1}\left(P^* + P_r\right) e^{-b_2 l_d}}{1 + \frac{b_2}{b_1} e - \left(b_1 + b_2\right) l_d},$$

$$c = \left(c_1 \frac{a}{b_1} e^{-b_1 l_d} - c_2 P^* - c_2 P_r\right)\frac{b_2}{c_1} e^{-b_2 l_d},$$

$$b_1 = 0.5\left(c_2 + \left(c_2^2 + 4c_1\right)\right)^{0.5}, \quad b_2 = 0.5\left(-c_2 + \left(c_2^2 + 4c_1\right)\right)^{0.5},$$

$$c_1 = \frac{4kA}{r^2 \nu_f \lambda}\left(1 - 2\nu_f k\right)\left(\mu + \frac{2A}{\lambda}\right) \text{ and } c_2 = \frac{2k}{r}\left(\mu + \frac{2A}{\lambda}\right)$$

l_d is the debond length, obtained by first solving the implicit equation

$$P_d = a\, e^{-b_1 l_d} + c\, e^{+b_2 l_d}, \qquad (4)$$

which was obtained by setting $P(x=l_d)$ to $(P_d + P_r)$, the critical load to propagate the crack. The reader is referred to [3] and [4] for mathematical details of both analyses.

The objective of this work was to measure interface properties in two composite systems with particular emphasis on the effect of roughness. This involved interface (pushout) testing and the subsequent data analysis as well as characterization of the interfacial roughness. The latter included characterization of a variety of (virgin) ceramic fibers, since the interfacial roughness is often controlled by the starting morphology of the fiber [8]. Characterization of the fibers required the use of multiple characterization techniques in order to measure roughness over a wide range of length scales.

2. EXPERIMENTAL PROCEDURE

2.1 Pushout testing

Two composites were examined. Each has been described previously. The reader is referred to the references indicated below for details of the processing. For simplicity, the composites will be designated by the numbers assigned below.

1. SCS-6/borosilicate glass (custom composition from Corning Glass Works, designated "E") [2]

2. Nicalon/aluminosilicate glass (Corning 1723) [9]

Both of the composites were unidirectional layups. The elastic modulus, Poisson's ratio, and coefficient of thermal expansion (CTE), α, of the fibers and matrices are shown in Table I. Thin slices were cut from the composites with the fibers perpendicular to the faces. Both faces of the samples were diamond polished to a 1 μm finish. The pushout specimen of composite 1 was 1.87 mm thick and that of composite 2 was 0.198 mm thick.

The pushout apparatus has been described previously [2,9]. Tests on composite #1 employed a 100 μm diameter flat bottomed tungsten carbide cylindrical loading probe. Tests on composite 2 employed a custom made truncated diamond cone (70° included angle with a 10 μm diameter flat). These fibers could only be pushed 3 to 5 μm due to the conical nature of the loading probe. The tests were run at a constant displacement rate of 127 μm/min (#1) or 12.7 μm/min (#2). In each case, the fibers were subsequently pushed back in to examine the seating behavior.

2.2 Characterization of fiber roughness

Commercial fibers come in a wide range of diameters and morphologies, hence the need to characterize surface topography over a wide range of length scales. This necessitates the use of multiple characterization techniques. The fiber roughness was examined using the scanning electron microscope (SEM),

scanning laser profiler (SLP), laser interferometric microscope (LIM), and atomic force microscope (AFM). The SLP consists of a stepper motor attached to a precision linear motion stage which steps a fiber through the measurement area of a scanning laser micrometer. The laser beam width is 1 μm and the minimum step length is 0.5 μm. The vertical resolution is ~0.2 μm, and the minimum fiber diameter which can be measured is approximately 100 μm. The technique is particularly good for large fibers which show relatively long range roughness (>50 μm), since the scan length is effectively unlimited. This work employed a Zygo, Model 5610, LIM. At maximum magnification the spatial resolution is 0.25 μm. A ~10 nm vertical resolution is typical, although the unit is capable of significantly better under the best of operating conditions. This technique is good for large fibers which show intermediate range roughness (~3-50 μm). The AFM used in this work was a Digital Nanoscope II. The unit achieves angstrom level vertical resolution. Spatial resolution depends on the scan length, 400 points being sampled per scan. For a standard 10 μm scan length, the spatial resolution is 25 nm. The AFM is particularly well suited to measurements on textile diameter fibers and others which have short range roughness (<3 μm). In no case is any special specimen preparation required. The Textron SCS-6, BP Sigma, Saphikon and Advanced Crystal Products sapphire, Nippon Carbon Nicalon, and DuPont FP fibers were examined.

3. RESULTS AND DISCUSSION

3.1 Characterization of fiber topography

It was observed that the fiber fabrication technique has a profound influence on the nature of the fiber surface roughness. This can be readily explained by examining the various fiber fabrication techniques. Existing large diameter (monofilament) ceramic fibers are produced by either chemical vapor deposition (CVD) or melt growth. In CVD, substrate fibers are pulled through a long, heated reaction chamber in which reactant gasses flow. The deposit builds up over the coarse of time as the fiber traverses the reaction chamber. At any given instant deposition is occurring on several feet of fiber. The result is a fiber which is highly resistant to momentary process deviations. Such deviations effect a long length of fiber, and only slightly.

The situation is almost completely reversed in melt growth, in which a single crystal fiber is pulled slowly from a melt, with a seed crystal used to initiate growth in the desired orientation. Here, the fiber is formed by solidification across an interface rather than deposition on a substrate. Solidification, obviously, occurs over only atomic dimensions at any given instant. The result is a fiber which is extremely susceptible to momentary deviations in temperature, pull speed, etc. Compounding the effect is the axi-symmetric nature of the resulting roughness in these fibers. Process deviations result in distinct diameter variations or undulations, whereas the nodular roughness characteristic of CVD fibers (see below) is randomly oriented, minimizing the overall roughness amplitude.

Commercial textile diameter fibers are generally produced by a fiber spinning process, in which a viscous solution or mixture is forced under pressure through a die. The fibers may be spun from a heated or solved pre-ceramic polymer, a heated or solved gel, a fine particle suspension, or some combination. The fiber

tow is rapidly cured, cooled, or dried and then heat treated. Surface forces promote smooth, round fibers, but, gravity, shrinkage, sintering, and fiber interactions during the cure and pyrolysis promote irregularity. The ovality of certain fibers is a classic example. Most of the textile diameter fibers remain amorphous through pyrolysis and are extremely smooth. Those fabricated from crystalline constituents are, clearly, crystalline and exhibit distinct surface roughness as a result.

In CVD, the morphology of the deposit is dependant on a host of system parameters, but the resulting fibers generally have a nodular surface (Figure 1), with the nodules ranging up to ~10 μm in diameter. For the SCS-6 fibers examined, the average peak-to-valley roughness (over ~100-300 μm) was ~250-300 nm, with an RMS roughness of ~25-35 nm. Fibers produced by melt growth exhibit a highly variable topography and require fairly long range characterization (Figure 2). Each batch of sapphire fiber that was examined was quite different, hence it is not possible to list typical roughness values. Diameter variations of several μm over a few mm of length are not uncommon, although much smoother fibers can be grown.

The Nicalon fiber remains amorphous through pyrolysis and is extremely smooth (Figure 3). Characterization is incomplete, but roughnesses on the order of a few tens of nm's appear to be typical. In this case, although the virgin fibers are quite smooth, they typically degrade during composite fabrication, producing a carbonaceous interface layer. The resulting interface roughness may be quite different than that of the starting fiber. Fiber FP represents the other extreme among textile diameter fibers. Its surface is quite rough (Figure 4), the individual nodules presumably being crystallites. Peak-to-valley roughnesses are on the order of 200 nm, similar to the SCS-6 fiber.

Although similar in absolute roughness, in must be realized that the order of magnitude difference in diameter of the Fiber FP and SCS-6 makes a huge difference in the overall effect of the roughness. For a given matrix, the stress associated with displacing the Fiber FP far enough to maximize the radial fiber/matrix displacement would be much greater than that associated with displacing the SCS-6 a similar amount (maximized radial displacement). Another obvious difference is that the SCS-6 must be displaced approximately 5 μm before the roughness induced friction is maximized, whereas the Fiber FP need only be displaced approximately one half μm before a similar maximization occurs. In some of the sapphire fibers which have been examined, a displacement of up to 100 μm or more would be required. The significance of the roughness, then, depends in large part on the magnitude of the fiber/matrix displacement (crack opening displacement (COD)) which will actually be observed in a composite in service.

At present, the amount of damage that can be tolerated is somewhat speculative. It can be argued that the brittle nature of the matrix in addition to the various fiber and matrix imperfections (porosity, inclusions, broken, displaced, or misaligned fibers) which distinguish real composites from the models that are studied, virtually guarantee that real composites in real applications will be at least locally microcracked. If the COD is limited to just a few μm, then longer range roughness will be largely irrelevant.

3.2 Pushout Tests

Figures 4 and 5 show the pushout and pushback data for composites 1 and 2, respectively. The system compliance has been removed from the pushout curves in order to show the actual debonding behavior. Note that in composite 2 displacement is plotted against stress rather than load. This is necessary since the fiber diameter varies. In this case, an effective diameter for each fiber was calculated by measuring two perpendicular diameters and averaging.

The use of a flat bottom diamond probe for pushout tests on textile diameter fibers represents a distinct improvement over the use of nanoindentation. Such probes avoid both fiber damage and significant radial loading.

Tables II and III show the interface properties calculated for the composites using the analysis of Kerans and Parthasarathy (no roughness) [3]. See also [10] and /9/, respectively, for more details. Note that in each case the interface toughness is quite small, often 0. This is consistent with the nature of the carbon rich interface that is known to exist in these composites. Similarly, the friction coefficient, μ, is low, ~0.13. This is consistent with an independent measure of μ for graphite on glass (μ=0.15) by Gupta [11]. The calculated residual stresses are higher than what would be calculated from the data in Table I, the fiber volume fractions, and an assumed ΔT over which the stresses develop. However, there is disagreement in the literature about the true values of α (radial) for the fibers, and the ΔT's are merely educated guesses.

The subsequent analysis of Parthasarathy and Kerans [4] has also been applied to the data of composite 1. The analysis requires that a roughness period and amplitude be known [in principle, it is possible to calculate both of these parameters from the data using a more advanced curve fitting program]. The period can be readily calculated from either the roughness characterization or the seating drop. The period used, 11.3 μm, was the average period of the seating drop for this specimen. The amplitude, however, is more difficult to establish. In particular, it is not clear whether it is the average roughness amplitude that is important or the extremes. In addition, how much of the roughness is offset by highly localized elastic and/or plastic deformation is not known. From the roughness characterization, roughness values ranging from 25 to 300 nm are possible. Using Equation 4 below (which derives from [3]), with the

$$\Delta = \frac{\pi r^2}{k} \cdot \Lambda \cdot \left(\frac{A}{r}\right) \left(e^{2\mu kt/r} - 1\right) \qquad (4)$$

magnitude of the seating drop, Δ, and the sample thickness, t, it was possible to assume a roughness amplitude, A, and calculate μ. By simultaneously adjusting A and iterating it was possible to arrive at an amplitude that gave the same μ from both Eq. 3 and 4. This was taken as the correct value. The calculated amplitude ranged from 20 to 28 nm, very close to the RMS roughness value obtained by examining fibers.

However, it can be (and has been [2]) argued that the measured seating drop underestimates the roughness amplitude for a number of reasons, and that an "effective" seating drop, measured from the immediately post peak sliding friction to the bottom of the seating drop, would be a better measure. If this value of Δ is

used, the calculated A ranges from 115 to 305 nm, closer to the typical peak-to-valley roughness. Table IV shows the calculated interface parameters for each of these choices of Δ. It is seen that the calculated μ is decreased as the assumed roughness amplitude increases. Additionally, the calculated residual stress is increased slightly. The two sets of values in Table IV should represent upper and lower bounds to the true values. The fact that they differ little is reassuring. The fact that they vary little from the values in Table II indicates that the roughness has relatively little effect at these small displacements. The radial stress due to the roughness varies along the length of the debond, but using Eq. 1 and the assumption of Eq. 2, at the top of the fiber (the point of maximum stress), the roughness induced stress would be ~4 MPa for an A of 25 nm and ~47 MPa for an A of 275 nm, given a maximum fiber displacement of 1.5 μm. Upon complete debonding, the roughness induced stress would be maximized, the corresponding stresses are ~16 MPa and 176 MPa, respectively.

It is seen that the roughness induced stresses are relatively small during debonding. In this case, the stress (displacement) was limited by the sample thickness, but the issue of how large the fiber/matrix displacement will be within a composite in service, remains. If the maximum crack opening displacement (COD) is limited to 1 or 2 μm, then the debond length will be remain short and the contribution of this fairly long period roughness will be relatively small. In the limit of a failing composite which is sustaining COD's on the order of up to a few 10's of μm, the roughness will play a major role. Interestingly, composite 2, which contains the finer diameter Nicalon fibers, exhibits a roughness period on the order of 1 μm (Figure 5). In this case the roughness will play a major role early in the debonding process.

SUMMARY

Pushout tests have been used to examine interface properties in two ceramic matrix composites. The fiber roughness has been examined experimentally and the effect of roughness has been included in one case. It was seen that the roughness period was too large to have a major effect on the behavior given the relatively short debond length. The nature of the fiber roughness was seen to depend on the fiber fabrication technique. The period of the fiber roughness has implications regarding its usefulness in optimizing composite properties.

REFERENCES

1. P. D. Jero, and R. J. Kerans, Scripta Metall., **25**, 2457-2462 (1991).
2. P. D. Jero, R. J. Kerans, and T. A. Parthasarathy, J. Am. Cer. Soc., **74** [11], 2793-2801 (1991).
3. R. J. Kerans and T. A. Parthasarathy, J. Am. Cer. Soc., **74**, [7], p 1585-1596 (1991).
4. T. A. Parthasarathy, R. J. Kerans,and D. B. Marshall, Submitted to J. Am. Cer. Soc.
5. W. C. Carter, E. P. Butler, and E. R. Fuller, Scripta Metall. & Mater., **25**, 579-584 (1991).
6. T. J. Mackin, P. D. Warren, and A. G. Evans, Acta Metall. & Mater., **40**, 1251-1257 (1992).
7. C. K. Bhihe and A. G. Evans, Cer. Eng. & Sci. Proc., In press.

8. P. D. Jero, T. A. Parthasarathy, and R. J. Kerans, Cer. Eng. & Sci. Proc., **13**, [7-8], p 64-69 (1992).
9. P. D. Jero, T. A. Parthasarathy, and R. J. Kerans, Cer. Eng. & Sci. Proc., In press.
10. T. A. Parthasarathy, P. D. Jero, and R. J. Kerans, Scripta Metall. & Mater., **25**, p 2457-2462 (1991).
11. P. K. Gupta, J. Am. Cer. Soc., **74**, [7], p 1692-1694 (1991).

Table I. Selected properties of the composite constituents.

	SCS-6	Nicalon	E	1723
E (GPa)	410	200	69	87
α (x 10^6/°C)	~4.0*	~3.8**	4.0*	5.4**
ν	0.15	0.20	0.23	0.25

* RT -500°C ** RT-700°C

Table II. Interface properties calculated for composite 1.

Fiber	μ	σ_N (MPa)	G (J/m^2)	Fiber	μ	σ_N (MPa)	G (J/m^2)
1	0.169	57.5	0.0	5	0.123	53.5	0.0
2	0.101	60.8	0.0	6	0.132	53.0	0.0
3	0.153	51.8	0.3	7	0.128	51.2	0.0
4	0.150	50.4	0.3	ave.	0.136	54.0	0.1

Table III. Interface properties calculated for composite 2.

Fiber	μ	σ_N (MPa)	G (J/m^2)	Fiber	μ	σ_N (MPa)	G (J/m^2)
1	0.127	143	0.2	10	0.065	251	0.0
2	0.129	130	0.0	11	0.098	180	0.0
3	0.044	192	0.0	12	0.108	134	0.0
4	0.125	166	0.0	13	0.156	132	3.3
5				14	0.187	115	2.9
6	0.100	241	0.0	15	0.067	209	0.0
7	0.132	147	3.0	16	0.139	193	0.0
8	0.206	127	0.0	17	0.321	49	0.0
9	0.118	183	0.0	ave.	0.133	162	0.6

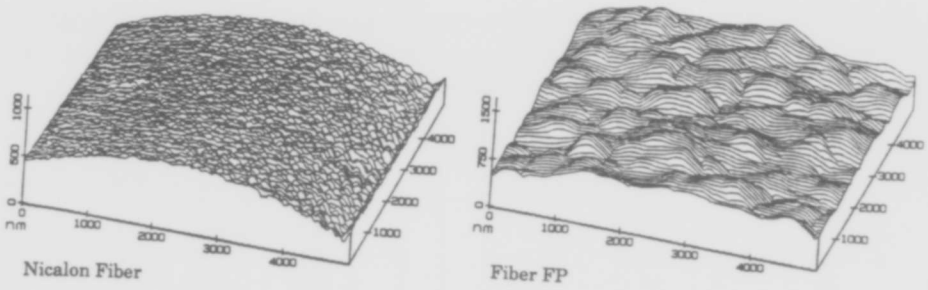

Figure 3. Surface topography of Spun fibers. AFM images.

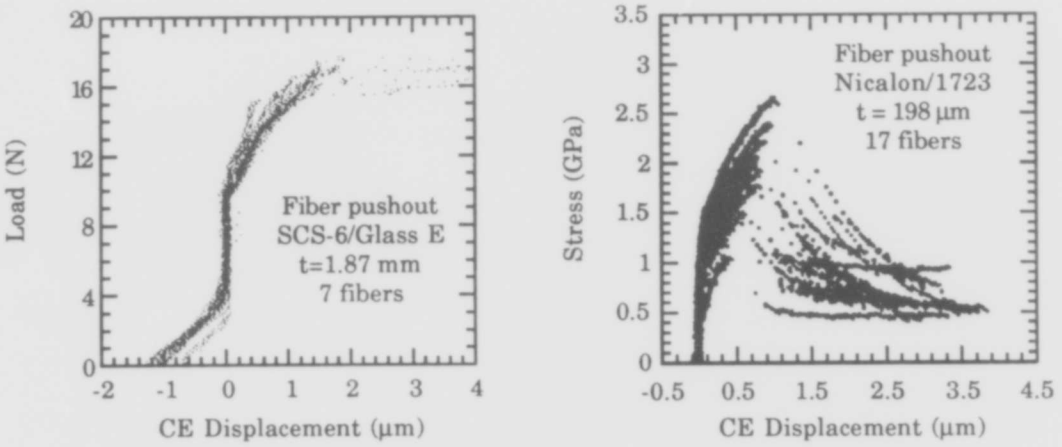

Figure 4. Pushout load-displacement curves for composites 1 and 2.

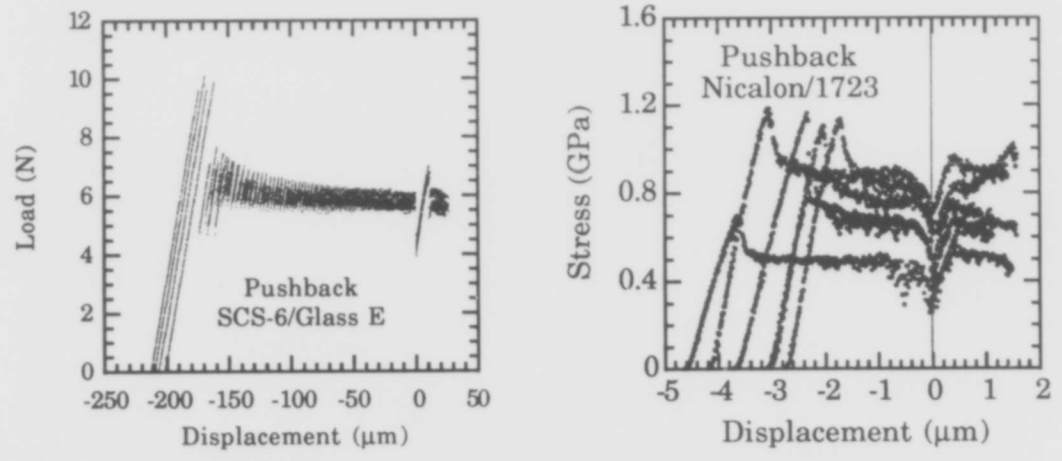

Figure 5. Pushback load-displacement curves for composites 1 and 2.

Table IV. Interface properties calculated for composite 1 with roughness contribution included, (left) based on "absolute" seating drop and (right) based on "effective" seating drop.

Fiber	A (nm)	μ	σ_N (MPa)	G (J/m^2)
1	16	0.166	57.5	0.0
2	27	0.098	61.2	0.0
3	21	0.140	53.1	0.0
4	24	0.136	52.0	0.1
5	26	0.117	54.0	0.0
6	25	0.125	53.4	0.0
7	22	0.122	51.6	0.0
ave	23	0.129	54.7	0.0

Fiber	A (nm)	μ	σ_N (MPa)	G (J/m^2)
1	115	0.154	58.3	0.0
2	305	0.061	64.5	0.0
3	220	0.089	58.2	0.0
4	260	0.079	57.4	0.0
5	295	0.068	58.2	0.0
6	260	0.079	57.2	0.0
7	255	0.074	55.7	0.0
ave	244	0.086	58.5	0.0

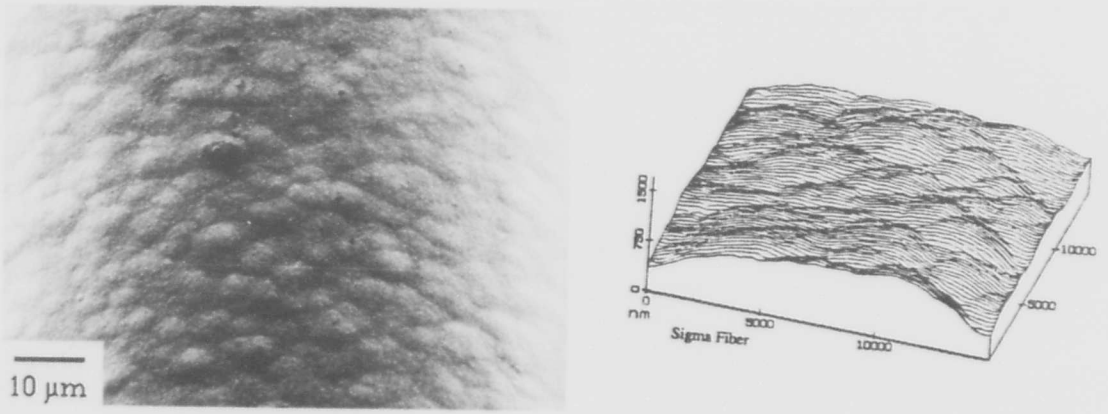

Figure 1. Surface topography of CVD SiC fibers. Micrograph of SCS-6 (left) and AFM image of Sigma fiber (right).

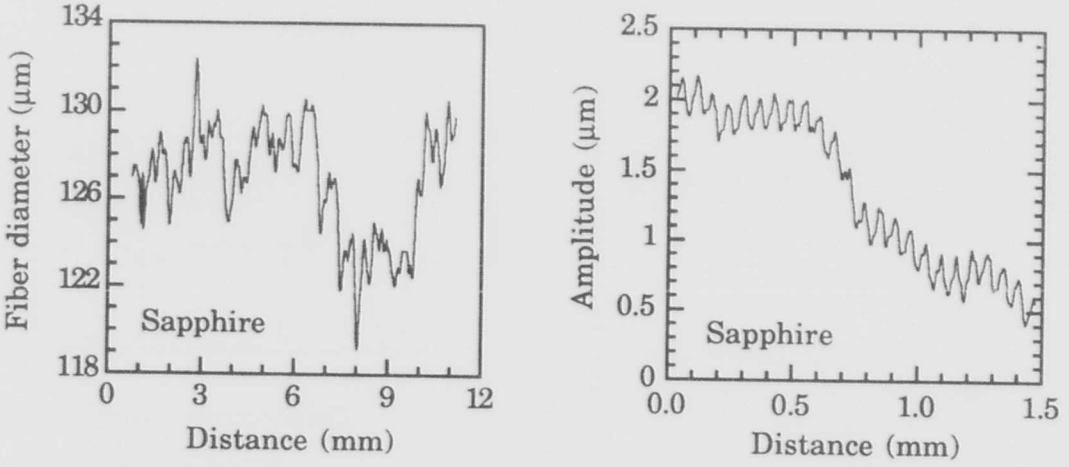

Figure 2. Surface topography of melt grown fibers. Examples of long range variations (left) and shorter wavelength undulations.

MICROMECHANICAL FAILURE MODES IN BRITTLE MATRIX COMPOSITES

by

Nicholas J. Pagano
WL/MLB
Wright-Patterson AFB
OH 45433-6533
United States

I. SUMMARY

Ceramic-and glass ceramic matrix composites are being touted for application in high-temperature structural components. Before their potential can be realized, however, understanding of the significance of the fracture modes that occur at very low stress levels well beneath those commonly assumed to initiate microcracking in the literature, will be essential. Unfortunately, at this point in the technology development, the precise definition of these mechanisms, i.e., the geography of the fracture plane(s), has been described rather incompletely in experimental research. In most cases, the experimental observations only provide views of these cracks at their intersection with a surface of the composite. Thus, in this presentation, we will provide some predictions of failure scenarios based upon a hypothetical idealized initial flaw in the matrix-an annular crack in a plane normal to the fibers of an unidirectional composite. Although many of the properties needed for the modeling study have not been realistically determined, especially the in-situ strength/ fracture properties, and the fracture criteria itself incorporates an undetermined parameter, i.e., initial flaw size, it is hoped that the modeling can serve to determine the nature of the parameters that require measurement and to help establish the sensitivity of the response to these parameters, as well as to guide experimental efforts to attempt validation of the failure processes hypothesized. The complexity of these processes seems to demand an iterative approach between the analyst and experimentalist.

According to the new model, interface damage in the form of matrix cracking and/or debonding may be developed as a function of the stress concentration produced by the annular crack. This secondary damage may then set up a synergistic increase in the applied energy release rate. For the cases considered here, this enhanced energy release rate entered the population of matrix $\mathcal{G}_c$ only for the non-uniform situation, where locally increased fiber spacing is encountered. Of course, this is partially due to the larger potential cracking area in the matrix. On the other hand, the small annular cracks permitted in the model in regions of large fiber volume fraction, were shown to be almost universally immobile. This suggests that uniform, high fiber volume fraction materials will be endowed with crack growth resistance. The fact that much higher values of $\mathcal{G}$ are available in matrix-rich regions may be responsible for the observation[3] that matrix cracking occurs in such regions, however, the small size and detection difficulty of potential matrix cracks in fiber-dense regions must also be considered.

The present model includes in its scope the perennial problem of the competition between the respective stresses causing crack deflection and fiber penetration at the fiber-matrix interface. The conclusion on this issue is that, for the composite class considered here, and ignoring dynamic and statistical effects, the state of stress on the interface at the point of maximum stress is such that matrix damage (due to σ_z^m) or debonding (due to σ_r) would precede fiber failure, even for the highest interface strengths that one can expect in these materials. Even when the annular crack impinges on the interface itself, the ratio σ_r/σ_z^f is so large that debonding would be expected. Therefore, practical efforts to degrade interfacial strength for the purpose of promoting crack deflection may be fruitless or even negative in many cases.

II. INTRODUCTION

We will make predictions employing a recently developed variational model[1] of an

Presented at an AGARD Workshop entitled 'Introduction of Ceramics into Aerospace Structural Composites', April, 1993.

axisymmetric concentric cylinder which may contain damaged regions in the form of annular or penny-shaped cracks in the constituents and/or debonds between them. The work attempts to examine in closer detail than analyses currently available[2, 3] the mechanics of failure in BMC once a flaw has been formed within the matrix. It should be noted that we start with the viewpoint discussed by Kim and Pagano[4] that initial failure in BMC occurs within a single cell or at random in various cells and is assumed to be a planar transverse matrix crack which is stopped (or deflected) as soon as it encounters the nearest fiber-matrix interfaces and does not extend any further. This is in contrast to the global steady state cracking mode in which a single matrix crack traverses and bridges all the fibers as studied in the famous ACK model[5] and refined by Budiansky, Hutchinson, and Evans[6]. In this regard, it represents the cylindrical geometry counterpart to the model of Wang et al[3] and the micromechanical version of the models that examine short cracks in homogeneous, orthotropic media, such as those by Marshall, Cox, and Evans[7] and McCartney[8]. Unfortunately, such models that represent the fibers and matrix as "layers" provide inaccurate geometric details as, for example, the ratio of fiber spacing to fiber diameter is very much higher than that in a composite having the same volume fraction of fibers arranged in a hexagonal pattern (See Fig. 1). There is substantially less distortion of these details in the concentric cylinder model utilized in the present work, although the idealization of an initial annular crack in this case carries its own question of credibility. We have called this failure mechanism the *full-cell cracking mode*[9], which may or may not include interfacial debonding (See Fig. 2).

An important feature of this work lies in the fact that very large (non-singular) stresses can be developed on the fiber-matrix interface in or near its intersection with the plane of an annular matrix crack and that these stresses may cause damage in the matrix (possibly the fiber as well) at the interface prior to propagation of the annular crack. Various failure scenarios may then develop depending on the magnitude and mix of the interlaminar stresses, the matrix energy release rate, and the respective ultimate properties of the interface and constituents. One of these scenarios which will be further explored examines the possibility of crack deflection at the interface, which of course represents a key controlling feature of a useful BMC. Included in this work is the presentation of a model which approximates the response in a region where the volume fraction differs from the average value. The behavior under consideration here is governed by numerous factors such as the thermoelastic and strength/fracture properties of the constituents, geometric details such as fiber diameter, spacing and volume fraction, initial annular crack dimensions and location, interface characteristics (which may not all be identified at this time), loading parameters, residual processing stress state, and, perhaps, interphase properties. Because of the multitude of parameters, we shall perform this investigation in the mode of a case study rather than attempting a systematic study of all the parameters and focus on bulk material properties typical of present composite systems under study in which the fibers are Nicalon and the matrix a glass-ceramic. Furthermore, we shall take advantage of the relative technical simplicity of a composite having a radial compressive stress at the fiber-matrix interface after processing. (The full-cell cracking mode may be generated by flaws other than the annular one assumed here, however, it seems quite reasonable to assume that such a flaw approximates one which must develop sometime prior to the formation of a full-cell transverse crack).

Somewhat representative (isotropic) values of elastic properties for the constituent materials will be assumed. The thermoelastic moduli and geometry are taken as

$$E_f = 200 \text{ GPa} \qquad E_m = 100 \text{ GPa}$$

$$\nu_f = 0.2 \qquad \nu_m = 0.4$$

$$\alpha_f = 2.7 \times 10^{-6}/°C \qquad \alpha_m = 3.2 \times 10^{-6}/°C$$

$$\Delta T = -1000°C, \ \frac{d^2}{a^2} = \frac{5}{3}, \ \frac{\ell}{a} = 20$$

The given ratio of d/a corresponds to a fiber volume fraction of 60% in the concentric cylinder. These dimensions will be subsequently modified by applying a factor of 8×10^{-6}, a realistic value of fiber radius (in m).

Although we have utilized a specific set of material properties the work should be considered, in addition, as an example of the use of advanced mechanical models in predicting microcracking events and some comments will be made regarding trends as governed by changes in these properties.

III. VARIATIONAL MODEL

The axisymmetric damage model was developed [1] in order to approximate the elastic stress field and strain energy release rates of bodies in the form of concentric cylinders as shown in Fig. 3. The model is generated by subdividing the body into regions consisting of a core and a number of shells of constant length and satisfying the Reissner variational equation with an assumed stress field within each region.

In order to study the conditions leading to the development of the *full-cell cracking mode* of Fig. 2, we shall consider an idealized model in which the fibers are arranged in a hexagonal array as shown in Fig. 4(a). The (z) dimension normal to the figure is constant and the body is subjected to a uniform (composite) uniaxial stress field on its ends and a constant temperature change. The *full-cell cracking mode* may be generated by a single annular crack surrounding the central fiber of Fig. 4(a) and lying in a plane normal to the fiber direction and extending the same radial distance in both directions. We focus on the region surrounding the central fiber bounded by a cylinder extending to the central surface of the crack r = d. This leads us to consider the axisymmetric element shown in Fig. 4(b), where continuity conditions are to be prescribed at r = d. We now assume that the representative volume element of the uncracked composite can be represented by a concentric cylinder model having fiber and matrix radii a, d, respectively, and we consider the boundary conditions to be imposed on the cracked concentric cylinder. In particular, we consider the surface r = d. At points well removed from the crack region (the results from the analysis will determine the affected zone) the boundary conditions are those corresponding to a uniform macroscopic stress state. For the concentric cylinder approximation in the present case, these conditions are the vanishing of shear and radial tractions. At points on the surface close to the crack, the boundary conditions are not so simple, however, we choose to impose a constant radial displacement and zero shear stress at (d,z) since these lead to zero slope of the crack surface, $\partial w/\partial r$ at (d,0). Thus we avoid the cusp which would result from the application of zero radial stress. As usual in fracture mechanics problems, we solve by superimposing solutions for a cracked and uncracked body. The former in this case is for a pressurized crack with constrained surfaces at r = d and z = ℓ such that the normal displacements and the shear stress all vanish. The actual (entire) body has the length 2ℓ.

A comment about failure analysis is in order here. In the event that the stress components at a given location are finite, we assume that failure will be governed by the maximum values of the stresses at the point as a first approximation. Subsequent research to develop refined failure criteria will depend on the iterative correlations of modeling and experimental studies. Here we refer to the stresses that would be calculated by elasticity since singular values do not arise in the present formulation. For crack-tip stress fields, we shall employ a critical energy release rate criterion, where an approximate value of $\mathcal{G}$ is computed from the model. Of course, this assumes that stresses can exceed the "strength" value in a crack-tip region. Hence the two-pronged approach may not be entirely consistent. However, we must remark that both approaches have been employed under the stated conditions to successfully predict failure. Finally, for points at which the stress singularity is of the form x^{-l}, where l is a constant and x the distance from the singular point, we shall only speak of ratios of stresses, e.g., $\frac{\sigma_r}{\sigma_z}$, which, having the same λ, are constant in the singular zone. Hence we use the

approximate values of stresses at the (elasticity) singular point calculated from the variational model to determine the relative propensity for a failure mode of a given type to occur[10]. It would seem that these different methods of estimating failure conditions can be unified by use of an average stress or point stress criterion [11, 12] for each. However this would require a major speculation, in which we do not care to indulge at this time, regarding an additional dimension. Where necessary, plausible values of material strengths and matrix critical energy release rate are assumed to attempt discrimination between competing failure mechanisms, plausible values of material strengths and matrix critical energy release rate are assumed. In subsequent work, we will assess the meaning of computed stresses in terms of their impact on failure and failure modes.

IV. GENERAL APPROACH

Our procedure consists of first examining a region of relatively high (.60) volume fraction, which seems to be near the upper limit for practical composites. We then introduce an annular matrix crack which could result from the processing conditions. The nature of the predicted stress field and energy release rate then guides the concoction of several additional fracture mechanics problems in a fairly exhaustive analysis. All of these respective failure modes are possible, given the right conditions, where the "right conditions" are certain combination of a geometric scaling factor, constituent and interface strengths and critical energy release rates. For example, under various conditions in which we allow arbitrary selection of material and geometric parameters, any of the failure modes displayed in Fig. 5 can take place. We then focus on the conditions implied by the use of reasonable bulk values of the latter properties to determine the likelihood of the associated failure modes. From this point, we investigate the influence of fiber spacing, which is expected to be very significant[3] by developing a new model in which a lower value of volume fraction is assigned to the unit cell It should be noted that, in all this work, the boundary value problems have been posed as "what if" exercises, i.e., we do not presume to know the length of the initial annular crack so it is treated as a parameter. Furthermore, the subsequent problems formulated are of the same nature in that they are assumed from observation of the stress field, not derived from a'priori knowledge or theory of crack growth behavior.

V. MODEL RESULTS

Selected results for interface stresses and energy release rates for various crack lengths are presented in Table 1. The values given represent the maximum magnitude of each stress component at the interface. Two loading conditions are considered: i) the effect of a constant temperature change of -1000°C and (2) the same temperature change in conjunction with an additional applied displacement e_0, where $\varepsilon_0 = .001$. The value of strain corresponds to a composite stress of approximately 160 MPa. The latter value of strain is in the vicinity of that required to initiate matrix transverse cracking in a wide class of glass-ceramic composites[4]. The reported stresses can be linearly interpolated or extrapolated to any value of ε_0 while $\mathcal{G}$ is a quadratic function of the axial matrix stress in the uncracked body and linear in a.

In the as-processed composite ($\varepsilon_0 = 0$) it is clear from Table 1 that the critical stress components are σ_z and σ_q in the matrix phase at the interface, however, once load is applied, either with or without the transverse crack, σ_z becomes dominant. We should point out that failures caused by σ_q would tend to take the form of radial cracks, which cannot be treated with the present model (this work is in progress).

We now employ the previous results to postulate a logical sequence of failure events, starting with the as-processed composite, which, as we have just seen, develops large values of σ_z in the matrix. Subsequent axial loading increases this tension, even at low values of ε_0. We should also observe here that the uncracked σ_z stresses (corresponding to b/a = 1.291) reported in the table act not only at the interface, but throughout the entire region. But

σ_r, the interfacial normal stress, is initially compressive. Therefore the appearance of transverse tensile matrix cracks would be expected based on bulk matrix tensile strengths of the order 100 MPa. If many of these cracks occur, we assume they are sufficiently far apart so that they do not interact. Thus we are led to presume the presence of a transverse annual matrix crack, after which the entire stress field will be redistributed. Since the crack length of the initial flaw is not known, we shall treat it as a parameter to be varied arbitrarily. This leads to the remaining results displayed in Table 1. The stresses reported in the table are the maximum values at the interface. While the theoretical stresses at the crack tip are unbounded, their effect is represented by the energy release rate $\mathcal{G}$. In assessing these results, it is important to keep in mind that they presume no failures other than the postulated annular crack occur and also that ε_0 is essentially an arbitrary quantity which can be much greater or much less than the value .001. But, as we shall see presently, the matrix and interface would usually need to possess extremely high strengths to support imposed values of ε_0 much larger than .001.

Some important predictions follow from the data reported in Table 1. Firstly, although a significant stress concentration in fiber axial stress is present, this component would not develop appreciable values compared to the fiber strength, which is in the neighborhood of 2 GPa[13], except at values of ε_0 much larger than those corresponding to observed initial cracking in glass-ceramic systems. As we have already seen, the matrix axial stress σ_z is always quite large and increases with crack length, however, as the crack length increases (or b decreases) the ratio of interfacial radial tensile stress σ_r to the matrix σ_z increases drastically. Thus at large crack lengths, debonding would tend to precede transverse matrix cracking at the interface. Furthermore such debonding would take place at strains ε_0 less than .001 for typical glass-ceramic composites where estimates of the interfacial tensile strength† range from 10 MPa[14] to 40 MPa[15], depending on the nature of the fiber surface treatment among other material and processing variables. Of course, the interfacial strength would also depend on the shear stress τ_{rz}, however, we have little or no data by which we can incorporate this effect. Therefore, the effect of τ_{rz} is not included in our failure hypothesis. The preceeding failure analysis also depends upon the assumption of an immobile initial crack, which, by comparing the calculated values of $\mathcal{G}$ with the range of critical bulk values 8 - 45 N m^{-1} (Reference 3), does suggest immobility. Thus, unless the initial transverse crack extends all the way to the interface, which is possible since the so-called "effective flaw" size in the matrix is at least several fiber diameters in length, the initial failure scenario consists of transverse matrix cracking followed by either interfacial matrix cracking or interface debonding, depending on the initial crack length. Subsequent crack linking may follow. In the event that the initial matrix crack extends all the way to the interface, the scenario will differ and will be discussed later.

While the ability to experimentally discriminate between two different failure scenarios within a realistic composite is at best a complex task, the added insight fostered by the present fundamental treatment may be important.

VI. CRACK DEFLECTION

We now inquire into the situation b = a, where the crack tip just touches the interface. For this problem, the model gives results of 1072 MPa for σ_r and 2536 MPa for σ_z^f, where the values represent an approximation of a singular stress field. As mentioned earlier, the present model does not produce singular stresses, but very high values which increase with the number of shells used to subdivide the body. One can justify the use of point-or average-stress failure criteria[11] or possibly rely on the ratios of the stress components, but not the stresses

† These are based on experiment-theory correlations using large diameter silicon carbide fibers in a glass-ceramic matrix.

themselves to predict failure. In the present example, the relatively high ratios of radial and shear stress to fiber axial stress at the interface suggest the subsequent failure mode of debonding rather than fiber penetration (recall that the fiber tensile strength is several orders of magnitude higher than the interface tensile strength for the data cited earlier). Therefore, in the extreme case in which the matrix crack impinges on the interface, as well as for all other relatively long cracks under the present conditions, crack deflection (debonding) is expected in lieu of fiber failure. Furthermore careful consideration of the stresses displayed in Table 1 suggests that the magnitude of interfacial strength, as far as its effect on the phenomenon of crack deflection, would not be an issue in the present class of composites according to the model and hypotheses given here. Table 1 also suggests that an important mechanism to consider is that of a matrix crack impinging on a debonded interface. Although Wang et al[3] consider an analogous physical problem in a layer model (fibers and matrix represented by lamina or layers), we observe here the case where the debonding is caused by the matrix crack.

At this point in the study in which nominal values of material properties and perfect interfacial bonding have been assumed, we see that the energy release rate is insufficient to propagate an initial transverse matrix crack at applied load levels corresponding to values known to create the *full-cell cracking mode* (Fig. 2) in typical glass-ceramic composites. We have, however, shown that the initial flaw causes sufficiently large stresses, in particular σ_z^m and σ_r, to produce subsidiary failures at the interface. Which of these stress components incites such a failure depends upon their ultimate values which in turn may vary considerably within the present class of materials. We have also demonstrated the improbability of fiber fracture under the stated conditions. Guided by these results, we now consider a series of problems designed to determine if the subsidiary failures can provide a mechanism to produce the *full-cell cracking mode*. We will present these as demonstration problems, rather than attempting an exhaustive parametric study.

VII. POTENTIAL SECONDARY FRACTURE MECHANISMS

We now assume that a small transverse matrix crack develops at the interface. We arbitrarily select the r/a values of the crack-tips to be 1.05 and 1.15. If $\mathcal{G}$ is suffrciently increased, the larger crack may grow and linking of the two can occur. However, the effect on $\mathcal{G}$ of the larger crack is very small. We next investigate the energy release rate of the short (inner) crack. Again, this value is quite small, suggesting crack-tip immobility. Although we have only considered a limited range of crack-tip locations, the smallness of $\mathcal{G}$ suggest that linkage does not occur.

We should clarify one aspect of this problem, i.e., it was shown that two cracks having an initial separation would not merge. Our inability to quantize the lengths of incipient flaws, however, does imply the existence of a possible linkage mechanism, where either crack is so long that the mere appearance of the second flaw causes it to touch or intersect the original one. This mechanism is not included in the present analysis.

In the next case we examine the other plausible subsidiary failure mode-debonding of the fiber-matrix interface caused by the stress concentration in radial stress in or near the plane of the annular crack. Again, the pressurized crack problem is solved. For simplicity, we shall only treat the limiting case of a long debond region of length 2ℓ. Furthermore, we let the boundary conditions on the interface be represented by

$$\tau_{rz}(a, z) = 0$$
$$u_r(a,z),\ \sigma_r(a,z) \text{ continuous}$$

or, "smooth interface" conditions, which only approximate the physical situation since $\sigma_r(a,z)$ is not compressive everywhere.

The curve of Fig. 6 indicates a larger value of $\mathcal{G}$ than for the case of a perfectly bonded interface. We see that $\mathcal{G}$ is enhanced by a factor that increases with crack length. As the crack tip approaches very close to the interface, however, the energy release rate is still

somewhat below the minimum value required to propagate the crack for the assumed range of 8 - 45 N/m cited earlier at $\varepsilon_0 = .001$ and DT = -1000°C. The accuracy of the present model is insufficient to pinpoint $\mathcal{G}$ in this range. Again, we provide an indication of the effect of the subregion details as shown by the slight discontinuity near b = a. Thus the *full-cell cracking mode* may lie in the realm of "probable" or "possible" for the matrices having the lower $\mathcal{G}_C$ values and the effect of the material property and modeling assumptions may be crucial for precise prediction of the event.

VIII. MATRIX ANNULAR CRACK EMANATING FROM THE INTERFACE

At this point we shall consider one more parameter in our case study of the *full-cell cracking mode* in the present class of composites. This parameter is the location where the annular crack originates. So far we have assumed that it would emanate from the midpoint between the fibers. We shall now pose the problem in which the annular crack initiates and grows outward from the fiber matrix interface. In order to justify use of the concentric cylinder model we might assume that two cracks initiate at r = a and 2d - a and grow towards each other. The pressurized crack problem is treated under perfectly bonded interface conditions. We have let the crack-tip location be defined by $r = b_1$, so that in this case, b_1 increases with crack length. However, the energy release rate is comparable to that of the previous situation. Hence, annular cracks of crack-tip radius $b_1 < d$ originating at the interface are not likely to propagate.

The case study examined a single composite (although we have not assumed a unique set of strength or fracture properties) under a given loading condition to assess the consequence of a single annular transverse crack in the matrix. Based on the present model, the only plausible explanations for the appearance of the *full-cell cracking mode* (Fig. 2) are

1) Due to stress concentration at the interface caused by the annular crack, debonding occurs which in turn increases the energy release rate causing it to propagate to the interface. This would only occur, at best, for the lower range of $\mathcal{G}_C$ that has been cited.

2) When the initial annular crack is formed, it simply consumes the entire plane between fibers. Subsequent debonding takes place, almost independent of interface strength, due to the very high radial tension at the interface.

Another mechanism, involving a transverse crack caused by stress concentration at the interface intersecting the original annular crack, is postulated but is beyond the scope of the present modeling exercise. It should be recalled that we have not assumed a length for the initial annular crack; the length was examined parametrically, i.e., varied arbitrarily. This concludes our case study of the particular composite of interest. The bottom line is: Growth of an annular crack to produce the *full-cell cracking mode* in a composite having the elastic properties and strength range assumed here with a volume fraction of .60 is very unlikely. This suggests that a unidirectional composite with well-controlled phase geometry and high volume fraction should be very resistant to initial crack growth of the matrix.

We now proceed to examine the plausibility of annular crack propagation in a region of the composite which has a lower volume fraction, hence, a larger fiber spacing. According to Wang et al[3], the matrix cracks initiate in such a region.

IX. VARIABLE VOLUME FRACTION/FIBER SPACING

So far in this work, we have assumed that the composite phase geometry is perfectly uniform with a fiber volume fraction of .60 throughout the medium. While debonding in the presence of an annular crack is very likely in that case, the growth of the annular crack to generate the *full-cell cracking mode* is improbable. Now suppose that we consider a region of material within the composite where the volume fraction is significantly lower, or equivalently, the fiber spacing is greatly increased, while the average fiber volume fraction is preserved. For example, suppose that we consider a local region in which the fiber volume fraction is

.20. We model this medium as shown in Fig. 7, where we imagine that the central fiber and its surrounding six neighbors of Fig. 4 are embedded within a homogeneous material characterized by the thermoelastic moduli of the host composite ($V_f = .60$). The radii of the inner rings are defined by the area ratio of .20, with the first composite ring being endowed with the effective properties corresponding to that value. The outer radius of the composite region is taken as 200a to simulate infinity since the uncracked stresses are evaluated by means of a computer code[16] written for a finite body. The stresses in the uncracked problems to be superimposed on those of the crack problem are computed through the model of Fig. 7 and will be discussed shortly. The model for the pressurized crack problem is unaffected by this new geometry, aside from the fact that its radii are governed by the smaller volume fraction. The curve showing the energy release rate for the pressurized crack problem is given in Fig. 8. Clearly, by comparison with Fig. 6, we observe an order of magnitude jump in the energy release rate for the longer cracks in this region for the case of unit pressure on the crack surface. Lowering the fiber volume fraction of the central region (say, to .10 or .05) would have the effect of increasing $\mathcal{G}$ even further. The significance of these results can be grasped more firmly by computing the actual energy release rate and stresses under a loading condition known to produce full-cell cracking, i.e., $\varepsilon_0 = .001$ and $\Delta T = -1000°C$. These results are displayed in Table 2. Again, we must caution that these results are based upon the presence of an annular crack of assumed length and no other damage. The Table 2 results, in conjunction with ranges of strengths and critical energy release rates assumed earlier, suggest longer cracks (small b) may propagate for matrix critical energy release rates in the lower end of the range. However, for long cracks, the interface radial stress and matrix axial stress become incredibly large. As before, the interface debonding mode is dominant in this range. Also as before, axial matrix cracking at the interface would be dominant for short cracks. Finally, as before, the analysis shows that we expect no fiber failure except, of course, from statistical weak spots which are not incorporated in the present model.

X. SECONDARY DEBONDING IN MATRIX-RICH REGIONS

Our final example deals with the effect of debonding on the energy release rate of the annular crack in the matrix-rich region (large fiber spacing) of the composite shown in Fig. 7. As we have just seen, a fairly long annular crack will generate very large radial tension at the interface which tends to cause debonding. In turn we wish to examine the effect of debonding on the energy release rate of the annular crack that produced the debond. Thus, as before, we assume sliding interface boundary conditions imposed in the pressurized annular crack problem, leading to the curve depicted in Fig. 8. The trend is similar to that seen earlier in Fig. 6, i.e., the effect of the debonding is to increase the energy release rate of annular cracks, the magnitude of the effect growing with increasing length of the annular crack. In this region, the interactive effect produces energy release rates within the median and high range of values of $\mathcal{G}_c$ for glass-ceramic matrix materials. Thus, a true synergistic effect takes place where the original annular crack causes interfacial debonding, which in turn magnifies the energy release rate of the annular crack.

XI. FINAL REMARKS

We have examined by means of a recently developed variational model, the phenomenon we call the *full-cell cracking mode*, in which an annular matrix crack surrounds a given fiber and eventually propagates to the fiber-matrix interface, while we suppose that the symmetric reflection of this crack grows to the interfaces of the neighboring fibers. Only one combination of constituent thermoelastic moduli were considered - this being representative of composites made from Nicalon fibers and certain glass-ceramic matrices. An important restriction is the assumption that $\alpha_m > \alpha_f$, thus inducing a process stress state consisting of axial tension and radial compression in the uncracked matrix according to the concentric cylinder model. However, in the presence of an annular matrix

crack, the radial interface stress reverses to tension, setting up the possibility of debonding under small tensile loads applied to the composite. Furthermore, the expansion coefficients only affect the uncracked solution in terms of the difference $\alpha_m - \alpha_f$, provided the elastic constants and volume fractions are unchanged. Hence, the given results can be easily converted for different thermal expansion mismatches. If this mismatch is such that the uncracked interfacial radial stress is tensile, however, the axial stress in the matrix will be compressive and the crack problem reverts to a non-linear contact problem, possibly in the presence of debonding caused by the process stresses.

As noted in the text, given the right conditions, i.e., particular combinations of geometric scaling parameter (a), ultimate strengths, and critical energy release rates, numerous failure scenarios can take place once an annular crack is introduced in the matrix phase. The maximum stresses are the same in geometrically similar bodies with the same phase thermoelastic moduli and the scaling factor for $\mathcal{G}$ is ap^2, where p is the axial matrix stress in the uncracked body. We have used conventional failure criteria in conjunction with bulk properties to interrogate the possible scenarios for the Nicalon and glass-ceramic matrix class of composites. According to the new model, interface damage in the form of matrix cracking or debonding may be developed as a function of the stress concentration produced by the annular crack. This secondary damage may then set up a synergistic increase in the applied energy release rate. For the cases considered here, this enhanced energy release rate entered the population of $\mathcal{G}_c$ only for the non-uniform situation, where increased fiber spacing is encountered. Of course, this is partially due to the larger potential cracking area in the matrix. On the other hand, the small annular cracks permitted in the model in regions of large fiber volume fraction, were shown to be almost universally immobile. This suggests that uniform, high fiber volume fraction materials will be endowed with crack growth resistance. The fact that much higher values of $\mathcal{G}$ are available in matrix-rich regions may be responsible for the observation[3] that matrix cracking occurs in such regions, however, the small size and detection difficulty of potential matrix cracks in fiber-dense regions must also be considered.

In this first-order study, we have not included the presence of an interphase region, however, such a region can be recognized within the existing model. The difficulty here is the lack of information on in-situ interphase thermoelastic properties and/or bonding conditions.

The present model includes in its scope the perennial problem of the competition between the respective stresses causing crack deflection and fiber penetration at the fiber-matrix interface. The conclusion on this issue is that, for the composite class considered here, and ignoring dynamic and statistical effects, the state of stress on the interface at the point of maximum stress is such that matrix damage (due to σ_z^m) or debonding (due to σ_r) would preceed fiber failure, even for the highest interface strengths that one can expect in these materials. Even when the annular crack impinges on the interface itself, the ratio σ_r/σ_z^f is so large that debonding would be expected. Therefore, practical efforts to degrade interfacial strength for the purpose of promoting crack deflection may be fruitless or even negative. We might point out, however, that the ratio σ_r/σ_z^f would decrease as the fiber/matrix modulus ratio decreases.

Perhaps it is useful to re-emphasize here that the failure mode treated here is that of matrix microcracking, in contrast to the mode of 'steady-state cracking'[6] in which all fibers bridge the damaged matrix. The latter mode has been extensively treated in the literature[5-8] but detailed experiments[4] have shown steady-state cracking is not the appropriate initiation mode, at least in a broad class of Nicalon/glass-ceramic matrix composites. Furthermore, local matrix microcracking (which we have labelled as the full-cell cracking mode) initiates at low stress levels. For example, the photomicrographs of Fig. 2 show evidence of matrix microcracking at composite stress levels as low as 70 MPa. The present model attempts to characterize this behavior in a fracture

mechanics setting. Aside from details of the local and average phase geometry, the input variables are the usual ones needed to conduct such an analysis, i.e., phase thermoelastic moduli and matrix fracture toughness. If subsidiary failure modes take place, however, interfacial strength/toughness parameters, such as interface tensile strength, will also be required. Of course, the proper way to characterize interfacial strength remains an open question. Clearly the model, especially the version which permits variable fiber spacing, is also amenable to failure prediction via a stress-based criterion.

What is needed now is a systematic experimental effort in which the experimentalist carefully determines the conditions at the initiation of full-cell cracking, i.e., composite stress or displace-ment and the very important details of the failure region, such as the fiber spacing of all neighboring fibers to define the true shape and size of the failure surface. In this way, we can begin to establish the veracity of the model in its representation of the geographic details, and hopefully to begin the interchange leading to the determination of that elusive parameter - the initial crack length (or inherent flaw size), if appropriate. Such work is now in progress. It's impact on the assumptions and predictions made via the present model will be reported soon.

ACKNOWLEDGEMENT

The author would like to express his sincere appreciation to Ms. Charleen Baldwin and Mrs. Barbara Hager for their very careful and skillful preparation of the text and artwork for this manuscript.

REFERENCES

1. Pagano, N.J., "Axisymmetric Micromechanical Stress Fields in Composites". Proceedings of 1991 IUTAM Symposium on Local Mechanics Concepts for Composite Materials Systems, Virginia Polytechnic Institute and State University, Blacksburg, VA, Oct. 29, 1991.

2. He, H. and Hutchinson, J.W., "Crack Deflection at an Interface Between Dissimilar Elastic Materials", Int. J. Solids Structures, 25, 9 (1989), pp. 1053-1067.

3. Barsoum M., Kangutkar, P., and Wang, A.S.D., "Matrix Crack Initiation in Ceramic Matrix Compcsites Part I: Experiment and Test Results"; Wang, A.S.D., Huang, X.G., and Barsoum, M., "Matrix Crack Initiation in Ceramic Matrix Composites Part II: Models and Simulation Results", Comp. Sci and Technology, 43, 3 (1992), pp. 257-282.

4. Kim, R.Y. and Pagano, N.J., "Crack Initiation in Unidirectional Brittle Matrix Composites", J. Am. Ceram. Soc.,74, 5 (1991), pp. 1082-1090.

5. Aveston, J., Cooper, G., and Kelly, A., "Single and Multiple Fracture", in The Properties of Fiber Composites, Conference Proceedings, National Physical Laboratory, Guildford, UK. IPC Science and Technology Press, Ltd. (1971), pp. 15-26.

6. Budiansky, B., Hutchinson, J.W., and Evans, A.G., "Matrix Fracture in Fiber-Reinforced Ceramics", J. Mech. Phys. Solids, 34 (1986), pp. 167-189.

7. Marshall, D.B., Cox, B.N., and Evans, A.G., "The Mechanics of Matrix Cracking in Brittle-Matrix Fiber Composites", Acta Metall, 33 (1985), pp. 2013-2021.

8. McCartney, L.N., "Mechanics of Matrix Cracking in Brittle-Matrix Fiber-Reinforced Composites", Proc. Roy. Soc. London, A-409 (1987), pp. 329-350.

9. Pagano, N. J. and Brown, H. W., "The Full-Cell Cracking Mode in Unidirectional Brittle Matrix Composites," Composites, 24, 2 (1993), pp 69-82.

10. Cornie, J.A., Argon, A.S. and Gupta, V., MRS Bulletin, 16 (1991), pp 32-36.

11. Whitney, J.M. and Nuismer, R., "Stress Fracture Criteria for Laminated Composites Containing Stress Concentrations", J. Comp. Mat., 8 (1974), pp 253-265.

12. Folias, E.S., "Failure at a Fiber-Matrix Interface in a Composite Subjected to an Applied Load", J. Comp. Mat., 25, 7 (1991), pp 869-886.

13. Prewo, K.M., "Fiber Reinforced Ceramics - New Opportunities for Composite Materials", Proc. 4th Japan-U.S. Conference on Composite Materials (1988), pp 24-40.

14. Chatterjee, A., Mah, T., and Kerans, R.J., "Residual Stresses and Their Effects on Transverse Properties and Interfacial Debonding in SiC Fiber Reinforced Glasses", presented at First International Ceramic Science & Technology Congress, Anaheim, CA, Oct 31-Nov 3, 1989.

15. Lilley, R., personal communication.

16. Pagano, N.J., and Tandon, G.P., "Elastic Response of Multi-directional Coated - Fiber Composites", Comp. Sci. and Technology, 31 (1988), pp 273-293.

TABLE 1

	$\varepsilon_o = 0$							$\varepsilon_o = .001$					
b/a	σ_z^f	σ_θ^f	σ_z^m	σ_θ^m	σ_r	τ_{rz}	$\mathcal{G}$	σ_z^f	σ_θ^f	σ_z^m	σ_θ^m	σ_r	τ_{rz}
1.05	25.84	7.46	109.34	106.57	30.96	14.20	146	344.95	48.06	323.42	211.34	117.57	42.01
1.10	-5.72	-4.36	79.69	81.88	5.87	7.78	.124	251.58	13.09	235.70	138.32	43.34	22.98
1.14	-18.76	-8.86	67.74	73.43	-2.60	4.56	101	213.01	-0.20	200.38	113.32	18.29	13.48
1.20	-29.93	-12.65	59.00	66.30	-10.75	1.86	064	179.99	-11.43	174.52	92.23	-5.80	5.50
1.291*	-35.96	-15.66	53.94	62.60	-15.66	-0-	-0-	162.14	-20.33	159.55	81.27	-20.33	-0-

*Uncracked

Energy Release Rates and Maximum Interface Stresses for imposed ε_o plus $\Delta T = -1000^\circ C$, $V_f = 0.60$

TABLE 2

	$\varepsilon_o = 0$							$\varepsilon_o = .001$						
b/a	σ_z^f	σ_θ^f	σ_z^m	σ_θ^m	σ_r	τ_{rz}	$\mathcal{G}$	σ_z^f	σ_θ^f	σ_z^m	σ_θ^m	σ_r	τ_{rz}	$\mathcal{G}$
1.08	222.8	109.8	292.5	259.2	192.8	47.4	1.63	878.5	318.0	814.9	617.0	549.5	131.8	12.6
1.12	166.8	93.9	235.3	213.4	142.9	37.1	1.55	723.2	259.4	655.3	489.5	410.0	103.5	12.0
1.48	101.8	44.0	86.5	62.4	56.2	16.8	0.85	294.5	137.3	240.9	175.4	171.5	46.7	6.58
2.236*	-33.0	-8.2	60.2	70.8	-8.2	-0-	-0-	166.0	-10.6	167.7	91.9	-10.6	-0-	-0-

*Uncracked

Energy Release Rates (N/m) and Maximum Interface Stresses (MPa) for imposed ε_o plus $\Delta T = -1000^\circ C$ in Non-uniform Composite

s/d

v_f	HEX.	CCM	LAYER
.01	8.52	9.00	99.00
.01	2.01	2.16	9.00
.01	1.13	1.24	4.00
.01	0.74	0.83	2.33
.01	0.51	0.58	1.50
.01	0.35	0.41	1.00
.01	0.23	0.29	0.67
.01	0.14	0.20	0.43

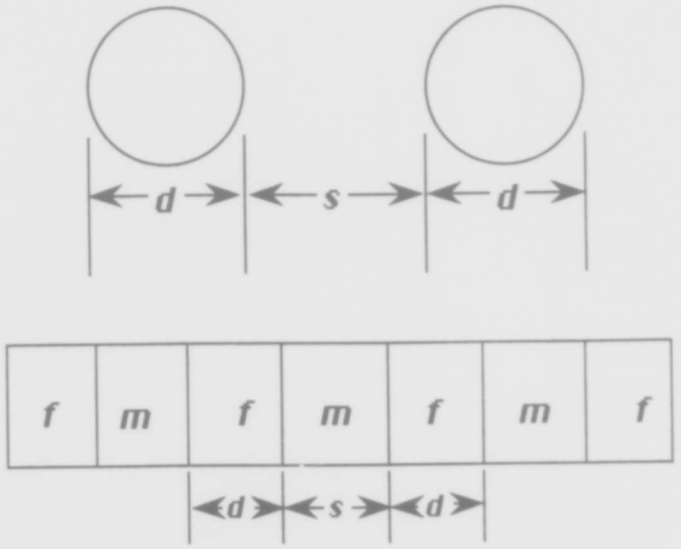

Fig. 1 Fiber Spacing/Diameter Ratios for 3 Models (Equiv. Ea)

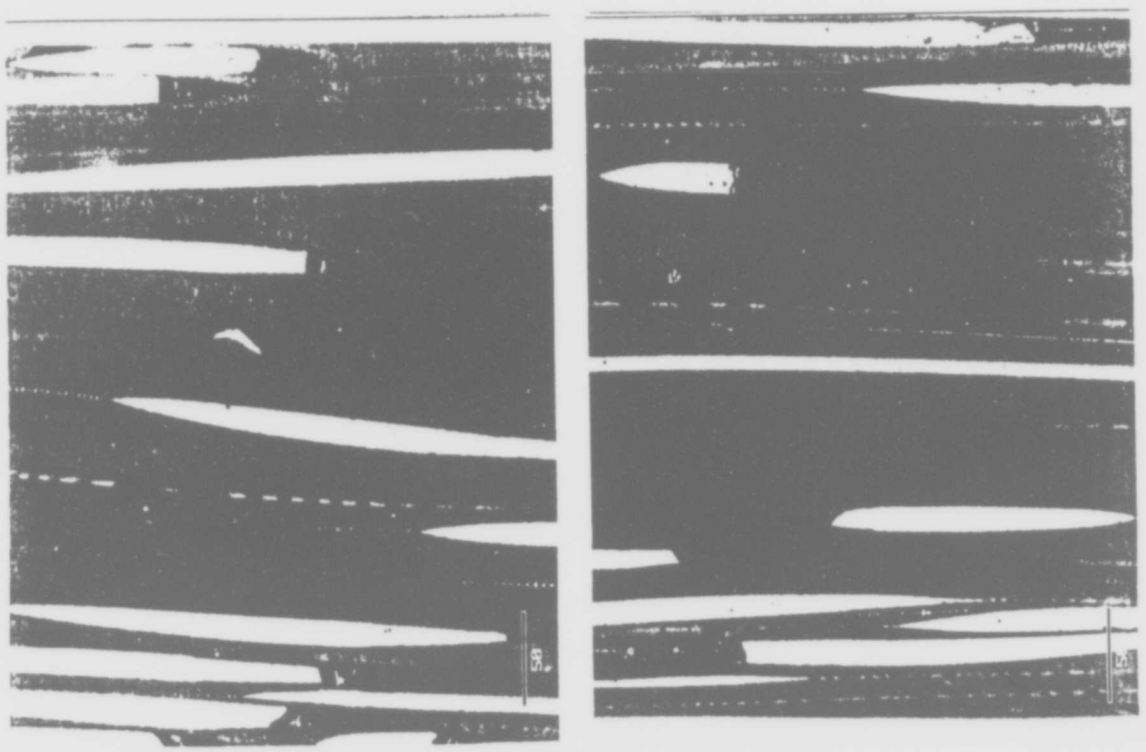

Fig. 2 Microcracking in a SiC - CAS Composite at 70MPa.

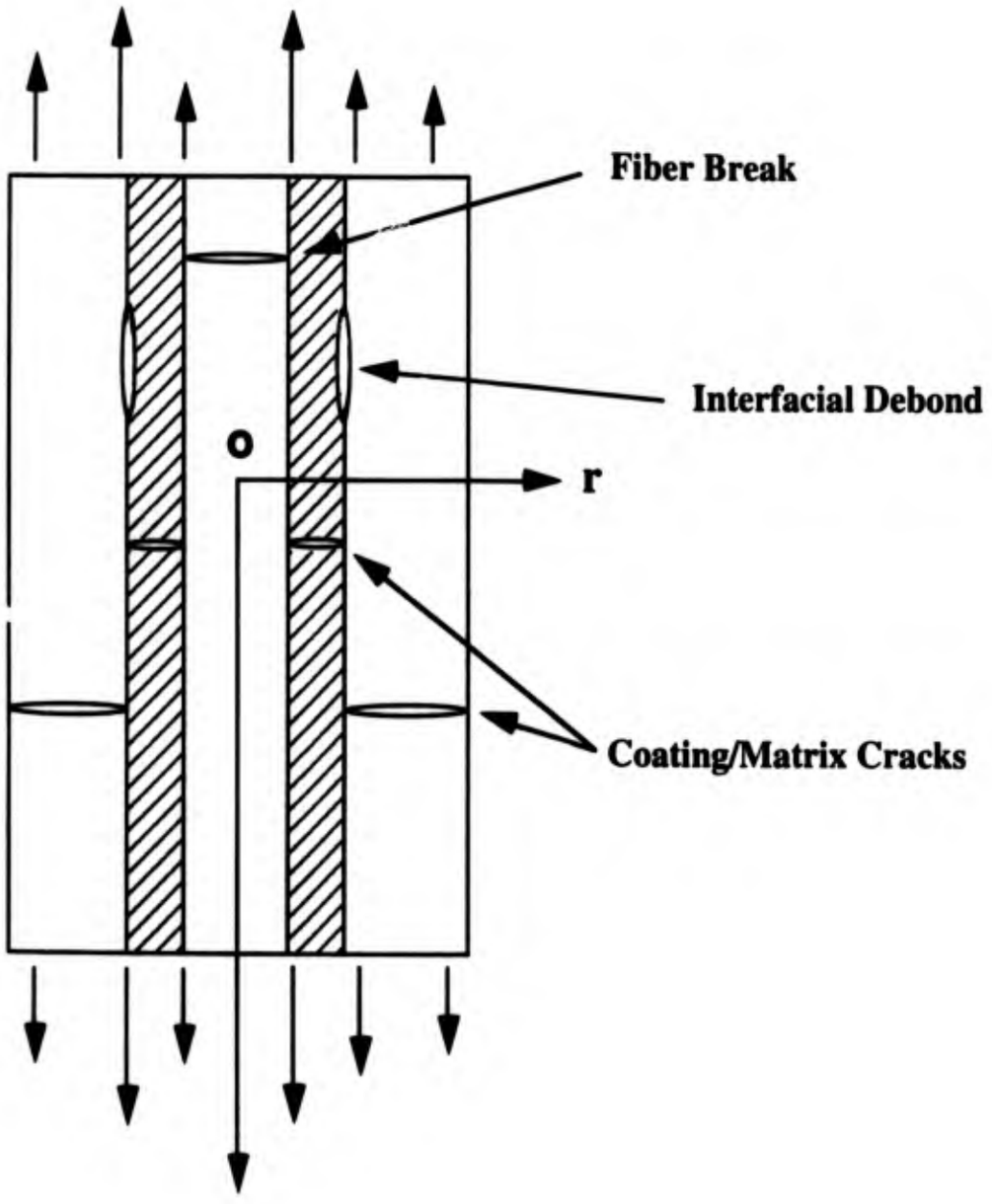

Figure 3. Axisymmetric Damage Model

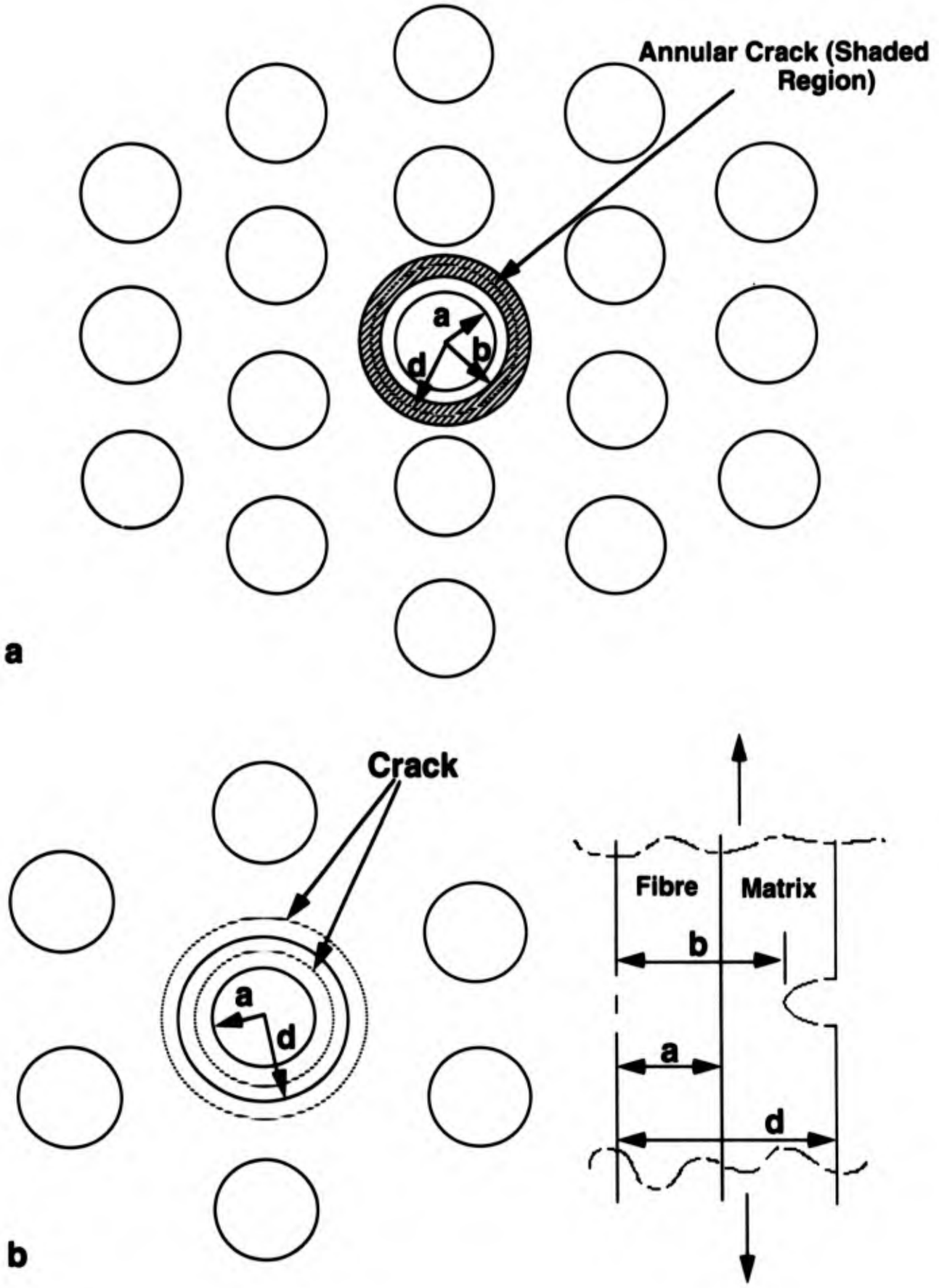

Fig. 4 (a) Postulated annular crack in a hexagonal array; (b) geometry of annular crack in a composite cylinder

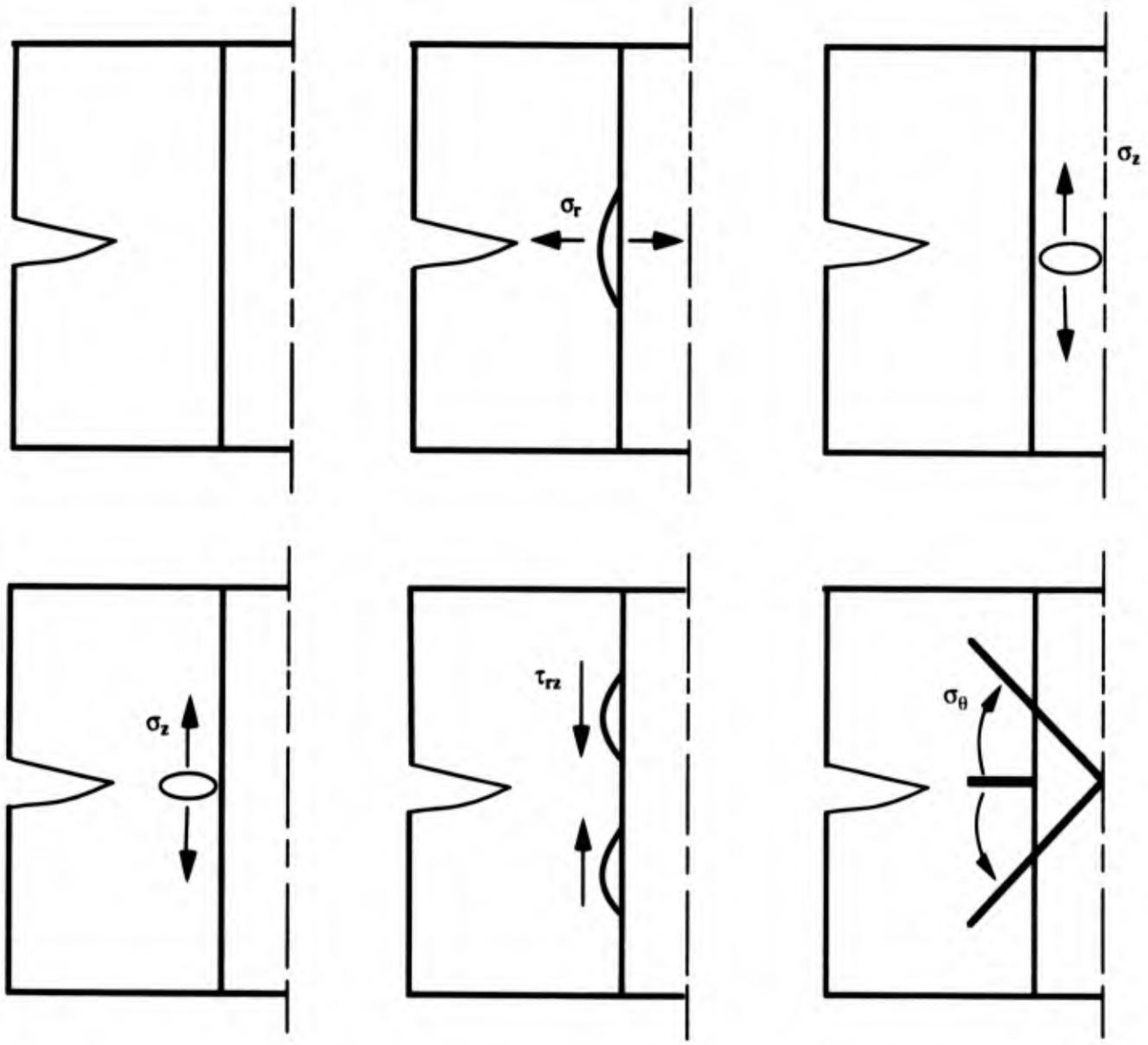

Fig. 5 Potential Subsidiary Cracking Prior to Propagation of Main Crack

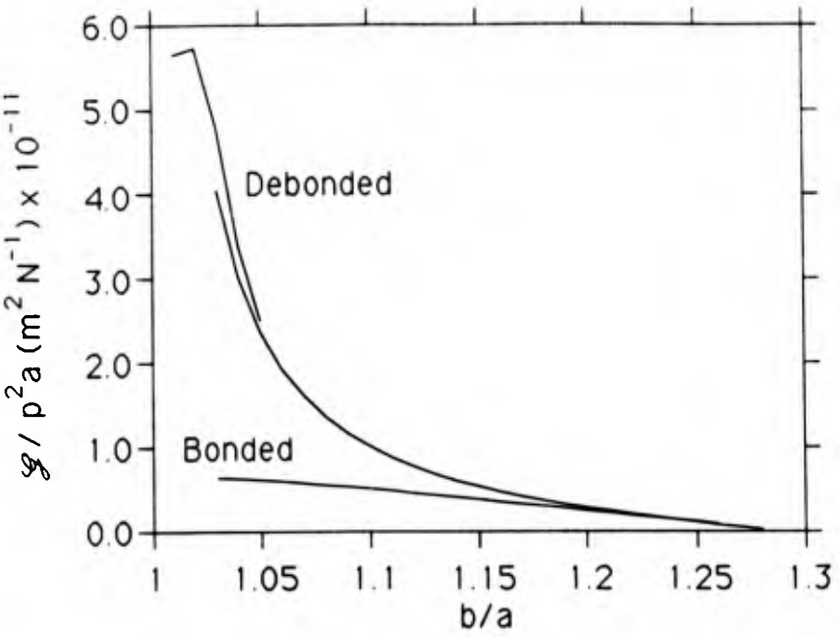

Fig. 6 Energy release rates for bonded and debonded interface, $V_f = 0.6$

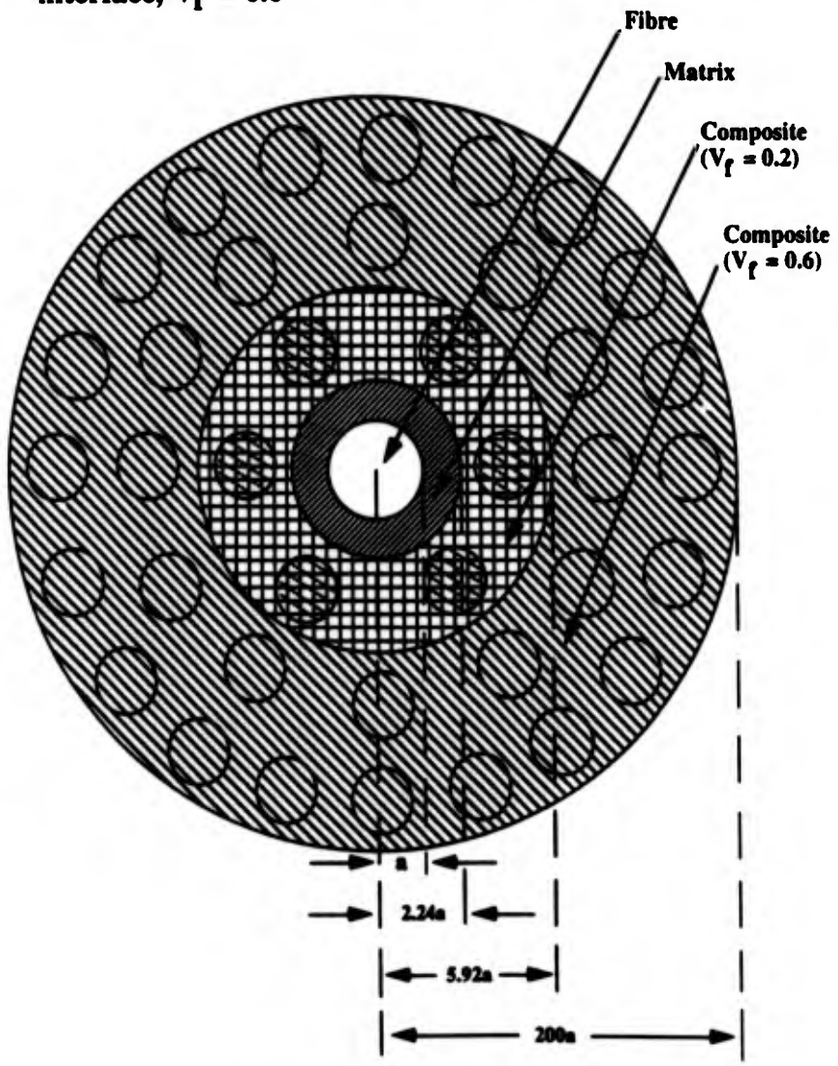

Fig. 7 Model for non-uniform composite

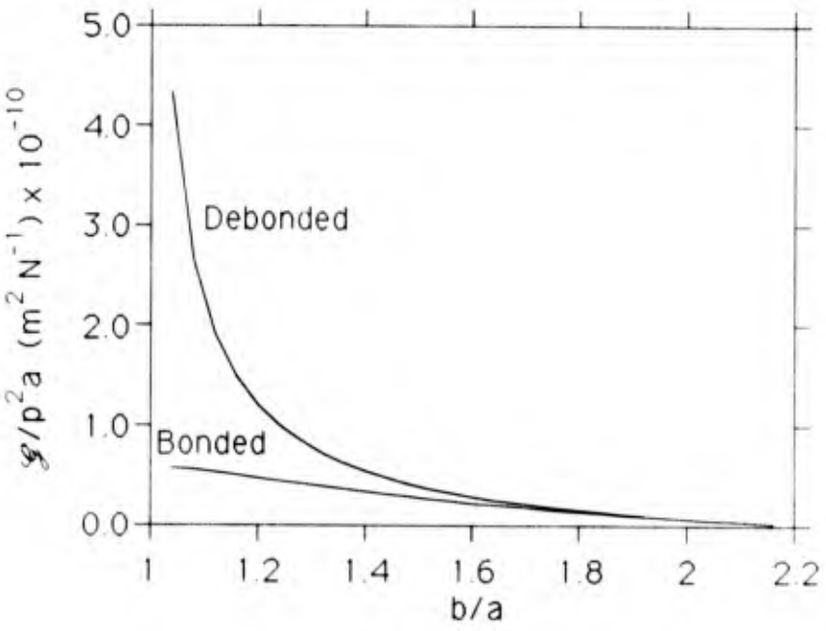

Fig. 8 Energy release rate bonded and debonded interface in non-uniform composite, V_f = 0.2

Caractérisation micromécanique des composites à matrice céramique à l'aide de la technique de microindentation instrumentée

M. Parlier
B. Passilly
O. Sudre

Office National d'Etudes et de Recherches Aérospatiales
Direction des Matériaux
BP 72
92322 Châtillon Cedex, FRANCE

1. SOMMAIRE

Les différentes possibilités d'investigation micromécanique associées à l'essai d'indentation Vickers instrumentée en force et déplacement sont décrites. Dans le cas des céramiques renforcées par des fibres longues, il est possible de déterminer la dureté et le module d'Young des constituants ainsi que les caractéristiques mécaniques de l'interface fibre-matrice, à savoir, l'énergie nécessaire à sa décohésion et la contrainte moyenne de rechargement par cisaillement sur la longueur de l'interface qui est désolidarisée.
Des exemples d'application sont donnés sur les composites à matrice oxyde (mullite, vitrocéramique) ou covalente (carbure de silicium) renforcée par des fibres SiC-Nicalon. L'effet des traitements de vieillissement sous air à haute température est abordé.

2. INTRODUCTION

Les céramiques renforcées par des fibres longues peuvent présenter une certaine tolérance aux dommages contrairement aux céramiques monolitiques. Pour cette catégorie de composites à matrice céramique (CMC), l'endommagement est caractérisé par une multifissuration progressive de la matrice sans rupture des fibres. Ainsi que l'ont montré Aveston, Cooper et Kelly [1], dans le cas d'un renfort unidirectionnel, tel que sa fraction volumique soit élevée, la matrice est progressivement débitée en blocs orthogonaux aux fibres. Toutefois, compte tenu de la singularité de contrainte qui existe au droit de la fissure matricielle et à l'interface fibre-matrice, il faut que la fibre et la matrice puissent se déplacer l'une par rapport à l'autre pour accommoder le champ de contrainte locale.

Pratiquement, cela implique que la liaison fibre-matrice ne soit pas trop forte pour autoriser localement la décohésion de l'interface. Le rechargement de la matrice de part et d'autre de la fissure matricielle résulte alors du transfert de charge des fibres vers la matrice dont on suppose qu'il s'effectue par cisaillement sur la longueur de l'interface qui est désolidarisée.

D'autre part, pour obtenir des contraintes limites élevées, il faut que la matrice soit suffisamment densifiée et que les fibres ne soient pas altérées lors de l'élaboration du composite.

Expérimentalement, la technique d'indentation Vickers instrumentée en force et déplacement permet à la fois :

- de déterminer les caractéristiques intrinsèques - dureté Vickers H_v, module d'Young E -de la région indentée et ainsi de vérifier l'incidence des paramètres d'élaboration sur la fibre et sur la matrice ;

- de caractériser mécaniquement l'interface fibre-matrice en déterminant l'énergie nécessaire à sa décohésion G_c ainsi que la contrainte de cisaillement τ caractérisant le rechargement fibre-matrice sur la longueur de l'interface qui est désolidarisée.

Dans un premier temps, nous allons développer pour chaque type de caractérisation, le principe de l'essai et la modélisation correspondante. Ensuite, nous donnons des exemples d'application au niveau des constituants et de l'interface fibre/matrice. Enfin, une estimation des contraintes d'origine thermique s'exerçant sur la fibre est proposée.

3. PRINCIPE DE L'ESSAI DE MICRO-INDENTATION

3.1 Indentation d'un milieu homogène.

L'essai de microindentation est usuellement utilisé pour déterminer très localement la dureté d'un matériau. Pratiquement, il s'agit de quantifier la déformation plastique rémanente provoquée par l'application ponctuelle d'une charge au moyen d'un indenteur pointu. L'indenteur le plus usité est une pyramide en diamant de type Vickers (base carrée ayant un angle entre faces de 136° et un angle entre arêtes de 158°). Lors du chargement, la profondeur de pénétration h_m se décompose en une composante

Presented at an AGARD Workshop entitled 'Introduction of Ceramics into Aerospace Structural Composites', April, 1993.

plastique h_p et une composante élastique h_e conformément à la représentation de la figure 1a. Après suppression de la charge, la dureté Vickers H_v s'exprime par le rapport entre la force maximale appliquée F_m et la surface de l'empreinte rémanente qui correspond à la déformation plastique déterminée par la mesure de la diagonale D de l'empreinte :

$$H_v = \frac{2 * \sin(68°) * F_m}{D^2} \qquad [1]$$

Pour les matériaux céramiques qui sont caractérisés par une très faible plasticité, la charge ne doit pas exéder quelques dixièmes de newton pour éviter la formation de fissures dans le prolongement des diagonales de l'empreinte. De ce fait, la dimension de l'empreinte est généralement inférieure à la dizaine de micromètres.

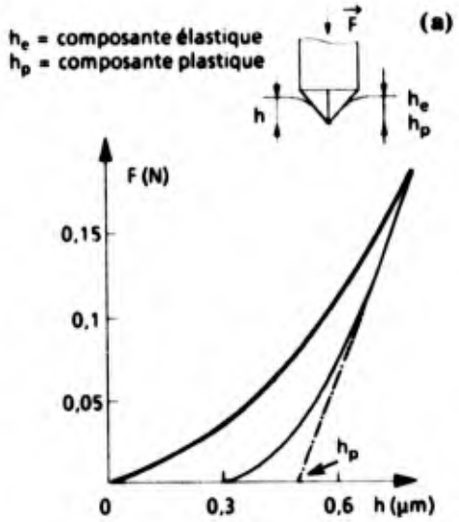

Figure 1 : Courbe d'indentation dans un milieu homogène (a); Comportement élastoplastique.

La figure 1b présente la courbe expérimentale de pénétration de l'indenteur en fonction de la force qui peut être décrite par une loi en puissance selon l'approche de Meyer [2] :

$$h_m = \alpha * F^{\beta} \qquad [2]$$

En exploitant la partie de cette courbe correspondant au déchargement, Loubet [3] a proposé de calculer le module d'Young E en supposant que la déformation plastique est constante durant cette phase de l'essai.

L'établissement des équations pour déterminer le module d'Young résulte d'une analyse antérieure proposée par Snedon [4] :

$$\frac{1-\nu^2}{E} + \frac{1-\nu_0^2}{E_0} = \frac{dF}{dh} * 4 * \sqrt{\pi} * (h_p * \tan\theta)^{-1} \qquad [3]$$

$$H_v = \frac{F_m \cos^2(68°)}{4 * h_p^2 * \sin(68°)} \qquad [4]$$

F_m étant la force maximale appliquée, dF/dh la pente de la courbe lors du déchargement, h_p la profondeur plastique, θ le demi angle entre les faces de la pyramide Vickers, E, ν, Eo, ν_0 étant respectivement le module d'Young et le coefficient de Poisson du matériau et du pénétrateur.

Cette approche a été validée sur les matériaux céramiques en utilisant des monocristaux de silicium (liaisons covalentes) et d'alumine α (liaisons iono-covalentes) pour lesquels la dureté et les propriétés élastiques sont bien établies. Les valeurs de dureté et du module d'Young sont reportées sur la figure 2.

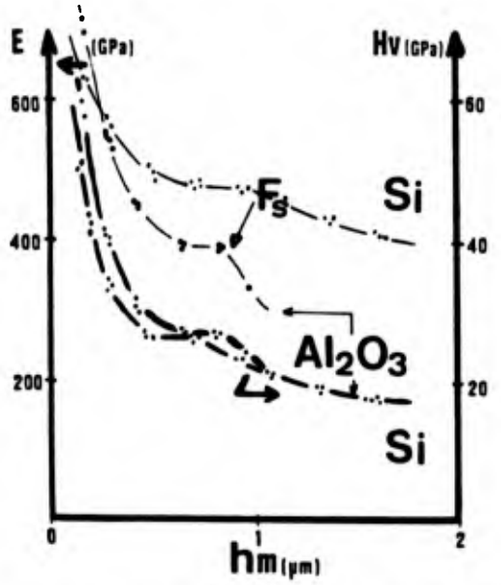

Figure 2 : Détermination de E et H_v par microindentation en fonction de h_m sur des monocristaux de Si et Al_2O_3-α

Pour les faibles valeurs de chargement, les mesures sont entachées d'erreurs expérimentales (émoussage de la pyramide Vickers, précision de l'instrumentation,...) [5]. Pour les charges trop élevées, il y a fissuration de la céramique, ce qui modifie la réponse élastoplastique du matériau et les résultats sont alors dépendants du taux d'endommagement. Dans le domaine intermédiaire et jusqu'au seuil de fissuration, les résultats sont indépendants de la charge et

les valeurs du module d'Young sont en bon accord avec celles déterminées à l'échelle macroscopique (tableau 1).

	Silicium	Alumine α
Orientation	100	110
E (GPa)	127*	350/400**
Hv (GPa)	11.5*	23***
E mesuré (GPa)	127 ± 7.5	391 ± 7
Hv mesuré (GPa)	13 ± 0.9	24.5 ± 0.8

Tableau 1 : Mesures de E et Hv par microindentation sur monocristaux et comparaison avec les valeurs admises : * (23), ** (24), *(25)**

3.2 Indentation d'une fibre.

Dans le cas des matériaux céramiques renforcés par des fibres longues, Marshall [6] a été le premier à utiliser un indenteur Vickers pour appliquer une charge sur une fibre de faible diamètre (environ 15 micromètres pour la fibre SiC-Nicalon) qui se présente perpendiculairement à la surface du matériau poli. Si la liaison fibre-matrice n'est pas trop forte, le niveau de contrainte appliqué est suffisament élevée pour provoquer le glissement de la fibre dans sa gaine de matrice. La figure 3 présente une courbe d'indentation réalisée sur un composite SiC-Nicalon/SiC brut d'élaboration. La première partie de la courbe correspond à la réponse élastoplastique de la fibre qui peut être décrite par une loi en puissance (Stade I). Le changement de pente correspond à la décohésion de l'interface fibre-matrice qui intervient pour une force F_d. La contrainte critique de décohésion s'exprime alors par la relation :

$$\sigma_d = \frac{F_d}{\pi * R^2} \qquad [5]$$

où R est le rayon de la fibre. En l'absence de contraintes thermiques résiduelles, une analyse énergétique simple [7] permet de relier cette contrainte de décohésion à l'énergie de décohésion G_c :

$$-\sigma_d = \sqrt{\frac{4 * E_f * G_c}{R}} \qquad [6]$$

où E_f est le module d'Young de la fibre. Le signe "-" rend compte d'une contrainte de compression due à l'indentation.

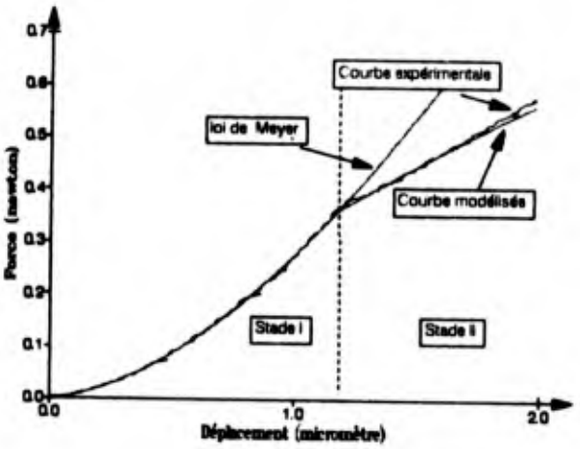

Figure 3 : Courbe d'indentation sur un composite SiC/SiC: Comparaison avec la courbe modélisée selon l'approche de Marshall.

Le stade II correspond au glissement relatif fibre-matrice. En supposant que ce dernier soit purement frottant sans frettage de l'interface, et en négligeant la déformation de la fibre sous l'effet de la charge, Marshall et Oliver [8] considèrent que le rechargement fibre-matrice s'effectue à contrainte de cisaillement τ constante. Une analyse uniaxiale permet alors de calculer la longueur de glissement fibre-matrice u en fonction de F, τ et G_c :

$$\forall F \geq F_d \quad u = \frac{F^2 - F_d^2}{4 * \pi^2 * R^3 * E_f * \tau} = \frac{F^2}{4 * \pi^2 * R^3 * E_f * \tau} - \frac{G_c}{\tau} \qquad [7]$$

Si on analyse un cycle de chargement-déchargement-rechargement, il est également possible de déterminer la contrainte thermique axiale σ_z^{res} supportée par la fibre. Dans le cas simple où l'interface fibre-matrice est initialement désolidarisée (cas du composite SiC/MLAS au § 7) et si $u_{res} / u_{max} < 1/2$ (fibre en compression axiale), on peut calculer σ_z^{res} à partir du formalisme proposé par Marshall et Oliver [9] :

$$\sigma_z^{res} = \frac{F_z^{res}}{\pi * R^2} = \frac{F_m}{\pi * R^2} * \frac{1}{2} * \left(1 - \sqrt{\frac{u_{res}}{\Delta u}}\right) \qquad [8]$$

F_z^{res} est la charge axiale résiduelle, $\Delta u = u_{max} - u_{res}$, u_{max} et u_{res} étant respectivement la longueur de glissement fibre-matrice maximale et résiduelle après suppression de la charge.

4. DISPOSITIF EXPERIMENTAL ET PROCEDURE DE DEPOUILLEMENT.

Le schéma de principe de l'appareillage d'indentation

Vickers instrumentée est représenté en figure 4. Il est construit sur la base d'un microscope optique. Ce dernier est équipé d'une tourelle porte objectif sur laquelle est positionnée la cellule d'indentation, de la même façon qu'un objectif. L'échantillon, monté en pince, est positionné sur un capteur de force. La motorisation de la mise au point du microscope permet d'atteindre des vitesses de chargement de 2 à 50 millinewtons/seconde. Le déplacement de l'indenteur par rapport à la surface de l'échantillon est mesuré à l'aide d'un capteur capacitif issu des travaux de A. Bruère [10]. En utilisant une bande passante de 10 Hertz, la résolution est de 10 nanomètres pour une distance capteur-surface de l'échantillon de 300 micromètres. Le capteur de force autorise la mesure d'efforts jusqu'à 1 newton avec une précision de 0.5 millinewtons inhérente à sa grande souplesse, mais qui rend l'ensemble particulièrement sensible aux vibrations. De ce fait, une isolation vibratoire du moyen d'essai s'est avérée nécessaire. Le système est piloté par un micro-ordinateur qui permet d'acquérir les courbes d'indentation.

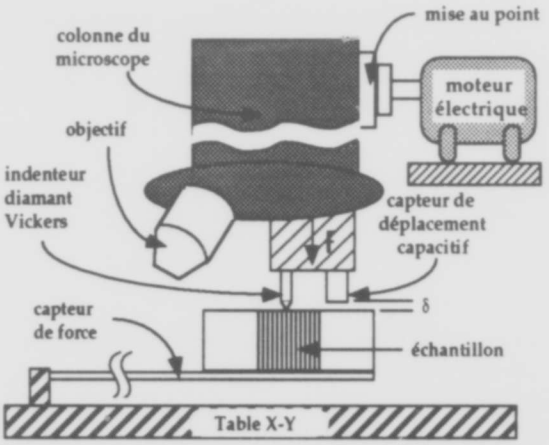

Figure 4 : Schéma de principe de l'appareil de microindentation

Le capteur de déplacement mesure la variation de la distance d vis à vis de la surface du matériau qui correspond à la déformation élastoplastique h_m à laquelle se superpose le glissement fibre-matrice u au-delà de F_d. L'exploitation de l'essai d'indentation se fait en quatre étapes : (i) estimation de la force seuil de décohésion F_d, donc de σ_d ; (ii) extrapolation de la déformation élastoplastique de l'ensemble fibre et indenteur au delà de F_d (stade II) ; (iii) détermination du glissement fibre-matrice u en retranchant la déformation élastoplastique h_m au déplacement d mesuré par le capteur ; (iv) détermination de l'énergie de décohésion G_c et de la contrainte de cisaillement τ à l'interface. En utilisant l'équation [7] relative à la modélisation de Marshall, on détermine la valeur de τ, seul paramètre ajustable, qui s'approche le plus de la courbe expérimentale (figure 4).

Les échantillons d'indentation se présentent sous forme de parallèlépipèdes tels que les grandes faces soient perpendiculaires aux directions principales de renforcement. L'une de ces surfaces est ensuite polie à la pâte diamant jusqu'à une granulométrie de 0.25 micromètres.

5. MESURE DE LA DURETE ET DU MODULE D'YOUNG DES CONSTITUANTS DANS UN CMC.

La détermination du module d'Young à l'aide de la technique d'indentation instrumentée suppose que l'on réalise plusieurs essais pour obtenir une mesure indépendante de la charge comme cela a été démontré au § 3.1. Pour faire des essais sur des fibres ou sur des régions de matrice peu étendues, il convient donc de procéder à des cycles de charge/décharge partiels en augmentant progressivement la charge jusqu'au seuil de fissuration.

La figure 5 illustre un essai pratiqué sur une fibre SiC-Nicalon NLM 202 dans une matrice Nasicon, le composite étant élaboré par pressage à chaud à 1050°C [5]. Le module d'Young ainsi mesuré étant identique à celui de la fibre brut, on en déduit que les conditions d'élaboration n'ont pas altéré les propriétés élastiques du renfort.

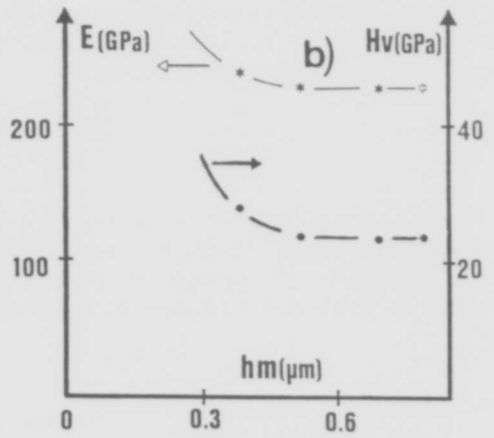

Figure 5 : Détermination de E et H_v par microindentation sur une fibre SiC-Nicalon dans une matrice NASICON.

Le tableau 2 résume quelques résultats locaux concernant des composites à renforts fibreux ou particulaires [5]. On constate que la présence de

précipités de zircone permet d'augmenter le module d'Young et la dureté. Dans un composite à matrice vitrocéramique LAS (Li_2O-Al_2O-$6SiO_2$), le suivi du module d'Young à l'échelle locale est un bon indicateur pour apprécier l'homogénéité de la cristallisation et son degré d'avancement en fonction des traitements thermiques.

Matériau - Lieu d'intentation		E (GPa)	Hv (GPa)
Composite SiC/Nasicon*	Fibre SiC	220 ± 10	-25
	Matrice avec ZrO_2	106 ± 5	7,2 ± 0,9
	Matrice sans ZrO_2	88 ± 5	5,7 ± 0,7
Composite SiC/LAS**	Matrice	66 ± 2	8 ± 0,4
Monolithe de Mullite***		180 ± 17	12,4 ± 0,8
Monolithe de Mullite + 10% ZrO_2		240 ± 15	15,7 ± 2

Tableau 2 : Mesures de E et Hv par microindentation sur composites et monolithes :
*** (élaboration par voie sol-gel à 1050°C),**
**** (élaboration par voie verrière à 1320°C),**
*****(frittage de poudre à 1600°C)**

6. CARACTERISATION DE L'INTERFACE FIBRE-MATRICE DANS LES CMC.

Les exemples concernent deux types de CMC à renfort fibreux de carbure de silicium (SiC-Nicalon NLM 202 de chez Nippon Carbon) : SiC-Nicalon/Mullite élaboré à l'ONERA par pressage à chaud de tissus préimprégnés par voie Sol-Gel [11]. Pour les renforts unidirectionnels (1D) et bidirectionnels (2D), le taux volumique de fibres est d'environ 40%.

Les composites SiC-Nicalon/SiC ont été caractérisés à l'état brut et après vieillissement de 100 heures sous vide et sous air, à une température de 1000°C [12]. Les courbes caractéristiques d'indentation sur les composites bruts d'élaboration et après vieillissement sont reportées sur la figure 6. La contrainte critique de décohésion σ_d, l'énergie de décohésion Γ au sens de l'approche de Marshall $G_c = 2\Gamma$ et la contrainte de cisaillement interfaciale τ sont répertoriées dans le tableau 3. Les valeurs moyennes et les écarts-types mentionnés sont donnés sur dix essais sélectionnés d'une part, pour que le taux surfacique de matrice et de fibres avoisinantes soit équivalent, et d'autre part, pour que le rayon des fibres soit compris entre 7 et 9 micromètres. Pour les composites à renforts 1D et 2D (tissus taffetas), la décohésion est marquée et se produit à des niveaux de contraintes sensiblement différents. L'exploitation du stade II de glissement montre une augmentation significative de la contrainte de cisaillement τ qui passe de 33 à 63 MPa respectivement pour les composites à renfort 1D et 2D. L'ondulation des fibres dans le composite à renfort 2D peut expliquer cette différence.

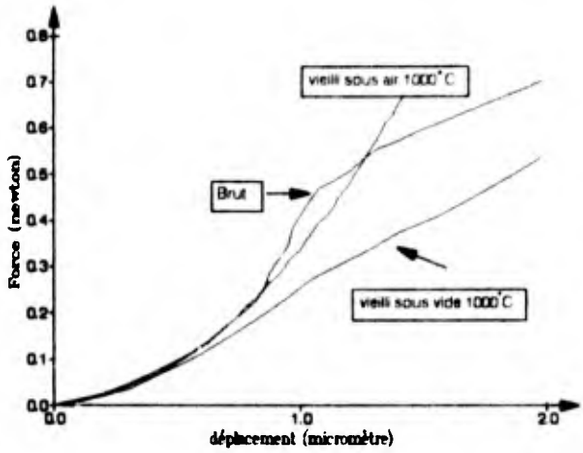

Figure 6 : Courbes d'indentation sur composites 2D SiC/ SiC brut et après vieillissement.

Composite	σ décohésion moyen MPa	Γ décohésion moyen J/m²	τ moyen MPa
1D brut	1100 ± 200	6 ± 2	33 ± 8
2D brut	1500 ± 230	12 ± 4	63 ± 15
2D sous vide 1000°C	1100 ± 100	6,5 ± 2,5	67 ± 11
2D sous air 1000°C	IND	IND	IND

Tableau 3 : Mesure de σ_d, Γ, τ par microindentation sur des composites SiC-Nicalon/SiC (IND : indéterminé)

Pour le matériau oxydé à 1000°C pendant 100 heures, aucune décohésion ne se produit. Seule la déformation élastoplastique de la fibre est enregistrée. L'observation de l'interface a été réalisée par microscopie électronique à balayage couplée à un spectromètre à dispersion d'énergie. Les analyses ont ainsi révélé la présence d'oxygène qui n'est pas observable à l'état non vieilli. Fillipuzzi [13] propose que l'interphase de carbone, initialement présente dans les composites SiC/SiC, s'oxyde avec formation d'oxydes de carbone (CO_2 et/ou CO) ce qui entraînent la création de pores à l'interface fibre-matrice. La diffusion de l'oxygène dans la porosité conduit alors à la formation de silice à la surface de la fibre. La présence de la couche de silice interfaciale a également été remarquée pour des composites SiC/SiC traités sous atmosphère oxydante à des températures plus élevées [1400°C) par Mozdzierz et Backhaus-Ricoult [14].
Après vieillissement sous vide à 1000°C pendant 100 heures, la décohésion se produit pour des charges plus faibles que sur le composite SiC/SiC brut.

De plus, dans le stade 1, on note une déformation élastoplastique différente, qui peut être attribuée à l'affaiblissement des caratéristiques mécaniques (E ou H_v) de la fibre.
Il est également possible d'évaluer la contrainte de cisaillement interfaciale τ en déterminant l'espace interfissures du réseau de fissures qui se développe perpendiculairement au renfort fibreux. Pour un composite 1D SiC-Nicalon/SiC caractérisé par une contrainte à rupture d'environ 450 MPa, la longueur moyenne L_m des blocs de matrice est de 34 micromètres (longueur minimale d'environ 20 micromètres). En appliquant le formalisme développé par Aveston, Cooper et Kelly [1] puis par Zok et Spearing [15], τ est respectivement estimé à 110 MPa et 125 MPa (en considérant une énergie de rupture de la matrice de 10 J/m²). Le désaccord avec la mesure de τ issue de l'essai d'indentation peut provenir du mode de sollicitation de l'interface qui n'est pas équivalent dans les deux essais. En particulier, dans l'essai d'indentation, le cisaillement axial de l'interface s'accentue contrairement à l'essai de traction du fait que la fibre est initialement soumise à une contrainte de compression d'origine thermique pouvant atteindre 300 MPa [16]. De plus, dans les deux approches, le modèle utilisé pour déterminer τ ne prend pas en compte la déformation de la fibre (effet Poisson) ainsi que la contrainte de frettage estimée à 200MPa.

En ce qui concerne les composites 2D (tissus 4 dir) SiC-Nicalon/Mullite, il est possible de modifier la composition de l'interphase fibre-matrice et de la matrice en ajustant le rapport molaire Al_2O_3/SiO_2 du gel et de la poudre successivement utilisé lors de l'étape de préimprégnation du tissu. Pour les deux compositions étudiées [17], les évolutions de dureté au niveau des constituants et de la contrainte de cisaillement interfaciale sont répertoriés dans le tableau 4, avant et après vieillissement de 3 heures à 900° C sous air. D'après les mesures de microdureté, les fibres ne sont pas altérées par les conditions d'élaboration ou de vieillissement et la matrice présente des caractéristiques équivalentes à celles des mullites frittées sans renfort fibreux. Il est à noter que la composition plus riche en alumine est moins densifiée et de ce fait, elle est moins rigide. L'augmentation de la contrainte de cisaillement à l'état brut a été corrélé à l'enrichissement du verre de mullite en alumine et à la formation de cristaux aciculaires de mullite en plus grand nombre et de plus grandes dimensions, certains d'entre eux étant en contact direct avec la fibre [18].

Composition des composites		Porosité ouverte en volume	E (GPa)		τ (GPa)
gel	matrice		20°C/apres recuit à 900°C		
Al/Si (atomique)	Al_2O_3-SiO_2 (molaire)		Fibre	Matrice	
1	6-4	10	20/17,5	12,5/12,5	20/ > 100
1,33	7-3	20	20/20	9/8,5	60/ > 100

Tableau 4 : Mesures E et τ par microindentation sur les composites 2D SiC-Nicalon/mullite : Influence de la composition du gel d'interphase et de la matrice

Après vieillissement, l'interface fibre-matrice se rigidifie probablement en raison de l'oxydation superficielle de la fibre SiC-Nicalon comme cela a déjà été constaté dans d'autres matrices de type oxyde ou SiC [19]. Corrélativement, la résistance en flexion chute progressivement et le mode de rupture devient de plus en plus fragile.
Pour optimiser les propriétés mécaniques des composites, il convient donc de trouver un compromis entre la composition chimique et la température de frittage afin d'obtenir une matrice la plus dense possible tout en limitant l'adhésion fibre-matrice.

7. EVALUATION DES CONTRAINTES THERMIQUES RESIDUELLES DANS LES CMC.

L'étude [20] a porté sur le composite 2D (taffetas) SiC-Nicalon/SiC caractérisé au § 6 et sur un composite 2D (satin) SiC-Nicalon/verre céramique MLAS (mélange MgO-Li_2O-Al_2O_3-SiO_2) élaboré à l'ONERA par pressage à chaud d'un tissu préimprégné de poudres synthétisées par voie Sol-Gel [21]. Dans les deux cas, le taux volumique de fibres est proche de 40%. Les valeurs caractéristiques de la contrainte de cisaillement interfaciale et de la contrainte thermique longitudinale sont répertoriées dans le tableau 5.

Composites	R (μm)	E_m (mn)	U_{mat} (nm)	U_{res} (nm)	τ (MPa)	σ_L^{res} (MPa)
SiC/MASL	7	80	362	140	5,3	-53
SiC/SiC	7,8	500	510	10	65	-670

Tableau 5 : Détermination de σ_L^{res} au niveau de la fibre dans un composite SiC/MASL et SiC/SiC

Pour le composite 2D SiC-Nicalon/MLAS, les courbes d'indentation présentées dans la figure 7 sont en bon accord avec le modèle évoqué au § 3-2 dans le cas d'un cycle de chargement-déchargement-rechargement. Les faibles valeurs relevées pour l'énergie de décohésion et la contrainte de cisaillement interfaciale ont été corrélées à la

présence de carbone à la surface de la fibre SiC-Nicalon [22]. Cependant, le fait que la fibre soit en compression est inattendu car les phases cristallines qui doivent se développer sont caractérisées par un coefficient de dilatation thermique plus faible que celui de la fibre : $1.10^{-6}°C^{-1}$ pour le spodumène-ß structure keatite et $2,6.10^{-6}°C^{-1}$ pour la cordiérite ß. Ce désaccord peut provenir de la présence d'une proportion importante de phase vitreuse résiduelle dont il faudrait préciser le comportement dilatométrique.

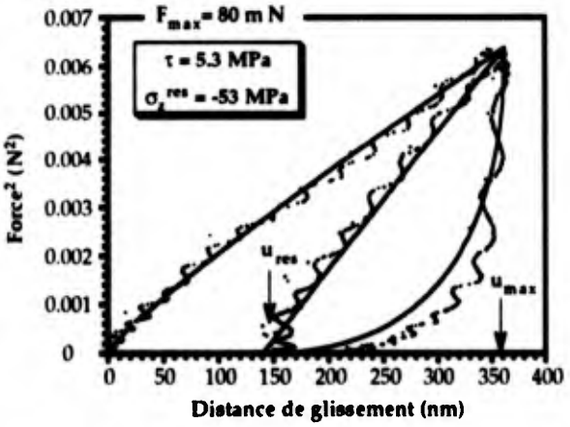

Figure 7 : Courbe de charge-décharge-recharge d'une fibre SiC dans une matrice MLAS.

En ce qui concerne les composites 2D SiC-Nicalon/SiC, l'exploitation de l'essai représenté dans la figure 8 est fait en supposant que : (i) la décohésion de l'interface se produit de façon stable au fur et à mesure du chargement, (ii) l'augmentation de la longueur de glissement lors du rechargement est liée à une diminution de la contrainte de cisaillement interfaciale (environ 15% dans ce cas). Dans ces conditions, la fibre est soumise à une contrainte thermique axiale de compression d'environ 600 MPa, soit pratiquement une contrainte deux fois plus élevée que celle issue de la modélisation en déformation plane à l'échelle d'une fibre enrobée de matrice [16].

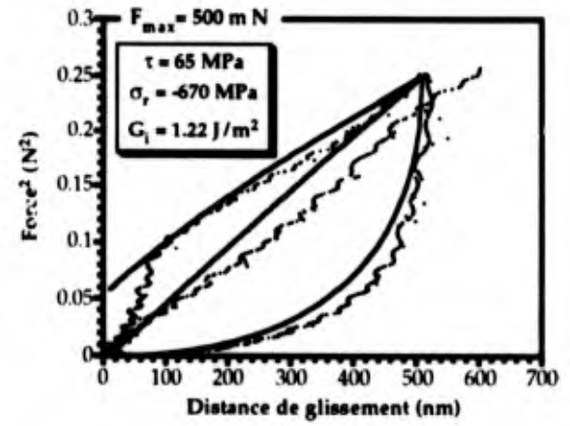

Figure 8 : Courbe de charge-décharge-recharge d'une fibre SiC dans une matrice SiC.

Ces essais préliminaires ont permis de mieux appréhender l'approche proposée par Marshall et Oliver [9] mais l'appareillage devra être amélioré pour éviter les phénomènes d'oscillation observés sur les courbes d'indentation. De ce point de vue, le pilotage du déplacement de l'indenteur par un dispositif piezoélectrique est envisagé.

8. CONCLUSIONS.

La technique d'indentation Vickers instrumentée apparait donc comme un moyen d'investigation micromécanique qui permet de caractériser localement la matrice et les fibres (dureté, module d'Young) ainsi que l'interface fibre-matrice (énergie de décohésion, contrainte de cisaillement interfaciale, contrainte d'origine thermique s'exerçant sur la fibre).

Il est ainsi possible d'agir ultérieurement d'une part, sur la formulation de la matrice ou de l'interphase fibre-matrice et d'autre part, sur les paramètres d'élaboration pour optimiser les caractéristiques mécaniques des composites. Il est également possible de caractériser la dégradation des composites après des traitements de vieillissement correspondants aux conditions de fonctionnement.

Pour mieux appréhender les évolutions se produisant à l'interface fibre-matrice pendant l'utilisation, un nouveau moyen d'indentation automatisé et fonctionnant à chaud (600°C) sous atmosphère contrôlée est en cours de développement.

Bibliographie

1. Aveston, J., Cooper, G.A., Kelly, A."Single and multiple fracture". Conference proceedings of National Physical Laboratory, Teddington, UK, 1971. Edité par IPC Science and Technology Press, 1971, p 15-26.
2. Meyer, M.A."Some aspects of hardness of metals, Thèse de doctorat, Delft, 1951.
3. Loubet, J.L. "Etude des courbes d'indentation. Cas du poinçon conique et de la pyramide Vickers", Thèse de l'Université Claude Bernard-Lyon I, n° 1332, 29 septembre 1983.
4. Snedon, I.N. "The relation between load penetration in the axisymetric Boussinsq problem", Int.J.Eng. Sci, n° 1, 1965, p 47-52.
5. Lagrange, J.L., Passilly, B., Parlier, M., Colomban P.- "détermination des propriétés mécaniques locales des constituants de composites céramique-céramique" Comptes-Rendus des 8e Journées Nationales sur les Composites, 1992, p 241-252, Palaiseau.
6. Marshall, D.B., " An indentation méthod for mesuring matrix fiber frictional stresses in ceramic composites", Journal of American Society, 1984, Vol 67, n° 12, C259-C260.

7. Outwater, J.D., Murphy, L.C.,"On the fracture energy of unidirectional laminate. 24th Annual Technical Conference of Composites, New-York, 1969, Paper 11C.
8. Marshall, D.B., Oliver, W.C., "Measurement of interfacial mechanical properties in fiber reinforced ceramic composites", J. Amer. Ceram. Soc., 1987, vol 70, p 542-548
9. Marshall, D.B., Oliver, W.C.- "An indentation method for mesuring residual stresses in fiber-reinforced ceramics". Mat. Sci. Eng, 1990, A 126, p 95-103.
10. Bruere, A.- "Métrologie sans contact par méthode capacitive", Journées AFCIQ métrologie 1989.Marshall, D.B., Evans, A.G.- "Failure mechanisms in steel reinforced epoxy resin composite". J. Amer. Ceram. Soc., 1985, 68, p225-2318.
11. Brevet FR 9101237 du 4 février 1991, "Matériau composite céramique fibre-matrice multicouche et procédé pour son élaboration".
12. Passilly, B., Sudre, O., Parlier, M., "Caractérisation mécanique des interfaces dans les composites céramique-céramique", A paraître dans la Revue des Composites et des matériaux avancés, 1993.
13. Fillipuzzi, L.- "Oxydation des composites SiC/SiC et de leurs constituants : approche expérimentale, modélisation et influence sur le comportement mécanique", Thèse de l'université de Bordeaux-I, n°593, 28 mars 1991.
14. Mozdzierz, N., Backhaus-Ricoult, M., "Evolution de la microstructure d'un composite SiC/C/SiC à haute température en fonction de l'atmosphère", Comptes-Rendus des 8e Journées Nationales sur les Composites, 1992, p225-239, Palaiseau.
15. Zok, F.W., Spearing, S.M., "Matrix crack spacing in brittle matrix composites", Acta Metall. Mater., 1992, 40, p 2033-2043.
16. Arnault, V.- "Relations entre microstructure et comportement mécanique des composites SiC/SiC : analyse du rôle de l'interface dans le processus de fissuration matricielle dans des matériaux multifilamentaires", Thèse de doctorat de l'INSA de Lyon, 21 décembre 1989.
17. Parlier, M., Grenier, T., Renevey, S., Passilly, B., Mouchon, E., Bruneton, E., Colomban, Ph., "Mullite and SiC Matrix SiC fibre composites for high température application", Proceedings of 4th International Symposium on Ceramic Matérials and Components for Engines, Göteborg (Sweden), june 10-12, 1991.
18. Bruneton, E., "Composites oxydes réfractaires-fibre SiC préparés par voie sol-gel", Thèse Paris VI, 1992.
19. Cutard, T., Fargeot, D., Gault, C., Huger, M., "Caractérisation par ultrasons à haute température de composites céramique-céramique." A paraître dans la Revue des Composites et des matériaux avancés, 1993.
20. Sudre, O., Passilly, B., Parlier, M., "Evaluation of thermal residual stresses in SiC/MLAS and SiC/SiC composites by microindentation push-down test" ; 17th annual conference on composites and advanced ceramics, January 10-15, 1993. Cocoa beach Fl. A paraître.
21. Brevet FR n° 8915987 du 4 décembre 1989 "Composition vitrocéramique Li-Al-Si-O et son procédé de fabrication".
22. Monthioux, M., "Interphace investigation of SiC/SiC and SiC/MASL by TEM", A paraître dans la Revue des Composites et des Matériaux Avancés, 1993.
23. Bhattacharya, A.K, Nix, W.D., Analys of elastic and plastic deformation associated with indentation testing in thin films on substrates", Int.J.Solids Structures, 24, n°12, 1988, p 1287-1298.
24. Pascal, P, "Nouveau traité de chimie minérale" sous la direction de P.Pascal, édité par Masson et cie, 1961.
25. Cook, R.F, Pharr, G.M., "Direct observation and analysis of indentation cracking in glasses and ceramics", J.Am.Ceram.Soc, 73, n°4, 1990, p 787-817.

ROLE OF INTERFACES ON THE CYCLIC FATIGUE BEHAVIOUR OF CERAMIC MATRIX COMPOSITES

D. Rouby
P. Reynaud
Groupe d'Etudes de Métallurgie Physique et de Physique des Matériaux - G.E.M.P.P.M. URA CNRS n°341
Institut National des Sciences Appliquées de Lyon
69621 VILLEURBANNE cedex - France

1. SUMMARY

Ceramics reinforced with continuous fibres exhibit delayed failure under pulsating load. A micromechanical model describing the fatigue effects is proposed. It is based on the decreasing of the shear stress at the fibre-matrix interfaces, resulting from interfacial wear due to the see-saw sliding. The main features of this model are the following :

During first loading cycle, the material exhibits multiple matrix cracking and some fibre breaks. During subsequent cycles the interfacial shear stress decreases, leading to increasing the failure probability of the bridging fibres. For a critical fraction of broken bridging fibres, instability occurs and the specimen fails, thus defining the lifetime. For lower peak stresses, but higher still than the proportionality limit, the material also evolves but no failure occurs (up to one million cycles), indicating that the interfacial shear stress decreases to a non-zero lower bound.

Fatigue induced changes of interfacial shear stress are also observed from fibre pull-out length analyses.

2. INTRODUCTION

The use of continuous fibre reinforced ceramics for aerospace structures such as space shuttles and very high speed aircrafts and for hot engines, offers opportunity for using the same material for both resistance to mechanical loads and thermal aggressions.

For ceramic-ceramic composites emphasis was made in the improving of the toughness, because this property is in fact very low in bulk ceramics [1,2]. In such materials, both fibre and matrix are brittle in nature and the toughnening finds its origin in the matrix crack tip shielding by bridging fibres which are at first intact and then broken, undergoing pull-out [3].

Clearly, the fracture properties of ceramic matrix composites are controlled by two main microstructure parameters : first the average fibre strength and the strength distribution (described currently by a weibull's statistics) and secondly the interface properties, particularly the interfacial shear stress associated with friction or debonding and controlled by adequate fibre coating and also residual thermal stresses.

When aircraft applications are considered, fatigue behaviour becomes a very important thing. At present very few works have been published about fatigue of ceramic-ceramic fibre composites [4-10]. It appears clear yet that this family of materials exhibits some delayed failure due to cyclic fatigue effects. However, unlike the fracture behaviour, no micromodelling is straigthforward to describe the microstructural origin of the observed fatigue effect and consequently for bringing into relief the pertinent parameters which are to be controlled and improved so as to reach material optimization. A very interesting pioneer model has been proposed for explaining the origin of the hysteresis of stress-strain loops observed experimentally during fatigue tests [11] ; the loops widening was still attributed to frictional shear strength at the interface and the fatigue damage related to the fraction of failed fibres. Nevertheless no discussion was made in connexion with the real cause of damage extension as a function of number of fatigue cycles.

The purpose of this paper is to describe a fatigue model based on a decrease of the interfacial shear stress (ISS) which may be due to wear phenomena connected with the alternate slip between fibre and matrix. The results of this model are in very good agreement with practical observation so long as fibres are orientated in the loading direction (in 1D or 2D composites) and provided that no great delamination damage occurs during testing.

In addition, we describe the effect of fibre radius on the interfacial shear stress measured by the indentation method. We also show how the interfacial shear stress changes by fatigue ; this parameter beeing evaluated indirectly from measurements of fibre pull-out length as a function of fibre diameter.

3. EXPERIMENTAL FATIGUE BEHAVIOUR

Tests are carried out at room temperature under tension-tension sinusoidal cycling, between zero and controlled maximum stress, S, at a frequency of 1 Hz. The results are here given for a cross-weave composite of SiC fibre (Nicalon™) bundles embedded in a SiC matrix obtained by chemical vapor infiltration (2D SiC/SiC). This composite is processed by the Société Européenne de Propulsion (S.E.P.) and is characterized by a failure strain of about 0.2-0.3 %. Similar results are obtained (but not described in this paper) for a cross-plied SiC(Nicalon)/glass-ceramic composite, processed by Aérospatiale. The MAS-L matrix is obtained by using the sol-gel route and hot-pressing.

Presented at an AGARD Workshop entitled 'Introduction of Ceramics into Aerospace Structural Composites', April, 1993.

Figure 1 shows the lifetime diagram. Depending on the maximum stress applied, three stages are observed :
i) samples broken at first loading, a certain scattering in the ultimate tensile strength (UTS) is observed ;
ii) fractures occured after a limited number of cycles (from 5 to 12,000) in relation to the maximum fatigue stress ;
iii) no fracture occured after a conventional number of cycles (typically : 10^6).

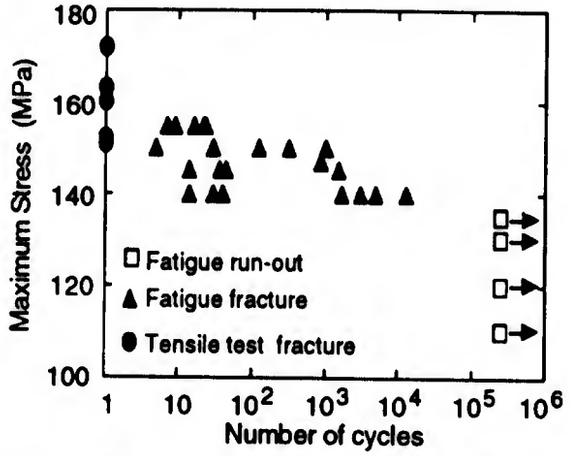

Fig. 1 : 2D SiC-SiC. Lifetime diagram.
Fatigue in tension-tension, 1 Hz, room temperature.

But the mechanical behaviour with cyclic loading remains similar whatever maximum stress is applied. As illustrated on Fig. 2a, the first stress-strain loading curve has a typical shape because of a response under loading similar to monotonic tensile test. It is interesting to notice that curves given on Fig. 2 correspond to a specimen not failed at 10^6 cycles (well below the fatigue limit) and it is clearly shown that the maximum fatigue stress is well beyond the limit of linearity.

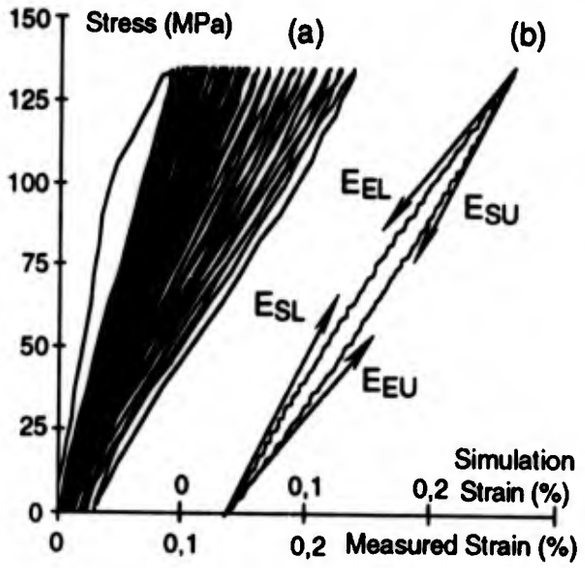

Fig. 2 : 2D SiC-SiC. Fatigue in tension-tension
(a) : example of recorded stress-strain loops
(b) : example of theoretical loop, definition of the tangent moduli.

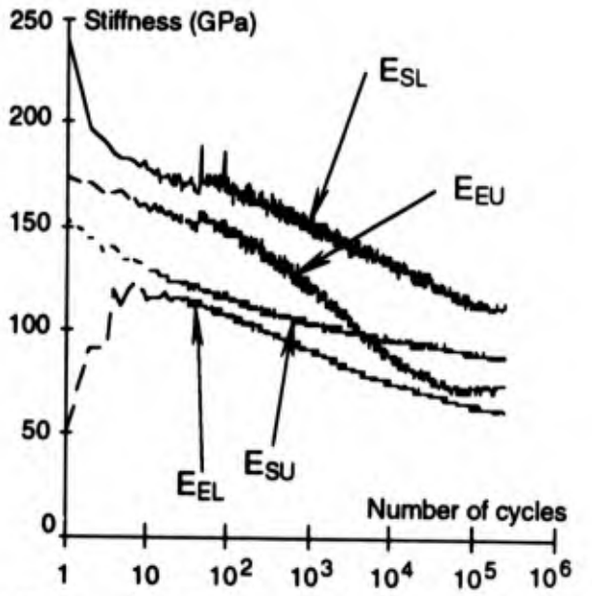

Fig. 3 : 2D SiC-SiC. Fatigue in tension-tension (S = 135 MPa). Tangent moduli as a function of number of cycles (no failure at 250,000 cycles).

Further hysteresis stress-strain loops are characterized by an increasing area and a decreasing main slope. A theoretical loop is given on Fig. 2b ; careful stress and strain measurements allow us to determine the evolutions of some stiffnesses (tangent modulus) in the loop : E_{SL} at start of loading, E_{EL} at end of loading, E_{SU} at start of unloading and E_{EU} at the end of unloading. Typical changes of these stiffnesses are shown on Fig. 3 : E_{SL} and E_{EU} (at the bottom of the loop) are higher than the other two, due to debris affecting the normal crack closure. So only E_{EL} and E_{SU} (at the top of loop) are significant with respect to fatigue behaviour.

Evolutions of these two slopes are given on Fig. 4 for different maximum fatigue stress values :
i) at low S, E_{EL} and E_{SU} are high, equal and remain constant during cycling : elastic behaviour, no damage, no failure ;
ii) at medium S (below fatigue limit), the stiffnesses are progressively decreasing ; E_{EL} decreases faster than E_{SU} and at a given number of cycles the two slopes evolve in parallel (stabilization stage), no fatigue failure occurs ;
iii) at higher S (beyond the fatigue limit), same evolutions are observed but the failure appears always before the stabilization stage.

More details upon the cyclic fatigue behaviour of 2D SiC-SiC composites and particularly the results concerning acoustic emission, can be found elsewere [12,13].

4. MODELLING OF FATIGUE BEHAVIOUR

The analysis of fatigue micromechanisms is presented in the case of a perfect unidirectional (1D) composite where the continuous fibres are randomly arranged parallel to the direction of the applied load. The influence of a more complicated architecture such as bidirectional (2D) woven composite will be discussed at each time if necessary.

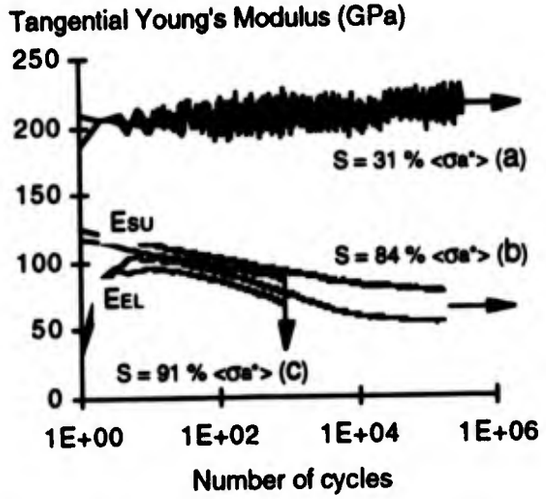

Fig. 4 : 2D SiC-SiC. Fatigue in tension-tension. End-of-loading (E_{EL}) and start-of-unloading (E_{SU}) stiffnesses versus N. (a) : S = 50 MPa (run-out); (b) : S = 135 MPa (run-out); (c) : S = 145 MPa (failure at 800 cycles)

4.1 Damage induced by tensile loading

During tensile loading the 1D composite undergoes multiple matrix cracking, following the ACK [14] scheme. The cracks are assumed running straight over the entire cross-section and regularly spaced with a given distance, d, between them (Fig. 5).

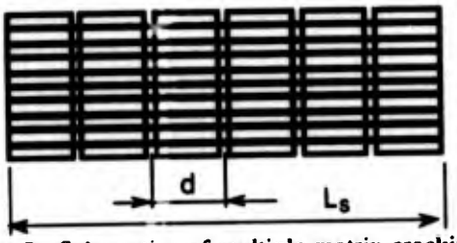

Fig. 5 : Schematics of multiple matrix cracking in 1D composite.

As loading proceeds, this distance decreases up to a saturation value. Saturation of matrix cracking is mainly due to the overlapping of the matrix unloading regions. But in some cases, an apparent saturation can be observed with larger distances, for example when local overstresses occur in the material near large voids introduced by the 2D woven architecture ; in this case the crack spacing should be more or less linked with the distance between large voids.

Near the matrix crack, the bridging fibres undergo overload and the peak stress, T, is given by the following relationship :

$$T = \frac{\sigma_a}{v_f (1 - q)} \qquad (1)$$

where σ_a is the applied stress on the composite, v_f is the fibre volume fraction and q is the proportion of broken fibres. To simplify, it is assumed that only the surviving fibres carry the load in the sliding zone. In the sliding zone, where the fibre stress, σ_f, increases to peak stress (Fig. 6a), the slope of the fibre stress is given by:

$$\left| \frac{d\sigma_f}{dx} \right| = \frac{2\tau}{r} \qquad (2)$$

with τ being the frictional interfacial shear stress (ISS) in the fibre/matrix sliding region, and r the fibre radius.

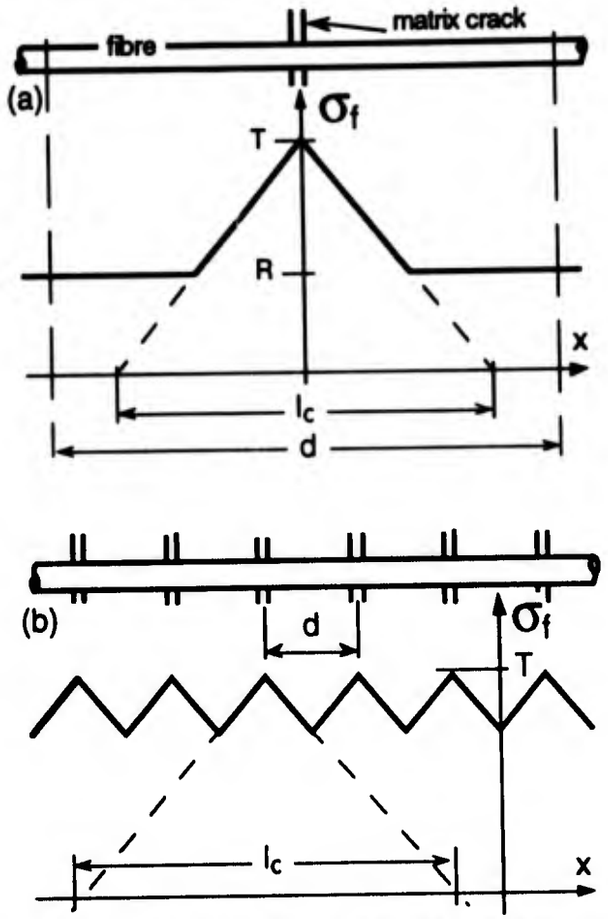

Fig. 6 : Fibre stress profiles resulting from matrix cracking. T : peak stress, R : nominal fibre stress. (a) : case of large crack spacing ; (b) : small matrix spacing.

According to crack spacing, two situations are to be considered (Fig. 6) :

i) if the mean distance d is greater than a critical fibre length, l_c, the sliding zones are not interacting and the overload profile is surrounded by a constant fibre stress (Fig. 6a). The level of this constant fibre stress is :

$$R = \frac{\sigma_a}{v_f} \frac{\eta}{1 + \eta} \qquad (3)$$

where η is defined by :

$$\eta = \frac{E_f v_f}{E_m (1 - v_f)} \qquad (4)$$

with E_f and E_m are the fibre and matrix modulus respectively. In this case, each bridged matrix crack is working independently from the other, and the specimen fails since one crack reaches the instability.

ii) if the distance d is smaller than the critical fibre length (Fig. 6b), the sliding regions are overlapping. When a fibre fails (near a given peak stress location), the resulting stress drop extends over several matrix blocks.

As a result, the bridged cracks are no more independent systems. Therefore the instability should be analyzed in the whole length of the specimen.

4.2 Composite failure under monotonic loading

For fatigue, there are several interests to analyze the failure under monotonic loading and particularly the ultimate tensile strength (UTS).

First, the UTS represents a characteristic data which is to be introduced in the lifetime diagram. Secondly, at the starting of a fatigue experiment, the first loading up to maximum fatigue stress introduces the initial damage consisting of a certain set of matrix cracks and a certain proportion of broken fibres ; this mechanism is typically working under monotonic loading. Thirdly, during load cycling some material parameters are changing and consequently fatigue failure will occur when the UTS (with the new parameters values) equals the maximum fatigue stress. And finally, for a given maximum fatigue load a scattering in the life times is commonly observed experimentally. This scattering should find its origin in the variability of fatigue effect and also in the variability of some parameters leading to the scattering observed for the UTS under monotonic loading.

The failure probability of the fibres is described by means of the Weibull's statistics, following the weakest link scheme : the probability of failure of a fibre element (link) of length δx can be expressed as follows :

$$F_1 = \left(\frac{\sigma_f}{\sigma_0}\right)^m \delta x \qquad (5)$$

where σ_f is here the stress sustained by the fibre element, m is the Weibull's modulus and σ_0 a scale parameter, related to the average fibre strength (under uniform load) :

$$\langle\sigma_{fu}\rangle = \sigma_0 L_f^{-1/m} \Gamma\left(1 + \frac{1}{m}\right) \qquad (6)$$

with L_f being the fibre gauge length used for the measurement of strength and Γ the well-known gamma function.

The analysis of ultimate failure of the composite (bridged crack) is similar in the principle to the well-known dry-fibre-bundle failure problem.

In the case of large crack spacing (assumption A), the surviving fibres in the bridging bundle undergo a stress profile as shown on Fig. 6a. The probability of fibre failure in such a system is calculated by using the same assumption and statistical analysis than Thouless and Evans [15] ; particularly fibre failure outside the slip length is ignored and the fibre stress is assumed to decrease linearly from the peak stress, T, to zero. The probability of fibre failure anywhere within the overload profile is found to be :

$$P_F(d > l_c) = 1 - \exp\left[-\frac{r\,T^{m+1}}{(m+1)\,\tau\,\sigma_0^m}\right] \qquad (7)$$

and can be considered as the fraction of broken fibres (q, see Equ. 1) at a given value of peak stress T. As the applied load increases, the fraction of broken fibres increases up to a critical instability value, q^*. Equation 7 can be easily maximized with respect to T, leading to the following instability condition :

$$\frac{r\,T^{m+1}}{\tau\,\sigma_0^m} = 1 \qquad (8)$$

That gives the critical fraction of broken fibres (subscript A refers to this first assumption : $d > l_c$) :

$$(q^*)_A = 1 - \exp\left[-\frac{1}{m+1}\right] \qquad (9)$$

and the UTS of the bridged crack :

$$(\sigma_u^*)_A = v_f \left(\frac{\tau}{r}\right)^{\frac{1}{m+1}} (\sigma_0)^{\frac{m}{m+1}} \exp\left[-\frac{1}{m+1}\right] \qquad (10)$$

For a specimen containing more than one matrix crack statistical fracture of a serial set of bridged systems as described above should be analyzed. For simplification, we will consider further that all cracks are exactly identical.

In the case of short fibre spacing (Fig. 6b) (assumption B), the fibre stress looks like saw-teeth. Some authors [16] considered that a fibre breaking anywhere within the entire sample gauge length (L_s, on Fig. 5) is unable to carry any load. In these conditions, the same analysis as before leads to a different instability condition. However the hypothesis of a single fibre failure within the gauge length does not seem very realistic, because of the existence of stress transfer mechanisms between fibre and matrix in the other matrix blocks.

A more complete analysis of UTS was recently proposed by Curtin [17]. It considers that each fibre in the composite can exhibit multiple failure, in the same way as a single filament embedded in a large failure strain matrix (assumption C). In that analysis, the load carried out by the broken fibres is taken into account. The analytical result (with a slightly different Weibull's expression) concerning the critical fraction of broken fibres is :

$$(q^*)_C = \frac{2}{m+2} \qquad (11)$$

and the UTS becomes :

$$(\sigma_u^*)_C = v_f \left(\frac{\tau}{r}\right)^{\frac{1}{m+1}} (\sigma_0)^{\frac{m}{m+1}} \left(\frac{2}{m+2}\right)^{\frac{1}{m+1}} \frac{m+1}{m+2} \qquad (12)$$

As a result, for the two most realistic assumptions, the critical proportion of broken fibres is only m dependent. In addition, the UTS (Equ. 10 and 12) only differs in the m dependent prefactor : the influences of the other material parameters (v_f, τ, σ_0 and r) are exactly the same. In order to simplify the presentation, the further analyses are only made with the assumption A ($d > l_c$).

If we take the hypothesis that some parameters (τ or σ_0) decrease during fatigue cycling, we see clearly that the potential UTS of the sample decreases. As, after a given number of cycles, this potential UTS reaches the maximum applied fatigue stress, the specimen will fail. Time dependent subcritical crack growth in the fibres leads to a decrease of effective fibre strength which can be described by a decrease of σ_0. In the material considered here, there are some arguments for retaining an effect of alternative sliding induced by the cycling of load, particularly the non-dependence of fatigue effect on test frequency [12,13]. In these conditions, the decreasing ISS

is a very good candidate to explain the observed fatigue effects. In the following sections the causes of the decrease of ISS as fatigue proceeds are discussed.

4.3 Changes of ISS during fatigue

The first hypothesis is to consider that the ISS decreases continuously as a function of number of cycles, N, up to a limiting value τ_∞ (Fig. 7). This decrease is mainly due to an interfacial wear, as discussed by Jero et al. [18]. This phenomenon is particularly effective when the matrix compresses radially the fibres, because of the thermal expansion mismatch. During the see-saw sliding, the asperities are mutually scraped off and this effect should be more pronounced with asperities of higher amplitude, that is at starting of fatigue test : the decreasing rate of ISS ($d\tau/dN$) should be lower for large cycle number. Having no further information about this mechanism and to simplify, a power law as below was chosen (Fig. 7a) :

$$\tau = \tau_0 N^{-t} \qquad (N < N_\infty)$$
$$\tau = \tau_\infty \qquad (N > N_\infty) \qquad (13)$$

where τ_0 is the initial ISS value before load cycling.

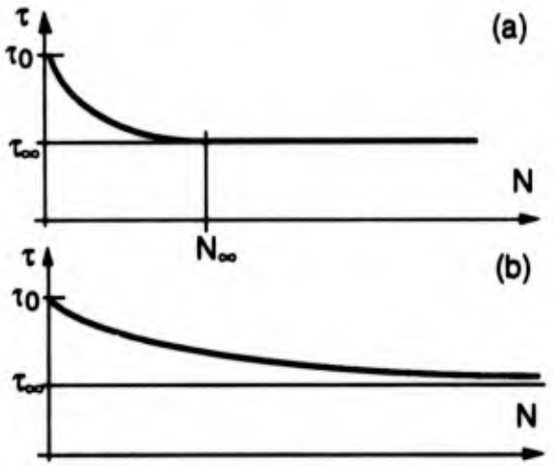

Fig. 7 : Expected changes of interfacial shear stress as a function of number of cycles.
(a) : power law (see Equ. 13) ; (b) : exponential law

The decreasing law is bounded by a limiting value ; this comes from non vanishing friction between fibre and matrix, due to long distance interactions : like changes in fibre diameter and cross-section shape, fibre bending (particularly in the case of woven clothes), etc. Another cause of ISS decrease can be originated from longitudinal splitting in the matrix. These cracks strongly reduce the thermal mismatch induced compression stress on the neighbouring fibres. This mechanism leads locally to easier friction. The effective ISS in a given cross section is therefore diminishing.

During one cycle, the fibre stress profile evolves as shown on Fig. 8 ; at each load rate inversion the sliding reverses (the slope of stress inverses) in a region close to the crack. In this present assumption, as the number of cycles increases, the ISS decreases regularly (according to Fig. 7a) and the width of the sliding zone increases. Since a decrease of ISS leads to an increase of broken fibres fraction, the overloading triangle at maximum applied fatigue stress exhibits a continuously decrease of sharpness and an increase of peak stress, as fatigue proceeds.

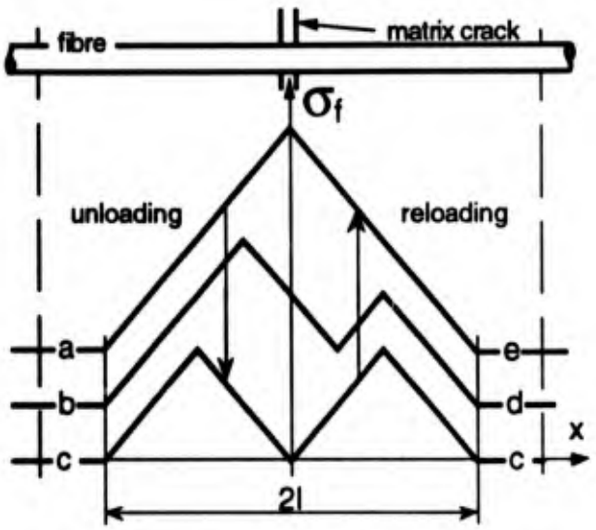

Fig. 8 : Schematics of fibre stress profiles during unloading (left) and reloading (right).(assumption A).

Some repeated indentation tests suggest that the ISS drops very sharply after the first slip and remains constant during the subsequent loadings. Applied to our fatigue problem, this effect leads also to a continuously decrease of an effective ISS, but with asymptotic tendency to τ_∞ (Fig. 7b).

At present no more informations are available to specify what is the real law of the ISS decrease. The curves on Fig. 7a and 7b are not very different in shape, so we choose arbitrarily the power law (Equ. 13) for taking into account the changes in ISS in a fatigue test.

4.4 Damage induced during first fatigue cycle

During the first fatigue cycle, the applied stress σ_a increases from zero to the maximum imposed fatigue stress , S.

Discussion about crack spacing

If S is lower than the the first matrix cracking stress ($S<S_0$), no matrix damage occurs during the first loading and therefore no subsequent fatigue effect may be observed : the specimen remains perfectly elastic.

Above S_0, there is multiple matrix cracking up to a certain amount, defined by an initial matrix spacing, d_0. As fatigue proceeds (with $S > S_0$), the decrease of the ISS and the associated stress transfer involve that the remaining matrix blocks are on the whole less loaded. Consequently the matrix damage remaining constant under the subsequent fatigue cycles can be considered, in a first approximation (i.e. the crack spacing is only depending on S).

In real composites however, the applied load induces cracks in the longitudinal bundles which are not running over the entire cross-section and also other cracks in the non-longitudinal parts of the microstructure. As an example, for a woven architecture, in the bundles

orientated perpendicularly to the load direction, classical fatigue effect, similar to that observed in polycrystalline ceramics [19], cannot be avoided.

Discussion about fraction of broken fibres

This fraction increases as the applied load increases. For the assumption $d > l_c$, one obtains :

$$\frac{\sigma_a}{\sigma_a^*} = (1 - q)\left[-\ln(1-q)\right]^{1/m+1} \exp\left[\frac{1}{m+1}\right](m+1)^{1/m+1} \quad (14)$$

The relation between σ_a/σ_a^* and q does not depend on the ISS ; of course the UTS σ_a^* is depending on it (see Equ. 10).

The initial fraction of broken fibres at first cycle, q_1, is obtained by taking the relative fatigue stress S/σ_a^* and resolving Equ. 14. If fibre Weibull's modulus increases, the initial fraction of broken fibres decreases. On the other hand, if the ISS decreases, σ_a^* decreases and for a given constant value of S, the initial fraction of broken fibres increases. This feature is at the origin of the main fatigue effect.

In real composites, both matrix and fibres exhibit scattering of failure stress and in some cases during loading, the region where fibres break overlap the zone where multiple matrix cracking works. This was clearly modelled by Pérès [20] for 1D composite.

4.5 Fatigue behaviour

In this section we analyse the influence of a succession of loading-unloading cycles on the occurence of failure and on stiffnesses.

Life-time diagram

At first cycle, the initial ISS is τ_0 and the loading up to S leads to the initial fraction of broken fibres q_1. During subsequent cycles, the fraction of broken fibres increases (as τ decreases, see Equ. 10 and 14 with $\sigma_a = S$). The theoretical evolution of the fraction of broken fibres as a function of ISS on Fig. 9, and the corresponding lifetime diagram is given on Fig. 10.

According to the level of S, several cases are to be considered :

i) for very high S values, q changes from zero to q* during first cycle : the specimen fails at first cycle at a stress σ_a^* (Equ. 10 with $\tau = \tau_0$) ;

ii) for high S, q changes from q_1 to q* : the specimen fails after a certain number of cycles (delayed fatigue failure). In this case the S value equals the UTS of the sample, given for example by Equ. 10, with $\tau < \tau_0$. One finally obtains :

$$\frac{S}{\sigma_a^*} = \left(\frac{\tau}{\tau_0}\right)^{1/m+1} \quad (15)$$

and using the proposed power law for the ISS change (equ. 13), the theoretical expression of the lifetime results in (for $1 \le N \le N_F$) :

$$\frac{S}{\sigma_a^*} = N^{-1/m+1} \quad (16)$$

Such a life-time law is in agreement with experimental measurements (see Fig. 1).

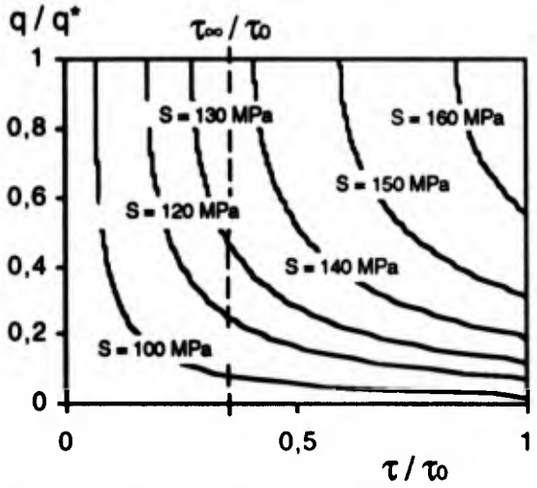

Fig. 9 : Simulated damage during fatigue. Proportion of broken fibres as a function of relative ISS change, for increasing maximum fatigue stress. (m = 6)

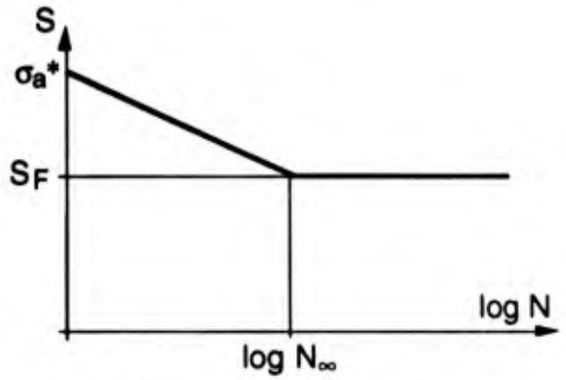

Fig. 10 : Theoretical lifetime diagram.

For the scattering observed in the experimental S-N curve, two main causes can be evoked :

i) the variability of the basic fatigue effect from one specimen to another : the parameters t and τ_∞ appearing in Equ. 16 should be distributed.

ii) the UTS under monotonic loading (given by Equ. 10 or 12) is governed by some distributed parameters (such as v_f, σ_0, $\tau=\tau_0$ or m). This means simply that a specimen having a potentially high UTS shows by fatigue an enhanced lifetime.

The scattering in lifetimes observed appears to be in agreement with a gaussian distribution of the UTS, or with a gaussian distribution of the ISS namely [12].

Analysis of the loading-unloading loops

From the fibre sress profile during loading and unloading (see Fig. 8), the stress-strain relationship can be easily calculated over basic length corresponding to matrix crack spacing. The theoretical hysteresis loop is symmetrical (parabolic laws), its width results from friction effects caused by the reverse slidings. In fact the loop is slightly open at zero load because the effective ISS has changed a little since the preceding loading. An example of theoretical loop is given on Fig. 2b.

In practice higher stiffnesses are commonly observed at low loads, by loading and unloading. This phenomenon

is attributed to debries located between the crack surfaces which hinder the crack closure at the end of unload. Our model does not take into account this feature. In these conditions, an analysis of the stiffnesses is more accurate at the top of the loops.

At the start of unloading, the stiffness given by the tangent modulus ($d\sigma_a/d\varepsilon$, for decreasing strain ε, and $\sigma_a = S$) is simply the undamaged 1D composite Young's modulus :

$$E_{SU} = E_x \tag{17}$$

with $E_x = E_f v_f + E_m v_m$, for perfect 1D composite.

At the end of loading, the tangent modulus ($d\sigma_a/d\varepsilon$, for ε increasing and $\sigma_a=S$) can be written as follows :

$$E_{EL} = \frac{E_x}{1 + \frac{\tau S}{2 v_f \tau d \eta (1+\eta)} \left(\frac{1+\eta q}{1-q}\right)^2} \qquad \text{for } d > l_c \tag{18a}$$

η is given by Equ. 4, and :

$$E_{EL} = \frac{E_x}{1 + \frac{1+\eta q}{\eta (1-q)}} \qquad \text{for } d < l_c \tag{18b}$$

In the case of slip length overlapping (as shown on Fig. 6b) the ends of loading and unloading curves become linear with a slope given by Equ. 18b.

Experimentally, as shown on Fig. 3 for 2D woven composite the end-of-loading stiffness decreases mainly according to Equ. 17 where τ decreases and q increases with increasing number of cycles. The increase observed at low number of cycles is seemingly due to the fact that the new damage occuring near the maximum load is very important and it affects the loading slope, because Equ. 22 is written with the assumption that both τ and q remain constant over the duration of the considered cycle ; clearly this assumption is not valid for the first cycle and probably also for few subsequent cycles. The higher the number of cycles, the smaller the new damage, hence after say 10 cycles this effect becomes negligible.

In addition, a progressive decrease of the start-of-loading stiffness is observed on Fig. 3. This phenomenon is probably due to some fatigue induced damage appearing in other regions of the microstructure than the 1D longitudinal bundles, certainly induced by the stiffness lowering of the longitudinal bundles which induces higher stress in the non-longitudinal regions (the bundles at 90°). Despite the complicated architecture of the 2D woven composite, an effective modulus $E_T(N)$, associated with the overall stiffness of the non-longitudinal (transverse) part of the material which is moreover supposed to be non-hysteretic, can be considered in a rule of mixture :

$$\left(E_{EL}\right)_{2D} = v_L E_{EL}(N) + v_T E_T(N)$$

$$\left(E_{SU}\right)_{2D} = v_L E_x + v_T E_T(N) \tag{24}$$

where v_L and v_T are the effective cross-section fractions respectively of the longitudinal and transverse parts of the composite. In these conditions, the difference $(E_{SU})_{2D}$ - $(E_{EL})_{2D}$ remains representative of the fatigue effects in the 1D longitudinal bundles. Finally if the multiple matrix cracking is fatigue sensitive, a decrease of crack spacing, d, can be expected ; this affects the rule of E_{EL} decrease but should no influence the E_{SU} stiffness.

In short : the stiffnesses involve the entire damage in the specimen, the final failure involves only the behaviour of the 1D longitudinal bundles. Of course in some cases such as a 2D composite orientated at ±45°, this very simplifying assumption is no more realistic. More work should be done for taking into account the damage accumulation in complex reinforcement architectures.

5. INTERFACE CHARACTERIZATION

In this section we briefly describe, particularly in the case of the SiC/MAS-L composite, the effect of fibre radius both on the ISS, measured by indentation technique, and on the fibre pull-out length, measured after specimen failure in tension.

5.1 Influence of the roughness on the ISS

The Nicalon™ Si-O-C fibre (from Nippon Carbon) is known to exhibit a large variation in diameter, from roughly 5 to more than 20 micrometers, with an average value close to 15 micrometers. This feature gives us a good opportunity for studying the interfacial characteristics as a function of fibre size. In addition, recent works clearly show that the interface roughness plays an important role in the frictional sliding mechanisms [18, 21, 22].

In the as-received material, the interface is bonded and a tensile thermal stress takes place. The debonding conditions are analyzed elsewhere [23]. After debonding and without external stress, the thermal expansion mismatch leads to a displacement, δ', between the fibre and the matrix surfaces, given by :

$$\delta' = r \Delta\alpha \Delta T \tag{20}$$

where $\Delta\alpha = \alpha_m - \alpha_f$ and $\Delta T = T - T_0$, with T : testing temperature and T_0 : matrix processing (stress-free state) temperature.

For the SiC/SiC composite ($\Delta\alpha\Delta T < 0$), the displacement δ' leads in fact to a compressive résidual stress ; for the SiC/MAS-L composite ($\Delta\alpha\Delta T > 0$), δ' corresponds to a gap at the interface.

The debonding is assumed to produce a certain roughness of the two created surfaces as described by Jero et al. [18]. In these conditions during post-debonding sliding, a radial displacement of the fibre and matrix surfaces takes place ; this displacement is controlled by the effective amplitude, δ, of the asperities. So long as $\delta' < \delta$, the resulting misfit leads to a compressive radial stress given by [24] :

$$\sigma_{rad} = -\frac{\delta - \delta'}{r} \frac{1}{A} \tag{21}$$

where $$A = \frac{1 - v_f}{E_f} + \frac{1 + v_m + v_f(1 - v_m)}{E_m(1 - v_f)} \tag{22}$$

The interfacial sliding is assumed to follow a Coulomb law and the ISS can be written :

$$\tau = -\mu \sigma_{rad} \tag{23}$$

with μ : coefficient of friction, considered as a constant.

This analysis neglects the effect of Poisson's radial expansion resulting from fibre compression during indentation test. In the cases described thereafter Poisson's expansion of fibre radius remains within 10% of the roughness amplitude. Finally the ISS is given by the following expression :

$$\tau = \frac{\mu\,\delta}{A\,r} - \frac{\mu}{A}\,\Delta\alpha\,\Delta T \qquad (24)$$

Fig. 11 shows how the ISS varies theoretically as a function of the inverse of fibre radius. For SiC-SiC composites the interface is always in compression (Fig. 11a) ; for SiC/MAS-L, there is a given radius r* where the thermal induced gap just equals the roughness amplitude and then the ISS vanishes (Fig. 11b).

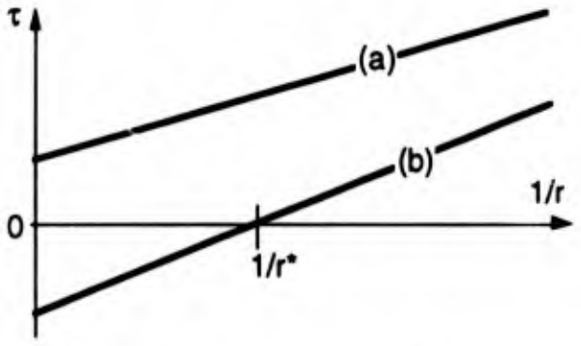

Fig. 11 : Interfacial shear stress versus 1/r.
(a) : $\Delta\alpha\,\Delta T < 0$; (b) : $\Delta\alpha\,\Delta T > 0$

5.2 Indentation measurements

The sliding resistance is measured by using a non-instrumentated micro-hardness tester (Testwell) following the method of Marshall [25], with an accuracy of about 30%. The fibre to test is carefully selected with regard to similar arrangement of and distances from neighbouring fibres. Its diameter is measured and the fibre is then impressed. If the indent is not centered or if there is the least sign of fibre splitting, this measurement is rejected.

The ISS related to sliding, τ, is shown in Fig. 12 as a function of the inverse of fibre radius. The ISS is seen to decrease in an overall fashion as the fibre radius increases. The observed scattering is caused by the low accuracy of measurement, and also by the natural variability of one fibre to another ; this includes variations of fibre and interface properties, and differences in the neighbourhood of each tested fibre as well. Some dots on Fig. 12 (corresponding to about 10% of the retained tests) stand well aside the main trend and concern mainly fibres of more than 20 micrometers diameter. This may be due to more pronounced irregularities in the fibre geometry such as sharper changes of the fibre diameter or the cross-section shape along fibre axis. Nevertheless the general trend of ISS change is in very good agreement with Equ. 24 (Fig. 11b). By taking $v_f = 0$, $E_m = 75$ GPa, $E_f = 200$ GPa, $\Delta\alpha = -2\,10^{-6}$ °C^{-1} and $T_0 = 1300$ °C, we obtain, with $r^* = 20$ µm, a roughness amplitude of $\delta = 46$ nm, for the material studied. The slope of the best fit line leads to a coefficient of friction : $\mu = 0.042$.

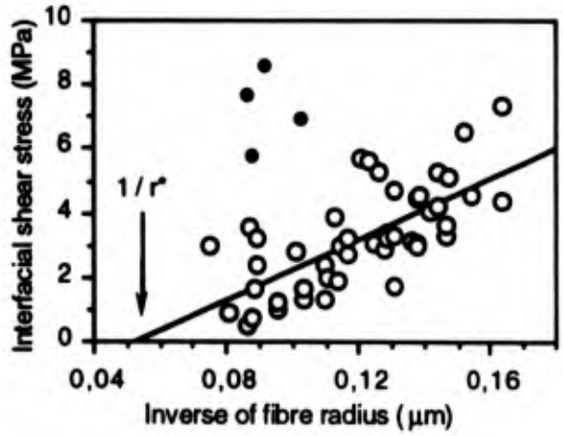

Fig. 12 : SiC/MAS-L. ISS versus 1/r.

5.3 Pull-out length analysis

In the case of a single matrix crack (or with large distance between them), the pull-out length was analyzed by Thouless and Evans [15] and by Sutcu [26]. An unidirectional composite (or a 0° ply in a laminate) without longitudinal discontinuities (woven clothes, macropores, ...) exhibits a saturation state in the multiple matrix cracking process ; this assumption is taken for the SiC/MAS-L material. In this case, the pull-out length was analyzed in details by Curtin [27] ; the average pull-out length is then given by :

$$\langle L_p \rangle = B \left(\frac{r}{\tau}\right)^{m/m+1} \qquad (25)$$

with

$$B = \frac{1}{4} \langle \sigma_{fu} \rangle^{m/m+1}\, L_f^{1/m+1}\, \Gamma\left(\frac{m+2}{m+1}\right) \left[\Gamma\left(\frac{m+1}{m}\right)\right]^{m/m+1}$$

where $\langle \sigma_{fu} \rangle$ is the average fibre strength an L_f the gauge length for measuring it ; $\Gamma(y)$ is the gamma function and m the fibre Weibull's modulus. Knowing that the ISS is also depending on the fibre radius, we obtain finally :

$$r \left(\frac{B}{\langle L_p \rangle}\right)^{m+1/m} = \tau = \frac{\mu\,\delta}{A\,r} - \frac{\mu}{A}\,\Delta\alpha\,\Delta T \qquad (26)$$

The left hand side term is obtained from Equ. 25 and the right hand side is simply the Equ. 24.

As a result, the average pull-out length is fibre radius depending as well.

5.4 Measurement of pull-out length

Tensile specimens of the cross-plied SiC/MAS-L composite were tested with an hydraulic MTS 810 machine. The failure was obtained by monotonic loading, either directly or after a great number of fatigue cycles (in the case described here the fatigue conditions are : 320,000 cycles with $S = 0.66\,\sigma_a^*$).

Afterwards the fracture surfaces are observed by optical microscopy. For each fibre, the diameter (2r) and the pull-out length (L_p) are measured. These measurements are only possible on the outer zone of the outer 0° plies of the laminate. In these regions the thermal constraints due to the 90° plies are less effective. The number of measurements is sufficient for a valuable analysis for the fibres having a diameter between 10 and 20 µm.

The average lull-out length <Lp> is calculated for each class of fibre radii, which are defined by the median radius plus and minus 0.25 μm. Typical results are given on Fig. 13 ; on this figure are only taken the averages of at least 20 fibres in each class.

One can see that the pull-out length increases as the fibre radius becomes larger. But the fatigued specimen exhibits overall higher pull-out length. Hence, the fatigue cycling leads to a significant increase of the pull-out length which can be only explained by a decrease of the ISS.

Fig. 14 shows, as a function of 1/r, the ISS calculated by using the left hand part of Equ. 26 (by taking also a fibre strenth of 1500 MPa and m = 4). As we can see, the ISS changes are in good agreement with the right hand part of Equ. 26.

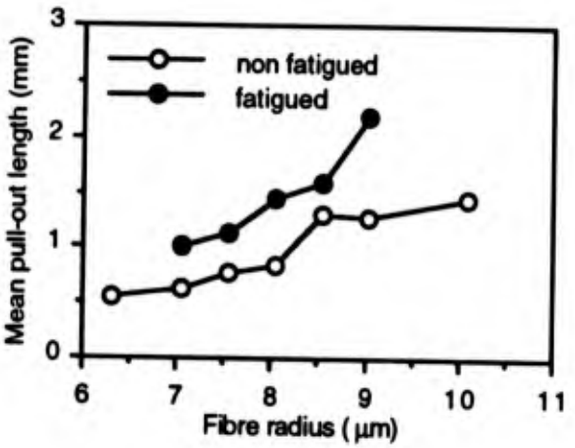

Fig. 13 : SiC/MAS-L.
Pull-out length versus fibre radius.

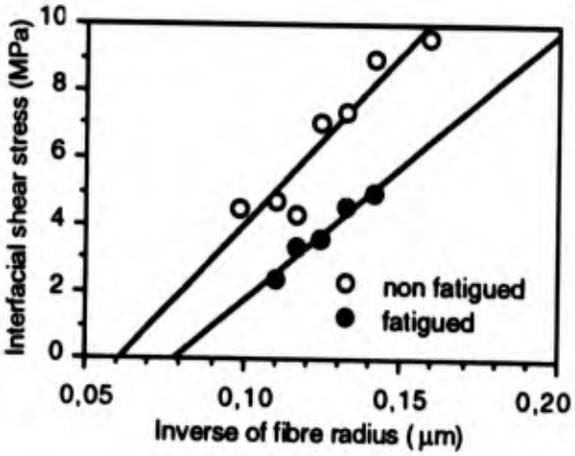

Fig. 14 : Interfacial shear stress versus 1/r.

Some parameters in the term B (Equ. 25) are not clearly quantified and therefore it is difficult to conclude about the absolute values of the obtained ISS. Nevertheless the straight lines on Fig. 14 exhibit seemingly the same ordinate at the origin and therefore the lower slope for the fatigued case indicates a decrease of the amplitude of the roughness. This result is in very good agreement with the idea of an interfacial wear due to the see-saw sliding during fatigue. Of course more work must be done in order to analyze more accurately the real wear phenomenon and to describe better the law of ISS decrease, which is only expected on Fig. 7.

CONCLUSION

Fatigue test in tension-tension at room temperature on 2D woven SiC-SiC composites revealed several main features :

i) The apparent fatigue limit is situated well beyond the proportional limit observed during tensile test.

ii) For fatigue tests conducted with a maximum imposed stress between the proportional and fatigue limit, the tangent moduli at the end-of-loading and at the start-of-unloading decrease gradually. After a given number of cycles, the difference between them stabilizes indicating stabilization of damage and test runs out without failure.

iii) For test performed beyond the fatigue limit, the stiffnesses evolve in a similar fashion as before, but failure occurs before the stabilization stage.

A micromechanical model describing the mechanisms which are at the origin of fatigue effect in the case of 1D composite is proposed. It is based on the continuously decrease of the interfacial shear stress, resulting from interfacial wear due to the see-saw slidings near the matrix cracks. As interfacial shear stress decreases, the fraction of broken fibres increases up to a critical instability value which determines the failure of the specimen.

The interfacial shear stress decreases from a given initial value to a non-zero limiting value. Depending on the damage introduced by the first loading, two situation can be considered : if this limiting value is reached before instability condition is fulfilled, the accumulation of broken fibres stops and the mechanical properties become stabilized ; if the critical fraction of broken fibres is reached before this stabilization takes place, the specimen fails.

The analysis presented here gives some analytical expressions of the lifetime diagram and of the tangent moduli of the stress-strain loops.

For 2D composites and other complex reinforcement architectures, some additional fatigue effects are expected to occur in the transverse regions of the material, modifying the rule of stiffness reduction as a function of number of cycles.

Finally the analysis of ISS measured by indentation method and evaluated from fibre pull-out length, shows clearly that fatigue cyling induces a decrease of the ISS, probably in connection with a decrease of the roughness of the asperities at the sliding interfacial surfaces.

ACKNOWLEDGEMENTS

This work was supported by the Centre National de la Recherche Scientifique, the Ministère de la Recherche et de l'Espace, the Direction des Recherches et Etudes Techniques and the Centre National d'Etudes Spaciales who sponsored two scientific associations : the Groupement Scientifique "Composites Thermo-structuraux" and the Groupement Scientifique "Comportements thermomécaniques des composites céramique-céramique à fibres".

Thanks are particularly due to M. Bourgeon, F. Abbé and J.M. Jouin from S.E.P., and P. Pérès and J.F. Jamet from Aérospatiale, for numerous and fruitful discussions and for providing the materials.

REFERENCES

1. A.G. EVANS and D.B. MARSHALL, The mechanical behavior of ceramic matrix composites, Acta Metall., 16 (1989), pp. 2567-83.
2. D. ROUBY and G. NAVARRE, Role of interfaces on mechanical properties of ceramic-ceramic fibre composites, in Structural Ceramics, Processing, Microstructure, Properties. Proc. of the 11th Risø Int. Symp, Risø National Laboratory, Roskilde, DK, 1990, pp. 127-44.
3. D.B. MARSHALL, B.N. COX and A.G. EVANS, The mechanics of matrix cracking in brittle-matrix fiber composites, Acta Metall., 33 (1985) pp. 2013-21.
4. D. LEWIS III, Cyclic Mechanical Fatigue in Ceramic-Ceramic Composites - An Update, Ceram. Eng. Sci. Proc., 3 (1883), pp. 874-81.
5. K. M. PREWO, Fatigue and stress rupture of silicon carbide fibre-reinforced glass ceramics, J. Mater. Sci., 22 (1987) pp. 2695-701.
6. K.M. PREWO, B. JOHNSON and S. STARRETT, Silicon carbide fibre-reinforced glass-ceramic composite tensile behaviour at elevated temperature, J. Mater. Sci., 24 (1989), pp. 1373-9.
7. R. TALREJA, Fatigue of fibre reinforced ceramics, in Structural Ceramics, Processing, Microstructure, Properties. Proc. of the 11th Risø Int. Symp, Risø National Laboratory, Roskilde, DK, 1990, pp. 145-59.
8. E.Y. LUH, R.H. DAUSKARDT and R.O. RICHIE, Cyclic fatigue-crack growth behaviour of short cracks in SiC-reinforced lithium aluminosilicate glass-ceramic composite, J. Mater. Sci. Lett., 9 (1990), pp. 719-25.
9. Z.G. WANG, C. LAIRD, Z. HASHIN, W. ROSEN and C.F. YEN, The mechanical behaviour of a cross-weave ceramic matrix composite, J. Mater. Sci., 26 (1991), pp. 5335-41.
10. L.P. ZAWADA, L.M. BUTKUS and G.A. HARTMAN, Tensile and fatigue behaviour of silicon carbide fiber-reinforced aluminosilicate glass, J. Amer. Ceram. Soc., 74 (1991), pp. 2851-58.
11. T. KOTIL, J.W. HOLMES and M. COMNINOU, Origin of hysteresis observed during fatigue of ceramic-matrix composites, J. Amer. Ceram. Soc., 73 (1990), pp. 1879-83.
12. P. REYNAUD, Etude du comportement en fatigue des matériaux composites à matrice céramique suivi par emission acoustique, Thèse de Doctorat, INSA de Lyon, France, 1992.
13. P. REYNAUD, D. ROUBY and G. FANTOZZI, La fatigue des céramiques composites. Analyse des matériaux de type SiC-SiC, Revue des Composites et Matériaux Avancés (in press).
14. J. AVESTON, G.A. COOPER and A. KELLY, Single and multiple fracture, in Proc. of Conf. on the Properties of fibre composites of the National Physical Laboratory. Surrey , IPC Sci. Technol. Press, London, 1971, vol. 4, pp. 15-26.
15. M.D. THOULESS and A.G. EVANS, Effects of pull-out on the mechnical properties of ceramic-matrix composites, Acta Metall., 36 (1988), pp. 517-22.
16. H. CAO and M.D. THOULESS, Tensile tests of ceramic-matrix composites : theory and experiment, J. Amer. Ceram. Soc., 72 (1990), pp. 2091-94.
17. W.A. CURTIN, Theory of mechanical properties of ceramic-matrix composites, J. Amer. Ceram. Soc., 74 (1991), pp. 2837-45.
18. P.D. JERO, R.J. KERANS and T.A. PARTHASARATHY, Theoretical analysis of the fiber pullout and pushout tests, J. Amer. Soc., 74 (1991), pp. 1585-96.
19. R.O. RITCHIE, Mechanisms of fatigue crack propagation in metals, ceramics and composites : role of crack tip shielding, Mater. Sci. Engineering, A103 (1988), pp. 15-28.
20. P. PERES, Analyse théorique et expérimentale du rôle des paramètres de microstructure sur le comportement des composites à matrice fragile. Thèse de Doctorat, INSA de Lyon, France, 1988.
21. W.C. CARTER, E.P. BUTLER and E.R. FULLER Jr, Micro-mechanical aspects of asperity-controlled friction in fiber-toughened ceramic composites, Scripta Metall. Mater. 25, 1991, pp. 579-584.
22. T.J. MACKING, P.D. WARREN and A.G. EVANS, Effects of fiber roughness on interface sliding in composites, Acta Metall. Mater. 40, 1992, pp. 1251-1257.
23. M. BENOIT, Ph. BRENET and D. ROUBY, Comportement des interfaces dans des composites céramique-céramique, Revue des Composites et des Matériaux Avancés (in press).
24. H.J. OEL and V.D. FRECHETTE, Stress distribution in multiphase systems : II, Composite disks with cylindrical interfaces, J. Am. Ceram. Soc., 69, 1986, pp. 342-346.
25. D.B. MARSHALL and A.G. EVANS, failure mechanisms in ceramic-fiber/ceramic matrix composites, J. Am. Ceram. Soc., 68, 1985, pp.. 225-231.
26. M. SUTCU, Weibull statistics applied to fiber faikure in ceramic composites and work of fracture, Acta Metall., 37, 1989, pp. 651-661.
27. W.A. CURTIN, Theory of mechanical properties of ceramic-ceramic composites, J. Am. Ceram. Soc., 74, 1991, pp. 2837-2845.

Mechanical Behavior of CMCs : Crack Growth Resistance and Creep Aspects

M. GOMINA
J.L. CHERMANT

LERMAT, URA CNRS N°1317, ISMRA
6 Bd du Maréchal Juin
14050 CAEN Cedex
France

1. SUMMARY

This paper deals with rupture and creep behavior of CMCs. The influence of the specimen geometry and size on the R-curve behavior for two types of SiC/C/SiC composite materials were investigated. The experimental results obtained using in-situ matrix crack lengths indicate that the shape of the resistance curve depends essentially on the predominant toughning mechanism (extensive matrix microcracking or fiber-matrix debonding) whereas the frontal process zone size is the same for both types of materials. K_R-Δa curves of SENB and small CT specimens rise as a consequence of the ligament which cannot contain the fully developped frontal process zone. Using large CT specimens, a minimum ligament size necessary to contain the frontal process zone and thus a K_R-Δa behavior free of structure size is observed.

Creep results obtained using three point bending tests are also presented for these materials and for SiC-MLAS materials,

2. INTRODUCTION

Continuous ceramic fiber-reinforced ceramic matrix composites (CMCs) are a category of structural materials which is favourably considered regarding the sustained efforts devoted to it. The reasons for that are their potential capabilities and the results more than encouraging obtained during these last few years. The potentialities are those of ceramic materials, i.e. low density and chemical inertness associated with a unique capability in the retention of strength at high temperature, plus the possibility to provide multidirectional reinforcement. Two steps are to be distinguished regarding the progress in the mastery of these materials : the elaboration and the mechanical characterization. The main results in the control of the elaboration processes indicate that efficient CMCs are obtained when the fiber-matrix bonding is weak enough. This is obtained when partial debonding occurs on cooling the materials from the elaboration temperature (for interphases subject to residual tension), or through the use of an interphase material (1,2). In such materials, the fracture energy is increased over the sum of the surface energies of the constituants by mean of interacting toughning mechanisms. The most important of them are: (i) the development of a non-linear process zone at the tip of the macroscopic crack (where matrix cracking and fiber-matrix debonding prevail) ; (ii) the shielding of the growing macrocrack tip by the intact fibers bridging the cracks walls in the wake; (iii) sliding and pull-out of the broken fibers from the matrix (governed by the frictional characteristics of the debonded interface). The reasons of the outstanding progress in the characterization of CMCs are twofold. On the one hand, it results from the various and recent experimental methods developped to assess the microstructural parameters which govern these mechanisms (3-6) and from the analytical approa-

Presented at an AGARD Workshop entitled 'Introduction of Ceramics into Aerospace Structural Composites', April, 1993.

ches proposed for modelling their effects (7-10). On the second hand, the progress in the mechanical characterization of CMCs follows from the extension of linear elastic fracture mechanics (LEFM) concepts to assess non-linear fracture toughness parameters, namely the R-curve behavior (11-15). Meanwhile, only few investigations deal with the effects of the specimen size and geometry on the fracture toughness of CMCs (16), although these enquiries had been encountered for heterogeneous materials such as concrete, mortar and rock (17,18). For CMCs the dependence of fracture toughness parameters on specimen size follows from the limited dimensions of laboratory test pieces comparatively to the extent of the process zone (frontal process zone and bridging zone). The specimen geometry and the loading configuration affect the fracture parameters since they determine the effective mode of crack surface displacement.
Very few works concern the creep behavior of CMCs, although creep results are very important as it informs on life-time and strain-time evolution for and arbitrary loading. One can only quote the investigations on 2D SiC/C/SiC (19), 1D SiC-Si_3N_4 (20), 1D or 2D SiC-1723 (21), 2D Al_2O_3-SiC (22) and 1D SiC-MLAS (23).

The purpose of the present study was to examine the effects of the specimen size and geometry on the R-Curve behavior for two types of SiC/C/SiC composite materials different by the fiber-matrix bonding. To accomplish this, in-situ matrix crack lengths were used for SENB and CT specimens with different relative notch lengths (24). Comparative investigation on the creep behavior of SiC/C/SiC and SiC-MLAS composites are also presented.

3. MATERIALS AND METHODS

3.1. Materials

The materials under study are two different types of 2D SiC/C/SiC composites elaborated by the Société Européenne de Propulsion, Etablissement de Bordeaux. The reinforcement consists in a stack of equilibrated bidirectional woven cloths of Nicalon fibers (NLM 202 ceramic grade type of ultimate strain ε_r^f =1%; Young's modulus $E_f \simeq 200$ GPa; 40 Vol. %). Prior to the deposit of the matrix, this fibrous architecture was coated with a thin layer of pyrocarbon (the interphase material, $\simeq 0.1$ μm thick).

Both the pyrocarbon and the β-SiC ceramic matrix (of ultimate strain and Young's modulus $\varepsilon_r^m \simeq 0.035$ % and E_m = 350GPa, respectively) were obtained using an isothermal-isobaric chemical vapor infiltration process (25). The remaining porosity is 10 to 15 Vol. % and the final density of the materials is $d \simeq 2.5$ g/cm^3. Morphological and physical properties of these materials have been extensively reported (26-29). The difference between the two types of the composites (termed type A and type B) lies in the texture of the interphase (30). Although the interphase material and the matrix are the same for both types, in type B materials the surface of the fibers had been pretreated prior to the deposit of the pyrocarbon. Hence type B materials show a more efficient load transfer capability from the fibers on the matrix, the ultimate strain is higher than 0.40 % whereas type A materials possess an ultimate strain value $\varepsilon_r \simeq 0.20$ %. For both types of materials the longitudinal Young's modulus is E_c = 230 GPa. Typical uniaxial tensile loading curves are shown in Fig. 1.

The SiC-MLAS materials elaborated by Aérospatiale, Etablissement de Bordeaux, consist in a unidirectional arrangement of SiC Nicalon fibers (32 vol.%) embedded in a MLAS matrix obtained by a sol-gel route. Physical properties of these materials include a density of 2.47 g/cm^3, a Young's modulus of 127 GPa and a 4 point bending strength of 800 MPa.

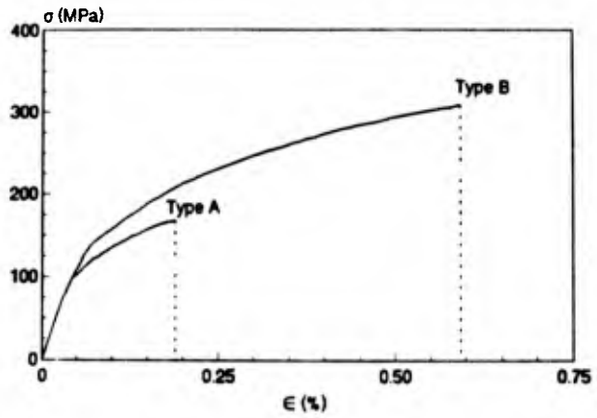

Fig. 1 : Behavior of the two types of materials under uniaxial tensile loading.

3.2. Specimens and mechanical tests

The dimensions of the three point bending test specimens were 100x10x3.5 mm^3 and 100x10x2.9 mm^3 for types A and B materials, respectively (span L = 90 mm and width W = 10 mm). The bending tests were displacement controlled with a cross-head speed v_T = 10 µm/min.

Two sizes of geometrically similar compact tension specimens in accordance with the specifications of ASTM Standarts E399-74 were tested (W = 20 and 40 mm, B=3 mm) and the displacement of the loading point was measured using a linear variable differential transducer connected between the loading axes. For both types of specimens, one large surface was finely polished using different grades of diamond paste and the notch plane was machined in the edge-wise direction. The relative notch depth was changed from 0.1 to 0.4 for the SENB specimens and from 0.2 to 0.5 for the CT specimens. All the tests were run on an electromechanical testing machine (Schenck RMC) equiped with a 100 KN load cell.

Creep tests were performed in three-point bending (20x5x2 mm^3), under vacuum (~ 10^{-4} torr) in a Sesame opening furnace in the 1173-1673K temperature range. The furnace is machine. Push rods were in tungsten with knives in TiC (ø = 5 mm). Displacement was measured on the external part of the device using several linear variable differential transducers (with an accuracy better than 1 µm). All tests were performed at constant stress in the 25-450 MPa domain.

3.3. Crack length measurements

3.3.1. *In-situ matrix crack length measurement on the polished surface*

In-situ crack length measurements were performed by monotoring the matrix crack tip position on the polished surface of the specimen during the test (31). The experimental setup consists in an optical microscope connected to a stage moving in a vertical plane parallel to the surface of the specimen. A camera was used for photographs; a video camera, a monitor and a magnetoscope could also be connected to the basic set for records.

3.3.2. *Post-mortem crack length measurement on the surfaces of rupture*

For each type of specimen and for each type of materials, identical specimens (same relative notch length, a_0/W) were loaded at different levels P_i and then unloaded, and loaded again until the reloading loop meets the preceding unloading loop. Then a hot sealing wax was pourred in the notch root in the aim to mark the crack walls. This operation was repeted a few times. The crack growth increment Δa_i is defined as the mean value measured on the front of the wax. The local compliance value, C_i (and the permanent displacement Δh_i) associated to P_i and Δa_i, was measured as the tangent line to the reloading loop passing through the unloading point (32). Because of the non-elastic fracture behavior, the local compliance C_i is different from the compliance C_i when no residual displacement is present.

3.4. Data reduction

The crack growth resistance curves were worked out either in the form of the potential energy dissipation per unit area of fractured surface, R, or in the form of the stress intensity-derived toughness parameter, K_R. The modified potential energy release rate R is presented as the sum of a pseudo-linear elastic term GR1 and a component GR2 including dissipation energies at the crack tip and in the wake regions (12,15) :

$$GR1 = \frac{P^2}{2B}\frac{dC}{da} \qquad (1)$$

$$GR2 = \frac{P}{B}\frac{d\Delta h}{da} \qquad (2)$$

$$R = GR1 + GR2 \qquad (3)$$

The analytical expression used for K_R is the general one for isotropic elastic specimens :

$$K_R = \sigma Y\sqrt{a} \qquad (4)$$

For SENB specimens σ is the maximum tensile stress applied in the beam corresponding to the current crack length a, and Y is a factor expressed as a function of the relative notch depth $\alpha = a_0/W$:

$$Y = 1.99 - 2.47\alpha + 12.97\alpha^2 - 23.17\alpha^3 + 24.8\alpha^4 \qquad (5)$$

For CT specimens, the analytical expression used for K_R is :

$$K_R = \frac{P}{BW^{1/2}}\, Y\,(a/W) \qquad (6)$$

where Y is the polynomial proposed by Srawley (33) :

$$Y = ((2+\alpha) / (1-\alpha)^{3/2})\,(0.886+4,64\alpha - 13.32\alpha^2 + 14.72\alpha^3 - 5.6\alpha^4) \qquad (7)$$

4. RESULTS

4.1. Loading curves and in-situ matrix crack lengths

4.1.1. *SENB specimens*

Figure 2a shows a monotonic loading curve, the associated in-situ matrix crack lengths and the crack lengths measured on the surfaces of rupture of identical specimens pre-stressed at different load levels as function of the displacement, for type A materials. A subcritical crack is observed on the surface of the specimen whereas no wax front is noted until the maximum load value is reached. From P_{max} onwards, the in-situ matrix crack length is identical to the one obtained using the wax. Type B materials behave totally different : two or more subcritical cracks develop from the notch root which are further connected by microcracks parallel to the loading axis. The macroscopic crack reflects the successive fractures of fiber bundles and is not fully controlled (Fig. 2b). So, both preceding methods for macroscopic crack length measurement fail. But as all the compliance lines (as defined above) meet at the origin O (0,0), we shall consider that type B materials behave linear elastic. Then for the SENB specimens of the type B materials, the crack length a is taken to be the equivalent crack which gives the same reloading compliance. The iterative expression derived from a Y(a/W) polynomial proposed by Wilson (34) is used to calculate crack growth increments (31,35,36).

$$\Delta a = a_n - a_{n-1} = \frac{W-a_{n-1}}{2}\,\frac{C^*_n - C^*_{n-1}}{C^*_n} \qquad (8)$$

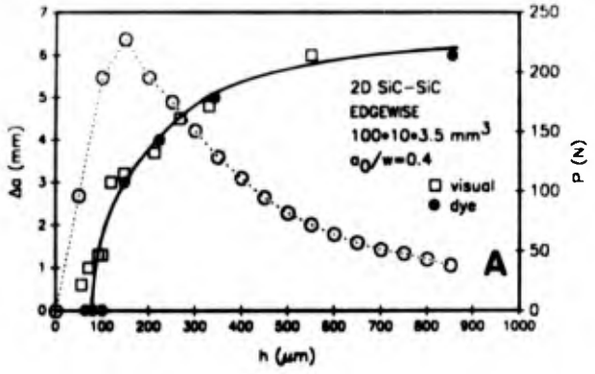

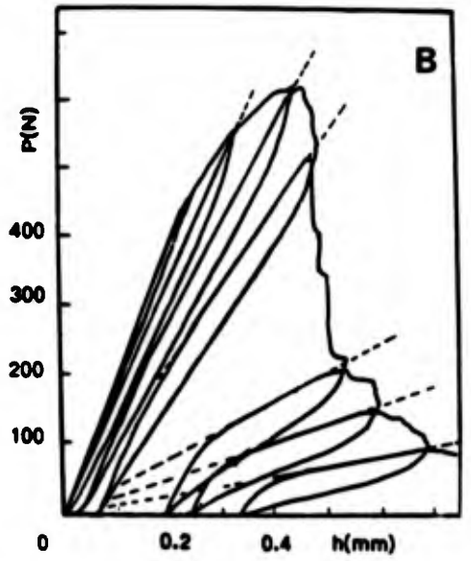

Fig. 2 : (a) Correlation of the monotonic loading curve (---) to the in-situ matrix crack lengths (•) and the crack lengths obtained using a wax (□) for SENB specimens of type A materials; b) loading-unloading curve for SENB specimen of type B materials.

4.1.2. *Compact Tension specimens*

The monotonic loading curves of figures 3a and 3b are relative to a small size specimen (W = 20 mm) and a large specimen (W = 40mm) of type A materials, respectively. The correlations of these loading curves with the macroscopic matrix crack growth show that damaging initiates in the earlier stage of the loading sequence, within the zone of apparent linear elastic behavior.

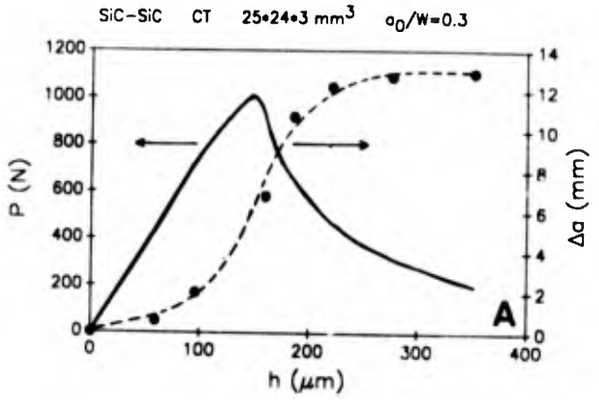

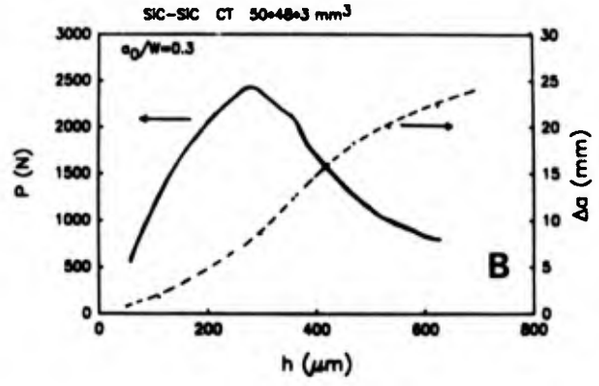

Fig. 3 : Monotonic loading curves (-) and associated in-situ matrix crack lengths for small (a) and large (b) specimens of type A materials.

4.2. Modelling the matrix crack

Usual compliance C^*, and local values, C (defined above), are presented in figure 4 as function of the matrix crack growth, Δa, for large compact tension specimens of type A materials. As the crack grows, the size of the bridging zone extends and for a given crack length value, the difference $C^*(a) - C(a)$ is linked to the importance of the bridging of the matrix crack by the fibers (37). Fig. 5 presents a schematic of the matrix crack in a unidirectional composite material (35). The usual compliance C^* is related to the portion a_n of the matrix crack where the crack walls are traction free a_r = (a)+(b)

(Fig. 5) and its increment is given by expression (8). The portion where the matrix is fractured but the fibers remain intact or are broken but can undergo sliding in the matrix seath is the bridged region $\tilde{a}_n$ = (c) + (d) (Fig. 5) which extent is evaluated by (38) :

$$\tilde{a} = (W - a)\frac{\Delta h}{h} = (W - a)\frac{C^* - C}{C^*} \qquad (9)$$

where (W - a) is the remaining ligament ; h and Δh are the total and residual displacements, respectively.

The matrix crack length is then :

$$\bar{a}_n = a_n + \tilde{a}_n = \qquad (10)$$

$$\frac{W - a_{n-1}}{2}\frac{C_n^* - C_{n-1}^*}{C_n^*} + (W - a_n)\frac{C_n^* - C_n}{C_n^*}$$

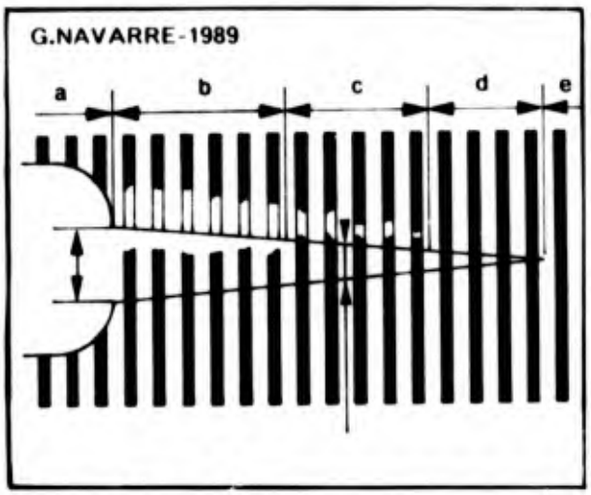

Fig. 5 : Schematic of a propagating crack in a unidirectional composite material : (a_0) is the notch; (b) crack mouths are traction free; (c) crack months are bridged by broken fibers; (d) matrix crack is bridged by intact fibers; (e) intact remaining ligament and frontal process zone.

For both types of specimens of type A materials, the crack lengths gained from expression (10) are shown to provide a fair description of the in-situ matrix crack lengths (Fig. 6a and 6b).

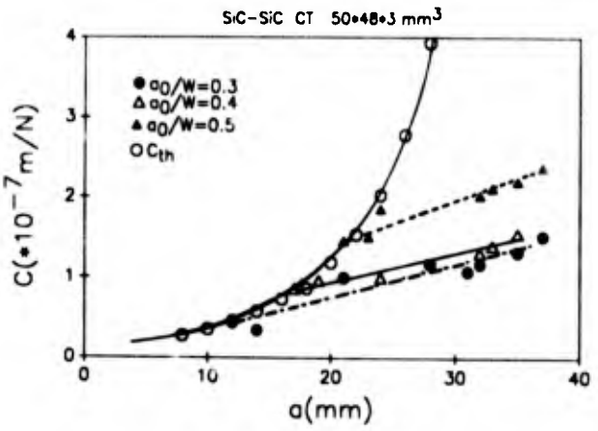

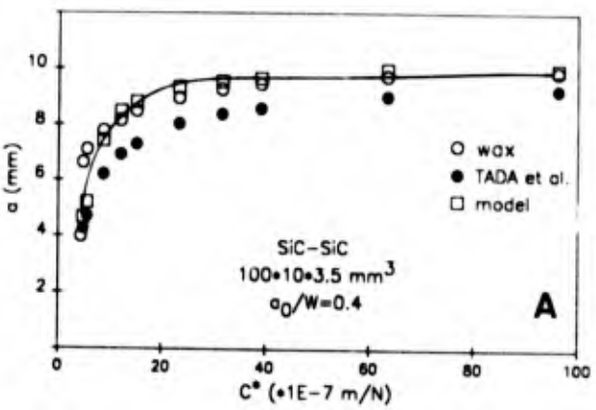

Fig. 4 : Illustration of the importance of the bridging effect by the differences between the local compliance C and C for large CT specimens of type A materials.

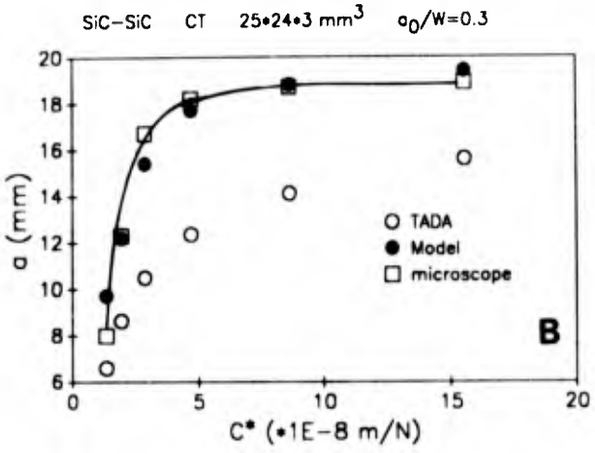

Fig. 6 : Intercomparison of experimental crack lengths for type A materials and results obtained from models : (a) experimental values are obtained using a wax; (b) experimental values are in-situ matrix crack lengths.

4.3. Crack growth resistance curves

4.3.1. *SENB specimens*

The non-linear fracture parameters R, GR1 and the GR2 are shown in Fig. 7a as function of the matrix crack length for type A materials. Starting from a low value ($\simeq$ 200 J/m^2), the resistance curve R increases slowly first in the domain of subcritical crack growth and then rises as the macroscopic crack extends toward the opposite side of the specimen. The quasi-elastic component GR1 remains very low with a plateau value of 630 J/m^2 during quasi-static crack propagation. In figure 7a the linear elastic energy release rate G_R^* is shown to be a fair estimation of the resistance R. The effects of the specimen thickness B and the relative notch length a_0/W on the resistance curve are shown in figure 7b. The influences of the crack bridging and the remaining ligament size on the resistance values appear clearly when intercomparing these curves.

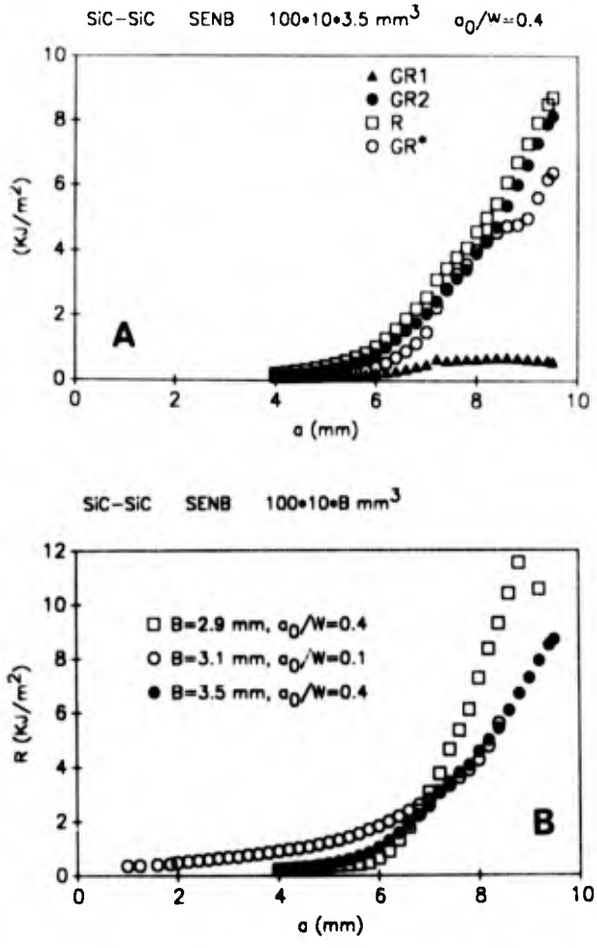

Fig. 7: (a) Non-linear fracture parameters R, GR1, GR2 and linear elastic energy release rate GR* as function of the matrix crack length, for a SENB specimen of type A material; (b) influence of the specimen thickness and of the relative notch length on the resistance curve.

Figure 8 shows the incremental work of fracture as a function of the effective crack length for a specimen of type B materials. The linear-elastic energy release rate reaches a saturation value of 15 kJ/m^2 after a subcritical crack growth of 2 mm. The K_R-curve rises from an initiation value $K_R^{in} \simeq$ 8 to 13 MPa$\sqrt{m}$ up to a plateau-like value of 40 MPa$\sqrt{m}$ for both monotonic loading and loading-unloading conditions (Fig. 9).

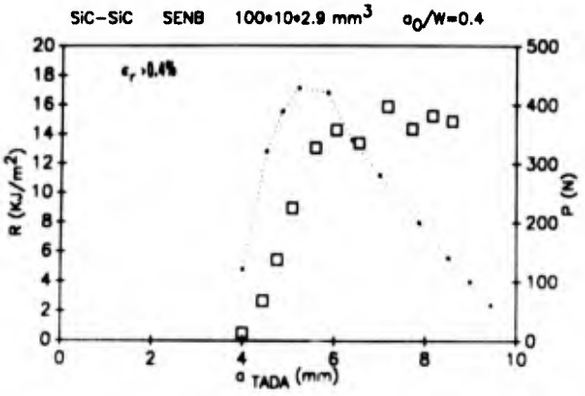

Fig. 8 : Incremental work of fracture as function of the effective crack length for a SENB specimen of type B materials. The dash line represents the loading curve.

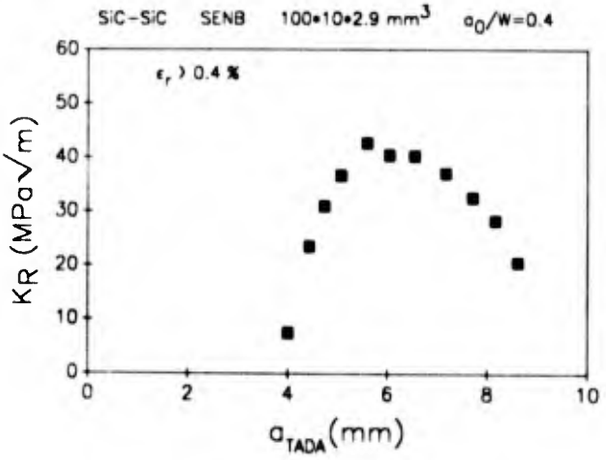

Fig. 9 : K_R-a curve for a SENB specimen of type B materials.

4.3.2. *CT specimens*

The linear elastic energy release rate G_R^* and the energy release rate when non-linear fracture mechanisms exist, R, are shown in figure 10a for type A materials. Both parameters increase continuously with the matrix crack length as we pointed it out for SENB specimens. At the opposite, the R curve of the large specimens of type A materials clearly exhibit a maximum value when the relative notch depth a_0/W is less than 0.5 (Fig. 10b) but the quasi-elastic component GR1 still remains at a low level. This behavior of the resistance curve is also observed for the elastic energy release rate $\overset{*}{GR}$ of small specimens of type B materials whatever the notch depth (Fig. 11a). The maximum values reached depend strongly on the relative notch length. At the contrary, the $\overset{*}{GR}$ curve of a large specimen with a relative notch depth $a_0/W = 0.2$ exhibits a steady state level of 23 kJ/m^2 by a crack extension $\Delta a \simeq 12$mm, (Fig. 11b). The K_R-curves of the small specimens of type A materials start at the same initiation value $K_R^{in} = 4.5$ MPa $\sqrt{m}$ and increase with a parabolic shape, whatever the initial notch depth (Fig. 12a).

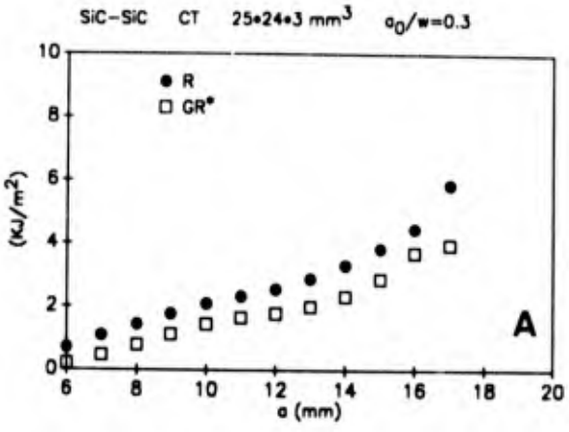

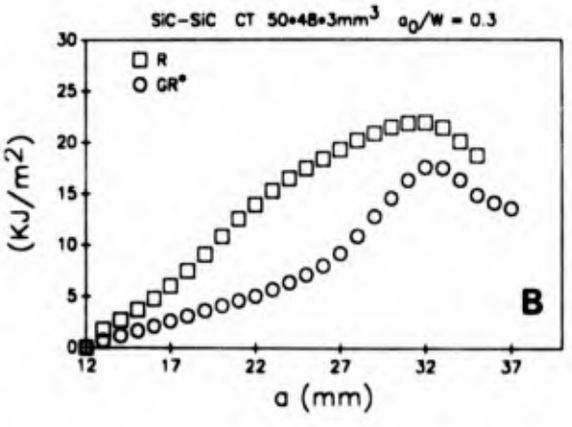

Fig. 10 : R and $\overset{*}{GR}$ as function of the matrix crack length for (a) small and (b) large CT specimens of type A materials.

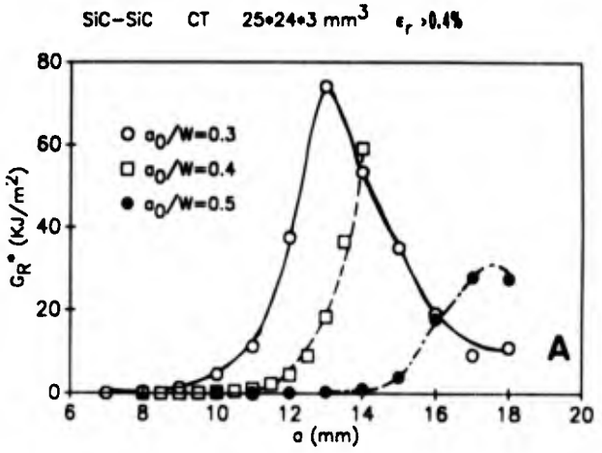

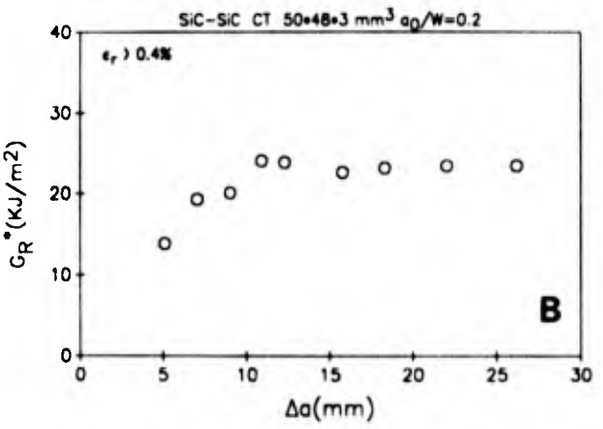

Fig. 11 : Linear elastic energy release rate for type B materials : (a) small size CT specimens; (b) large CT specimen.

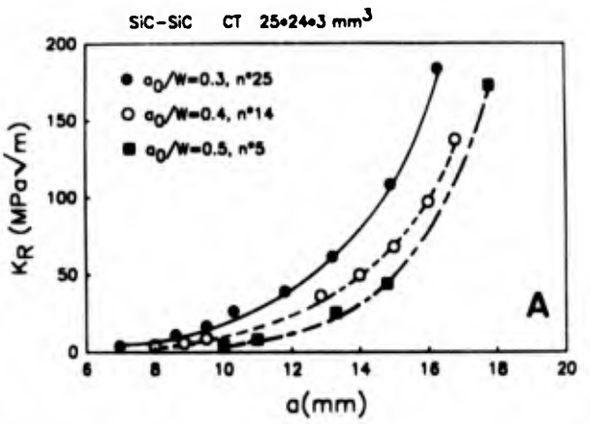

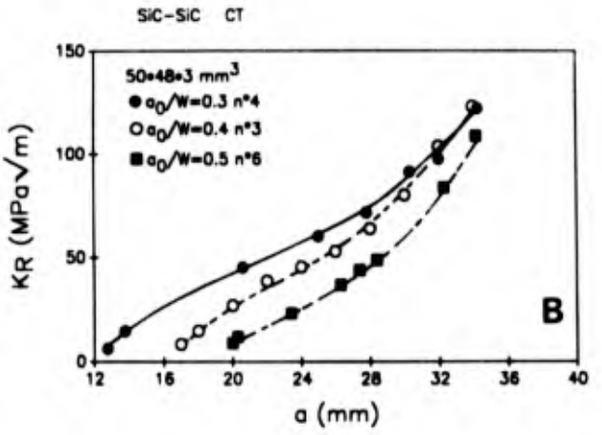

Fig. 12 : K_R-a curves for type A materials: (a) small and (b) large CT specimens.

The resistance curves associated to the large specimens with relative notch length $a_0/W \geq 0.5$ behave similarly but start from an initiation value K_R^{in} = 3.5 MPa$\sqrt{m}$ (Fig. 12b). The reduction of the relative notch length (a_0/W = 0.3 to 0.4) results in a totally different behavior of the K_R-curve, but the initiation value is unchanged.

For small specimens of type B materials, the K_R curves behave similar to those of indentical specimens of type A materials but the initiation value is much higher (K_R^{in} = 7 to 8.5 MPa$\sqrt{m}$) as a consequence of a less weak fiber-matrix bonding (Fig. 13a). An increase in the size of the specimen results in a K_R-Δa curve which increases up to a plateau value of 67 MPa$\sqrt{m}$ and then rises (Fig. 13b).

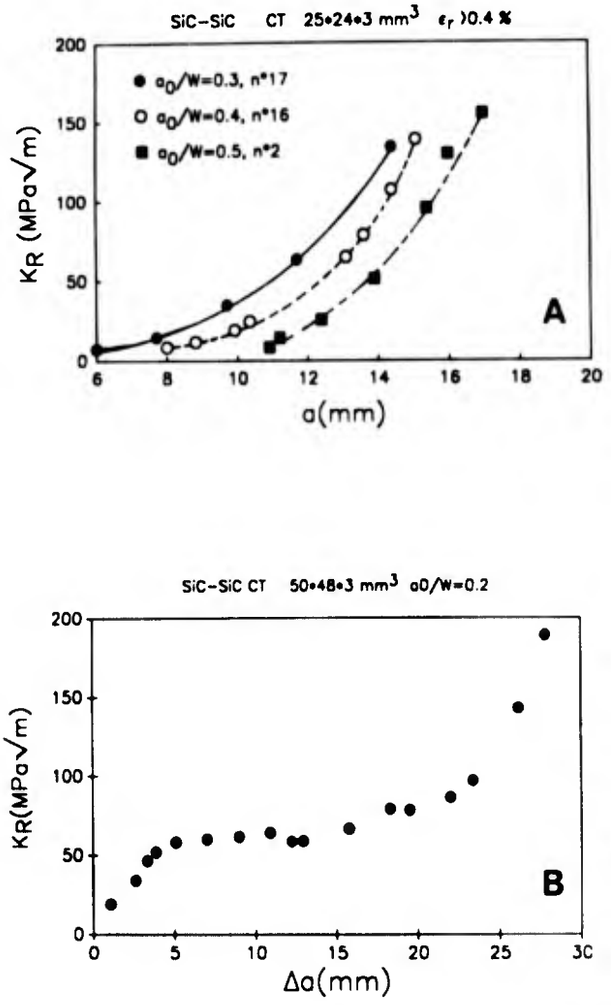

Fig. 13 : K_R-Δa curves for type B materials (a) small and (b) large CT specimen.

4.4. Creep results

The analysis of the steady-state creep rate, $\dot{\varepsilon}$, as a function of the applied stress, σ, indicates that in both cases several mechanisms arise depending on stress and temperature (Fig. 14) (19, 39, 40)

In the case of SiC/C/SiC, thanks to AlN marks (41), and then to an accurate localisation of the neutral axis, a deconvolution method has been proposed. From bending tests the curves of creep rate as a function of stress in tension and in compression have then been deduced. The obtained threshold stress values at 1473 and 1573K are of the same order of magnitude than that obtained experimentally during short time tests in tension (respectively 80 and 60 MPa). The stress exponent lies between 1.4 and 2 for low stress values respectively at 1473 and 1573K, and 5.6 and 3.2 for 1473 and 1573K at high stresses.

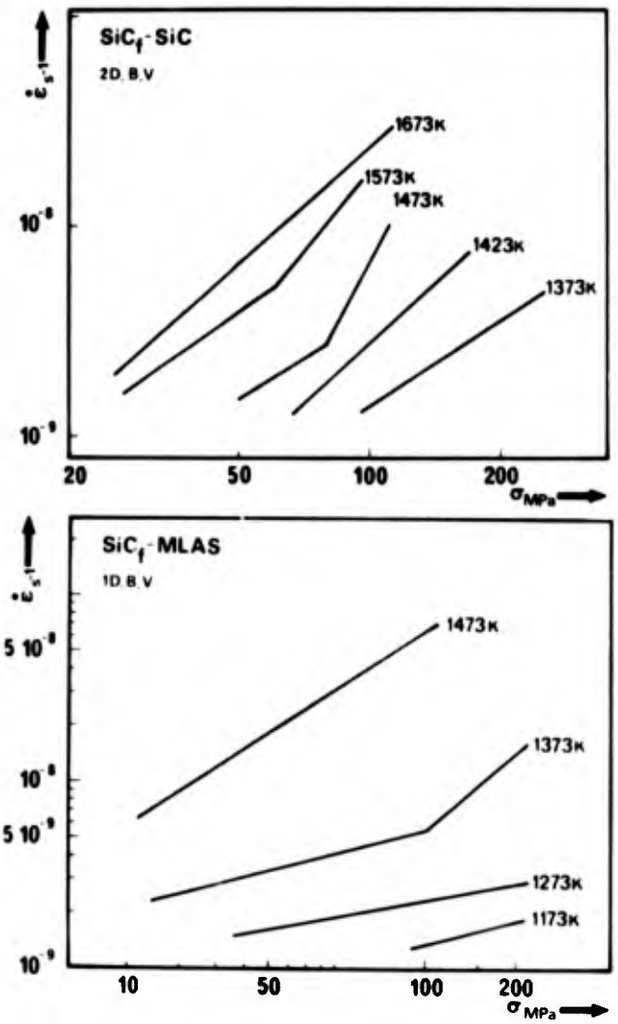

Fig. 14 : Change in the steady-state creep rate, $\dot{\varepsilon}$, as a function of the applied stress, σ, for 2D SiC-SiC and 1D SiC-MLAS tested in three point bending at different temperatures, under vacuum.

In the transitory and stationnary stages there exists a damaging zone with decohesion and microcracking. Its evolution has been modelled from the stress relaxation associated to the transitory stage, confirming the existence of the stationnary stage.

The origin of the change in stress levels on the fibers and the interfaces during the transitory stage is due to the fiber creep from 1373K and to the fiber recrystallisation over 1473K.

During the transitory and stationnary stages the damaging zone exists over a threshold stress value of which the change has been correlated to the measurements of interfacial shear stress, τ_i, by push-in method (39).

Taking into account the value of the damaging zone preceding the beginning of the tertiary stage and in introducing a parameter of continuum damaged mechanics, D, it has been possible to describe the tertiary stage and then the lifetime of this CMC from a damaging parameter, D, (from the Kachanov's analysis).

In the case of SiC-MLAS materials, the transitory stage has been modelled by a Zener cell (spring parallel to a Maxwell element) which takes into consideration the elastic behavior of the fibers and the viscoelastic behavior of the matrix (42).

As one can see on figure 14 in the stationnary state, three domains appear with lower values of n than for SiC/C/SiC. To each domain of stress exponent a certain damaging feature was observed in the tensile zone of the specimens (43,44) :

- low temperatures and low stresses : n = 0.3-0.4, with a damaging by decohesion and matrix microcracking parallely to the fibers,
- low temperatures and high stresses: n ∝ 1.4, with a damaging by decohesion and matrix microcracking parallely and perpendicularly to the fibers,
- high temperatures : n ∝ 1.0, no damaging by microcracking is observed during the stationnary stage ; the deformation of the composite is governed by the viscous flow of the vitroceramic matrix and the creep of the SiC fiber.

To explain the mechanisms responsible for the deformation for the two domains at low temperatures (n=0.3-0.4 and ∝ 1.4) the hypothesis of a weak fiber/matrix interfacial cohesion is proposed : it comes down to a supplementary deformation which is to add to that obtained during the transitory stage. Then one considers that parallel microcracking is linked to stress concentration arising at the interface.

5. DISCUSSION

5.1. Matrix crack, Bridging zone size

The combination of the in-situ matrix crack measurement using an optical microscope with the dye penetrant technique provides reliable natural crack length values in fibrous composite materials. Earlier investigations used directly optical crack length values measured on the surface of the specimen, (12,45), but with our SiC/C/SiC materials with $\varepsilon_r^m < \varepsilon_r^f$ it was worth to verify that the surface crack lengths were identical to the values measured on the surfaces of rupture. Moreover, this method is much more easy to implement than the one which consists in a drilling-hole in the specimen (46).

The interest in utilizing matrix cracks rather than effective cracks for the calculation of resistance curves is manifest when recalling that these materials are destined for high temperature applications. Then matrix fracture signifies the onset of permanent damage, the loss of protection provided by the matrix against corrosion and oxidation of the fibers.

The importance of the bridging zone size, represented by the difference between the matrix crack length and the value calculated using expression (8), is shown in figure 15 as function of the crack extension for a large CT specimen of type A materials. A steady state value of the bridging zone size is not observed even after a crack growth increment of 20 mm. Depending on the saw-cut notch length, the bridging zone size increases to 7.3 mm for a_0/W = 0.3 or 0.4 and 6.2 mm for a_0/W = 0.5, and

then decreases. These maximum values correspond to crack growth increments Δa = 14, 10 and 8 mm respectively, that means a total crack length a = 26 mm (from a_0 = 12 and 16 mm) and a = 28 mm (from a_0 = 20 mm). The decrease can be explained by the progressive fracture of the fibers located near the notch tip due to bending as the crack enters in the compressive zone of the remaining ligament.

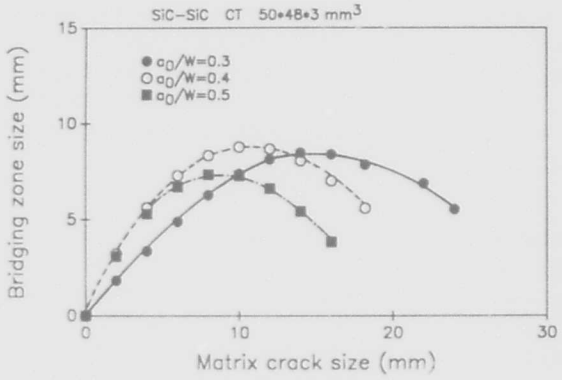

Fig. 15 : Variation of the bridging zone size as a function of the matrix crack size for large specimens of type A materials.

5.2. Resistance curves and frontal process zone size

The resistance curves R-Δa, GR^*-Δa and K_R-Δa for type B materials have been calculated assuming a linear elastic behavior because the reloading compliances met at the origin point. This behavior is confered by a relatively strong fiber-matrix bonding which induces an intense microcracking of the brittle matrix as a consequence of a good load transfer from the fibers on the matrix (Fig. 16a). As the fiber-matrix debonding is not favoured, very short pull-out lengths are observed on the surfaces of rupture and the fracture in the brittle matrix around the fibers is not fully brittle (Fig. 16b). Moreover, the application of the Irwin's relationship $K_R = (E' G_R^*)^{1/2}$ when using the steady state values of the K_R-Δa and G_R-Δa curves (67 MPa$\sqrt{m}$ and 23 kJ/m^2, respectively) gives E' =195 GPa which is consistent with the longitudinal Young's modulus E_c = 230 GPa. This testifies the linear elastic behavior of type B materials which is highly damage tolerant (47).

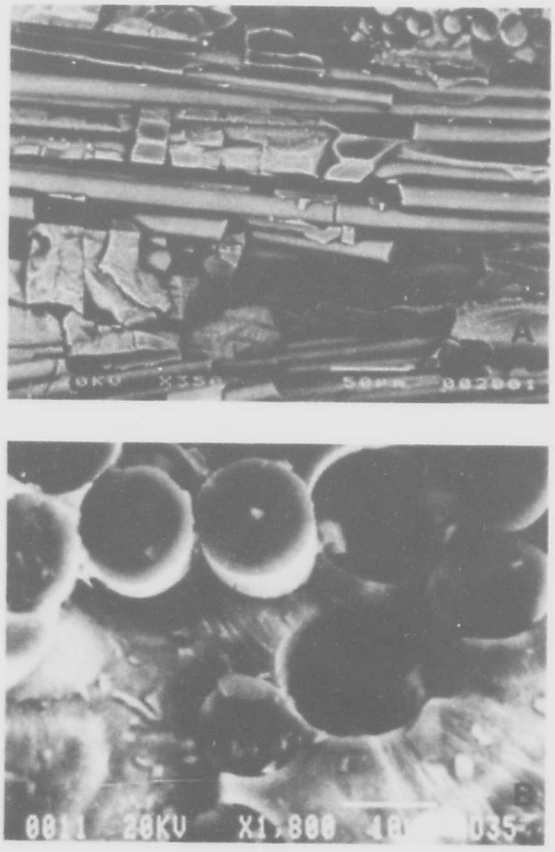

Fig. 16 : (a) Intense microcracking of the brittle SiC matrix; (b) short pull-out lengths and weavy fractures on the surfaces of rupture of type B materials.

From a notch depth a_0 = 8 mm, the K_R-Δa curve of figure 13b starts rising by a crack growth Δa = 16 mm. This corresponds to the interaction of the frontal process zone with the compression zone of the ligament or with the opposite side of the specimen. The maximum size of the frontal process zone along the direction of crack propagation is then W = (a_0+Δa) = 16 mm, which is consistent with the remaining ligament size when the bridging zone size starts decrea-

sing for type A materials. Hence, the continuous increase in the resistance curves of the SENB specimens of type A materials and the small CT specimens of both types of materials means that the ligaments ($W-a_0$) were too narrow for the frontal process zone to develop fully (9).

The effect of the frontal process zone size relatively to the ligament width on the behavior of the resistance curve is illustrated in figure 17 where the K_R-curves of the two sizes of CT specimens of type A materials are compared. Different domains are apparent, depending on the specimen size :

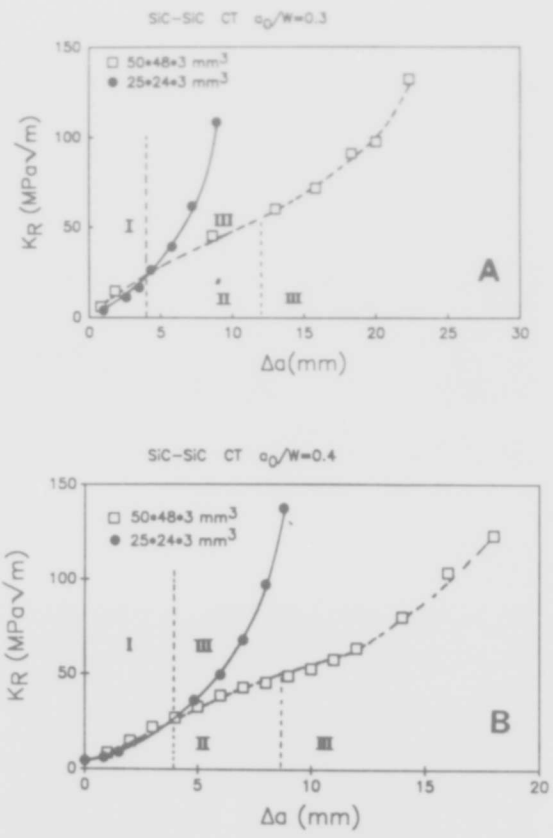

Fig. 17 : Comparison of the K_R-Δa resistance curves for a small and large CT specimen notched at $a_0/W=0.3$ (a) and $a_0/W = 0.4$ (b) . The different domains of behavior are depicted :

- in domain I ($\Delta a < 4mm$) the K_R values are identical for both sizes of specimen; this corresponds to the creation of a frontal process zone,
- domain II is observed only for large specimens. It is characterized by a full development of the frontal process zone size which propagates continuously within the ligament. Meanwhile, the matrix crack is bridged by the fibers and the size of this bridging zone has not reached a steady-state value. In domains I and II the K_R curves behave like $\sqrt{a}$, as far as the frontal process zone is totally contained within the remaining ligament,
- domain III is characterized by a parabolic behavior of the K_R-curve. For the small specimens this behavior is related to the wedge of the frontal process zone before it reaches a steady state size (insufficient size of the remaining ligament) while the matrix crack is bridged by the fibers and damage continues growing. Large specimens behave similarly as the frontal process zone stumbles over the compression zone of the ligament or the opposite side of the specimen. Figures 18 show an example of the surface of rupture of a CT specimen of type A materials.

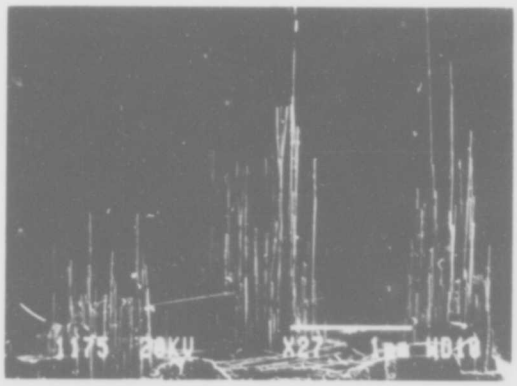

Fig. 18 : Long pull out lengths observed on the surfaces of rupture of a CT specimen of type A materials.

Again, the change in the behavior of the K_R-curves from domain II to domain III corresponds to a remaining ligament size of 16 mm. Meanwhile, this value has to be confirmed using larger specimens, i.e. W > 40 mm. In fact, for the same materials and using the data reduction formula (6), the results obtained by Conchin et al. (36) give an estimate of the frontal process zone size of 4 mm, which is low compared to the values discussed above. The discrepancy should be attributed to the methods used for crack lengths measurement (effective crack length versus matrix crack lengh). Thus, for the comparison of resistance curves, it is important to use not only the same data reduction formula, but also the the same method for crack length measurement.

5.3. Creep behavior

Comparison of SiC/C/SiC and SiC-MLAS indicates that at equivalent temperature, SiC/C/SiC materials are more creep resistant than SiC-MLAS, but it confirms that their domain of uses is higher.

In any case, the predominant mechanisms are matrix microcracking, decohesion and interfacial microcracking, fiber creep and for glass or vitroceramic matrix viscous flow.

Although these two materials are made from the same SiC fibers (Nicalon® NLM 202), the fracture and damaging features are in fact very different (Fig.19) : fiber pull-out decreases with temperature in the 1173-1473K domain for SiC/C/SiC, while it increases in the same domain for SiC-MLAS. That evidences clearly the predominant role of interfaces and the importance of their degradation.

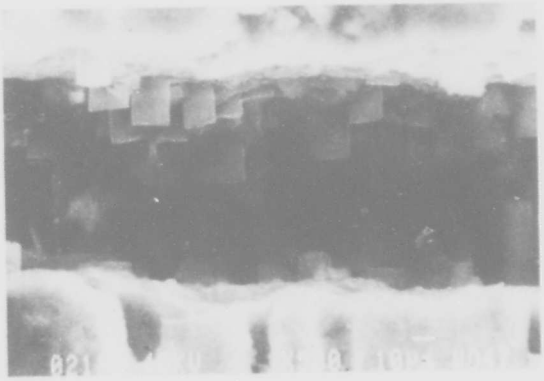

SiC-MLAS, 1373K

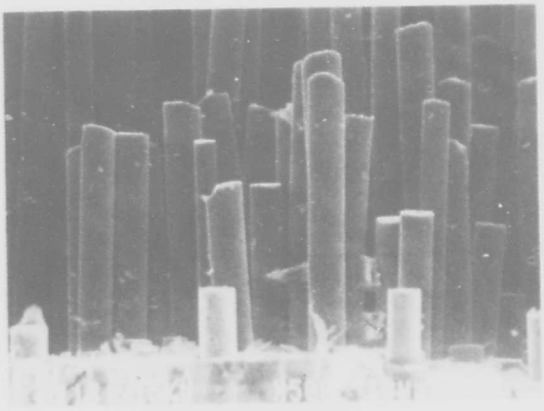

SiC-MLAS, 1473K

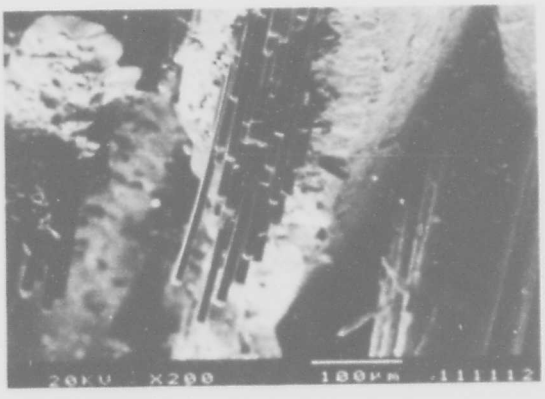

SiC/C/SiC, 1373K

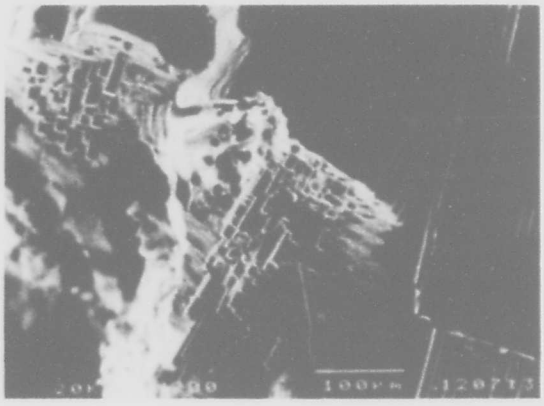

SiC/C/SiC, 1473K

Fig. 19 : Scanning electron micrographs of SiC-MLAS and SiC/C/SiC after creep tests at different temperatures.

6. CONCLUSION

In this paper we advocate the utilization of in-situ matrix crack length as far as possible, rather than an effective crack length, for the investigation of crack growth resistance of CMCs. The application of this method to SENB and CT specimens of bidirectional SiC/C/SiC materials shows that :

(i) SENB specimens may be suited for in-situ matrix crack length measurement, depending on the toughning mechanism specific to the type of materials, i.e the fiber-matrix bonding,

(ii) crack growth resistance curves obtained using SENB or CT specimens of small size (W = 20 mm) are strongly dependent on the specimen size because the full extend of the frontal process zone (≃ 16 mm) is larger than the ligament size,

(iii) for both types of materials, crack growth resistance curves non-dependent on specimen size are obtained when using large CT specimens (W = 40 mm),

(iv) intercomparison of the resistance curves of the two types of materials indicates that a weak fiber-matrix bonding is not a necessary condition for enhancing the fracture toughness. Tougher materials have been produced by promoting intense matrix microcracking (type B materials) against fiber-matrix debonding and pull-out of broken fibers (type A materials).

(v) attention must be paid when comparing resistance curves from different bibliographical sources : the crack length measurement method is important.

(vi) these CMC have a high domain of creep resistance where several mechanisms act and the aging of the fibers and of the interfaces must be taken into consideration

ACKNOWLEDGMENTS

This paper reports results from the thesis of ROUILLON M.H. (R-curve behavior of 2D SiC/C/SiC), ABBE, F. (creep of SiC/C/SiC) and KERVADEC, D. (creep of SiC-MLAS).
This work is part of national joint research programms in France created by CNRS, SEP, Aérospatiale, DRET, CNES, SNECMA and MRE(GS4C and GS Thermostructuraux) for investigations on CMCs. We thank SEP and Aérospatiale, for diligence in machining and delivery of the specimens.

7. REFERENCES

1. LOWDEN, R.A., and MORE K.L., "The effects of fiber coatings on interface shear strength and mechanical behavior of ceramic composites", Mater. Res. Soc. Proc., 1990, **170**, 205-14.

2. PROUHET, S., CMAUS,G., LABRUYERE, C., GUETTE, A. and MACKE, T., submitted to J. Am. Ceram. Soc.

3. AVESTON,J.,COOPER,G.A.,and KELLY, A., "Properties of fibre Composite", Proc. of National Physical Laboratory Conf., IPC Science and technology, Press Ltd, Surrey, UK, p 15 (1971).

4. MARSHALL, D.B. and OLIVER, W.C., "Measurement of interfacial mechanical properties in fiber-reinforced ceramic composites", J. Am. Ceram. Soc., 1987, **70**, 8, 542-548.

5. HSUEH, C.W., "Evaluation of interfacial shear stength, residual clamping stress and coefficient of friction for fiber reinforced ceramic composites", Acta Metall. Mater., **38** [3] (1990) 403-409.

6. CARTER, W.C., BUTLER, E.P. and FULLER, E.F. "Micromechanical aspects of asperity controlled friction in fiber-toughned ceramic composites", Scripta Metall. Mater. **25** (1991) 579-584.

7. WELLS, J.K., BEAUMONT, P.W.R., "Debonding and pull-out processes in fibrous composites", J. Mater. Sci., **20** (1985), 1275-84.

8. THOULESS, M.D., SBAIZERO, O., SIGL, L.S. and EVANS, A.G., "Effect of interface mechanical properties on pull-out in a SiC-fiber-reinforced lithium aluminum silicate glass-ceramic", J. Am. Ceram. Soc., **72** [4] (1989) 525-532.

9. ZOK, F. et HOM, C., "Large scale bridging in brittle matrix composites", Acta Metall. Mater., 1990, **38** [10], p. 1895-1904.

10. ZOK, F., SBAIZERO, O., HOM, C.L. and EVANS, A.G., "Mode I fracture resistance of a laminated fiber-reinforced ceramic", J. Am. Ceram. Soc., 1991, **74** [1], 187-193.

11. SAKAI, M., URASHIMA, K. and INAGAKI, M., "Energy principle of elastic-plastic fracture and its application to the fracture mechanics of a polycristalline graphite", J. Amer Ceram. Soc., 1983, **66**, 868-874.

12. MAI, Y.W. and HAKEEN, M.I., "Slow crack growth in cellulose fibre cements", J. Mater. Sci., 1984, **19**, 501-508.

13. SWAIN, M., and ROSE, L.R.F., Toughning of ceramics. In advances in Fracture Research, ICF6, Eds. S.R. Valluri et al., Pergamon Press, Exeter, 1984, **1**, 473-494.

14. SAKAI, M., and BRADT, R.C. "Graphical methods for determining the non-linear fracture parameters of silica and graphite refractory composites", J. Amer. Ceram.Soc., (1983) 66, 868.

15. GOMINA, M, THEMINES, D.,CHERMANT, J.L., OSTERSTOCK, F., "An energy evaluation for C-SiC composite materials", Int. J. Fract. **34**, (1987) 219.

16. COX, B.N., and LO, C.S., "Load ration, notch, and scale effects for bridging cracks in fibrous composites", Acta Metall. Mater., **40** [1], 69-80.

17. CARPINTERI, A., "Interpretation of the Griffith instability as a bifurcation of the global equilibrium", Advanced Research Workshop on Application of Fracture Mechanics to Cementitious composites, Sept. 4-7, 1984 Northwestern University Evanston, Illinois, USA.

18. BAZANT, Z.P. and KAZEMI, M.T., "Size effect in fracture of ceramics and its use to determine fracture energy and effective process zone length", J. Am. Ceram., Soc., 1990, **70**, 7, 1841-1853.

19. ABBÉ F., Thesis, Université de Caen, July 1990.

20. HOLMES J.W., "Tensile creep behaviour of a fibre-reinforced SiC-Si_3N_4 composite", J. Mat. Sci., **26**, 1991, p 1808-1814.

21. KHOBAIB M., ZAWADA L., "Tensile and creep behavior of a silicon carbide fiber-reinforced aluminosilicate composite", Ceram. Eng. Sci. Proc., **12**, 1991, p 1537-1555

22. ADAMI J.N, Thèse de Docteur ès Sciences Techniques, Ecole Polytechnique Fédérale de Zürich, 1992.

23. KERVADEC D., Thesis, Université de Caen, December, 1992.

24. ROUILLON, M.H., Thesis, Université de Caen, France, February 1993.

25. NASLAIN, R., "Two dimentional SiC/C/SiC composites processed according to the isobaric-isothermal chemical vapor infiltration gas phase route", J. Alloys Comp., (1992), **188**, 42-48.

26. BERNHART, G., LAMICQ, P., MACE, J., "Reliability of Ceramic/Ceramic Composites", Industr. Ceram., 1985, **790**, p 51.

27. LAMICQ, P.,BERNHART,G.,DAUCHIER, M. et MACE, J.G., "SiC-SiC Composite Ceramic", Am. Ceram. Soc. Bull., 1986,65 [2], p 336-338.

28. ABBE, F., CHERMANT, L., COSTER, M., GOMINA, M, CHERMANT, J.L., "Morphological characterization of ceramic-ceramic composites by image analysis" Comp. Sci. Tech. 1989, **34**, 37, p 109.

29. COJEAN, D., MONTHIOUX, M. et OBERLIN, A., "Phénomènes interfaciaux dans les composites SiC/SiC 2D de propriétés mécaniques variées", Comptes rendus des septièmes Journées Nationales sur les Composites JNC-7, 6-8 nov. 1990 Lyon, France (publiés par G. Fantozzi et P. Fleichmann, Paris, 1990), p 381-390.

30. MONTHIOUX, M., COJEAN, D., "Microstructures of interfaces related to mechanical properties in ceramic fiber reinforced ceramic matric composite", ECCM 5 (1992) 729-734.

31. GOMINA, M., "Crack length measurements in C/SiC Composite material", Int. J. Fract., 1987, **35**, R69-74.

32. GOMINA, M. and ROUILLON, M.H., "Etude de la résistance de composites; à fibres à la propagation de fissures naturelles", Comptes rendus des Septièmes Journées Nationales sur les composites JNC-7, 6-8 Nov. 1990, Lyon, France (publiés par G. Fantozzi et P. Fleichmann) p. 351-360.

33. SRAWLEY, J.E., "Wide Range Stress Intensity Factor Expressions for ASTM E399 standart Fracture Toughness Specimens", Int. J. Fract., 1976, **12**, 475-476.

34 WILSON W.K., Eng. Fract. Mech. 2 (1970) 169-171.

35. NAVARRE, G., Thesis, Université de Lyon, France, April 1990.

36. CONCHIN, F., BENOIT, M., ROUBY, D. and FANTOZZI, G., "Comportement à la rupture d'un composite céramique-céramique bidirectionel", Comptes rendus des Huitièmes Journées Nationales sur les Composites JNC-8, 16-18 Nov. 1992, Palaiseau, France (publiés par O. Allix, J.P. Favre et P. Ladevze) p 365-376.

37. SAKAI, M., "Fracture mechanics and mechanisms of fiber-reinforced brittle matrix composites", J. Ceram. Soc. Jap. (1991) 99 [10], 983-992.

38. FOURVEL P., Thesis, Université de Caen, France, September 1989.

39. ABBÉ F., CHERMANT J.L., J. Amer. Ceram. Soc., **73**, 1990a, p 2573.

40. ABBÉ F., CHERMANT J.L., In : "Creep and Fracture of Engineering Materials and Structures", edited by Wilshire B., Evans R.W., Proc. 4th Int. Conference, University College, Swansea, 1-6 April 1990, The Institute of Metals, 1990b, p 463.

41. ABBÉ F., CARIN R., CHERMANT J.L., J. Europ. Ceram. Soc., **5**, 1989, p 201.

42. KERVADEC D., CHERMANT J.L., In : "International Conference on Ceramic Matrix Composites" HTCMC-ECCM-6, Bordeaux, Sept 20-24, 1993, edited by Naslain R., 1993b, p...

43. KERVADEC D., CHERMANT J.L., In "8èmes Journées Nationales sur les Matériaux Composites", JNC8, 16-18 Nov. 1992, Ecole Polytechnique, Palaiseau, Proceedings edited by Allix O., Favre J.P., Ladeveze P., AMAC, 1992, p 63.

44. KERVADEC D., CHERMANT J.L. - In "5th International Conference on Creep and Fracture of Engineering Materials and Structures", University College Swansea, 28 March-2 April 1993, edited by Wilshire B., Evans R.W., The Institute of Materials, London, 1993a, p 401.

45. SHAH, S.P., "Fracture of cement and concrete", ICF6, Advances in Fracture Research, **vol 1**, 495-514. Eds S.R. Valluri et al., Pergamon Press, 1984.

46. MIYAJIMA, T. and SAKAI, M., "Fiber bridging of a carbon fiber-reinforced carbon matrix composite", J. Mater. Res., 1991,6, 539-547.

47. DESPIERRES, T., DRISSI-HABTI,M., GOMINA, M., "Comparative investigation of damage in two types of SiC/C/SiC composite materials under uniaxial tensile loading", to appear in the Proceedings of the third European Ceramic Society Conference.

48. ABBÉ F., CHERMANT J.L., In : "7èmes Journées Nationales sur les Matériaux Composites", JNC 7, 6-8 Nov., 1990c, Lyon. Proceedings edited by Fantozzi G., Fleischmann P., AMAC-CODEMAC, 1990c, p 401.

MICROSTRUCTURE AND MACROMECHANICAL BEHAVIOUR OF CMCs

by

M.H. Lewis, A. Chamberlain, A.M. Daniel, M.W. Pharaoh, A.G. Razzell and S. Sutherland
University of Warwick
Centre for Advanced Materials Technology
Department of Physics
Coventry CY4 7AL
United Kingdom

SUMMARY

A survey is presented of research aimed at an understanding of the relation between microstructure, interface properties and macromechanical behaviour of a range of silicate (glass ceramic) and nitride matrix composites.

For silicate CMCs, hot-pressing cycle (P/T) in relation to matrix chemistry and fibre type is critical in avoiding mechanical and chemical damage of fibres with consequent reduction in ultimate CMC strength.

Interfacial debond and shear stresses, measured via a fibre 'push-down' indentation technique exhibit a wide variation, dependent on CMC processing time, temperature and matrix chemistry and thermal expansion. 'Graceful' failure, typified by 3 stage stress-strain curves, may be obtained for debond energies Γ and shear stresses τ up to $\sim 20\ Jm^{-2}$ and ~ 50 MPa, respectively.

Interface-oxidation-induced property degradation occurs at intermediate temperatures (400-800°C) but is suppressed at higher temperatures by passive oxidation of SiC fibre ends which prevents further carbon interface removal by channelled reaction.

Higher temperature SiC (Textron CVD) monofilament based CMCs with Si_3N_4 (SRBSN) matrices have been fabricated using tape-cast matrix preforms. Partially sacrificial C-coatings on the monofilaments provide low Γ and τ interfaces and result in ideal composite response with separation between matrix cracking stress and ultimate stress, followed by filament pull-out. Although interface oxidation is a limiting problem for creep and stress rupture, these properties are superior to turbine superalloys.

1. INTRODUCTION

Of the many potential applications of ceramic materials in aerospace, the aero-engine field exemplifies the most demanding properties in relation to temperature, stress and environment, driven by the need for enhanced performance and efficiency. Improvements in materials and aerothermal technology over the past 50 years have resulted in increased thrust to weight ratios from 3:1 to 10:1 and take-off thrusts from 1000lbs to 50,000lbs. This trend would indicate respective values of 20:1 and 80,000lbs within the next decade, together with an aim of increased thermal efficiency via compression ratios up to 40/1 coupled with turbine entry temperatures approaching that for stoichiometric combustion (~2000K for kerosine). The attainment of such performance figures requires ceramic/metal substitution with the benefits of higher specific stiffness and strength at elevated temperatures.

After more than 20 years, in a number of national turbine-oriented programmes, few ceramic components have attained more than demonstrator-engine status. It is now generally recognised that for 'high-risk' aerospace applications the use of probabilistic failure criteria, intrinsic to brittle monolithic ceramics, is not acceptable without significant enhancement of fracture toughness (Kc).

The concept of 'damage-tolerance' via stress-transfer to high modulus aligned fibres following matrix microcracking in a service overload transient has been repeatedly demonstrated in CMCs. The classical 3 stage stress-strain response of long-fibre CMCs has also been modelled theoretically, consisting of a linear elastic range followed by a reduced modulus during progressive matrix cracking, reaching an ultimate stress at which fibre failure initiates and a final reduced-stress range associated with energy absorption during fibre pull-out. However, there are major problems in the application of CMCs concerning the difficulty and cost of fabrication, availability of small diameter ($\sim 10\mu m$) fibres with high temperature stability during fabrication or service and the synthesis of chemically-compatible and environmentally stable fibre/matrix interface layers which have a suitable debond and shear property within a range of high-temperature matrices. For one or more of these reasons it may be argued that existing CMCs have very limited application potential as aerospace materials, especially at temperatures above 1000°C. However, during the advance of new fibre syntheses, interface development and fabrication processes they will continue to be useful experimental models for generic CMC behaviour.

Presented at an AGARD Workshop entitled 'Introduction of Ceramics into Aerospace Structural Composites', April, 1993.

Most current CMCs based on polymer-precursor SiC-based fibres (Nicalon and Tyranno type) have a fortuitous combination of composition (Si-C-O) and non-crystalline structure which produces a controlled reaction with silicate matrices during fabrication, resulting in carbon-rich interfaces with appropriate debond/shear property. Based on the earlier work of Prewo et al [1], aluminosilicate glass composites such as Li_2O-Al_2O_3-SiO_2(LAS) have been used as matrices, in model composites, which form low thermal expansion phases on crystallisation (e.g. spodumene). More recently CaO-Al_2O_3-SiO_2 (CAS) matrix composites have been produced commercially (Corning, USA) and used in many basic studies of mechanical behaviour. However, relatively few research programmes have concentrated on the systematic variation in interface, matrix and processing parameters in comparing a wider range of microstructure with theoretical prediction. This has been the theme of a number of projects at Warwick which are reviewed in this paper. The research concerns a range of glass and glass-ceramic (silicate) matrix CMCs with differing chemistry and processing parameters together with higher-temperature CMCs composed of CVD SiC monofilaments within silicon nitride or sialon matrices.

2. GLASS AND GLASS-CERAMIC MATRIX COMPOSITES

2.1 Processing and Ultimate Strength

The ultimate theoretical strength (σ_u) of a unidirectional CMC has to be less than that given by the unrealistic assumption of equal load-sharing by all fibres in the cross-section;

$\sigma_u = V_f \bar{S}$, where V_f = fibre volume fraction (1)
and $\bar{S}$ = mean fibre strength

More realistic theories involve the statistics for fibre strength (specified by the Weibull modulus m); the treatments of Rosen [2] and, more recently, Thouless et al [3] yield similar values for σ_u but are based on differing assumptions about stress-distribution within fibres in relation to their failure origin. The Thouless et al analysis requires a knowledge of fibre/matrix interface shear stress τ and matrix microcrack spacing D in addition to m, fibre radius R and strength S;

$$\sigma_u = V_f\, S \exp\left[-\frac{1-(1-\frac{\tau D}{RS})^{m+1}}{m+1[1-(1-\frac{\tau D}{RS})^{m}]}\right] \qquad (2)$$

Using measured values for Nicalon fibres in various glass (borosilicate) and glass ceramic matrices these 'lower-bound' values for σ_u may be compared with experimental values from 3 point bend specimens (typical size 50mm X 3mm depth). In making this comparison it is clear that whereas the higher temperature fabricated glass ceramic matrix composites (GCMCs) provide reasonable agreement with equation 2, with lower temperature glass matrices σ_u, may approach the upper limit (Fig.1). A simplistic explanation (although not widely discussed in the literature) is that of thermal degradation of fibre strength and Weibull modulus which is known to occur in the isolated fibre state. Another possibility is that of surface mechanical damage induced by premature crystallisation and absence of totally viscous-flow-densification during hot-pressing. These observations have prompted a more detailed study and refinement of composition and processing variables in relation to fibre surface condition, covering a series of GMCs and GCMCs.

Critical features of the pressure/temperature cycle during hot pressing were a delayed pressure application until beyond the glass softening temperature and a critical choice of pressing isotherm in relation to crystallisation kinetics for GCMCs. Some of these features are summarised in Fig.2 which compares P and T profiles with the 'C-curve' for initiation of crystallisation. There is some control of the latter, and of glass softening range by selection of off-stoichiometric silicate compositions; the most convenient choice is near a eutectic join between primary phase (e.g. low thermal expansion aluminosilicates CAS-anorthite or MAS-cordierite) and binary silicate (wollastonite, $CaSiO_3$ or enstatite, $MgSiO_3$). This also facilitates control of matrix thermal expansion α relative to that of the fibre [4], for example cordierite ($\alpha \sim 2.6 \times 10^{-6}$) in phase-mixture with enstatite (α 8 x 10^{-6}) may span the range from negative to positive values with respect to SiC (Nicalon $\alpha \sim 3.1 \times 10^{-6}$).

In addition to P/T cycle and matrix composition, choice of fibre is important in minimising surface 'chemical' damage; carbon precoated Nicalon 607 inhibits interfacial cross-diffusion associated with the formation of C-rich layers by in-situ reaction and retains the pristine fibre surface topography and strength.

The remarkable elevation in GCMC bend strength associated with these combined processing/chemistry changes is illustrated in Fig.1. The MAS matrix composites have an unsurpassed strength near to the upper-bound in parallel with the borosilicate GMCs. A more limited range of processing variables have been applied to the CAS-matrix compositions but their strength is above that for near-stoichiometric CAS-matrix composites produced commercially (Corning, USA).

In comparing absolute values of ultimate strength with theory there are inevitable difficulties in using bend test data and the lack of precise data for fibre strength and Weibull modulus 'in-situ' after processing. However it is clear that there is little mechanical, thermal or chemical degradation in fibre properties with optimised processing since the lower bound strengths (assuming a

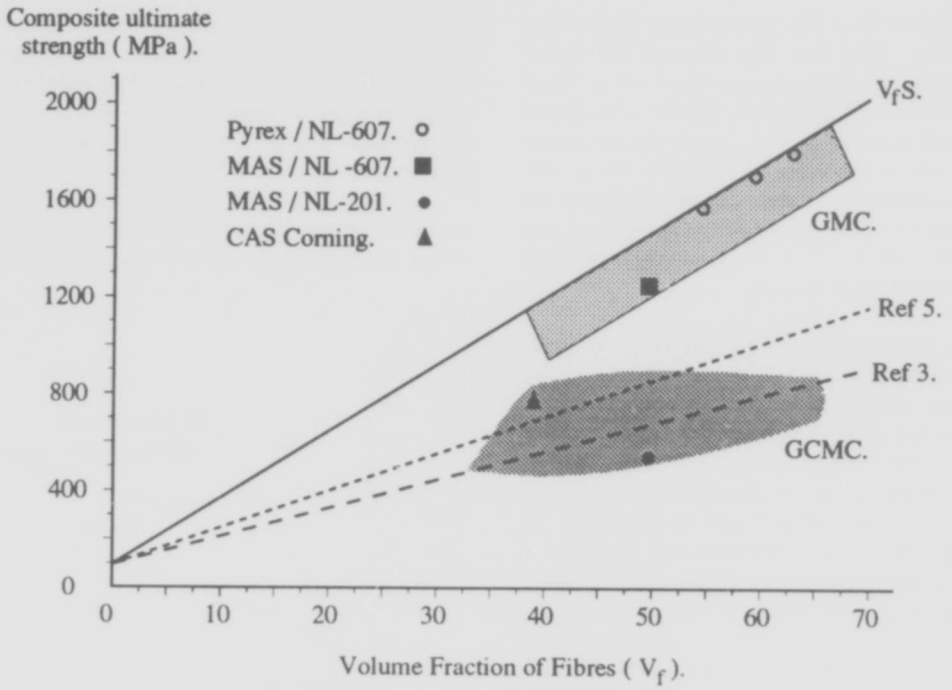

Fig.1 A sample of ultimate bend fracture stresses (σ_u) for GMCs and GCMCs illustrating the improvement in σ_u for MAS compositions relative to borosilicate matrix composites with optimised processing. The reference lines represent typical σ_u - V_f relations for tensile fracture according to theory [3,5].

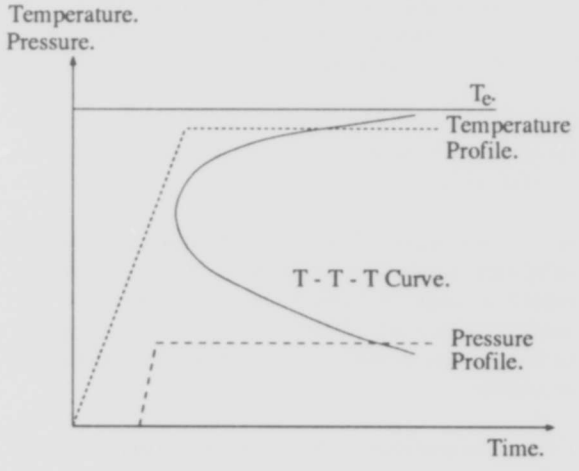

Fig.2 Typical pressure/temperature cycle for GCMC hot-pressing to optimise matrix densification and avoid fibre damage. Pressure application is delayed until glass softening and is followed by rapid densification in the interval before substantial matrix crystallisation (shown via the T-T-T curve in relation to liquidus temperature Te).

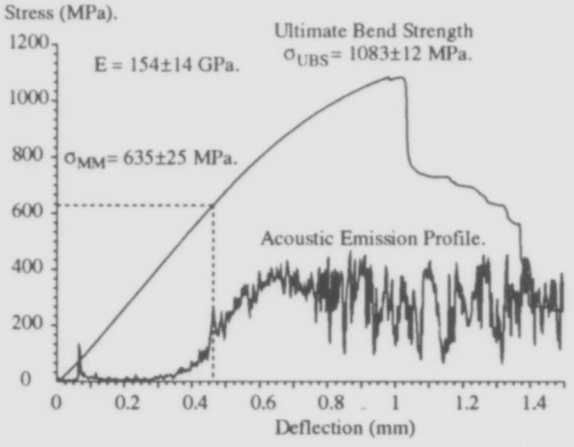

Fig.3 3 point bend stress/deflection plot for a high strength Nicalon 607/MAS matrix composite. Acoustic emission from the composite is recorded during the test to indicate the initiation of matrix cracking.

Weibull modulus of 3) in Fig.1 use pristine fibre values of ~ 2.7 GPa. This data also supports the recent refinement to theory which assumes that broken fibres may support load by matrix stress-transfer at positions remote from the fracture origin. Curtin [5] has shown that such analysis may increase σ_u by ~30% for m ~3-4. It is also necessary to correct experimental data for variations in interfacial shear property (τ), although for existing theories (equation 2) σ_u is a relatively insensitive (slowly decreasing) function of τ.

2.2 Interface Microstructure, Micromechanics and Matrix Microcracking

In addition to ultimate strength, values of matrix cracking stress and interfacial debond/shear stresses are critical parameters which dictate composite design criteria, for example, the notch sensitivity of CMCs [6]. In general high ratios of ultimate strength (σ_u) to microcracking stress (σ_m) are required and the latter is associated with low values for interfacial shear stress (τ) in systems with low interface debond energy (Γ). However, for environmentally sensitive interfaces, such as carbon in oxidising conditions, it is preferable to maintain a moderate σ_m to prevent atmospheric exposure.

An attempt has been made to use GMCs and GCMCs to experimentally model microcracking response in relation to variations in interface microstructure and micromechanical measurements of debond and shear property. Microcracking stresses may be estimated from the thresholds for significant acoustic emission from bend specimens, which is considered more reliable that the detection of non-linearity in stress-strain. Fig.3 is an example of acoustic signal in comparison with a 3pt. bend stress/deflection relation from the high-strength MAS matrix composite. To measure τ and Γ the technique pioneered by Marshall and Oliver [7] using indentation 'push-down' of exposed fibre ends on transverse polished surfaces has been used. A novel indent system, operating within a scanning electron microscope (SEM), has been developed [8] which has a higher load capability than conventional 'nano indentors' (20N compared to 0.1N). A smaller radius diamond indentor also enables greater fibre sliding distances (u), measured to a positional resolution of < 10 nm using a capacitive gauge attached to the end of a computer-controlled piezo 'inchworm' translator. Load (F) is continuously monitored to a precision of < 1mN using a 'hard' piezo load-cell directly interfaced with the diamond mounting. Within the SEM a simultaneous monitoring of image enables an exact indentor positioning and a correlation of interface debond and sliding events with discontinuities in load/displacement curves. Software has been developed to facilitate the subtraction of displacements due to indent-plasticity and to plot the F^2 vs u relation [8] from which Γ and τ are calculated using intercept and gradient, respectively.

The indentation response is dependent on interface microstructure and, in turn, on processing parameters and matrix and fibre chemistry [9]. Typical extremes in behaviour are exemplified (Fig.4) by a Nicalon 607/LAS composite (low α matrix), which exhibits continuous debond/shear, and the Nicalon/MAS composite in which the fibres have been CVD precoated with a double layer (C + SiC). The CVD conditions have created some reaction with the fibre which results in a high debond energy and rapid shear-crack propagation.

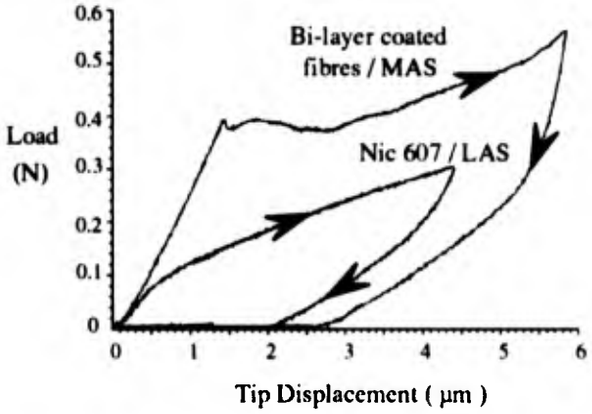

Fig 4. Force-displacement curves from fibre 'push-down' tests, using SEM-based microindentation [4,8]. The curves show extremes of behaviour from a Nicalon/LAS composite with low debond energy and shear stress (Γ = 2Jm^{-2}), τ = 14 MPa) to a Nicalon/MAS composite with bi-layer CVD interface which has a high debond energy (Γ = 60 Jm^{-2}) and shear stress (τ ~60 MPa).

Values of 2Γ and τ are listed in Table 1 for a range of GCMCs and interface types from which a few general conclusions may be obtained:-

(i) Interfaces produced by natural processing reaction or by carbon precoating followed by processing reaction exhibit a range of debond and shear parameter, the values of which are influenced by time and temperature of hot-pressing as well as matrix chemistry and thermal expansion.

(ii) The gradation in matrix microcracking stress (σ_m) follows that in τ but the precise correlation with theory is inhibited by the uncertainty in σ_m defined by the acoustic emission threshold.

Using appropriate values for V_f (~40%), fibre and matrix moduli, fibre radius (r = 7-8μm for Nicalon) and matrix fracture energy (Γ_m), combined with experimental values of τ, only moderate agreement with experimental σ_m values is obtained from the expression [10];

Table 1. Interfacial debond energies Γ and shear stresses τ for various glass and glass-ceramic matrix composites together with experimental and theoretical matrix microcracking stresses.

Composite.	2Γ / Jm^2	τ / MPa	α_m / $10^{-6}°C^{-1}$	σ_m / MPa	Theoretical σ_m / MPa	
					inc. res.stress	w/o res.stress
CAS/Nicalon as pressed	9.6 ± 1.2	25 ± 3		390 ± 30	450	370
CAS/Nicalon, 700°C	13.4 ± 7.8	87 ± 53	4.5	250 ± 30		
CAS/Nicalon, 1200°C	11.8 ± 1.8	25 ± 3		420 ± 30		
MAS/Nicalon - 607 As pressed	12.4 ± 5.4	48 ± 15	5.5	640	690	530
Borosilicate/Nicalon 607 950°C, 20min.	17.8 ± 8.6	111 ± 108	3.2	1000		
Borosilicate/Nicalon 607 1100°C, 20min.	20 ± 7	51 ± 9		600	510	510
LAS / Nicalon - 607	2.2 ± 0.8	14.5 ± 10	1.5	——	230	350
BMAS/Tyranno as pressed	1.2 ± 1.6	25 ± 7	2.7	——	450	490
BMAS/Tyranno 1200°C, 100hrs.	1.8 ± 0.8	28 ± 5		——		

$$\sigma_m = \left[\frac{6\tau\Gamma_m E_f E^2 V_f}{r\ E_m^2\ (1-V_f)}\right]^{\frac{1}{3}} - p\frac{E}{E_m}$$

(where p = longitudinal residual stress in matrix)

(iii) Typical composite behaviour (a 3-stage stress-strain relation) is observed for 2Γ and τ values up to ~20 Jm^{-2} and ~ 50 MPa, respectively. The theoretically-predicted debond condition Γ (interface)/Γ (fibre) < ¼ is apparently not obeyed, assuming typical Γ (fibre) values < 10 Jm^{-2}. Alternatively, measured values for Γ (interface) are too large.

(iv) The influence of thermal expansion mismatch between fibre and matrix on Γ and τ is visible in comparing LAS and CAS matrices which give rise to similar interface microstructures but a reversal (from-ve to + ve) in the α values relative to the fibre. For borosilicate matrices, which have similar α values to the fibre, the high Γ and τ values are dominated by the limited interface reaction thickness at the lower fabrication temperature.

(v) The insensitivity of Γ, τ and σ_m to high temperature (1000-1200°C) oxidising heat-treatment contrasts with that at lower temperatures (400-800°C); these differences are explained in the following section.

2.3 Thermal and Environmental Stability

The influence of heat treatment in oxidising (air) environment on interface properties and on macromechanical response has been studied principally for MAS and CAS compositions. The observed behaviour is generic for composites with C-enriched interfaces; a retention in strength with little change in interface behaviour above ~ 1000°C and a reduced strength with enhanced statistical spread in strength and interface property in the 400-800° interval.

The data, summarised in Table I, may be explained by the active oxidation (CO or CO_2 loss) of C-rich interfaces at intermediate temperatures by 'channelled', longitudinal, gas transport along fibre interfaces from exposed fibre ends. There is a limited fibre surface oxidative degradation and minimal fibre-matrix 'bridging', giving reduced fibre strength and considerable variation in τ. Above 1000°C passive oxidation of SiC (SiO_2 formation) inhibits continued 'channelled' reaction from fibre ends. Further oxygen ingress is limited, in the absence of matrix cracking, to diffusion through the glass-ceramic [11, 12]. Matrix diffusion is surprisingly slow in well-crystallised glass ceramics and, for example, in the CAS composition interface oxidation is limited to a few fibre diameters (10-30μm) from the free surface. In this surface layer fibre/matrix interfaces are totally 'bridged' by SiO_2 and exhibit immeasurably-high debond and shear levels consistent with zero interface crack deflection. An image of near-surface bridged interfaces in comparison with 'bulk; fibres is illustrated in Fig.5.

An important observation is the retention of composite (and hence fibre) strength in the protected state within silicate matrices even following long heat-treatment (> 100 hours) up to 1200°C. This is accompanied by a measurable change in order (or microcrystallite size) in Nicalon fibres and demonstrates that the key problem of strength-loss is related to changes in surface microstructure, probably oxidation-induced.

2.4 Time-Dependent Deformation

There is a limited literature on creep deformation or stress-rupture of long fibre CMCs although some attempts have been made to model composite creep rates, assuming efficient load transfer between matrix and fibre [13, 14]. Preliminary data has been obtained for bend and tensile creep of GMCs and GCMCs at stress levels below σ_m within two temperature regimes: that where both fibre and matrix undergo measurable creep in the isolated state (above ~ 1000°C for Nicalon) and that where fibres exhibit only elastic deformation.

There is approximate agreement with theoretical prediction:-

(i) Creep rates ($\dot{\epsilon}$) are largely fibre-controlled and hence much smaller than matrix rates

(ii) Nicalon/borosilicate glass composites are limited (by glass softening) to temperatures (400-600°C) where fibres are elastic and hence undergo transient creep; the rate of approach to zero creep (Fig.6) is related to matrix creep rate and hence temperature, which agrees with theory [13];

$$\dot{\epsilon} = \alpha\ \dot{\epsilon}_m[1 - (V_f/\sigma)\ \epsilon]^n$$

$$\text{where } \alpha = \left[\frac{E_m(1-V_f)}{E_f V_f + E_m(1-V_f)}\right](1-V_f)^n$$

and E_f, E_m are Young moduli of fibre and matrix, V_f = fibre fraction and n = matrix stress exponent

(iii) GCMCs above ~ 1000°C exhibit classical primary + steady state creep at a composite rate $\dot{\epsilon}_c$ dictated by load-sharing between fibre and matrix [14];

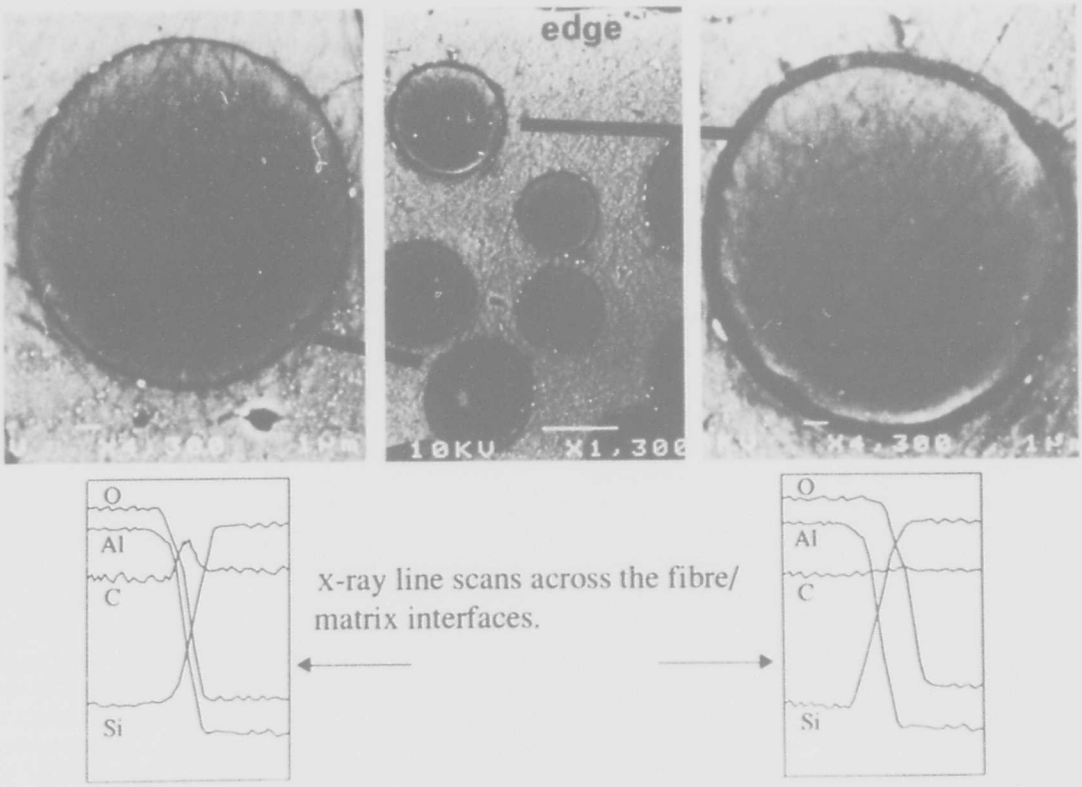

Fig.5 Sectional SEM image and X-ray analysis line scans illustrating interface oxidation (carbon removal followed by SiO_2 'bridging') only within 1-2 fibre diameters from the free surface after 100 hours at 1200°C. Fibres below this level are protected by slow oxygen diffusion rates through the CAS glass-ceramic matrix.

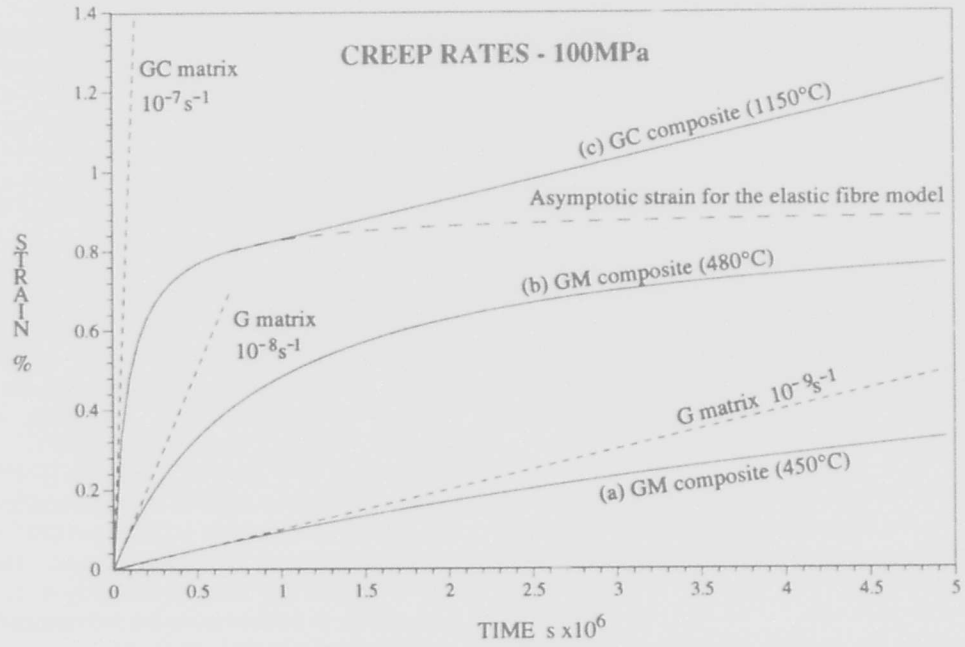

Fig.6 Creep curves modelled for U.D. Nicalon GMCs and GCMCs corresponding to differing temperature regimes: (a) and (b) typify transient creep (elastic fibres) for borosilicate matrix composites at 450°C and 480°C, respectively. Creep curve (c) combines transient and steady-state creep at a higher temperature (1150°C) where fibres and matrix undergo creep (fibre creep rates ~ 1% of matrix rates for Nicalon/MAS, CAS.

$$\sigma_c = \frac{\sigma_{fo} V_f \dot{e}_c^{\frac{1}{n}}}{\dot{e}_{fo}^{\frac{1}{n}}} + \frac{\sigma_{mo} V_m \dot{e}_c^{\frac{1}{m}}}{\dot{e}_{mo}^{\frac{1}{m}}}$$

where fibre and matrix creep rates ($\dot{e}_{fo}$ etc) for stresses (σ_{fo} etc) are measured in isolation and give stress exponents n and m, respectively.

A more precise quantitative comparison of theoretical and experimental creep curves will require data for $\dot{e}_{mo}/\sigma_{mo}$ relevant to specific compositions and microstructures of matrices. For temperatures above ~1100°C the stability of both fibre and matrix microstructure, with respect to crystal growth, may introduce a long-term transient creep. There is evidence that oxidative interface reactions in the critical 400-800°C interval may be responsible for reduced stress-rupture lifetimes, due to loss of fibre strength.

3. HIGH TEMPERATURE NITRIDE-MATRIX COMPOSITES

3.1 Processing Constraints and Microstructure

In the quest for higher temperature performance there is a recognition that currently-available polymer-precursor fibres are intrinsically unstable above 1100-1200°C. Whereas the ultimate solution may rest with oriented oxide monofilaments, there have been a number of CMC studies using CVD SiC monofilaments (Textron SCS) which have a modest strength retention and microstructural stability to ~1400°C. They may be incorporated within reaction-bonded silicon nitride (RBSN) at such fabrication temperatures [15] but matrix porosity results in a susceptibility to oxidation of pre-coated carbon-rich interfaces (typically using SCS6 grade filaments). A novel approach to matrix densification, at Warwick, utilises the SRBSN route of intermediate temperature nitriding/partial sintering, using a Si/Si_3N_4 powder mix containing a liquid-sintering aid, followed by a brief liquid sintering under pressure at ~1700°C [16,17]. Single layer filament + powder preforms are made by simultaneous filament winding and tape-casting which produces a regular microstructure on subsequent layer-stacking, nitriding and hot-pressing (Fig.7).

The CVD monofilaments appear to tolerate short excursions to the final sintering temperature with little change in the fine columnar SiC crystal size but with the appearance of microporosity (possibly due to free Si or C reaction/evaporation). A key to composite performance is the survival of part of the carbon precoating; the reaction $3C + Si_3N_4 \rightarrow 3SiC + 2N_2$ may be shown (using the MTDATA thermodynamic programme - NPL, UK) to proceed in favour of SiC above a critical temperature of ~1400°C at 1 atmosphere N_2 partial pressure. Continued reaction is limited by diffusion through the SiC reaction layer which is clearly visible in sectional micrographs (Fig.7) which illustrate the retention of >4μm of the, initially, 6μm carbon coating. The matrix is a typical liquid-phase sintered (SRBSN) microstructure of micron-sized βSi_3N_4 or β' Sialon crystals in a glassy residue of the sintering medium (MgO, Al_2O_3 and Y_2O_3 additives were used in varied combination [17]).

Interface microstructure is unstable for long heat-treatments in oxidising atmospheres (100-1000 hours in the 1000-1400°C interval) due to channelled reaction from fibre ends. Channel closure due to passive SiC/Si_3N_4 oxidation is less effective in these microstructures which have very large interface widths (~5 μm compared with ~50 nm in GCMCs).

3.2 Micro and Macromechanical Behaviour

Interfacial mechanical data, obtained from filament 'push-through' tests yield shear stresses, τ, of 2-4MPa, with little change from the relatively low debond shear stress (Fig.8). Debonding and shear occurs at the inner carbon interface of the fibre coating and not at the outer reaction interface (Fig.9). The low debond and shear values may result from thermally-induced separation over part of the interface due to the higher expansion coefficient of the fibre. There is little change in τ with oxidising heat-treatments up to ~100 hours at 1200°C, during which only partial carbon removal occurs. For longer times τ is reduced to negligible levels, with total filament debonding during specimen polishing.

Bend and tensile testing of unidirectional materials demonstrates a typical composite response of load-carrying ability after matrix cracking. Stress-strain curves (Fig.10) exhibit substantial non-linearity following the first 'burst' of acoustic emission but extensive multiple matrix microcracking is not common in view of the large fibre radii, low τ and low volume fraction (~25%); a theoretical estimate of crack spacing is in the 10mm range, orders of magnitude greater than for the fine SiC fibres which also have higher τ values in GCMC matrices. Extensive filament pull-out is observed, especially in tensile tests (Fig.11), with estimates of work-of-fracture from pull-out and fibre relaxation totalling 23kJm^{-2}. Estimates of residual filament fracture stress after 1700°C fabrication indicates a 50% strength retention (~1800 MPa). Values of flexure strength of 750 MPa and first cracking stress of 640 MPa are the highest recorded for this class of CMC containing SiC monofilaments. These values fall to 560 and 540 MPa, respectively at 1200°C with little change in fracture mode but with reduced 'pull-out' contribution to the work of fracture.

Specimens subjected to long-term high temperature oxidation exhibit linear behaviour to the maximum bend stress and a 40-50% reduction in the latter for 1000°C and 1400°C pretreatments. Acoustic emission occurs

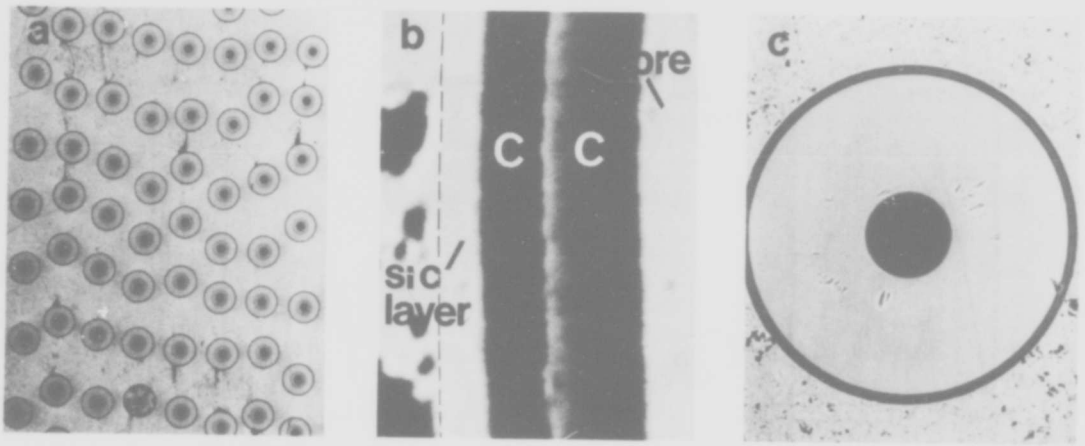

Fig.7 Sectional SEM images of a SiC monofilament/Si_3N_4 matrix composite showing filament distribution (a), partially-reacted interface layer (b) and filament microstructure after high-temperature (1700°C) fabrication.

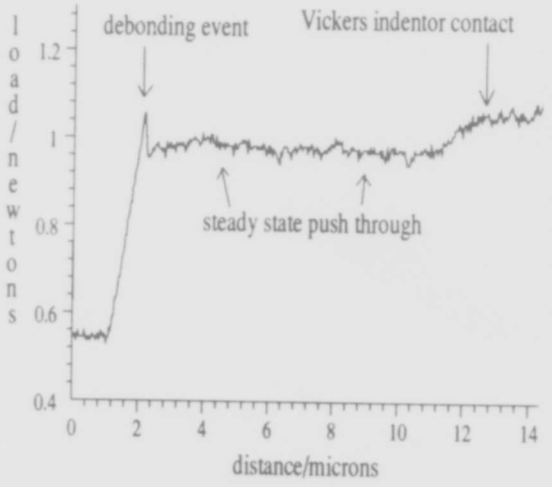

Fig.8 Force-displacement plot from an SEM-based indentation 'push-through' test to measure interface debond and shear stresses for SiC monofilament/SRBSN matrix composites. The peak force represents the initial debond, followed by frictional sliding of the filament at nearly constant force.

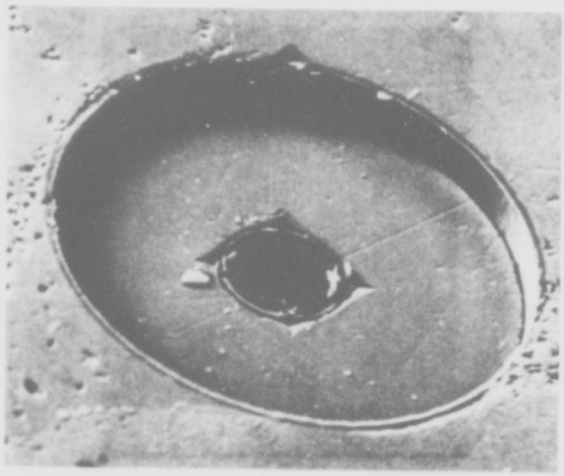

Fig.9 SEM image recorded after indentation 'push through' of a SiC monofilament, illustrating preferred debond and shear at the inner C/SiC interface.

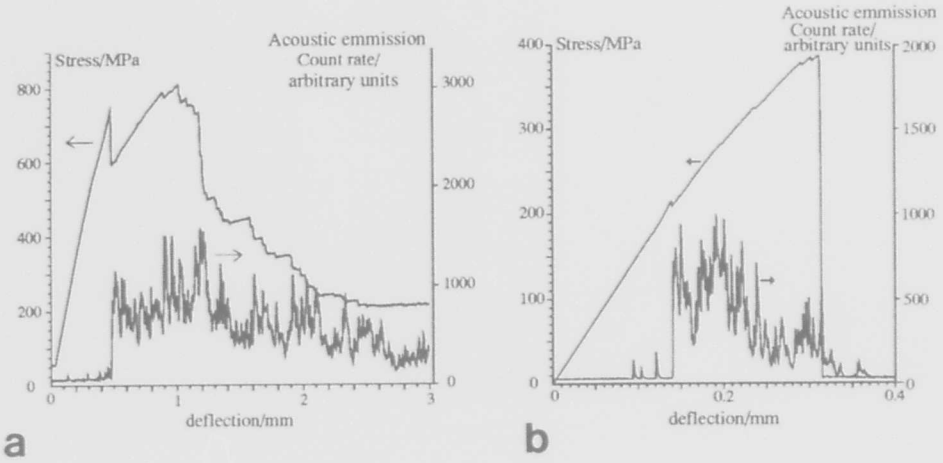

Fig.10 Stress-deflection and stress-elongation curves for 3 point bend (a) and tension (b) tests on a SiC monofilament/SRBSN matrix U.D. composite. Acoustic emission traces are used to detect matrix cracking for comparison with non-linearities in stress-strain plots.

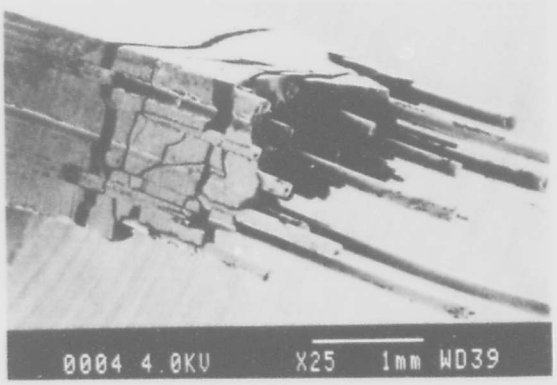

Fig.11 Tensile fracture surface from a SiC monofilament/SRBSN matrix U.D. composite showing extensive filament pull-out and matrix cracking.

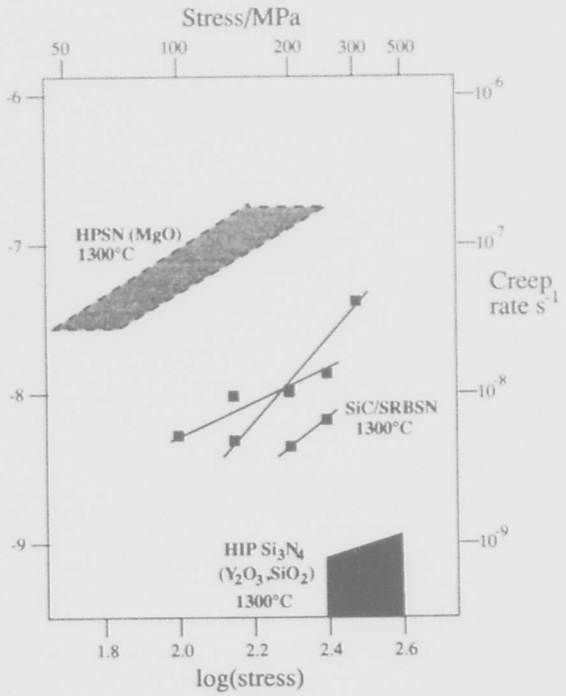

Fig.12 Bend-creep data for a SiC monofilament/SRBSN matrix U.D. composite compared with two grades of monolithic silicon nitride ceramic.

prior to peak stress in oxidised specimens, which may be related to fibre/matrix shear with reduced debond stress. Work of fracture is reduced in parallel with observation of smaller pull-out lengths and reduced filament strength, probably due to atmospheric interaction (it is known that uncoated monofilaments suffer a 50% strength reduction [18]).

3.3 High Temperature Creep and Stress-Rupture

Bend-creep has been studied at 1300°C for stresses between 150 and 300 MPa (i.e. below the matrix cracking stress in the linear part of the stress-strain plot for constant-imposed strain rate test). For all stress levels the creep curves may be resolved into transient and steady state components consistent with a partial load transfer to the monofilaments which have been calculated, from literature data [19], to creep in the isolated state at a slower rate than the composite. All creep curves have the form modelled in Fig.6, consistent with a temperature for measurable simultaneous creep of both matrix and fibre. Unlike GCMCs the disparity in matrix and fibre creep rates is not large; in Fig.12 a set of 1300°C creep data for two types of matrix Si_3N_4 in the monolithic state is compared with that for the composite which has a matrix microstructure more closely related to the HPSN (upper shaded area). The HIP Si_3N_4 is an example of a creep-resistant ceramic with an intergranular residue in the crystalline state. Although there is a considerable scatter in creep stress-exponents from bath-to-batch of the pressed composite (Fig.12) they are generally higher than unity, typical of the matrix ceramic containing glassy residues which act as creep-cavity nuclei.

Stress-rupture tests were conducted between 200 MPa and 400 MPa at 1300°C, using 500 MPa as a zero-time failure stress based on monotonic tests between 1200 and 1400°C. Unlike refined monolithic matrix ceramics, which may exhibit stress thresholds below which no failure occurs within 1000 hours [20], the composite appears to show an almost stress-independent failure limit at ~1000 hours. This is symptomatic of a time-dependent interface oxidation coupled with fibre strength degradation. The data has been plotted for comparative purposes in the form of a 'Larsen-Miller' diagram (Fig.13) which combines time (t) and temperature (T) on a single axis via a parameter $P = T \log (C + t)$. The constant C is empirically adjusted to enable data from different temperatures to fall on the same line. The data for various stages in evolution of 'superalloy' turbine materials is compared with that for the CMC which shows a significant increment in Larsen-Miller parameter P, at least for low stress levels.

4. CONCLUSIONS

The selection of pressure/temperature cycle in relation to matrix chemistry and initial fibre condition is critical in avoiding mechanical and chemical damage to fibre surfaces during fabrication of CMCs. With optimised conditions GCMCs with ultimate bend strengths in excess of 1 GPa are obtainable. High ultimate strength is important in relation to an ability to maintain moderate ratios of σ_u/σ_m for varying σ_m. The value of σ_m in GCMCs is most conveniently controlled via interfacial shear stress τ which varies, typically, from 10-50 MPa and is a function of time and temperature of fabrication as well as chemistry and thermal expansion of matrix relative to fibre. Measured values of fibre-matrix debond energy are sometimes higher than the theoretical limits predicted for ideal composite response.

Interface oxidation is a critical problem at intermediate temperatures (400-800°C) due to channelled reaction from fibre ends. This mechanism is suppressed above ~1000°C by channel-blocking with the SiO_2 oxidation product of SiC. A silicate-coating or preoxidation treatment of exposed fibre ends may resolve the intermediate temperature problem but a stress limit remains that for microcrack exposure of interfaces.

Textron CVD SiC monofilament-reinforced Sialon and Silicon Nitride matrices have been explored as higher temperature CMCs. A novel preform-preparation method using matrix tape-casting has been used in conjunction with SRBSN matrix chemistry/processing. Composite response and moderate fracture energy may be achieved utilising a partially-sacrificial thick C-rich interface which has a very low τ value (2-4 MPa). The oxidation problem of C-rich interfaces is retained at higher temperatures than for GCMCs due to the difficulty in channel-blocking of thick interfaces. Despite the oxidation problem creep and stress-rupture properties exhibit useful increments over turbine superalloys.

ACKNOWLEDGEMENTS

The research surveyed in this paper has been supported by the SERC and Rolls-Royce plc.

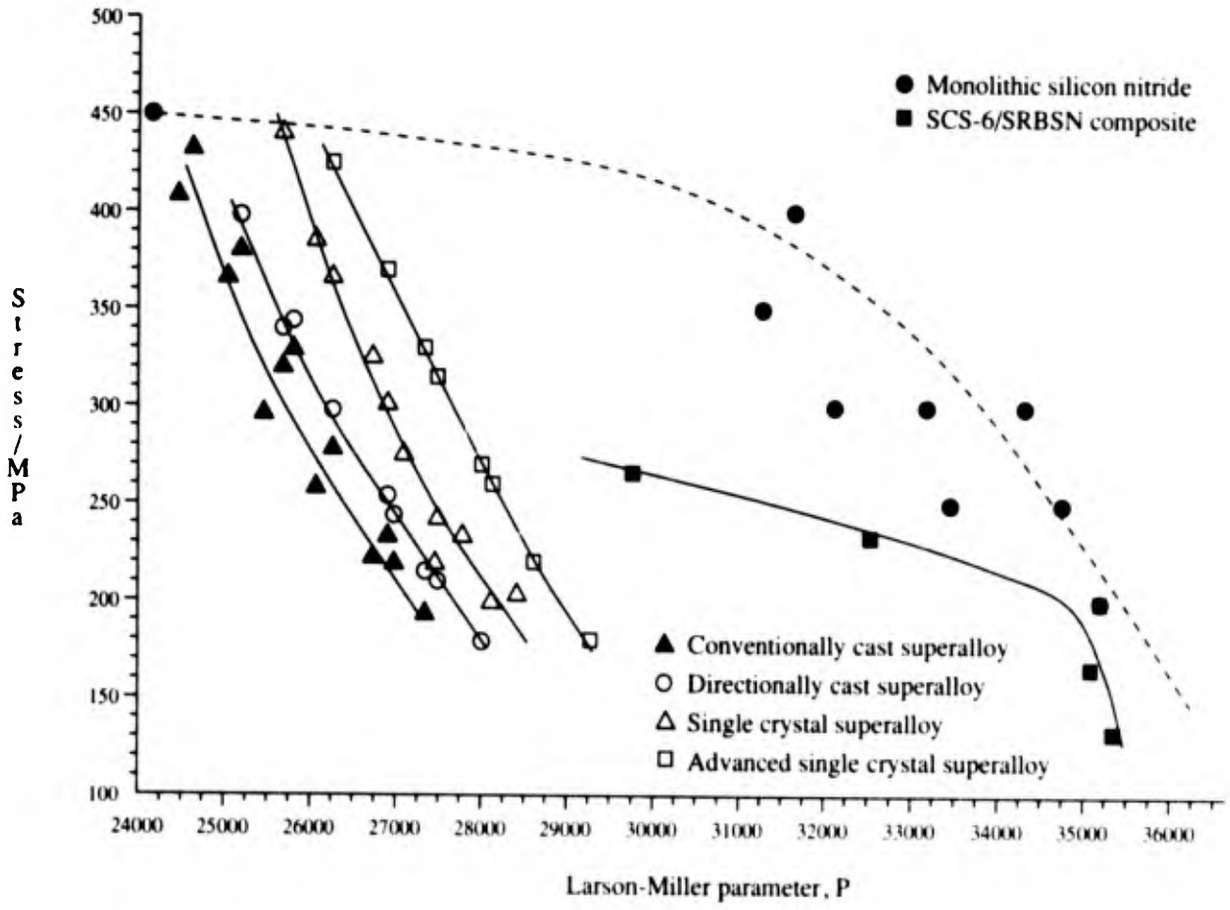

Fig. 13 Stress-rupture data for a SiC monofilament/SRBSN matrix composite compared with that for a range of turbine superalloys and a typical monolithic silicon nitride (data from [21]). The Larsen-Miller parameter ($P = T \log [c+t]$) is used to compare the time/temperature influence on a single axis.

REFERENCES

1. Prewo K.M. and Brennan, J.Mat.Sci. 15 (1980) 463.
2. Rosen B.W., AIAA Journal 2 (1964) 1985.
3. Thouless M.D., Sbaizero O., Sigl L.S. and Evans A.G., J. Amer. Ceram. Soc. 72, (1989) 525.
4. Lewis M.H., Daniel A.M., Chamberlain A., Pharaoh M.W. and Cain M.G., J. of Microscopy 169 (1993) 109.
5. Curtin W.A., J.Amer.Ceram.Soc. 74 (1991) 2837
6. Evans A.G. AGARD publication - this volume.
7. Marshall D.B. and Oliver W.C., J.Amer.Ceram.Soc. 70 (1987) 542.
8. Daniel A.M. and Lewis M.H., Ceram. Eng. and Sci. Proceedings, (in press, Amer.Ceram.Soc. 1993).
9. Lewis, M.H. and Murthy V.S.R., Comp. Sci. and Tech. 42 (1991) 221.
10. Budiansky B., Hutchinson J.W. and Evans A.G., J. Mech.Phys.Solids 2 (1986) 167.
11. Butler E.G. and Lewis M.H., in 'Ceramic Materials and Components for Engines' ed. R. Carlsson (Elsevier 1992) 32.
12. Pharaoh M.W., Daniel A.M. and Lewis M.H., J.Mat.Sci. in press (1993).
13. McLean M., Comp. Sci. and Tech. 23 (1985) 37.
14. Bullock E., McLean M. and Miles D.E., Acta. Metal. 25 (1977) 333.
15. Bhatt R.T. and Phillips R.E., J.Mat.Sci. 25 (1990) 3401.
16. Razzell A.G. and Lewis M.H., Ceram. Eng. and Sci. Proceedings, 12, (Amer. Ceram. Soc. 1991) 1304.
17. Razzell A.G. and Lewis M.H., J. of Microscopy 169 (1993) 215.
18. Foltz T.F., Ceram.Eng.Sci.Proc. 6 (1985) 1206.
19. DiCarlo J.A., J.Mat.Sci. 21 (1986) 217.
20. Tuersley I.P., Leng-Ward G. and Lewis M.H. in 'Engineering with Ceramics' ed. R. Morrell (Inst. of Ceramics, 1990) 231.
21. Watanabe K., Ozawa T., Kobayashi Y. and Matsui E., in 'Ceramic Materials and Components for Engines' ed R. Carlsson.

CERAMIC MATRIX COMPOSITE PARTS DESIGN

by

P. Lamicq and D. Boury
Société Européenne de Propulsion
B.P. 37
33265 Saint Médard en Jalles Cedex
France

SUMMARY

CMC are new materials with specific features regarding damage and rupture. A good CMC performs as non brittle, damageable material, with nearly no stress concentration sensitivity. Such behaviour is the base of their structural capacities. But past design experience has to be adapted to take advantage of this.

Several characterisation levels are necessary to achieve a material data base relevant for parts design. Standard deviation knowledge and tests coupons similarity with actual parts has to be checked carefully, as fiber volume fraction or residual porosity have an impact on test results. For long time uses, CMC performances are affected by fatigue and ageing. Mechanical or thermal fatigue, without oxydation or corrosion, is not detrimental to those composites. They can sustain millions of cycles at high stress levels. Chemical effects are of far greater importance, and may modify strongly strength and elongation to rupture. Life time predictions depend upon an accurate knowledge of environmental conditions, then a good set of representative tests.

Powerful mechanical and thermal code are used for optimised design analysis. At high load or elongation levels, non linear stress strain relationship has to be modelled. Stiffness matrix changes can be determined by simple tests, but tension shear interaction needs more sophisticated experiments. Statistical approaches for safety factors are under development and may be of interest for future methodologies.

Nevertheless, singularities of shape or thickness have to be dealt with specifically, and first in the load transfer areas. Results of analysis are compared with tests performed on technological sample, simplified in order to measure relevant data. Such failure criteria for complex load cases are still to be worked on, taking into account in plane and out of plane stresses and strains, and shear which may be strongly improved under compression.

0. INTRODUCTION

Scientists have always been passionately fond of extremes and the high temperature field does not make an exception to the rule. This field is particularly difficult to approach and therefore interesting for it presents the characteristic of complicating both the theoretical aspects, like aerodynamic or combustion, and more pragmatic considerations, such as the materials and structures that must keep on ensuring their functions in conditions that are becoming more and more severe while presenting constantly improved performances.

It is obvious that in these conditions, refractory metal materials are handicapped. For instance superalloys present too low operating temperatures, ranging from 900 K to 1250 K, and require an active cooling that reduces performance. Ultra-refractories, such as niobium or rhenium, are handicapped by deceptive mass or rigidity balances and high costs.

As for technical ceramics, which are well adapted to these conditions, their brittleness and defect sensitivity is often prohibitive for applications of structural type.

Ceramic matrix composites (CMC) are making up a new material family that presents a significant potential for thermostructure design. They show a good specific strength and stiffness up to high temperatures and these characteristics are associated to non-fragile behaviours which do correspond to the designer practical requirements.

This document, after a short description of the CMC most used by SEP designers, presents a thought on part design and dimensioning with these materials. An approach of the currently used general methodology is presented, followed by various comments specific to the use of these materials. Finally, we give some examples of singular behaviors, which are currently poorly controlled by simple modeling and require advanced rupture criteria.

Presented at an AGARD Workshop entitled 'Introduction of Ceramics into Aerospace Structural Composites', April, 1993.

1. C/SIC AND SIC/SIC C.M.C. DESCRIPTION

These two material families are currently the most used for designing themostructural-oriented parts or sub-systems in an oxidizing environment.

C/Sic are made up of a carbon fiber reinforcement, a pyrocarbon interphase and a silicon carbide matrix.

SiC/SiC are made up of a silicon carbide fiber reinforcement, a pyrocarbon interphase and a silicon carbide matrix.

Fiber reinforcements can be either bidirectional - consisting of a mere fabric stacking (2 D) or made up of layers that are bound together to form a multi-layer (2.5 D) - or three-directional in the case of carbon reinforcement by using the needling technique (3 D NOVOLTEX or SKINEX).

The interphase and then the matrix are deposited by chemical vapour infiltration (CVI) of a carbon or silicon carbide (SiC) precursor.

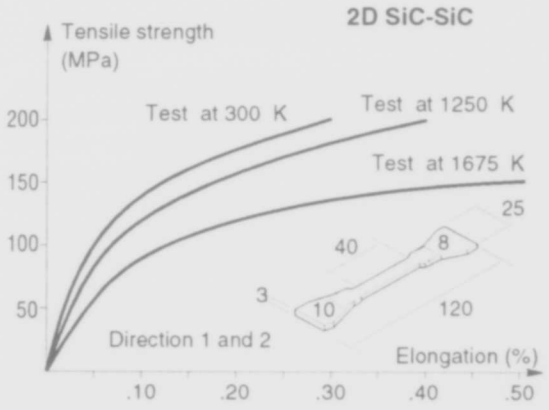

FIGURE 1 : SIC/SIC 2D STRAIN/STRESS CURVE

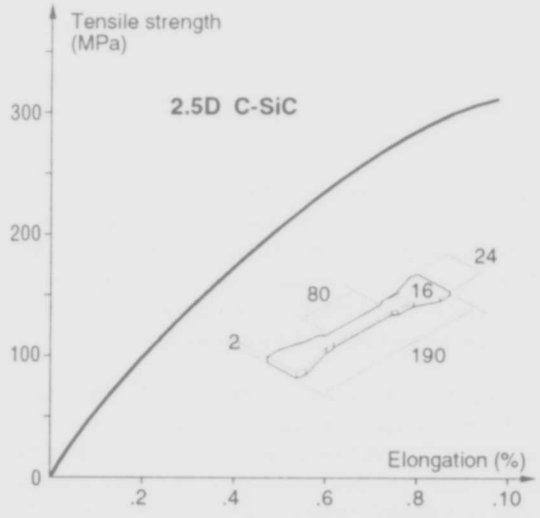

FIGURE 2 : C/SIC 2.5D STRAIN/STRESS CURVE

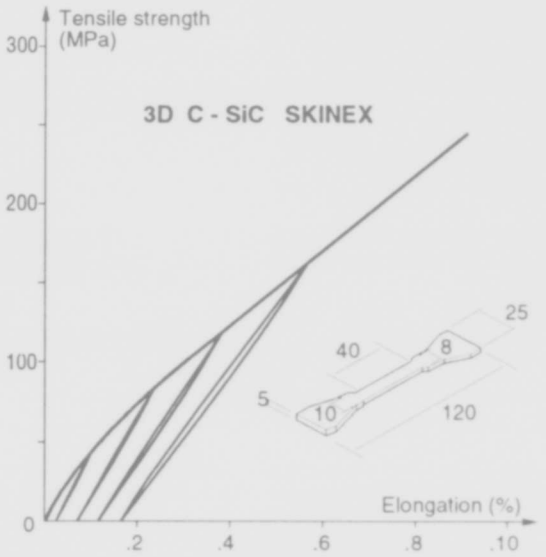

FIGURE 3 : C/SIC 3D SKINEX STRAIN/STRESS CURVE

Figures 1, 2 and 3 remind the mean behaviour laws (stress/strain) obtained for some examples that are the most representative of these materials. They are representative of average unaged material behavior for standard fiber ratio and density.

These curves show well the specific behaviour of these materials, that can be qualified as "elastic-damageable".

They are elastic because the discharge curves, that are quasi-linear, pass again close to the original deformation. A residual deformation, due to the fact that cracks are not completely closed, can be noted but remains limited and without great influence on design.

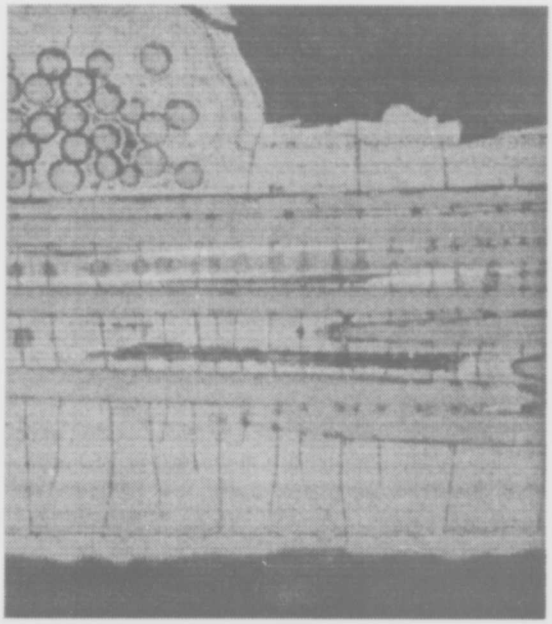

FIGURE 4 : STRESSED SIC/SIC MICRO-CRACKS SYSTEM

Such materials are damageable because, when placed under stress, the matrix cracks as its own elongation near 0.05% is much lower than that of the fibers which is higher than 1 %. Figure 4 shows a micro-cracks network for a bending stressed SiC/SiC sample. Cracks propagation and effect are currently under studies and modelings improving our understanding of mechanical behavior are proposed.

Owing to this micro-cracking mechanism, these materials profit by a notch propagation behaviour that is remarkable for a ceramic.

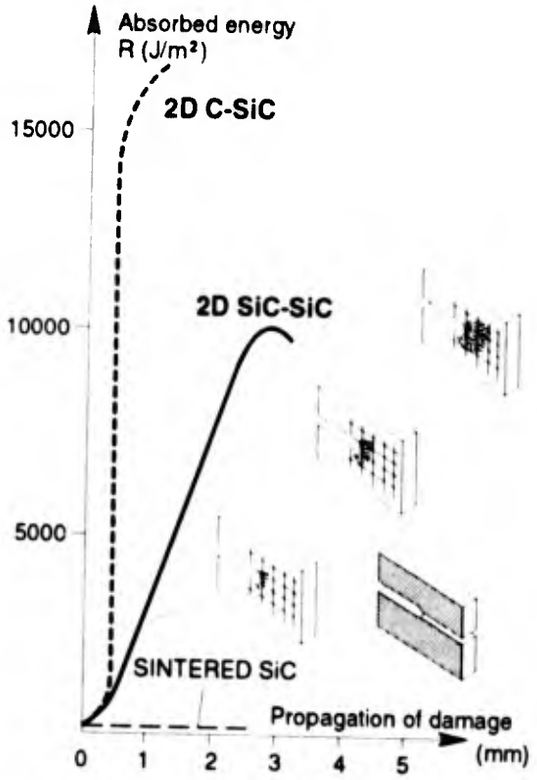

FIGURE 5 : CMC CRACK PROPAGATION RESISTANCE

Figure 5 that presents comparative test results with sintered ceramic, shows an improvement of 2 decades for the CMC benefit. This result is consecutive to the energy dissipation through the micro-crack network. This mechanism is the main foundation of the CMC behaviour and makes them usable for structural applications.

The strength potential at room temperature appears relatively low. On the other hand, the low evolutions with temperature lead to remarkable results at high temperature for unaged material. Average rupture values are higher than :

- 200 MPa for a 2D Sic/Sic up to 1450K
- 300MPa for a 2.5D C/SiC upto 1750K
- 230 MPa for a 3D C/Sic up to 1750K.

Figure 6 can be used to compare these strength performances with that of some usual metallic materials.

It can be noted that, from 900 K, upwards some specific features (reduced to density for iso-mass comparison) are comparable. At 1250 K, the mechanical advantage becomes obvious, due to the CMC low mean density.

However, this type of data, although very promising and obtained on industrialised material, is far from being sufficient to achieve a part or structure that can be competitive.

To use this material potential correctly, it is necessary to build up a significant know-how in design and dimensioning. This document takes stock of the knowledge and mastery acquired in this field.

	INCO 718 at 900 K	HAYNES 188 at 1250 K	C/SiC 2.5D up to 1750 K	SiC/SiC 2D up to 1450 K
DENSITY - kg/m^3	8200	8980	2100	2300
ULTIMATE TENSILE STRENGTH - MPa (minimum at 3 standard deviation)	1150	240	210	140
YOUNG'S MODULUS GPa (initial or elastic value)	165	150	65	220
SPECIFIC RUPTURE STRENGTH $MPa/kg/m^3$	140	27	100	61
SPECIFIC STIFFENESS $GPa/Kg/m^3$	20	17	31	95

FIGURE 6 : CMC VERSUS METALLIC MECHANICAL CHARACTERISTICS

2. CMC PART PROJECT

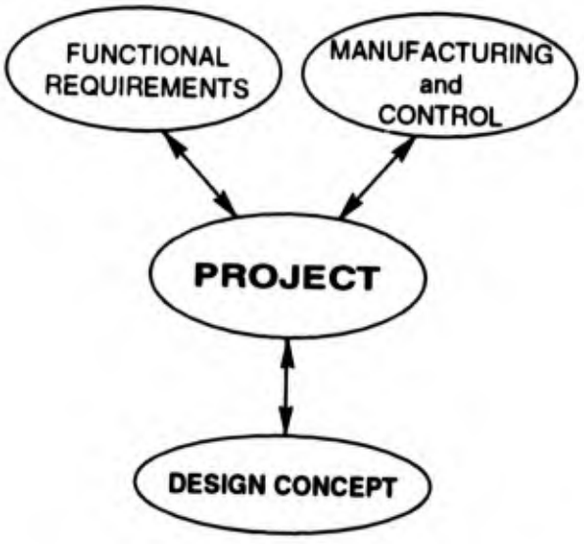

FIGURE 7

A lot of informations are required to choose a design concept for a CMC part project and it would be long to be exhaustive. Only the most important elements, indicated on figure 7, that need to be known to define a CMC part concept will be discussed.

The two following points, the understanding of the functional need and the knowledge of the manufacturing limits, are particularly important for these materials and have a strong influence on the results.

2.1. Functional requirements

This is one of the most important point of CMC part design since most potential users (rocket propulsion, military turbojet, thermal protection) have a "metal" culture that greatly influences the preliminary projects and often dictates design choices.

Thereby the design latitudes then offered to introduce a new material are reduced :

- difficulties to make the most of this material and the material real potential is under-used,
- the overall interest can be masked or underestimated. For example by omitting the positive effects induced by a lighter rotating machine or a reduced cooling, etc... or the negative effects which can follow a radiation increase. Such interactions must be considered very soon in order to correctly judge the snowball effect,
- interfaces with the structure can prove to be inadequate, for instance when the expansion coefficients and the thermal behaviours during the thermal transients of metal supports or structures and CMC parts are comparatively different.

It is essential to know the functional needs of the parts or structures to be made of CMC very soon in the project in order to facilitate their implantation and make the most of them.

The preliminary project must be the result of a close cooperation between the user and the CMC designer. An approach including a common engineering working-group is one of the most profitable.

2.2. Manufacturing possibilities

It is necessary to design a part than can be easily manufactured, even if its performance characteristics have to be slighdy altered.

The remarks and advices made in this chapter are closely related to the CVI densification process. They result from the experience accumulated by SEP in this field.

Shape simplicity

As for most long fiber composites, the general part shape must remain as simple as possible in order to achieve a fiber reinforcement with correct fiber orientation.

Complex structures with seamed or co-needled textures (stiffeners on a shell for exemple) can be performed. They remain expensive due to required handle manufacturing and level of control.

Nondelaminating texture

It is very difficult to ensure the reliability and reproducibility of 2D texture reinforcements. They are very sensitive to delamination and associated quality control costs are significant. Layer stacking should therefore be avoided if the product has to be industrialized and multi-layer 2.5 D or 3D reinforcement are to be recommended.

Thickness variation

Thickness variations are difficult to obtain with a "near net shape" pre-form approach. It is preferable to design parts with constant thickness. If needed, surface machining is correctly controlled, but requires the use of diamond tools and is cost generator. Machining should be limited to functional areas.

High thickness

Thick shells give rise to infiltration problems with a density that is lower in the core than on the surface. This will have to be taken into account in characterizations and calculations, increasing program duration and overall costs. Thick shells should better be avoided from the economical stand-point.

2.3. Other project drivers

Many other elements should also be taken into account to design a CMC part. The following general remarks throw a light on the acquired experience.

Technological aspect

This point deals more particularly with bonding and assembly mastery. Experience tells that the behaviour of metal screw bonds is generally correct and that CMC are resistant to local overstress.

Bonds obtained by brazing or CVD metal deposit are also possible according to temperatures.

At low temperatures adhesives bonding is possible. However, an area whose temperature is constantly less than 300K is exceptional on a thermostructure.

Cost and delivery aspect

CVI manufacturing process is naturally long because the deposit kinetics are slow. Nevertheless, the process real times are in fact very short with respect to the total manufacturing duration. Manufacturing times, for parts that are mostly prototypes, are now mainly dependant from an industrial organization which is still to be improved.

We also have identified materials inducing a lot of manufacturing operations, and of course long times, and those

with short manufacturing time. Costs and delivery times, that are still high for some new and complex parts, could be reduced :

- by rationalizing the types of CMC used
- by simplifying the parts to be manufactured
- by a production to be industrialized

Failure mode effect and criticity analysis (FMECA)

CMC characteristics do not suddenly decline as temperature rises. Their life duration diminishes but phenomena are very gradual so far as the aggression remain limited. This type of behaviour allows a temporary operation in degraded mode, like over heating, without disastrous outcomes. CMC are resistant to operating variations and fault tolerant.

3. CMC PART DESIGN

CMC system or part design is a new discipline with few solid bases but our expertise and mastery have now reached new levels where some methodologies can be settled.

As for any problematics, the same alternative between an analytical approach and an experimental approach is found in CMC design.

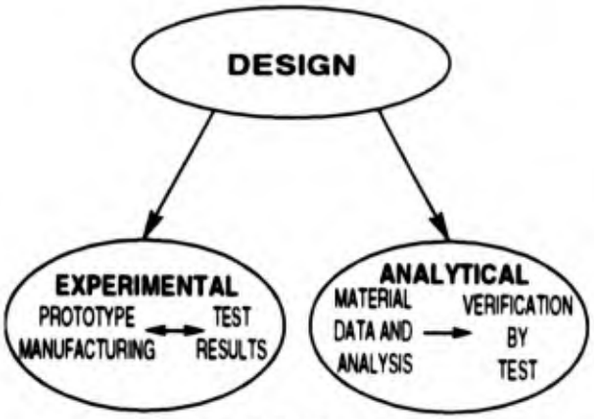

FIGURE 8

The experimental approach is based on an iterative process between prototypes manufacturing and large scale tests. It quickly provides an answer to a complex problem but presents major drawbacks in case of failure: the iteration cost and times are rapidly becoming prohibitive with respect to the high cost of prototype parts and the associated designing/manufacturing times.

The analytical approach is based on the understanding of the phenomena and mechanisms that come into play to lead to a theoretical justification of part dimensioning. Tests are only required for verifications. This approach requires more time at the beginning but gives much more satisfactory results, transposable to other projects.

After a first fifteen years CMC development phase with mainly a global approach, we now turn to an analytical approach, of course structured by the first results.

This analytical approach requires the mastery of three mains elements, namely material characterization, analysis and rupture criteria knowledge.

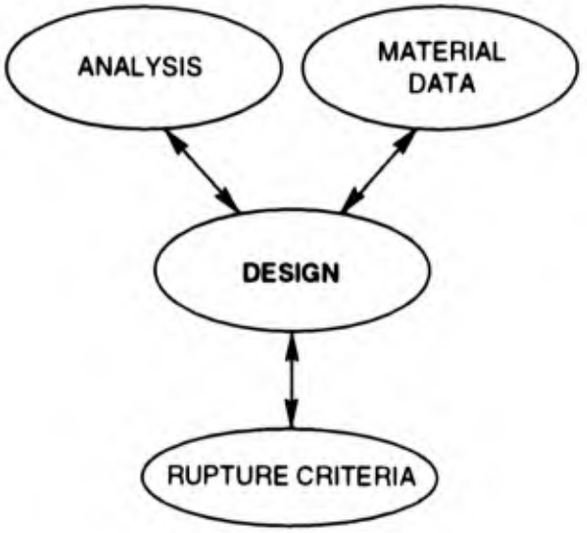

FIGURE 9

3.1. Material characterization

With every material, it is important to resort to the right level of knowledge of the materials according to the project progress and nature. According to this, a SEP classification (A/B/C/D/E) of the different characterization level was developed in order to clarify the data in this field. These levels are summarised figure 10 and described hereunder.

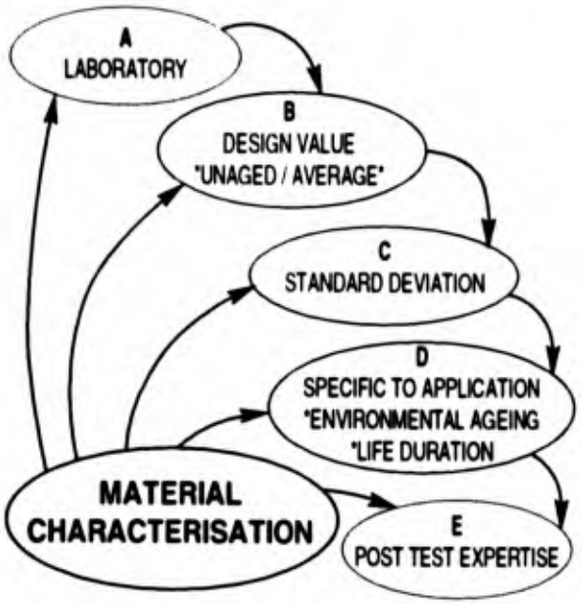

FIGURE 10

A - Laboratory

This characterization level, the lowest one, is only an estimation of a future material main features, on the basis of a few

test pieces and without quality control. It allow to check the coherence of a potential material with project requirement.

B - Material dimensioning

This characterization level gives access to the "mean" thermal and mechanical features of a material as fabricated (unaged). Only average values are known. The process is clearly defined, checked and industrial.

It can allow for temperature or density effects for example. This is important for materials densified by CVI.

C - Manufacturing dispersion

CMC dispersion is significant. It has to be allowed for by considering dispersion in a manufacturing batch and between different batches. This aspect particularly interfaces with the attempts of ultimate strength modelling.

D - Specific to application

Design must be performed by taking into account the mechanical characteristic losses or the thermal characteristic changes due to ageing during use.

This type of characterization requires the designer to be familiar with the material or structure degradation modes in order to define representative ageing tests.

This is particularly important for long-lasting uses (1000 h for example for military turbojets) where "real time" testing is impossible and therefore requires a hardening that has to be made pertinent.

Aggressive environments are very diverse ranging from acoustic fatigue to chemical degradation or erosion. For instance CMC present a good behavior to hydrogen embrittlement or chemical product ageing like acid, oil and derivated....Each case is specific but two types of ageing can be discussed in general words.

Oxidizing species ageing

SiC/SiC and C/SiC CMC are sensitive to oxidizing environments. Degradation is consecutive to crack opening under stresses. These cracks allow oxygen or other oxydizing species to come in contact with the "pyrocarbon" interphase or the carbon fibers, which leads with time to its destruction and part ruin.

These mechanisms kinetics depend on the temperature, the oxygen partial pressure and the strain level due to cracks width. They are studied and modeling are proposed.

Finishing treatments exists to slow down oxidation in long-lasting applications. They are conceived to fill up cracks when opening and increase life duration by several orders of magnitude.

Nevertheless, their efficiency is not unlimited and the performance degradation versus time has to be known for designing.

Fatigue ageing

CMC are hardly sensitive to fatigue and can withstand millions of cycles without significant decrease in their failure level. Fatigue limit is not clearly define but is higher than 2/3 of the initial ultimate tensile strength. Figure 11 gives as example tests results for a SiC/SiC material.

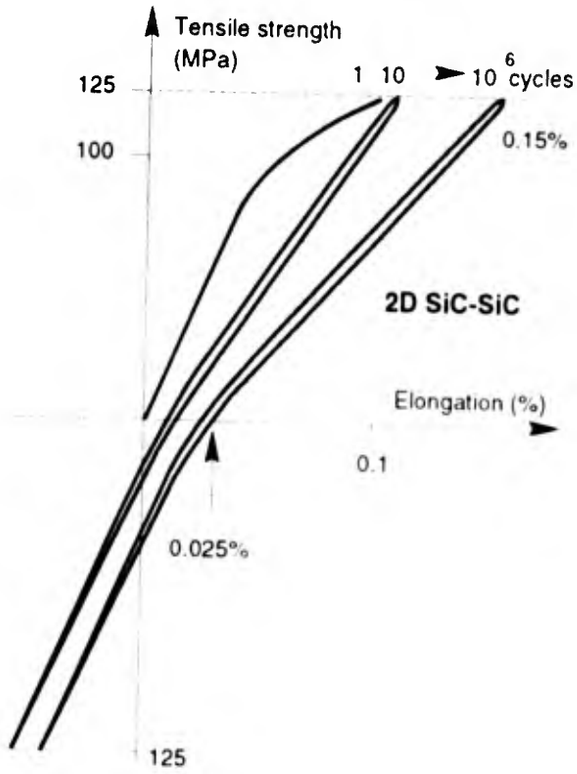

FIGURE 11 SIC/SIC FATIGUE RESULTS

This generic behaviour remains the same with high temperatures as long as other degradation such as oxidation do not intervene to mask it. Inert gaz thermal tests are in that respect the most relevant. Such fatigue behavior gives CMC great interest for cyclic application where metal materials have to face huge decrease of mechanical strength (only 1/3 of initial ultimate rupture strength after one million cycle).

E - Expertise after use

This level of CMC behaviour knowledge is the most important, for it makes possible to define the real degradations in use. This identification of the real problems is fundamental for design and manufacturing.

We can mention for example the phenomena of SiC matrix self-protection at high temperatures through the formation of silicon dioxide, which reduces oxidation effects.

Correct use of material characterisation data is mandatory for a safe design. For the firing of a prototype combustion chamber with 20 s duration, level B can be sufficient since firing degradations are negligible and the quality of each part can be checked before the fire test. For a pre-series pro-

duction of a part which must ensure 1000 h of operation, level C and D are compulsory.

These characterizations are long and expensive, but are unavoidable to build a part development. Two remarks can be made :

- the need for pertinent degradation models, that limit investigations, is essential,
- the basic material must be accurately defined, and the number of variants reduced to perform these characterizations and accumulate data. These considerations require for example the choice of a single process to manufacture the SiC matrix, the limitation to certain types of C or SiC fibers, and the selection of some texture families (multilayer 2.5D or needling for 3D).

In addition it is necessary to repeat that samples definition must be representative of part material. It is why some standard thicknesses of 3mm for 2D and 5 mm for 3D material are not retained when projects involve material thicknesses of 1 or 2 mm. Sample manufacturing process must also be in good accordance with part one, specific cares on densities is mandatory.

3.2. Analysis

According to the project progress, the used means are different.

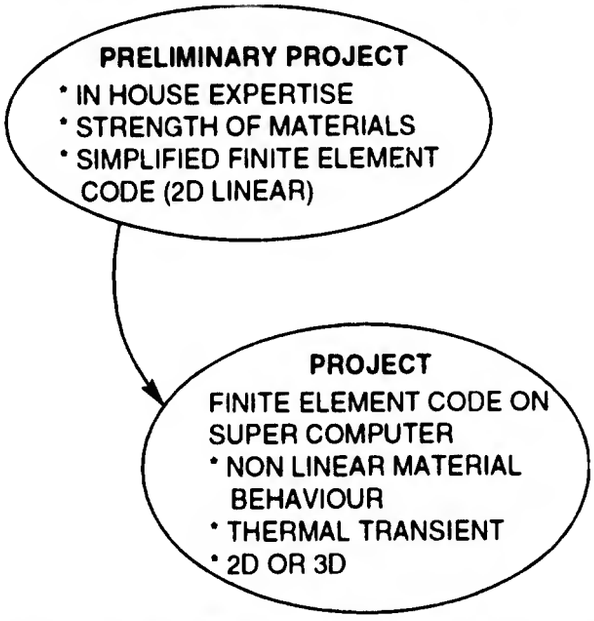

FIGURE 12 : PRELIMINARY PROJECT AND PROJECT TOOLS

At the preliminary project stage, the analytical formulas of materials strength, mechanical finite element linear 2D codes and transient 1D thermal codes for exemple are generally sufficient.

At project stage, non linear mechanical 2D and 3D codes and transient 2D or 3D thermal codes with radiation are generally used to perform thermal and mechanical analysis.

These powerful codes, and access to super-computor, are necessary in the fields where design margins are low. The CMC characteristics, although correct at high temperatures, remain low in the absolute (100 to 200 MPa). The calculation uncertainties of simplified models (thermal and mechanical load accumulation for example) cannot be covered by an important safety factor. This could lead to a redhibitory overdimensioning for the project (volume/mass).

The different types of calculations performed as part of CMC dimensioning are quite classical, but some particularities are remarkable and noted hereafter.

Thermal calculation

In most cases, one must resort to transient 2D or 3D thermal calculations while taking radiation into account. As we have to manage very hot parts, thermal exchange level by radiation due to high CMC emissivity near 0.8 is often higher than convective or conductive exchange. It can lead to introduce thermal insulation device.

Transient thermal analysis is required because dimensioning cases often occur during thermal transitory phases where differential expansions between the part and the support or on the part itself are maximum.

Luckily, CMC present a low thermal expansion coefficient, which often limits interfaces problems, and confer them a particularly high thermal stress resistance. This is interesting for applications like nozzle guide vanes for instance.

An important difficulty rests in the good assessment of thermal boundary conditions. The knowledge of the convective coefficient and of gas flow adiabatic temperature is often relatively empirical.

It is worth noticing that CMC materials are not ablative materials and erosion phenomena that can occur for example at the throat of combustion chambers remain minor.

Mechanical and thermomechanical calculations.

Finite element code are based on HOOKE laws to modelize stress/strain behavior of material. Such models developed for continuous and homogeneous material are used and validated at macroscopic level for CMC parts analysis involving a porous and composite material.

Local analysis axis system must be as respectful as possible of material fiber reinforcement orientation.

The damageable elastic behaviour of CMC's requires to perform iterative calculations (automated procedure) to assign each direction of the appropriate Young's secant modulus, linked to the strain in the same direction.

Current models are aimed at defining the effect of damage (strain) on shear modulus and Poisson's coefficient. Other works are performed to clear coupling relations between levels of damage in each direction and their influence on rigidity matrix coefficient.

The modelling approaches of such behaviours are promising but can not yet be applied for real analysis.

The material non linearity is generally an advantage because the locally overstrained areas will benefit by a pseudo-plasticity phenomenon.

Vibratory calculation.

These calculations are particularly long and sensitive to boundary conditions. The applied acoustic stresses are to a large extent approximated and part boundary condition modeling like attachment stiffness and degree of freedom is very critical.

In addition, the CMC damping coefficients are still badly determined. They are nevertheless much better than for metal materials as a consequence of the energy dissipation in the cracks and in the fiber/matrix interface. Values ranging from 6 to 12 % were measured.

A static pressure equivalent is in most cases assessed to avoid vibratory calculations with a dynamic response which are feasible but hardly processable for justification.

In general, CMC structures are stiffer than comparable, from a mechanical point of vue, metal structures. The following general remarks can be done for the CMC version versus an "equivalent" metal version :

- it is thicker and presents therefore a higher inertia
- it is lighter and "moving" masse is reduced.

For SiC/SiC material parts, that present a Young's modulus higher than common metallic material the natural frequencies will be greatly risen compared to the metal version. For C/SiC the situation will remains in general favourable in spite of a moderate Young's modulus.

Mechanical stress - σ - $\quad \sigma = P \times R / T$

Mass budget - M - $\quad M = \pi \times R \times T \times D$

Natural frequency - F - $\quad F = \frac{1}{2\pi} \times \frac{T}{R^2} \times \sqrt{\frac{3E}{5D}}$

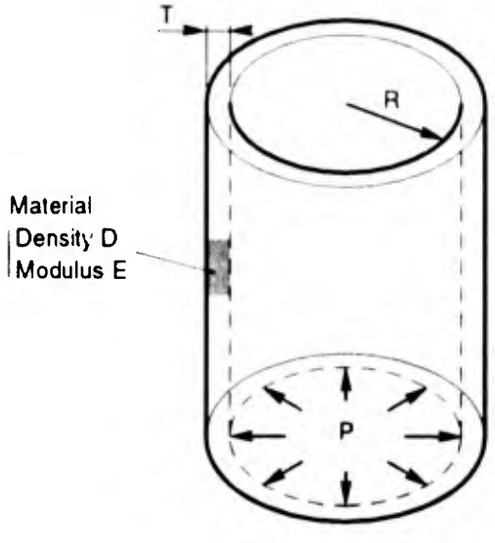

FIGURE 13 : GEOMETRY AND FORMULAS

	HAYNES 188 at 1250 K	SiC/SiC 2D	C/SiC 2.5D	C/SiC 3D SKINEX
DENSITY - kg/m^3	8980	2300	2100	2100
YOUNG'S MODULUS GPa	150	220	65	35
ULTIMATE TENSILE STRENGTH - MPa (minimum at 3 standard deviation)	240	140	210	160
THICKNESS	reference	+ 71 %	+ 15 %	+ 50 %
MASS	reference	- 56 %	- 73 %	- 65 %
FIRST NATURAL FREQUENCY	reference	+ 310 %	+ 55 %	+ 50 %

FIGURE 14 : COMPARATIVE RESULTS

This situation is illustrated by figures 13 and 14 showing the design and analysis of first natural breathing frequency for a cylinder whose design driver is internal pressure.

3.3 Rupture criteria and safety factors

To complete design, it is necessary to define the failure criteria that allow the characterization and calculation results to be exploited, and then compare the margin with the required safety factors.

The failure criteria retained with current characterizations are based on the material fibrous nature, and generally limited to one direction. Some rupture criteria for bi-axis local load are available but for specific case. They will be discussed in chapter 4.

Simple rupture criteria used commonly are described hereafter :

-Tension : the analysis give the stresses in the fiber direction. This value is compared to the material potential determined on a tension test piece.

-Compression : the failure criteria is badly controlled. The material generally behaves well and the limits obtained with a standart sample are compared with the values in the fiber direction.

-Interlaminar shear : the calculation results are compared with the mean value obtained with a double notch test sample.

-Translaminar shear : a comparison with a IOSIPESCU sample result is made.

Safety coefficients can be imposed by the requirement specification.

It is always higly important to discuss thoroughly with the costumer the origin of the values. Indeed, they often result from an experience acquired with another type of material, that has different behaviours and therefore different design margin requirements.

Considering the high CMC dispersion, a safety coefficient introduced in a statistical form in order to obtain a failure level, is a very constructive approach.

This method requires the following procedure:

- specify the mechanical, thermal or vibratory stresses in statistical form (mean value and standard deviation).
- determine the influence coefficients of loading on the stresses, from the reference calculation (partial derivative)
- perform a serie of calculation with random stresses to determine the stress mean value and standard deviation.

From these statistical results on stresses, the failure rate is calculated by comparison with the material potential mean value and typical deviation. Figure 15 summarizes this logic.

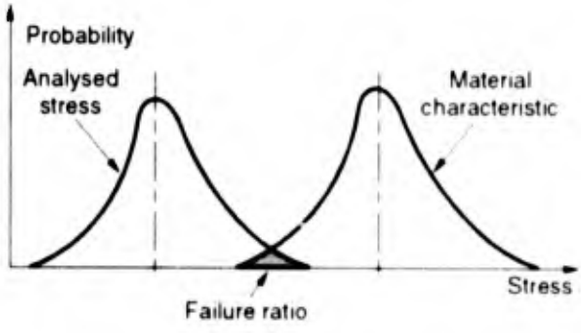

FIGURE 15 : STATISTICAL SAFETY FACTOR

If the material used is characterized at level D or E, and these results used for analysis, you just have then to use the above failure criteria and check safety factors.

Nevertheless, in many cases, the elementary characteristics (level B) are the only ones known to start the project, for example because of the choice of a particular texture suited for the part.

The following methodology, summarized on figure 16, is then recommended to determine the maximum stress allowable for the envelope analysis, and design correctly the part :

- level B characteristics : draw up a characteristic file for dimensioning (mean mechanical behaviour laws, thermal values), and define the average failure values.
- standard deviation : these materials present a noticeable dispersion on failure limits. A 10 % standard deviation, representative of the C/SiC and SiC/SiC population, can be considered by default. Design limits should be taken at -3* standard deviation.
- ageing : characteristic decrease in case of long-lasting stresses in an aggressive environment (oxidation) must be considered. It must be assessed for each case.
- safety factor : if not given by specifications, a minimum value of 1,4 is to be applied on stresses.
- failure criteria : use the simple 1D criteria applied on each fiber direction.

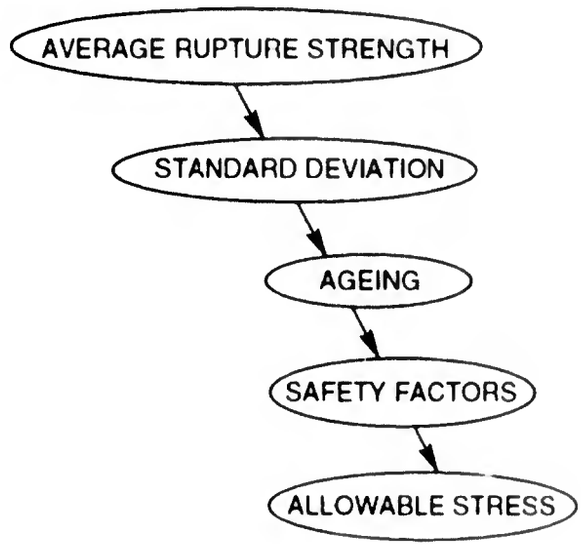

FIGURE 16 : DESIGN METHODOLOGY

4. SINGULAR AREAS AND COMPLEX RUPTURE CRITERIA

An adapted characterization and the mastery of calculation allow correct design of a CMC part current areas. A methodology exists for materials whose characterization is incomplete

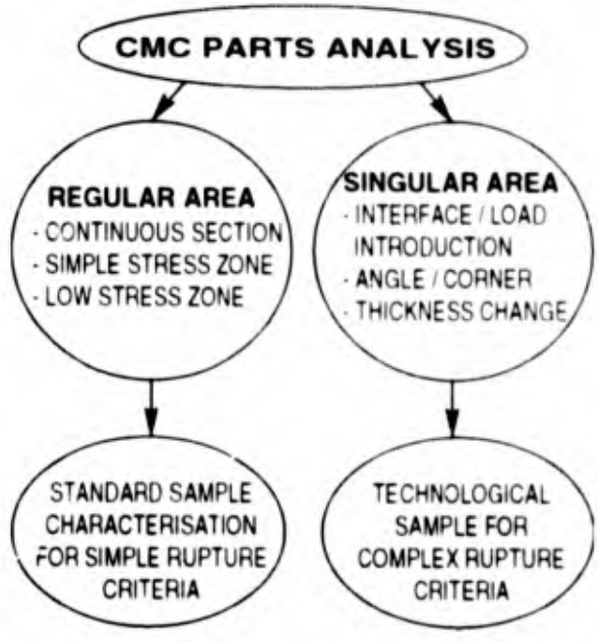

FIGURE 17 : REGULAR AND SINGULAR AREA

However, experience showed that parts generally include two types of areas with a different behaviour :

- regular areas where stress fields and geometries are simple. In these areas, the comparison between calculation and material standard characteristics is relatively easy and correct.
- singular areas: these are in particular shape accidents (angle, corner, thickness change..) or loads introduction areas (interface or bond).

In such singular area, stress fields are very complex and highly sensitive to calculation limit conditions. The standard characteristics resulting from test piece specifically defined for pure stressing are not adapted.

The realistic design of these areas can only be correctly done today by so-called technological samples, with a more experimental methodology.This chapter describes a technological sample, its objectives and the methodology of use. Some examples are then described.

4.1 Technological sample

The objective of a technological sample is to be as representative as possible of the real case in order to determine pertinent failure criteria for the case under consideration.

This representativity must of course regard the material and process which must be the same. It is then essential that the geometry and the mechanical (or thermal) load allow a stress field equivalent to the real case to be obtained. The comparison is made on the stress fields, and it is indeed, the invariant that has to be considered.

The question is in fact to define a low cost simplified part allowing margins to be quantified by a complex rupture criterion definition and behaviors to be specified by failure mode knowledge (FMECA).

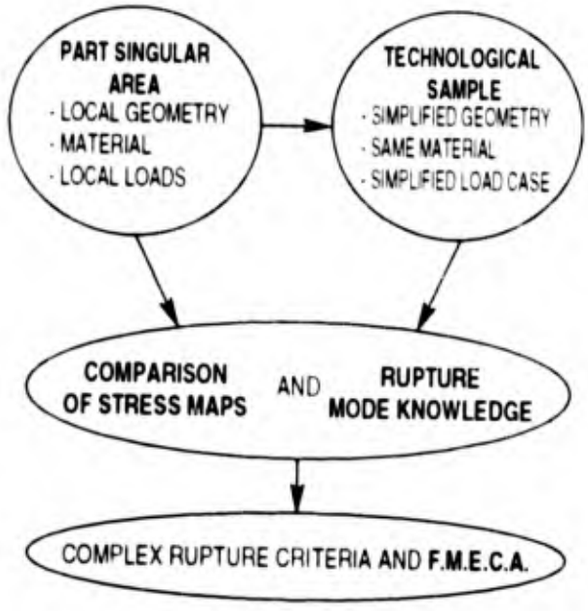

FIGURE 18 : TECHNOLOGICAL SAMPLE

This method presents also the advantage of disregarding the biases brought by the material model an the calculation code, as those are used in similar conditions.

Such methodology can be applied to bi-axis rupture criteria or more complex case.

4.2 Longitudinal shear under compression stress

This kind of load case is encountered for example on parts such as blade attachments or combustion chamber throat where the compression stress procedes from the radial thermal gradient in the throat.

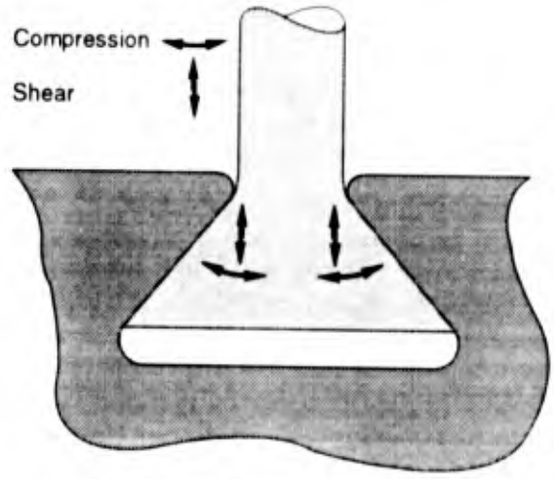

FIGURE 19 : BLADE ATTACHMENT

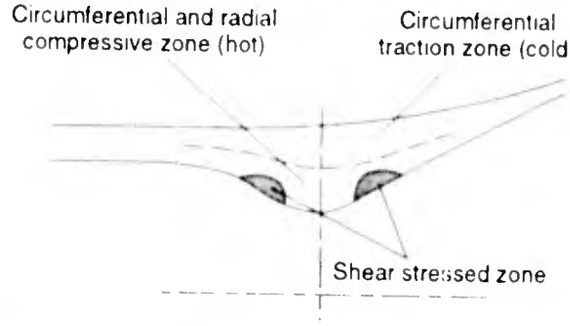

FIGURE 20 COMBUSTION CHAMBER THROAT

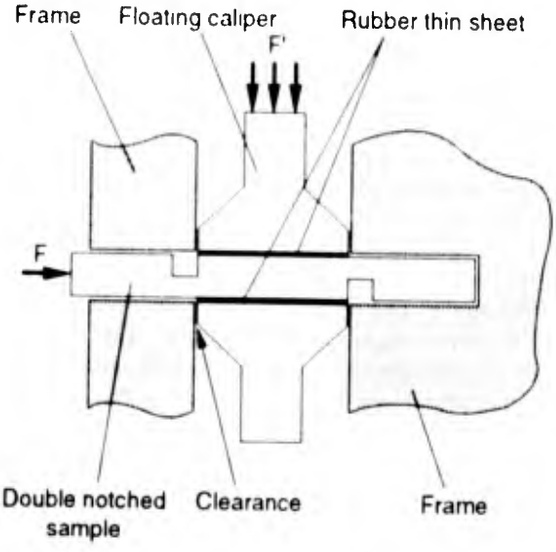

FIGURE 21 : TEST SAMPLE

Technological tests were carried out on the basis of a double notch test sample equipped with a compression device (figure 21). The mean used, floating caliper and thin rubber sheet interface, is far from being irreproachable and the stress field is not totally pure. However, the results are interesting and the tendancies clear. It also has to be noted

that the real cases will also be modelized with the introduction of an unavoidable distortion.

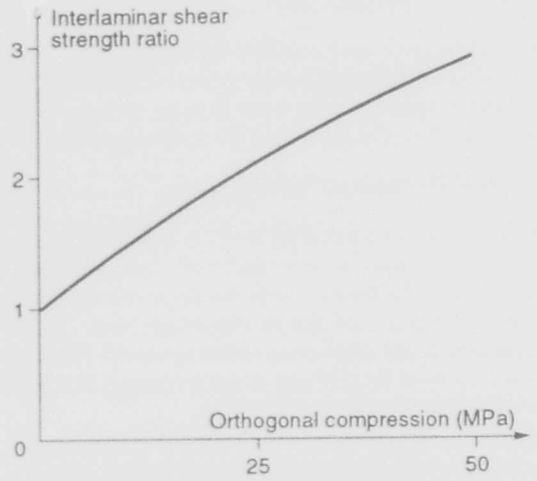

FIGURE 22 : TEST RESULTS

The curve in figure 22 indicates the results for the 2D C/SiC material. The interlaminar shear strength doubles for a compression stress of about 50 MPa. One has to reason upon these elements to define a failure criterion adequate for this specific bi-axis load.

4.3 Overstresses in rotational symetric flange

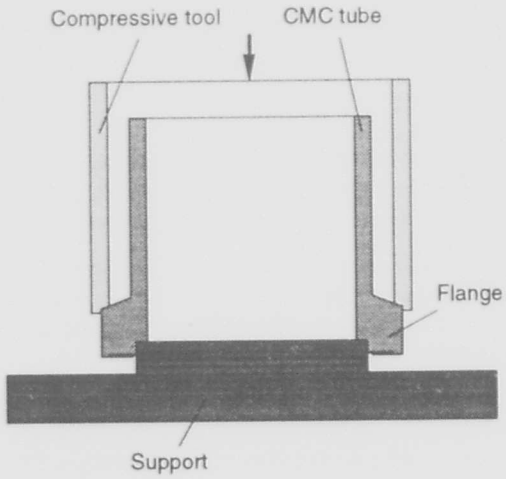

FIGURE 23 : ROTATIONAL SYMETRIC FLANGE DESIGN AND TEST DEVICE

Figure 23 presents the case of an rotational symetric flange with a torsion phenomenon applicable to different parts such as combustion chamber tubes or divergents (such "poor" geometry can be imposed by considerations that differ from pure mechanical requirement).

Regular design driver of such a flange is interlaminar shear stress. But the ring torsion causes the flexion of the tube thin part and very locally generates an important peak meridian tensile stress even with optimised finite element size.

Non linear analysed stress fields in meridian traction and interlaminar shear are presented on figure 24 and 25.

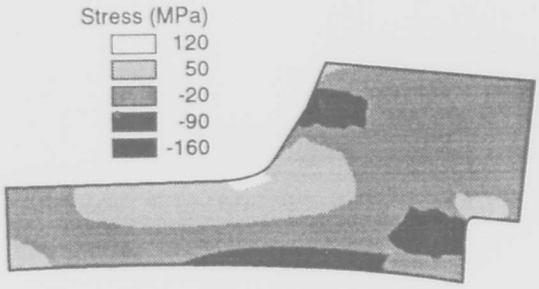

FIGURE 24 : FLANGE MERIDIAN TRACTION STRESS

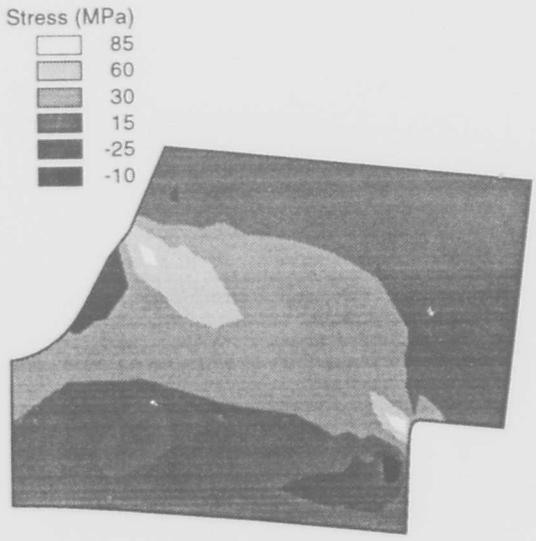

FIGURE 25 : FLANGE INTERLAMINAR SHEAR STRESS

	MERIDIAN TENSILE	INTERLAMINAR SHEAR
MATERIAL STRENGTH - MPa	70	80
ANALYSED PEAK STESSSES MPa	120	85
PERCENTAGE	+ 70 %	+ 6 %

FIGURE 26 : MATERIAL AND TEST RESULT

The failure test shows that the rupture occurs by shearing in the flange for a maximun local value that is 6% higher than the material capacities in very good accordance with material standard rupture value.

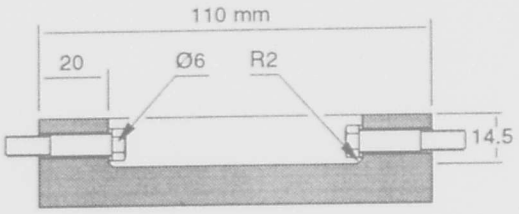

AXIAL SECTION

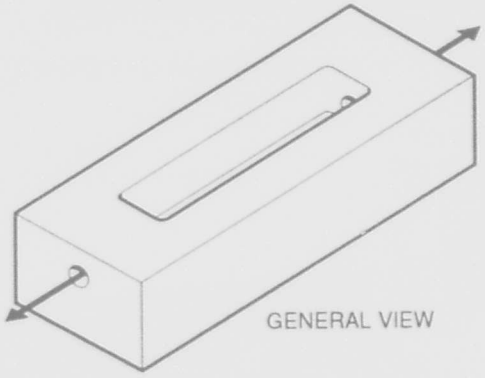

FIGURE 27 : BOLTED ZONE SAMPLE AND TEST DEVICE

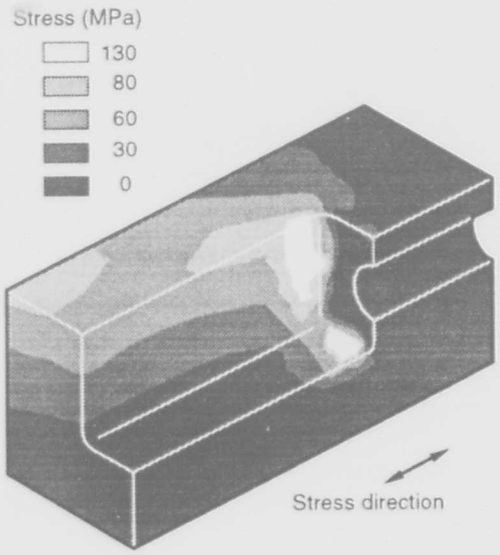

FIGURE 28 : LINEAR BOLT AXIS TENSILE STRESS

At rupture, the maximum meridian tensile stress reaches a value that is 70 % higher than the mean failure value of a standard traction sample. Sample examination do not allow to detect any meridional cracks.

This technological sample allow to conclude that the simple criterion in stresses on the most tensioned fiber is in this case very conservative, the local peakstressed zone is not relevant for FMECA and shear is the good design driver.

4.4 Overstresses in bolted zone

The test piece described in figure 27 is representative of a massive part attachment with machined grooves.The stress field of figure 28 obtained with 3D linear calculation for preliminary design indicates an axial tensile stress concentration area in the connecting radius under the fastening screw head.Axial traction tests of this technological sample showed that the rupture :

- did occur from the overstressed areas,
- for a maximum tensile value twice higher than the material capacities.

Such informations allow to estimate real margin. In that case, the use of linear analysis and consideration of the simple criterion would have been too conservative leading to an over-design.

More sophisticated non linear analysis of this sample will allow to define a relevant rupture criteria for such a couple geometry/load.

This exemple show also that CMC are able to whistand important stress concentration.

5 CONCLUSION

The know how in CMC design is beginning to be formalized. This allows better appreciation of the real potential and application possibilities of the materials that are still very new.

The experience acquired in refractory metal structure and part design and the methodologies developed are used for guidance in structuring these activities, but are not entirely transposable.

The degradation modes and the sensitive parameters differ from those already known and identified for metals or ceramics. Thanks to a better control of these aspects, it is now possible to improve the analysis and the characterization relevance.

Today, a structured approach much more specific to these materials appears following the first global experiments performed and providing a greater determinism and better design control.

CMC Design Consequences

W. Krenkel

German Aerospace Research Establishment
Institute of Structures and Design
Pfaffenwaldring 38 - 40
7000 Stuttgart 80
Federal Republic of Germany

1. SUMMARY

Ceramic matrix composites (CMC) have widely demonstrated their feasibility and performance although no series production has been achieved. Today's status is characterized by long production times, high material qualities with high reproducability and experience in the first structural components. Some unsolved problems are the joining and attachment of CMC parts, the lack of adequate nondestructive testing methods and the insufficient oxidative stability for long term applications. This paper deals with general valid design aspects as a consequence of the CMC materials characteristics and the demand for structural components of high reliability.

2. INTRODUCTION

In uncooled conventional structures the application range is limited to approximately 1000°C by the thermal stability of metallic alloys. Monolithic ceramics are well known for their high service temperature capability, however their low fracture toughness and thermal shock resistance restrict their applicability as a load bearing material within large parts. Reinforcing ceramics by continuous fibres seems to be the only suitable way to create lightweight structural materials for the highest temperature applications.

One of the main restrictions of a commercial use of CMC are their costs - not just the costs of the raw materials but the inherently high production costs due to long processing times. Presently available CMC materials are produced by the isothermal chemical vapour infiltration (CVI) technique, which leads to superior properties, but it is a very time consuming (several months) and therefore very expensive process. As a consequence, alternative techniques are now under development like the gradient CVI, the Si-polymer pyrolysis and the silicon infiltration of C/C. With manufacturing times of only days to weeks from the design to the finished component these processes may allow the opening of the market for a broader range of industrial applications of CMC.

Another aspect of the need for shorter processing times is the lack of experience with these new materials. As their application will be mostly in fail safe constructions, their reliability must be high and their performance must be well known. This presupposes a high learning rate and shorter loops during the materials development to get an adequate knowledge to

Presented at an AGARD Workshop entitled 'Introduction of Ceramics into Aerospace Structural Composites', April, 1993.

design or to predict the life of a CMC component in service.

To enhance the performance of ceramic matrix composites some large scale governmental material programms have been initiated. Between 1979 and 1989 the US Department of Defense and other agencies funded a research programme on CMC with a total of about $250 million [1]. As most important topics the improvement of reinforcements, the fibre/matrix interface, cost-effective processing, testing methodology and oxidation stability were investigated.

Japan's MITI is currently sponsoring an eight-year programme of basic materials development which started in 1989. One essential goal is to raise operating temperatures of carbon/carbon from 1700°C to 2000°C. The tensile strength and stiffness will be increased to 700MPa and 200GPa, respectively, after heating for 20 hours in air at 2000°C and 200 hours at 1800°C [2].

Topics of this long-term R&D programme are the development of suitable protective coatings, an increase of resin char yield and the improvement of chemical vapour infiltration process and pitch based carbon fibres.

In Europe, the French company SEP is leading in the CMC development by the CVI process which results in excellent material properties. A family of C/C, C/SiC and SiC/SiC materials can be produced in different furnaces and some demonstration parts have already been realised [3]. In Germany, the work focuses on the development of faster and therefore less expensive processes. Nevertheless, despite all these international efforts the status today is far away from series production of CMC components.

Generally, composite materials are critically dependent on the interface between the fibre and the matrix. Therefore, the reinforcing fibres, the matrix system and the manufacturing process greatly influence the properties of the material. This is even more true for ceramic matrix composites where the fibre/matrix bondings directly determine the microstructure and the material properties. Their microstructure is characterised by an inherent porosity, a complex chemical composition and more or less low bonding forces. Although different processes lead to CMC materials with different compositions and properties, some general rules and consequences for the design with CMC can be deduced from today's data and will be described in the remainder of the paper.

3. FIBRE REINFORCEMENT AND THERMAL STABILITY

The reinforcing fibres and the fibre/matrix bonding have a dominant influence on the fracture behaviour and the mechanical properties of CMC. To obtain energy dissipating effects at the interface in order to avoid catastrophic failure, low adhesion between fibre and matrix must be achieved. This is a detrimental requirement for polymer composites where strong bondings, reached by special fibre treatments lead to high properties. Therefore, no direct correlation can be expected between fibre strength and the mechanical properties of CMC.

The main future markets for CMC materials are applications in high temperature structures as substitutes for metals or monolithic ceramics. The temperature capability has to exceed at least 1000°C, for very short exposures more than 2000°C. In most technically relevant applications the service conditions are oxidative and the exposure times should be as long as possible. For space applications like TPS and hot structures life times of some ten hours are required while for gas turbines and major terrestrial applications the goal are hundreds to thousands of hours under hot service conditions.

The recent development of CMC is mainly based on carbon and silicon carbide fibres. The thermal stability of carbon fibres is dependent on the mode of graphitization. Tests with HT, IM and HM carbon fibre bundles showed different decreases in mass and strength after exposure in nitrogen (Fig. 1). As a result, influence of temperature is more pronounced than that of the exposure time. Generally, all carbon fibres are very sensitive to oxygen and degrade very fast in air above ca. 450°C with a subsequent reduction in mechanical properties.

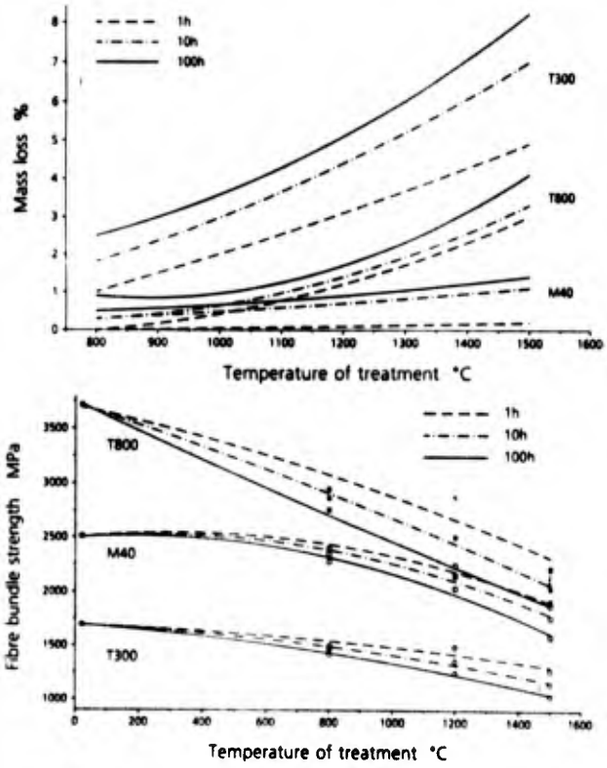

Figure 1: Mass Loss and Strength Degradation of Carbon Fibres with Modes after Exposure in Nitrogen

Two main polymer-derived ceramic fibres are commercially available: Tyranno fibres from Ube Industries and Nicalon by Nippon Carbon (Table 1). These fibres are based on silicon carbide, fabricated by pyrolysis of organo-metallic precursors to yield a continuous, weavable fibre of about 7µm diameter. However, the processing leaves a residue of free active elements like carbon and oxygen which degrade the fibres at ca. 1100-1200°C (Fig. 2).

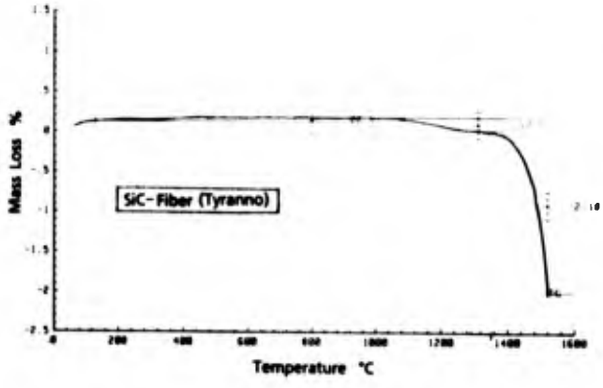

Figure 2: Thermogravimetric Analysis of Tyranno Fibre

In different countries there are major efforts to produce more stochiometric and therefore more stable fibres, but at the moment, they are on a laboratory scale. At present all commercially available, weavable SiC type fibres are very expensive and manufactured in Japan.

In order to achieve the desired pseudo-ductility and to increase the oxidation resistance, coatings of multilayer systems are under development. The lack of bonding provides lower fibre/matrix shear strength and allows crack deflection and fibre pull out effects. The coatings can be applied by different processes like the CVD or sol-gel deposition. The influence of fibre coating can be considerable on strength level and fracture toughness, as shown in Table 2 for C/SiC resp. SiC/SiC materials, manufactured by the Si-polymer route [4]. Nevertheless, fibre coating is not a sufficient method to increase the oxidation resistance of CMC, especially for carbon fibres. The procedure itself is costly and is restricted to smaller amounts of textile preforms.

Generally, today's application range of C/SiC and SiC/SiC materials is restricted by the thermal and oxidative resistance of their reinforcing fibres.

4. PROCESSING OF CERAMIC MATRIX COMPOSITES

There exists a number of different processes for manufacturing ceramic matrix composites. A general overview is given in Table 3. All processes can be divided into two types, the chemical and the liquid phase route. Among all these possibilities only chemical vapour infiltration and polymer pyrolysis have reached a level of technical feasibility. Generally, three different processes are used to manufacture CMC components:

- CVI (isothermal or with gradients)
- liquid infiltration of silicon polymers and subsequent pyrolysis
- liquid silicon infiltration of porous C/C and subsequent chemical reaction to SiC

As processing has a great influence on design concepts, the current state-of-the-art of these processes is now described.

4.1. Chemical Vapour Infiltration

Presently available CMC materials, particularly C/SiC and SiC/SiC are generally produced by the CVI technique. Large furnaces with diameters of up to 2.5 meters have been installed at SEP to manufacture particularly CMC components for the hot structures of Hermes. These facilities allow a scaling-up to volume production, but the already discussed long furnace holding times prevent the isothermal CVI process from entering broader industrial fields. This process, initially developed for the manufacture of carbon/carbon, is well documented in the literature [3, 6].

A fibrous preform is placed inside the furnace and must be held during the early stages of infiltration in a graphite mold to define the correct fibre volume content of the finished component. A common precursor used to form SiC matrices is methyltrichlorosilan, the normal process temperatures lie at 1000 - 1200°C. The preform is infiltrated with steady gas flow rates, but concentration gradients between the surface and interior tend to block off the surface by deposited matrix, preventing further deposition within the preform. The sealed surface can be machined and re-infiltrated, but handling of poorly infiltrated preforms can be difficult. The materials properties are very high and the geometry of components can be complex.

A thermal gradient/forced flow process was originally developed by Oak Ridge National Laboratory [7] and is being applied by the German firm MAN in pilot facilities [8, 9]. Specially prepared preforms allow pressure and temperature gradients over the components to be realised (Fig. 3). The reduction of the total infiltration time to about two weeks, the restriction to symmetrical and simple shapes (eg flat plates, tubes) while maintaining the high strength values of the isothermal CVI are the main characteristics of this process.

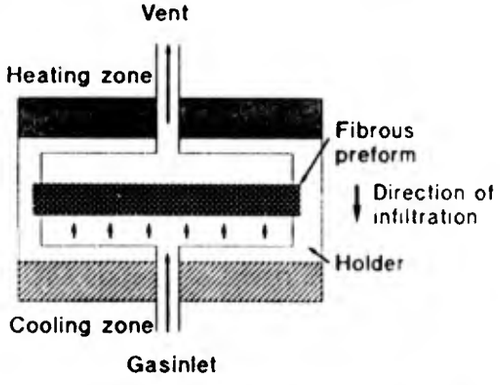

Figure 3: Schematic lay-out of a Gradient CVI reactor [9]

4.2. Pyrolysis of Si-Polymers

This liquid phase route is based on the pyrolysis of ceramic precursors (eg silane or siloxane). Large scale components can be fabricated in technologies, similar to the fabrication of fibre reinforced plastics [4, 10] (Fig. 4). Prepregs are made of Si-polymer, fiiler material and continuous fibres and laminated to the desired shape. The parts are cross-linked and densified in an autoclave and subsequently pyrolysed in inert atmosphere. Due to the decomposition of the precursor several reinfiltration steps are necessary to close the open porosity. The properties are lower compared to CVI but the main advantages of this process lie in the processability of highly integrated, complex shaped structural components.

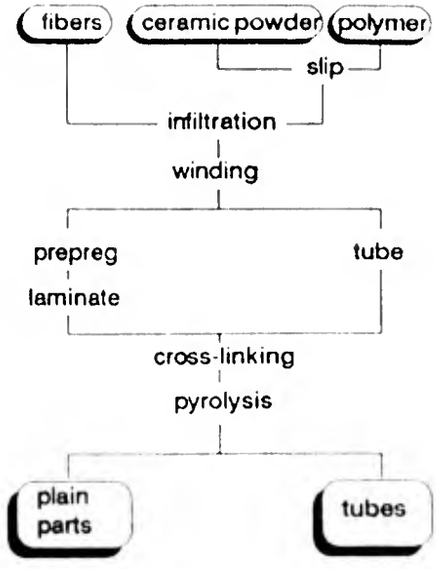

Figure 4: Scheme of the polymer infiltration - pyrolysis technique [10]

4.3. Liquid Silicon Infiltration

The liquid silicon infiltration of porous carbon/carbon with subsequent chemical reaction is an alternative technology to produce CMC structures with lower costs and shorter manufacturing times. The resulting C/C-SiC material shows an internal protection of the load

carrying carbon fibres and different structural components have already been realised [11,12,13].

The process allows a component production period of about two weeks and is based on two principal steps: shaping in the CFRP stage and ceramization of the matrix (Fig. 5 and 6). As precursors, one-part thermoset systems are used to fabricate laminates with 2D- or 3D-reinforcements. By resin transfer moulding (RTM) as well as autoclave technology flat plates, tubes and structural components are manufactured. Generally, the autoclave process is preferred for large spherical shaped components with 2D-fibre reinforcement, whereas more integrated structures with 3D-fibre skeletons are manufactured by RTM.

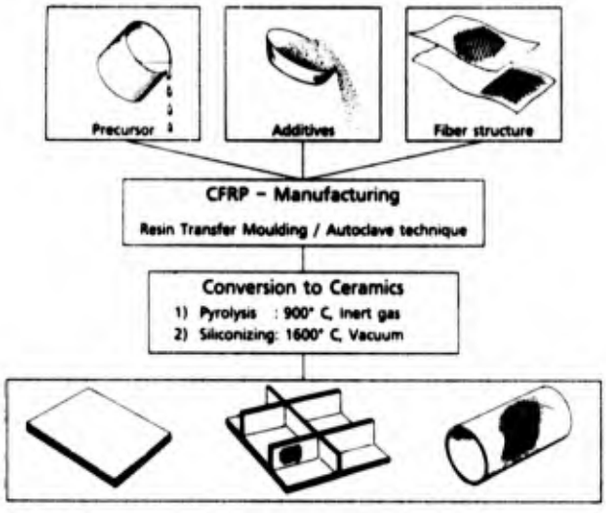

Figure 5: Schematic Illustration of the Liquid Infiltration Process

During pyrolysis (900°C) the matrix adopts a crack pattern as a result of the precursor shrinkage and induced forces by the stiffer fibres. After this thermal treatment the composites show a crack pattern with translaminar channels resulting in an open porosity of about 20%.

During the subsequent siliconizing process (1550°C) one takes advantage of the low viscosity of silicon and its high reactivity with carbon. Within the channels the liquid silicon infiltrates the C/C-composite very quickly driven by capillary forces and the subsequent exothermal reaction with matrix carbon leads to the cracks being filled by SiC. The key points of the manufactured C/C-SiC are the protection of load carrying carbon/carbon areas by silicon carbide to increase the oxidation resistance while maintaining the high damage tolerance of carbon/carbon.

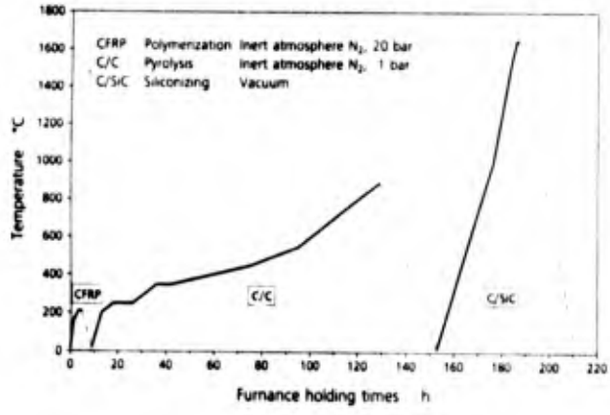

Figure 6: Temperature Profile and Furnace Time of the Liquid Infiltration Process

The state-of-the-art process allows a high flexibility in design and manufacturing of materials with moderate strength levels. The key points for higher strength lie in an appropriate fibre/matrix interface.

As no tooling after shaping is necessary the whole process is realised in a near-net-shape technique resulting in integral structures. Figures 7 to 10 show the sequences in manufacturing by RTM a multi spar component of 270×270×35mm^3 as an intake flap of a hypersonic propulsion system. No joints and no interruption of load carrying fibres are characteristics of this design concept.

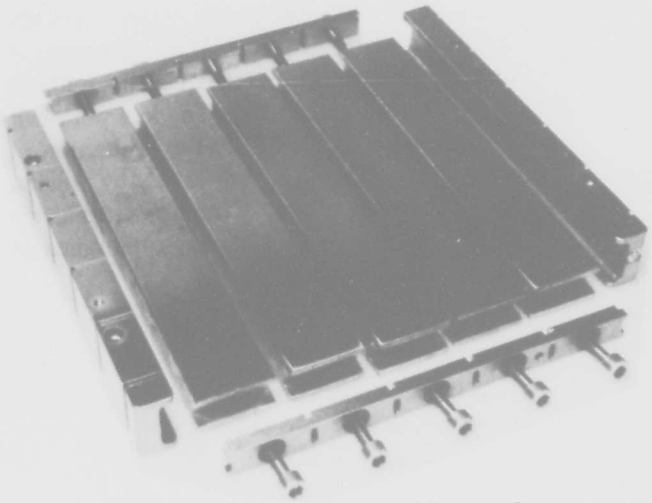

Figure 7: Arrangement of Inserts for the Preform Set-Up

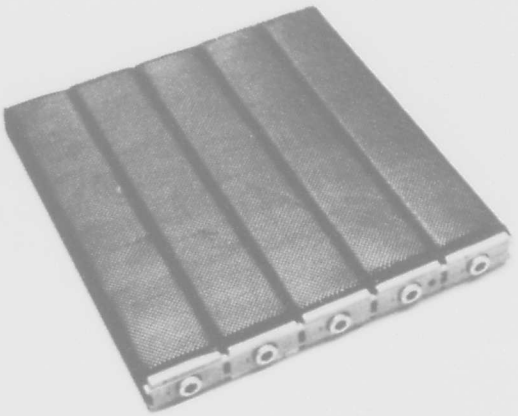

Figure 8: Assembled Carbon Fibre Preform

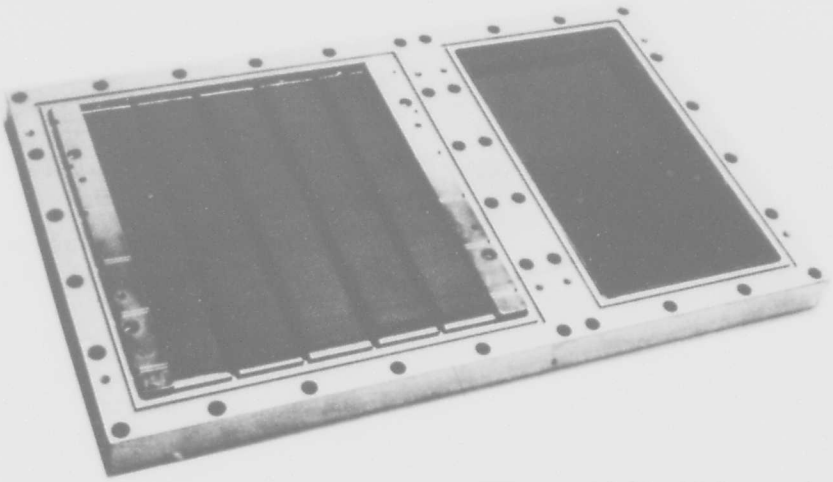

Figure 9: RTM Arrangement of a Two-Chamber Mold with Inserted Fibre Preform (left) and Molten Precursor (right)

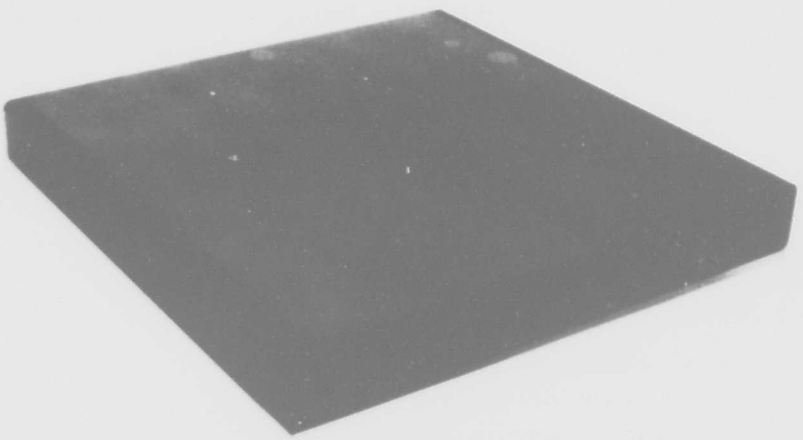

Figure 10: CFRP Component ($270 \times 270 \times 35 mm^3$) Manufactured in a Near-Net-Shape Technique

5. DATA BASE BY REAL FLIGHT EXPERIMENTS

The use of CMC materials in future space transportation systems presupposes extensive evaluation in ground test facilities with wide ranges of Mach number and gas flow. Thus large investments are needed to simulate the flight envelope, mainly the reentry trajectory, with material samples and full-scale components required over a large domain. These very expensive tests are usually carried out in plasma wind tunnels to simulate the high heat fluxes occuring in reentry conditions.

Furthermore, functional tests with combined thermal and mechanical loads have to prove the reliability of structural parts before their implementation in vehicles' primary structures.

In Europe, several different test facilities are available, eg the solar furnace in Spain (Almeria), plasma wind tunnels in Germany (Stuttgart, Cologne) and high enthalpy facilities in France (Bordeaux).

The development of experimental aircraft as technology demonstrators is a common way to get reliable flight test data. The Bell X-15 which flew nearly 200 times before it was cancelled in 1968, or the Lockheed SR-71, actually under discussion as a carrier for half-scale NASP engine cowling and exhaust nozzle, are examples from the pre-Shuttle time. Today, research vehicles and flight test programmes are projected for NASP (X-30) as well as for the Japanese HOPE (OREX) to gain experience of other technologies with new reusable heat protection systems.

Presently, there are only two vehicles with CMC hot structures, the US Shuttle and the Russian Buran. While the Shuttle has accumulated up to now launch and flight experience from 55 missions over a 12 years flight period, the generally similar Buran has flown once in a three-hour automated test flight in 1988.

Over the life of the Shuttle programme, experience showed that for about 60-70% of the time an orbiter will be out of service for some reason. Cost estimations of one Shuttle flight amounts to between 200-500$ million with marginal costs of about 40$ million per launching.

Summarizing these facts it has to be expected that an experimental winged vehicle to evaluate advanced CMC thermal protection systems will be extremely expensive and will not be able to satisfy all the demand for flight opportunities. To get high reliability in CMC design and characteristics the best way would be a step-by-step learning process by successive reentry testing. A solution would be the use of capsules for low cost flight opportunities with reentry capability [14]. Although for example the heat fluxes are considerably higher compared to winged spacecrafts (about a factor ten) the conservative design approach of partially replacing the ablative heatshield by CMC shingles allows a fast increase of knowledge about the materials behaviour under severe conditions. Enhancing reliability, lower launch costs and no scaling down of experiments are some main advantages of CMC testing in capsules.

6. DESIGN CONSEQUENCES

Generally, the substitution of metals by CMC in primary structures requires a new design philosophy. Basic investigations in manufacturing, testing and integration are necessary for optimization in several iterative loops. Therefore, a high availability of CMC materials must be guaranteed.

Series production or an even broader application of CMC presumes low-cost processes with short manufacturing times to allow a rapid implementation of design changes. The most time consuming steps of current CMC fabrication are the furnace holding times, due to either low deposition times when infiltrating by chemical vapour (CVI) or several re-infiltration and pyrolysis steps for the polymer route of C/SiC fabrication.

In regard to microstructure, composition and characteristics ceramic matrix composites differ from all other structural materials and represent a separate class of material. Although there are considerable differences between the individual materials and processes, some generally valid statements about an appropriate component design can be done.

6.1. Properties and Design Stress Level

The mechanical and thermal properties of ceramic matrix composites, manufactured with processes as described in section 4, are published in literature and summarized in Table 4. All values refer to C/SiC resp. SiC/SiC with bidirectional reinforcements and fibre contents of more than 40%. Both CVI processes, isothermal and with gradients, lead to high mechanical properties with ultimate tensile strength levels of ca. 350MPa at room temperature and under static loads. The corresponding values for ceramic composites fabricated by the polymer route are considerably lower. For these processes higher strength levels can be achieved by lower fibre matrix bondings, realised for example by additional fibre coating or by thermal fibre pretreatments. In the case of Si-polymers several re-infiltration cycles with the liquid precursor and subsequent pyrolysis increase the tensile strength considerably (see Table 2).

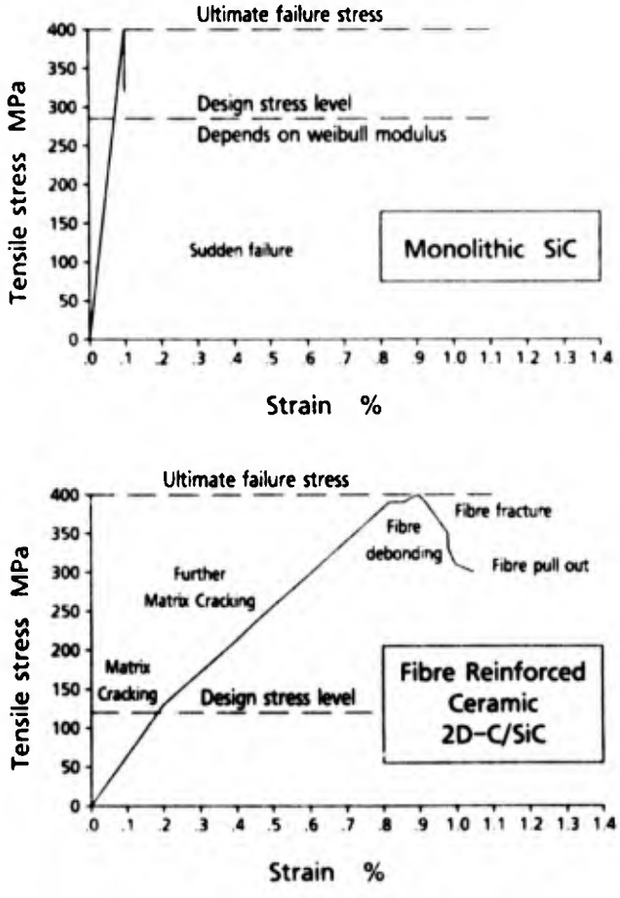

Figure 11: Stress/Strain Diagrams of Monolithic and Bi-Directional Reinforced C/SiC

In comparison to monolithic ceramics with their brittle failure behaviour damage tolerant CMC materials show at the same stress level failure strains an order of magnitude higher (Fig. 11) as a result of irreversible energy absorbing mechanisms like matrix cracking, fibre debonding and pull out. Principally, the total stress/strain curve can be divided into a first zone of linear-elastic behaviour with no essential decrease in stiffness, although some matrix cracks occur from the very beginning, and a second zone with distinct decrease of composite stiffness characterised by pronounced matrix cracking. The transition point cannot clearly be defined for CMC materials, but the corresponding stress level is much lower than the ultimate failure stress of the material.

If the transition point is accepted as the maximum allowable stress level, the best CMC materials with static strength levels of about 350MPa would have a maximum design stress of 100-150MPa, corresponding to 0.2-0.3% strain. Furthermore this design stress has to be reduced by adequate safety factors. Summarising, the usable stress levels of CMC are much lower than the characteristics in Table 4.

6.2. Limits in Time and Temperature

The lifetime of CMC structures is limited by the thermal stability of the fibres. Currently available CMC materials are short time materials and allow applications at high temperatures in the range of minutes to some hours, depending on environmental and load conditions. SiC/SiC materials are limited by recrystallisation effects of the ceramic fibres, which starts far below the ultimate application temperature of ca. 1200°C. C/SiC materials show a certain amount of oxidation resistance, but oxidation can rapidly occur by oxygen diffusion via inherent matrix porosities and microcracks or from exosed fibre ends. At present no oxidation protection systems are available in the near future which allow long term applications in the range of some tens or hundreds of hours. Combinations of fibre protection, internal protection and surface coating are promising approaches but such highly sophisticated protection systems will be extremely expensive and are restricted to some few applications. In all other cases one has to

accept the limited lifetime of C/SiC structures. As a consequence, new design concepts must allow a fast and reliable replacement of expired or damaged structures. This requires high temperature joining techniques with advanced materials and joining procedures. On the other hand, highly integrated, complex structures would minimize the number of joints, therefore suitable manufacturing process with near-net shape technology must be available for new design concepts.

6.3. Low Cost Material for Model Structures

CMC materials, manufactured by chemical vapour infiltration, show very high and reproducible properties. However, costs and delivery time are also very high and due to strategic reasons their availability is not guaranteed. To force the implementation of these materials into new markets and to solve basic problems like high temperature joining and attachment of structures, model structures with lower but representative performance must be available. These model structures should be manufactured within short times and at low costs. As a result CMC materials and structures are available in short development loops and will increase knowledge and experience in designing with this new class of materials.

7. CONCLUSIONS

In comparison to monolithic ceramics CMC have the potential of higher damage tolerance. Energy absorbing mechanisms like matrix cracking, crack deflection and fibre pull out can locally decrease stress peaks, resulting in ultimate strains up to 1%. At present the process of chemical vapour infiltration and the liquid phase routes are at different levels of development, thus leading to CMC with different properties.

Due to limits in oxidation and temperature stability of available fibres, the application of CMC at present is restricted to three domains:

- For application temperatures below 800-1000°C large, thin walled components may be fabricated, which cannot be realised in monolithic ceramics. Generally, the lower the stress level and temperature, the higher the application time.
- In temperature ranges above 1000°C CMC materials are primarily candidates for extreme lightweight structures of limited lifetime.
- Due to their high properties under abrasive and corrosive conditions CMC can partially replace monolithic ceramics and super alloys in components, where the material strength level is no critical feature.

The future achievement of CMC depends critically on the development of fibres with increased thermal resistance and of cost efficient fabrication processes. Beyond that the improvement of oxidation protection as well as the development of adequate joining techniques are of high interest. With continuing development, CMC are expected to be used in space (thermal protection systems, hot structures), aeronautical (combustion chambers, engine flaps) or terrestrial HT applications (heat exchangers, tooling devices, brake disks).

8. REFERENCES

[1] Sheppard, L.M., *Enhancing Performance of Ceramic Matrix Composites*, Ceramic Bulletin, Vol 71, No. 4, 1992

[2] Dornheim, M.A., *MITI Pursues Improved High-Temperature Materials*, Aviation Week & Space Technology, August 17, 1992

[3] Desnoyer, D., Lacombe, A.,Rouges, J.M., *Large Thin Composite Thermostructural Parts*, Proc. Internat. Conf.: Spacecraft Structures and Mechanical Testing, Noordwijk, The Netherlands, 24-26 April 1991

[4] Ostertag, R., Trabandt, U., *Fibre-Reinforced Ceramic Components by Filament Winding for Intermediate Temperature Applications*, Proc. Internat. Symp. 'Advanced materials for lightweight structures', ESTEC, Noordwijk, The Netherlands, 25-27 March 1992

[5] Hüttinger, K.J., Greil, P., *Keramische Verbundwerkstoffe für Höchsttemperaturan-*

wendungen, BDLI-Werkstofftag, Hamburg, 13-15 Nov. 1991

[6] Heraud, L., *Main Characteristics and Domains of Application of C/SiC and SiC/SiC Ceramic Matrix Composites*, Proc. Verbundwerk, Wiesbaden, Germany, Febr., 1990

[7] Stinton, D.P., Besmann, T.M., Lowden, R.A., *Advanced Ceramics by Chemical Vapour Deposition Techniques*, Ceramic Bulletin Vol. 67, No. 2, 1988

[8] Mühlratzer, A., *CVI-Verfahren zur Herstellung faserverstärkter Keramik*, CCG-Seminar Faserkeramikwerkstoffe - Eigenschaften und Anwendungen, Stuttgart, 24-25 Nov. 1992

[9] Mühlratzer, A., Handrick, K., Köberle, H., Peetz, K., *New Process for Lightweight Ceramic Matrix Composites*, Proc. Internat. Symp. 'Advanced materials for lightweight structures', ESTEC, Noordwijk, The Netherlands, 25-57 March, 1992

[10] Haug, T., Ostertag, R., Schäfer, W., *Fiber Reinforced Ceramics for Aerospace Applications*, SAMPE European Chapter 1992

[11] Krenkel, W., *Fiber Ceramics for Reentry Vehicle Hot Structures*, IAF, Malaga, 1989

[12] Kochendörfer, R., *Liquid Silicon Infiltration - A Fast and Low Cost CMC-Manufacturing Process*, ICCM, Honolulu, 1991

[13] Krenkel, W., Schanz, P., *Fiber Ceramic Structures Based on Liquid Impregnation Technique*, IAF, Montreal, 1991

[14] Hald, H., Schöttle, U.M., *Analyse und Konzeption eines Hitzeschildexperiments mit einer C/SiC-Faserkeramikkachel für die EXPRESS-Kapsel*, DGLR-Jahrestagung, Berlin, 1991

[15] Data Sheet Sintec Keramik GmbH, 1991

TABLES

	Unit	HT (T300)	HM (M40)	UHM	Pitch	Nicalon (NL-200)	Tyranno	Si_3N_4
Manufacturer	-	Torayca	Torayca	Tonen	Idemitsu	Nippon-Carbon	UBE	Tonen
Composition	-	C: 95%	C: 100%	Pitch	Pitch C: 95% H: 5%	SiC: 65% SiO$_2$: 23% C: 12%	Si: 48% C: 28% O: 18% Ti: 4%	Si: 60% N: 37% O: 3%
Price roving/fabric	DM/kg	80/200	250/800	5000/-		1000/2500	1200/2000	
Number of fil.	-	1000-12000	1000-12000	3000	3000	500	400-1600	6000
Diameter	µm	7.0	6.5	10	10	15	11	10
Tensile strength	MPa	3500	2700	3300	3600	2500-3000	2800	2500
Young's modulus	GPa	230	400	700	250	180-200	206	300
Elongation	%	1.5	0.6	0.5	1.5	1.4	1.5-2.0	~1.0
Density ρ	g/cm^3	1.75	1.80	2.15	2.0	2.55	2.3-2.4	2.5
Spec. electr. resistance ρ	Ωm	$20 \cdot 10^{-6}$	$8 \cdot 10^{-6}$		$10 \cdot 10^{-6}$	10	10	
Coefficient of thermal exp. α	K^{-1}	$-0.5 \cdot 10^{-6}$	$-0.5 \cdot 10^{-6}$	$-1.5 \cdot 10^{-6}$		$3.1 \cdot 10^{-6}$	$3.1 \cdot 10^{-6}$	
Spec. heat c	J/(kgK)	0.71	0.71			$1.14 \cdot 10^{-3}$	$0.79 \cdot 10^{-3}$	
Heat transfer coefficient λ	kJ/(mhK)					41.88		
Dielectric constant ε_r	-					9		
Temp. of app. T_{max}, air/inert	°C	400/1700	500/2000	500/2000		-/1200	1000/1300	-/1200

Table 1: Selection of Carbon and Ceramic Fibres for CMC Materials

CMC / Properties 3/92		C/SiC			SiC/SiC		
Infiltration Cycles		1	1	3	1	1	3
Fibre Coating		-	PyC	PyC	-	PyC	PyC
Porosity	%	20-25	20-25	10-15	20-25	20-25	10-15
Density	g/cm³	1.6-1.7	1.6-1.7	1.9-2.0	1.9-2.0	1.9-2.0	2.3-2.4
Tensile Strength	MPa	100-120	180-260	250-300	30-40	140-160	180-200
Elongation	%	0.2	0.4-0.6	0.4-0.6	0.1	0.4	0.2
Young's Modulus	GPa	60-80	60-80	70-80	80	80	90
Interlaminar Shear Strength	MPa	4	2	12	6	6	20
Bending Strength	MPa	100-120	80-100	190-210	150-160	160-190	280-300
Bending Strength 1000°C	MPa	-	-	-	150-160	160-190	280-300
Bending Strength 1100°C	MPa	-	-	-	150-160	-	
Lamination: 0/90° UD-Prepregs					Fibre Content: 45-55 %		

Table 2: Properties of CMC Materials Manufactured by the Si-Polymer Route

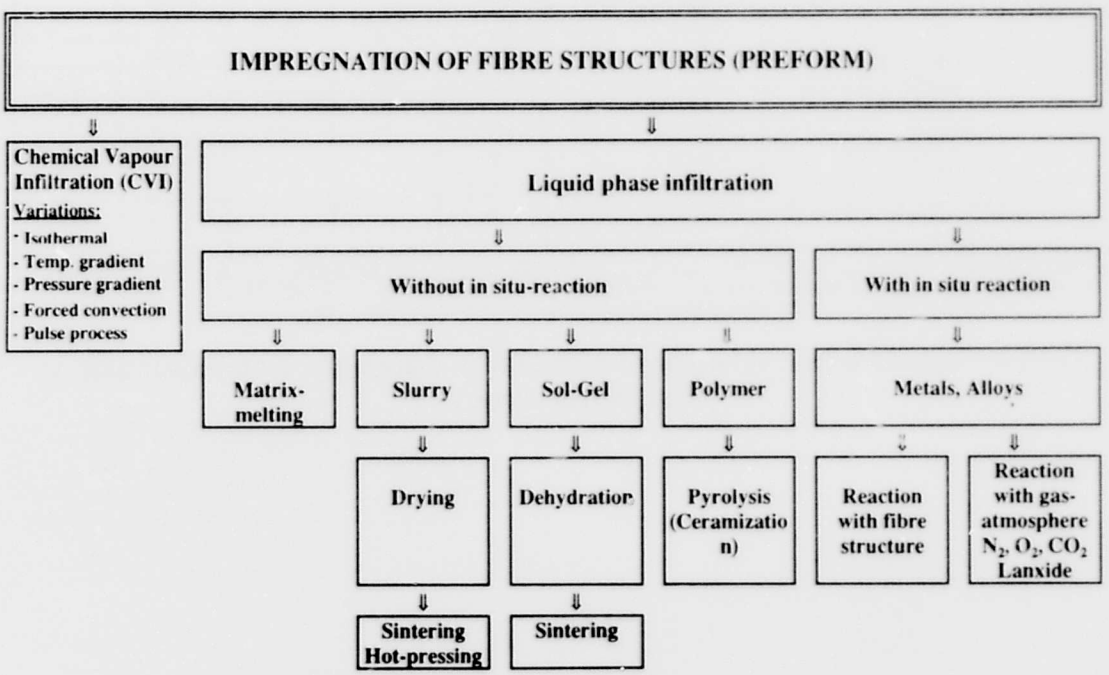

Table 3: Manufacturing Processes for CMC Materials [5]

Properties	Units	CVI-Route				Polymer Route (*)			Monolith. Ceramic
		Isothermal		p,T-Gradient		Si-Polymer		Si-Infiltration	
		C/SiC	SiC/SiC	C/SiC	SiC/SiC	C/SiC	SiC/SiC	C/C-SiC	SSiC
Tensile strength	MPa	350	150-200	270-330	300-350	100-120	30-4[illegible]	90-110	
Elongation at break	%	0.9	0.3-0.5	0.6-0.9	0.5-0.8	0.2	0.1	0.23	
Young's modulus	GPa	90-100	170-230	90-100	180-220	60-80	80	60-70	405
Compression strength	MPa	580-700	300-580	450-570	440			300	2900
Flexure strength	MPa	500-700	280-400	450-560	500-600	100-120	150-160	160-200	350-400
Shear strength	MPa	35	25-40	45-55	65-75	4	6	55-60	
Open Porosity	%	10	10	10-15	10-15	20-25	20-25	3-7	
Fibre content	Vol.%	45	40	42-47	40-50	45-55	45-55	55-65	
Density	g/cm^3	2.1	2.5	2.1-2.2	2.3-2.5	1.6-1.7	1.9-2.0	1.8-1.95	3.1
CTE ∥	10^{-6}1/K	3 (1)	3 (1)	2 (2)	4 (2)	3	3	1-2 (3)	4.1
CTE ⊥		5 (1)	1.7-3.4 (1)	5 (2)	4 (2)	5	2.5	4-6 (3)	
Thermal conductivity ∥	W/mK	14.3-20.6 (1)	15-19 (1)	14	20			10-15 (4)	105
Thermal conductivity ⊥		6.5-5.9 (1)	5.7-9.5 (1)	6	10			6-8 (4)	
Specific heat	J/kgK	620-1400	620-1200	600				1150-1850	660
Manufacturer		SEP [3]		MAN [8]		Domier [4]		DLR	Sintec [15]

∥ = parallel, ⊥ = perpendicular to fibre direction, (1) = RT-1000°C, (2) = 100-1000°C, (3) = RT-1500°C, (4) = 200-1700°C.
(*) Values without additional fibre coating and after one infiltration cycle

Table 4: Typical Mechanical Properties of 2D-CMC in Comparison to Monolithic SSiC as Published in Literature

Integrated Approach in Modelling, Testing and Design of Gradient-CVI Derived CMC Components

D. Sygulla, A. Mühlratzer and P. Agatonovic
MAN Technologie AG
8000 München 50, Bauschingerstraße 20
Germany

SUMMARY

Ceramic composite materials with continuous fibres in a SIC matrix, manufactured by CVI, have shown benefits for structural applications due to high fracture toughness and damage tolerance under operational conditions. However, the production time associated with the hitherto applied CVI technique entails development cycles of hardly acceptable long duration. Therefore, there is growing interest for the CVI technique to manufacture reliable CMC parts, focusing special attention on a more efficient production technology. In this paper a current attempt to develop and qualify a new CVI process, the so-called gradient-CVI, is described and discussed. This process offers increased productivity appropriate for industrial production and excellent material properties.

LIST OF SYMBOLS

CMC	Ceramic Matrix Composites
CVI	Chemical Vapour Infiltration
GAST	Gas Cooled Solar Tower
C/SiC	Carbon-fibres/Silicon-carbide matrix
SiC/SiC	Silicon-carbide fibres/Silicon-carbide matrix
2D	2-dimensional
3D	3-dimensional
E_{CMC}	Young's modulus of CMC
E_F	Young's modulus of fibres
E_M	Young's modulus of matrix
E_D	Mean cyclic Young's modulus
E_{COM}	Young's modulus of cracked composite
V	Volume fraction of fibres
γ_M	Fracture energy of matrix
R	Fiber diameter
ν	Poisson's ratio
ε_M	Strain in matrix
τ	Shear stress
Δ	Matrix crack distance
σ_M	Matrix normal stress
σ_S	Matrix crack saturation stress
σ_B	Rupture stress
K_c	Critical fracture toughness
GFRP	Glas fibre reinforced plastics
CFRP	Carbon fibre reinforced plastics

1. INTRODUCTION

The need for structural materials that allow reliable operation under high temperatures has posed a real challenge for the current technological development especially for future supersonic transport. The mechanical and physical properties of ceramics, such as, high temperature strength, low weight and low thermal expansion, offer an advantage over other materials for the use in lightweight structures operating under high temperature conditions. However, the conventional monolithic ceramic materials manifest a wide scatter in strength properties and they are known to be extremely sensitive to stress concentration and to the presence of very small flaws. This shortcoming of the monolithic ceramic materials can be overcome with CMC materials.

The application of ceramic as a structure material, was initiated at MAN Technologie many years ago in the development and testing of the ceramic heat exchanger for a solar power station (GAST). A further step was the development program of components for the "adiabatic" diesel engine, where MAN Technologie has gained experience with the use of ceramic matrix composite materials. The engine was mocked-up with a piston insert of SiC/SiC, a cylinder head plate, ceramic flame-sprayed valves and a cylinder liner in the exhaust channel, consisting of monolithic Al_5TiO_2, [1, 2]. In a series of different component and engine tests, the ceramic composite materials with continuous fibres in a SIC matrix, manufactured by CVI, have shown benefits in structural applications, [3]. High fracture toughness and damage tolerance under dynamic load conditions at appreciable stress levels were clearly demonstrated. However, it became evident that the long production time associated with the hitherto applied CVI technique entails development cycles of hardly acceptable duration. From simple geometrical design changes to testing required turn-around times of up to 1 year. Therefore, industry has focused special attention on the CVI technique to manufacture reliable CMC parts since an efficient production technology is a mandatory prerequisite for a broadened utilisation of CMCs. The so-called gradient-CVI offers increased

Presented at an AGARD Workshop entitled 'Introduction of Ceramics into Aerospace Structural Composites', April, 1993.

productivity appropriate for an industrial production and excellent capabilities to produce high performance materials. A current attempt to develop and qualify this new CVI process is described and discussed in this paper. The process, using temperature and pressure gradients throughout a fibrous preform, was originally introduced for the manufacture of carbon/carbon composites, [4] and was successfully transferred to the SiC matrix infiltration at the Oak Ridge Laboratory in the USA, [5]. This paper describes, as far as is known, a first approach to the industrial scaling-up of the gradient CVI-process for the manufacturing of SiC matrix composites.

Another important condition, in terms of cost-effectiveness of CMC components, is the appreciation of an integrated design concept as CMCs are typical engineered materials, i.e., the design of a component has to adequately combine operational demands, manufacturing needs and limits, and the inherent anisotropy of the properties of the composite material.

2. SELECTION OF MANUFACTURE AND DESIGN CONCEPT

Extension in the use of CMC materials requires not only solutions to a number of technical problems, but also changes in the outlook of designers which are accustomed to concepts more appropriate for conventional materials.

Traditionally, most designs are based on previous experience and similar designs, with some modifications introduced to fulfill particular requirements. According to this, many designs tend to evolve gradually as a series of modifications of the same basic plan. The designer is trying to make his best judgement concerning the expected behaviour of a new structure on the basis of information and measurements from previously realised designs. Taking this approach in case of the CMC materials can lead to serious problems. When designing a structure to be made of metal, for example, the designer specified the stress level below elastic limits to be safe. Local strain increase above the elastic limit yields to plastic deformation, but will seldom cause fracture, because the metallic material can adapt to some strain increase and failure can appear only after a thousands of repeated cycles at the same level. In bulk ceramics no significant plastic deformation can occur without failure. The conventional monolithic ceramic materials manifest a wide scatter in strength properties and since they do not yield, they are not capable to redistribute high local stresses as typically other design materials will do. Due to this brittleness, bulk ceramic is very sensitive to stress concentrations and looses total strength even if a very small flaw is present. Therefore, designing with ceramics is very different from designing with metals, which are much more tolerant of local stress peaks, flaws etc. This shortcoming of the monolithic ceramic materials can be overcome with the ceramic composite materials by combining the advantages of both the monolithic ceramics and diminishing their weaknesses. It is clear that both CMC ingredients, fibre and matrix, correspond to bulk ceramics. But their composite behaviour changes strongly, making CMC-materials attractive. Thus, both experience in metallic as well as in bulk ceramic materials is less relevant and may not be directly applied to CMC parts.

On the other hand, glass fibre composite parts deformation and fracture mechanisms are completely different to CMC materials, too. For CFRP and GFRP materials the function of the relatively weak matrix is to bond the fibres together, providing the strength, that is lacking in the matrix. Again the corresponding behaviour and the design experience is less relevant for the CMC application with the brittle SiC matrix. However, virtually any form of fibre lay-up that is possible with plastic composite, including three-dimensional fibre architecture, is also possible with CMC. Based on this, the preform manufacture experience can be very valuable for CMC applications, but the same forms should never be applied prior verification.

Based on above findings it is clear that nearly no background from valid experience with other kind of material is available. Moreover, direct transfer of these experiences may be very erroneous and can lead to inefficient and unreliable designs of CMC structures.

In essence, CMC structures should really be considered as structures rather than as materials. Accordingly, it is essential to have an integrated design process based on the synthesis of the material, structure and manufacture processes and/or requirements and capable of balancing the relevant manufacturing and design variables within of the solution. Thus, the design of a component has to adequately combine operational demands, manufacturing needs and limits, and the inherent anisotropy concerning the properties of the composite material.

The concept of the integrated design of the CMC structures is the essential part of the MAN-approach. Based on this, the following research priorities for development work were selected:

- Efficient parts manufacture, compatible with a commercial/ industrial environment, guaranteeing low cost and low time to perform all operations that comprise component production. Time like money, material, man power etc. is a resource defining the profitability, i.e., simple acceleration of the manufacturing process can lead to a significant increase in the profitability and overall efficiency. To this end, development and

qualification of a new gradient-CVI process, with an increased productivity appropriate for an industrial production, is the main subject of the developmental work, explained in more detail in the next chapters.

- Quality and the ability to inspect the product are most important to the success of CMC materials. The high sensitivity of both ceramic constituents to any kind of defects requires the establishment of appropriate NDI methods fully capable of assuring acceptable quality and the conformance with the reliability requirements. The parts must be designed so that the quality control actions can be reliably performed on all components and over the whole volume.

- Quality control means conformance with the requirements when manufacturing a batch of parts with the spatial geometry. Under these conditions, the importance of treating CMC as structures rather than as materials gets full attention. One must be sure that important properties, examined and validated, using typical one dimensional laboratory specimens, are also achieved on the components.

- The above requirements of quality assurance lead inevitably in the case of ceramic applications, to structure elements of uniform shape, which, after careful NDI control and preparation of interface surfaces, may be assembled in structures of different geometries. At the same time, the gradient-CVI process favours regularly shaped parts. Therefore, MAN Technologie's design concept relies on the utilisation of standardised parts, such as stiffened plates, profile beams and spars and tubular elements, to yield their short manufacturing cycles at a cost advantage. This "Building Box" principle requires reasonable joining methods for complex parts. Different approaches are under development depending on the load conditions of the particular operation. However, because of the severity of the joining of the CMC parts problem, extensive fastening should be avoided. In this respect, therefore, careful optimisation of the design is necessary.

- High reliability of the final product means, in addition to high performance and reliability in service, the possibility to repair or replace a damaged component with an acceptable effort. Also, in this respect, the use of parts assembled in the structure allows individual proof, repair and replacement of damaged components and is, therefore, advantageous. The corresponding maintenance system, fully proved in the case of metallic structures, is for the purpose of CMC structures even more promising. However, the weak point is the design of reliable joints.

- Using accurate machining (grinding) of all interface surfaces can prevent high residual and assembly stresses to appear under fastening/joining operations. Although the extensive and expensive machining has to be avoided, the distortions under basic manufacture conditions cannot be avoided and their removal by machining is desirable and possible. It is clear that in the case of integrated structures the removal of residual stresses may not be possible.

3. MANUFACTURING PROCESS

The manufacture of CMC components on the basis of the gradient-CVI process comprises three major working steps, which are

- Preparation of stabilised fibrous preforms near to net shape
- Infiltration of the fibre coating material and of the SiC matrix in one process
- Machining as appropriate

These working steps are described in the following in more detail.

3.1 Preform preparation

Whenever possible commercially available 2D-woven fabrics are used, for economic reasons, to build up the fibrous preform. Usually the fabrics are laid-up by hand into appropriate moulds. During this procedure a resin which can be a purely organic one or a silicon bearing polymer, is put between the fabric layers in a quantity which provides sufficient strength to set and keep the shape but avoids the impairment of the subsequent vapour infiltration process. Prior to the CVI step, the shaped preform is mounted in a flanged holding tool and then the adhesive resin is cured and pyrolyzed under inert gas. Thus, a stabilised, self-supporting preform ready for CVI is obtained.

3.2 Matrix infiltration by the gradient-CVI process

The holding flange with the preform is mounted into the CVI furnace in a way that the flange and the wall of the fibrous preform separate the furnace chamber into two parts which are, in terms of an infiltration gas flow, upstream and downstream. A sketch of a gradient-CVI reactor principle is shown in Figure 1. When the gas flow is let in the CVI furnace, a pressure gradient results at the porous preform walls. Its amplitude depends on the gas flux, the wall thickness and the fibre architecture of the preform. During the infiltration run, the pressure gradient increases with the proceeding matrix growth.

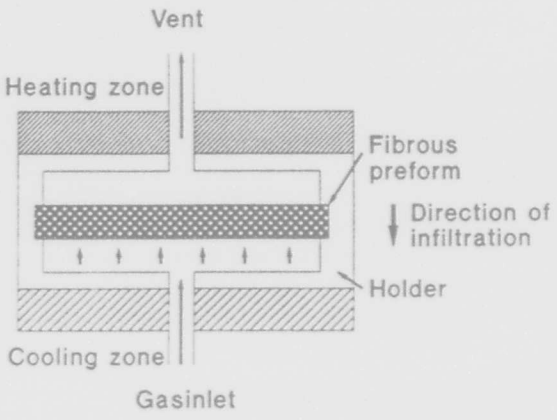

Figure 1: Sketch of a gradient CVI reactor

The SiC premior gas is methyltrichloro-silane (CH_3SiCl_3) in excess hydrogen as carrier gas.

A temperature gradient which is inverse to the pressure gradient is applied to control the local distribution of the matrix deposition within the preform. At the beginning of the infiltration process, the down-stream side of the preform body is typically heated to 1450 ^{o}K for the SiC matrix process whereas the up-stream side is held at a lower temperature at which SiC deposition does not yet occur. This means that the densification of the fibrous structure by SiC matrix growth proceeds from the rear to the front side against the gas flow direction and thus allows a permanently open access for the feed gas throughout the densification process, until the growth front reaches the up-stream surface. The progress of the growth front is driven by the increase of the thermal conductivity where the pores are filled with SiC matrix.

In comparison to the isothermal/isobaric CVI process, the gradient-CVI exhibits two essential differences:

- a markedly higher gas flow
- a raised deposition temperature.

Both of these features involve a remarkably higher deposition rate which would cause soon clogging of the surface near pores and exclude complete densification when applied in the isothermal/isobaric process. This higher useful deposition rate reduces the time required for densification of a certain thickness by at least one order of magnitude.

A pilot plant for the gradient-CVI process is shown in Figure 2. This equipment provides a working capacity of 220 liters and allows, as it is fully automatized, continuous infiltration runs without personal control.

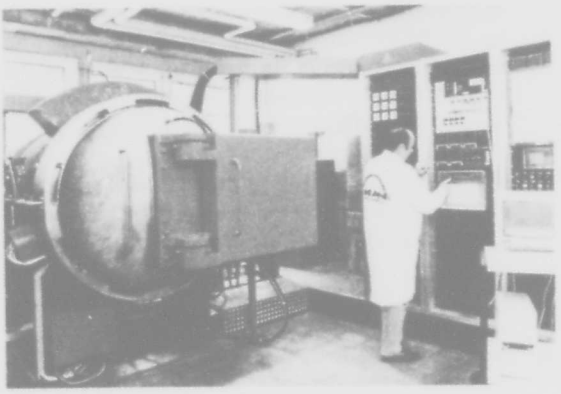

Figure 2: Fully automised pilot plant for gradient CVI

3.3 Final machining and joining

Manufacture of CMC parts is mainly based on near-net-shape processing. However, as already stated, the final machining, especially on all contact surfaces at connecting joints, cannot be avoided. The final machining of CMC parts is performed by diamond grinding and drilling, including also, if necessary, cutting by a high power laser. The high hardness of the material makes the machining operation difficult and very expensive. On the other hand, there are no degradation effects through the machining and the strength of the parts is not reduced by cutting of the fibres. Moreover, by the adequate form, smoothing, avoidance of the residual stresses, preloading, etc., the strength of a structure can be significantly improved.

Joining is done with metallic fasteners, made of refractory metals if the service temperature is beyond the maximum temperature level for usual metallic fasteners. The high compressive and shear strengths of the CVI-derived ceramic composites make this kind of joining a very reliable one. Furthermore, it provides the important advantage of an easy dismounting for inspection, and repair in case of local damage.

A further metallic joining method which has already been tested is brazing with reactive brazes. However, probably due to the typical residual porosity of CVI derived CMCs, the reliability of brazed joints is not yet satisfactory so that additional development work is necessary. Furthermore, this is the joining method with the strictest temperature limitation.

Where only low mechanical loads occur, joints with ceramic cements, preferably with SiC powder filler, are applicable. In this case it is necessary to machine the joining surfaces accurately to ensure a uniform tight contact. The cement volume should be kept at a minimum and the support by fixations is favourable. Good experiences were gained with silicon organic polymers (polycarbosilames and - silazanes) as bin-

ders in the ceramic cement. Upon their pyrolysis under inert gas they form an amorphous SiC residual which fits to the SiC matrix composite material.

A very promising development route, which provides inherently joined elements, i.e., over interlaced fibres, relies on the utilisation of 2D- and 3D-woven shaped fibrous structures. The current development is oriented towards higher fibre volume contents, comparable to those obtained with stacked 2D-fabrics and multidirectional in-plane fibre orientation.

3.4 Feasible forms

As already mentioned, the gradient-CVI process favours regularly shaped parts. Examples of feasible geometric are even and curved plates, cylinders, angular tubes, boxes and U-section beams. These parts can be provided with engineering elements such as flanges, corrugated sections, thickness variations, and integrated ribs of some millimeters in height.

Furthermore, with the gradient-CVI method it is possible to realize wall thicknesses which are beyond the capability of the conventional CVI process, e.g., plates with 25 mm thickness have successfully been infiltrated by gradient-CVI.

Examples of manufactured basic parts are shown in Figure 3 and Figure 4 demonstrating, at the same time, the principle of how such parts are assembled to a complex component.

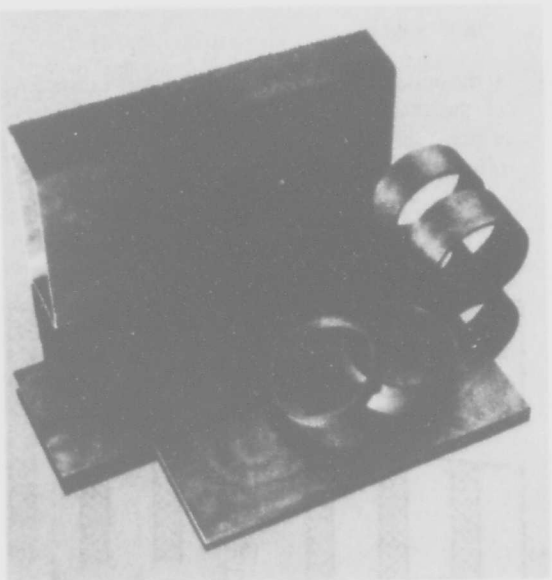

Figure 3: Basic parts, manufactured with gradient-CVI

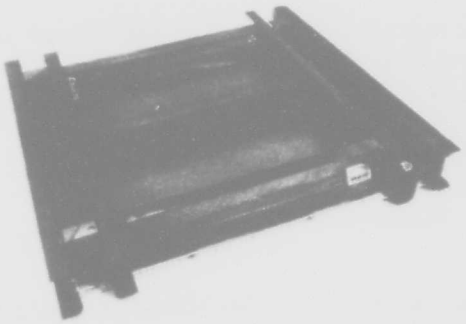

Figure 4: Assembly of gradient-CVI parts to a complex component

4. DESIGN PROCEDURE

CMC materials exhibit very different and more complex response to applied loads compared to other materials and provide remarkable mechanical characteristics in comparison with bulk ceramics. Different analyses has been performed to relate the strength properties under tensile conditions, especially first matrix cracking, to microstructural behaviour, as fibre sliding in the matrix, fibre bridging and pull-out in the crack wake and the fibre rupture. The achievement of the adequate strength properties of the CMC structures depends on the knowledge of the role played by each of these features during deformation and development of the failure. Therefore, the improved modelling of the behaviour, which is based on micro-structural features, can provide significant contribution to the understanding of the behaviour and prepare preliminary information necessary for the adequate structure design.

The analytical modelling of the mechanical behaviour is performed not only for the purposes of ceramic adequate integrated design, but also for the optimisation of basic material.

4.1 Analytical modelling of the behaviour

The first kind of problems relate to the determination of the "elastic" modulus. The elastic modulus of a single, uni-directional ply composite, in the direction of the fibre, can be given by the law of mixtures:

$$E_{CMC} = V \cdot E_F + (1 - V) \cdot E_M \,. \qquad (1)$$

However, a general feature of the stress-strain curve of a tension test is that the initial linear elastic region is followed by a non-linear stress increase up to a maximum where the failure occurs. Generally the onset

of non-linear deflection coincides with the first formation of matrix cracks.

Due to matrix cracking the composite's strength and modulus progressively reduce down to minimum values, corresponding to the situation where the applied load is carried by the fibres alone, bridging the cracks:

$$E_{COM} \cong V \cdot E_F \qquad (2)$$

Furthermore, for woven 0/90 systems, stretching or compressing the fibres tends to reorient the later thus inducing little non-linear effects. Therefore, the non-linear effects are present in the system, as a combination of different effects. It should be noted that at failure the stress is relatively low, but the strain is high compared to that for monolithic ceramics. It is in such materials that large strains-to-failure can be achieved. However, this increased straining requires some sliding of the matrix over the fibres, so that stress increase after matrix cracking is non-linear. The ultimate load carrying capacity is determined by fibre failure and pullout.

The first cracking of the matrix in the CMC system is the consequence of the lower strain capability of the matrix compared to the fibre. For crack onset in the matrix two conditions are necessary: the strain in the composite must reach the fracture strain of the matrix and supply the energy required for the fracture process. Based on this, the strain necessary for the matrix crack onset is given by, [6]:

$$\varepsilon_M = \left[\frac{12 \cdot \gamma_M \cdot \tau}{R} \cdot \frac{V_F^2}{V_M} \cdot \frac{(1 - V^2)^2 \cdot E_F}{E_M^2 \cdot E_{CMC}}\right]^{1/3} \qquad (3)$$

This relationship is the basis of the so-called ACK analysis (Aveston-Cooper-Kelly). Based on this relationship some consistency between flexure and tension test results can be expected. However, in case of the internal stresses due to the fibre-matrix mismatch, the fracture strain relationship must be modified by superposing/subtracting the relevant part of strain.

It can be seen from (3), that the crack initiation strain is positively influenced by the fibre volume fraction and the reduction in fibre diameter. This is also valid for woven fabrics considering that the fibre volume fraction is varying from 0 to 100 % of the nominal value with 50 % as the mean.

If the fibres have sufficient strength to remain intact after a crack extends completely through the matrix, then the formation of multiple, regulary spaced matrix cracks will precede failure of the composite. In fact, the crack spacing is the consequence of the interaction of the slip zones necessary for the full load transfer between the fibres and the matrix and, therefore, can be also determined based on the fibre strength, dimensions and the shear strength of the interfaces.

The cracks develop successively up to the overlapping of the effects of the neighbouring cracks or up to saturation density:

$$\Delta = \frac{R \cdot \varepsilon_M \cdot E_F}{2 \cdot \tau} \cdot \frac{E_M \cdot (1 - V)}{E_F \quad V} \qquad (4)$$

The corresponding stress is called saturation stress, (σ_S). The crack spacing is directly dependent on the fibre fraction, and this means that the matrix is weakened both by matrix fraction reduction and increase in number of cracks, so that increase in fibre volume fraction is, for practical purposes, limited.

For 1D reinforced composites which exhibit multiple cracking, a method to describe formation of the first matrix crack has been also developed based on fracture mechanics approach, [7]. Separation of the surfaces of a matrix crack is restrained by fibre reinforcement. This "closure" effect prevents further crack growth. Therefore in the analysis, a matrix crack is formed in two hypothetical steps:

- the bonds across the crack plane are cut and the stress causing the crack to open is applied (Figure 5 a)
- at the end of each fibre that lies within a distance d of the crack tip a reverse traction is introduced which allows the fibres to be rejoined (Figure 5 b).

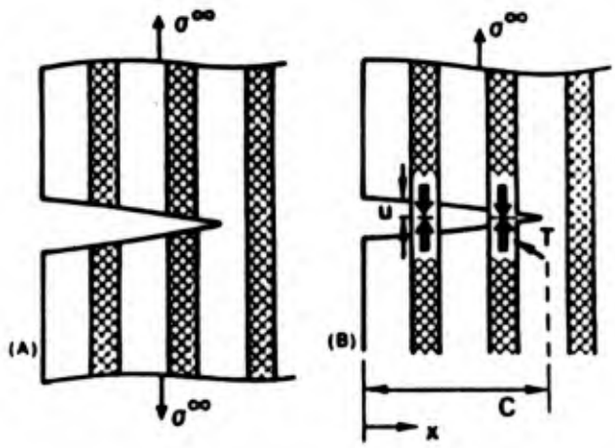

Figure 5a and 5b: Closure effect of matrix and fibers

According to this approach the crack initiation is controlled by the fracture toughness parameter of the matrix (K_C) and friction forces at interface between the fibre and matrix (τ):

$$\sigma_M = \left[\frac{12\cdot(1-\nu^2).K_c^2\,\tau\cdot E_F\cdot V^2\cdot(1-V)\cdot(1+\eta)^2}{E_M\cdot R}\right]^{1/3}$$

where

$$\eta = \frac{E_F V}{E_M(1-V)}$$

Again it can be seen that a high fibre volume fraction and a small diameter insure that a sufficient number of fibres bridge the matrix crack, preventing their propagation. Another advantage of the small fibre diameter is that the fibre length required for full fibre-matrix load transfer (critical length) is also small.

Concerning the interface between the fibre and matrix effect, which is characterised by the shear strength, (τ), the relationships are more complex than both above equations indicate. If the fibre-matrix interfacial bonding is strong, the stress concentration on fibres at the crack tip, during matrix crack propagation, will generally be high enough to fracture the fibres. Because of this CMC should contain fibres that are weakly bonded to the matrix, so that matrix cracks only can propagate around the fibres and not through them, thus allowing the bridging of the crack and limiting crack extension.

Cyclic loading leads to further significant differences in the behaviour and, is consequently, in overall performance of the CMC materials, in contrast to other materials. The stiffness of the material change depending on the loading and unloading prestrain in the tensile direction and loading in compression after crack closing, (Figure 6). At the tensile side the loop develops with a mean width ($\Delta\varepsilon$) that corresponds to the sliding effects between the fibres and the matrix. Based on this, the interfacial strength τ can be measured. At the same time, the mean tensile slope (E_d) of the cycle continously reduce with the increase of the initial prestrain. On the other hand, the compression modulus generally equals the initial slope of the CMC before matrix cracking. Non-consideration of the stress-strain relationship variation is a handicap to reliable designing with these materials leading to the inaccurate evaluation of the stress distribution in the components under operational loading and the inproper use of the material. The tensile-compression stiffness asymetry, which is dependent on the load level, is also responsible for the inadequacies of bending load measurements for the purposes of the material characterisation.

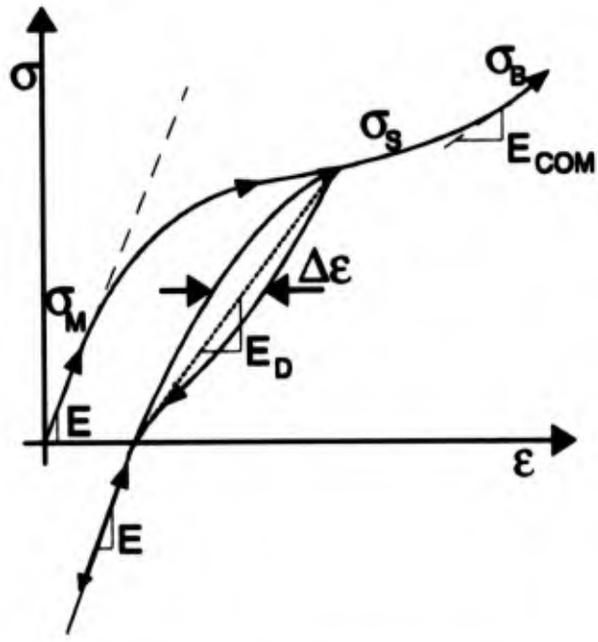

Figure 6: Scheme of cyclic behaviour of CMCs

4.2 FE-Modelling

The major drawback of the analytical models is that they are limited to the idealised conditions, as for example, unidirectional fibre strengthening, matrix isotropy, etc. Even the evaluation of the "elastic" modulus, based on (1), is only valid for matrix without any porosity effects. Therefore, the kind of modelling which is based on microscopic observations in the composite and its direct implementation in the model may be very useful. For these purposes, the FEM model, besides being a method used for the prediction of the behaviour of structural systems, can also be used to model the different phases, ingredients, and effects at microscopic level and to predict the overall macroscopic behaviour of the CMC system.

To verify the benefits of the combined FEM-microscopic approach, the in-phase ply stacking, observed on CMC micrographs, has been modelled and investigated, as shown in Figure 7. For the purpose of the analysis the failure of the fibre bundles and matrix is assumed, based on rupture strain. In this first analysis, no consideration of the sliding at interfaces between the fibre and matrix has been introduced.

During calculation the conditions are varied in order to gain knowledge about the behaviour of different "material configurations". The results show that the best agreement with the experimental results is found after introduction of the "voids" in the matrix material. The effect of voids was bigger than expected (Figure 8). The stiffness of the system, by eliminating the part of matrix material reduces, and the stress distribution changes considerably. The stress change is a product of both high concentration at pores and loading by fibres.

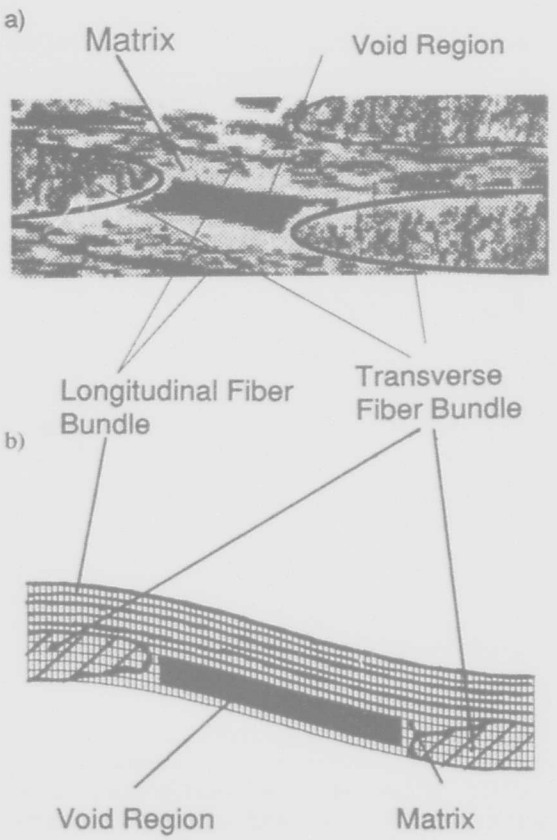

Figure 7: Microscopic cross section of C/SiC, a) and the approriate FEM model, b)

The previous analysis shows that voids induce more cracking and are also responsible for non-linear macroscopic behaviour. In typical CMC material with 2D-woven fabrics, the volume fraction of the pores within of the matrix is nearly the same as the fibre fraction in the loading direction under tensile loading conditions. Therefore the effect of pores should be significant.

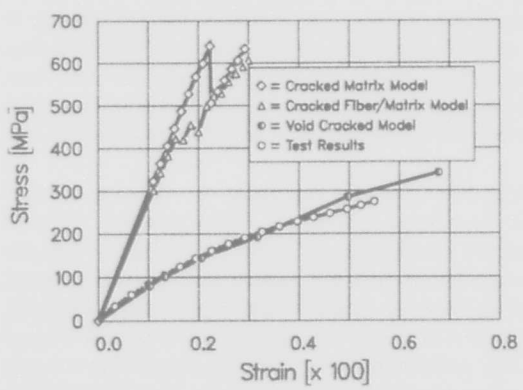

Figure 8: Comparison of test results to computed results with different CMC models

On the other hand, comparison of some results for different CMC materials have shown that 2D-materials may be nearly accurate represented by the 1D-version of the same materials if the stress-strain curve is scaled down according to the fibre fraction change in one direction (mostly 50 % for 2D-CMC) (shown shematically in Figure 9 according to [8]). Based on this, one can assume that the behaviour of 2D-CMC is mainly controlled by the fibre lay-up in the direction of the loading. Even in the case of woven 2D-fabrics, the differences were so small, leading to the conclusion that the contribution of the fibre curvature may be also negligible.

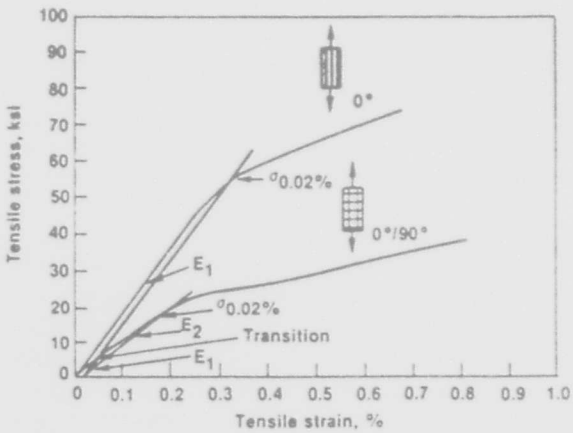

Figure 9: Tensile stress-strain curves for 0° and 0°/90° SiC/LAS at room temperature

Generally, previous results show that further modelling effort is necessary and very desirable, both for the fundamental understanding of the behaviour and for the optimisation of the CMC basic structure. The corresponding investigation must concentrate on the sensitivity analysis of CMCs to the variation in parameters and features of the basic components included in the composition of the material.

Although the analysis shows that the FE method is a very important tool that can efficiently aid the investigation of the microstructural aspects, the presented results are preliminary, and have to be verified by further examination. The results were presented here to show the influence of porosity, which is usually neglected in different models, at first also in the simplest one, of the so-called "law of mixture" (1) for the evaluation of "elastic" modulus.

4.3 Material characterisation

For the practical application in addition to the tensile rupture strain capability other characteristic of the materials may also be very important, as for example, general performance under stress condition (stress concentration, bi-axial stress conditions, shear strength), fatigue behaviour, creep and environment effects.

For all high temperature materials the maximum utilisation temperature is also very important. This is for CMC on SiC/SiC basis limited to 1200 °C, where for the C/SiC materials the application up to 1600 °C is possible. In the last case, however, the oxidation protection of the sensitive C-fibre is necessary. For C/C materials the temperature limit is much higher, but the problem of oxidation protection is even more serious.

Development of matrix cracks strongly influences the deformation behaviour of CMC material under fatigue conditions. However, after intensive matrix cracking during the first cycle, further crack growth is nearly fully prevented by the fibre closure effect, so that life time up to millions of cycles can be achieved with the material, inspite of the matrix cracking.

Important design material characteristics of typical CMC materials manufactured by gradient CVI method based on test results will be presented and discussed.

5. PRESENTATION OF RESULTS AND DISCUSSION

5.1 Specimen tests

The material data of the CMCs obtained with the gradient-CVI process, i.e. SiC/SiC and C/SiC are compiled in Table 1.

Properties		SiC/SiC	C/SiC
Fiber volume fraction	vol %	40-50	42-47
Porosity	vol %	10-15	10-15
Density	g/cm^3	2.3-2.5	2.1-2.2
Tensile strength	MPa	300-400 (0°/90°)	270-330 (0°/90°)
Rupture strain	%	0.5-0.8	0.6-0.9
Flexure strength	Mpa	500-600	450-500
Compression strength ‖	MPa	650	450-570
⊥	MPa	850-950	600-700
Shear strength‖	MPa	65-75	45-55
⊥	MPa	130-160	110-140
Low Cycle Fatigue (LCF)	cycles	$5.3 \cdot 10^5$ at ±310 MPa	$8.6 \cdot 10^6$ at ±160 MPa
Young's Modulus	GPa	180-220	90-100
Coeff. of therm. expansion ‖	10^{-6} ·1/K	4	3
⊥	10^{-6} ·1/K	4	5
Thermal conductivity ‖	W/mK	20	14
⊥	W/mK	10	6
Heat Capacity	J/kg·K	600	620

Table 1: Material properties of SiC/SiC and C/SiC, manufacturd by gradient CVI method

For tensile tests, flate plate specimens were used with the size of 10 mm x 120 mm x 3 mm. The strain tolerant behaviour, known for continuous fibre reinforced material, is clearly demonstrated by the stress-strain curve from a tensile test shown in Figure 10. The results confirm the quasi-plastic material behaviour, typical for this type of CMC, which depends on matrix cracking and load transfer to the fibres. With a density of 2.45 g/cm^3 the material possesses a high specific strength and it exhibits a considerable strain to rupture. The adequate interlaminar shear strength and the high compressive strength render joining by bolts possible as described above.

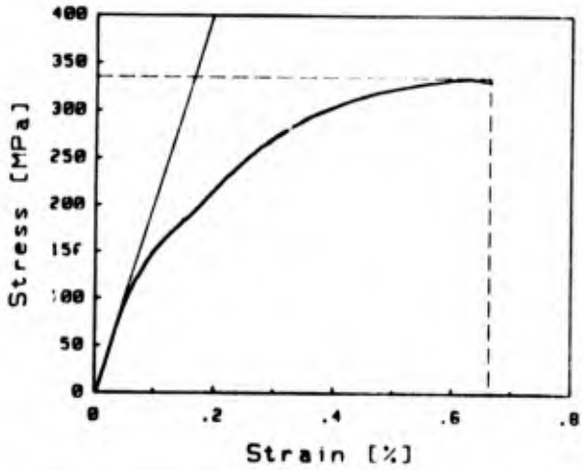

Figure 10: Stress-strain curve of a SiC/SiC tensile test

Different material lay-up compositions were investigated in tensile tests to clarify the influence of the laying-up angle of the woven carbon fibre fabrics on the rupture strength and rupture strain, see Figure 11.

Even in the case of an orientation in $[+45°/-45°]_n$ to the applied tensile load (that means no fibre was oriented in load direction) the rupture strength and the rupture strain was considerably high. The amount of quasi plastic deformation is nevertheless very good.

The fibre volume fraction in load direction is increased with the $[0°/90°, 30°/-60°, 60°/-30°]_n$-material compared to the $[+45°/-45°]_n$, but is lower in relation to the $[0°/90°]_n$-oriented material. The results with the orientation in $[0°/90°, +45°/-45°]_n$ are inbetween the latter curves. The material offers a wide band of possibilities for the design of components as the strength and stiffness can be adapted to the requirements of the design by choosing the appropriate material layering.

The results of the notched tensile tests (plate with hole, K_t = 2.43) show that the material is not sensible to stress concentrations, compare Figure 12 to Figure 11. This is the most powerful advantage of CMC in comparison to conventional, monolithic ceramic. Together with the previous mentioned "quasi plastic

deformation", which are both untypical for monolithic ceramic, the material can be used for design purposes in aerospace applications.

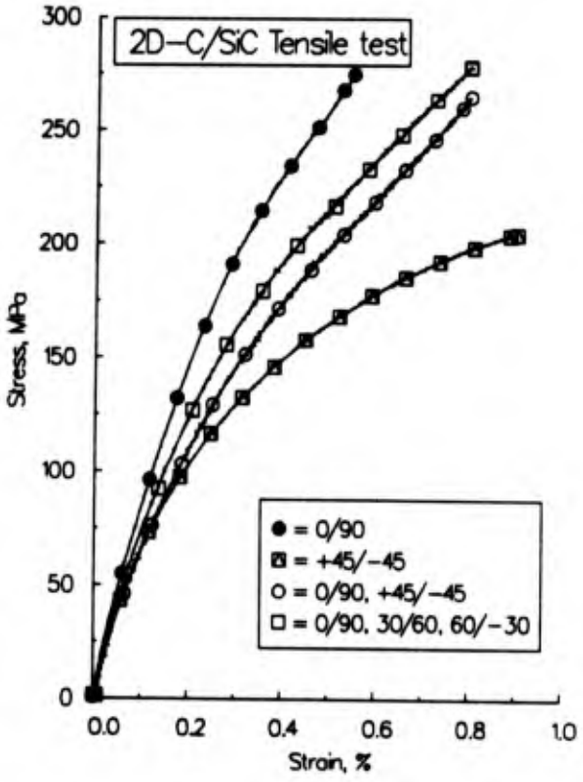

Figure 11: Tensile test results of C/SiC with different ply orientations

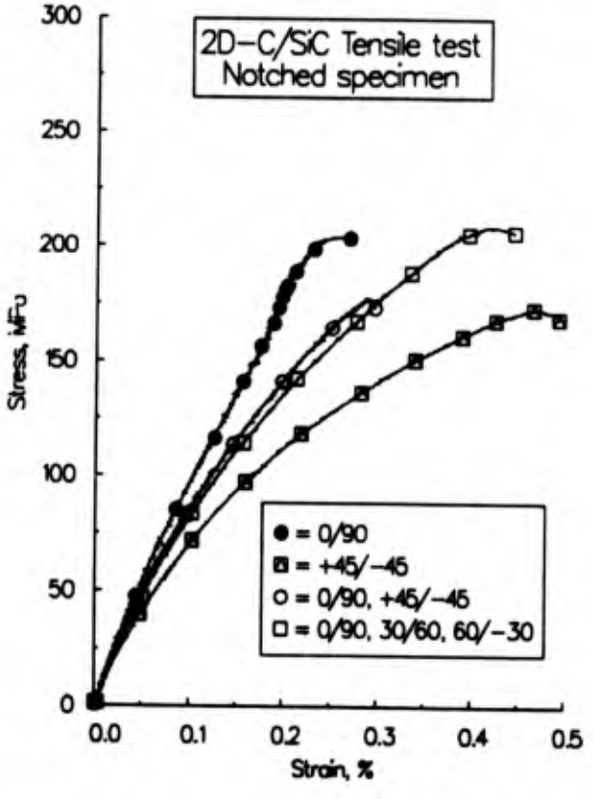

Figure 12: Tensile test results of notched C/SiC specimen with different ply orientations

A further material property of C/SiC and SiC/SiC, well known from monolithic ceramic, is that they maintain the strength even at high temperature levels up to 1300°C. Figure 13 presents a comparison of tensile test results at 1000°C and at 1300 °C in vacuum with 0°/90° C/SiC material. After the 1000°C temperature test the remaining part of the specimen was again tested at room temperature. There is little reduction of the strength after high temperature test although the sample was already loaded up to 273 MPa. The high temperature results prove the remaining high strength of C/SiC. The 1300°C-curve is slightely above the the 1000°C-curve, which is probably caused by temperature effects between matrix and fibre.

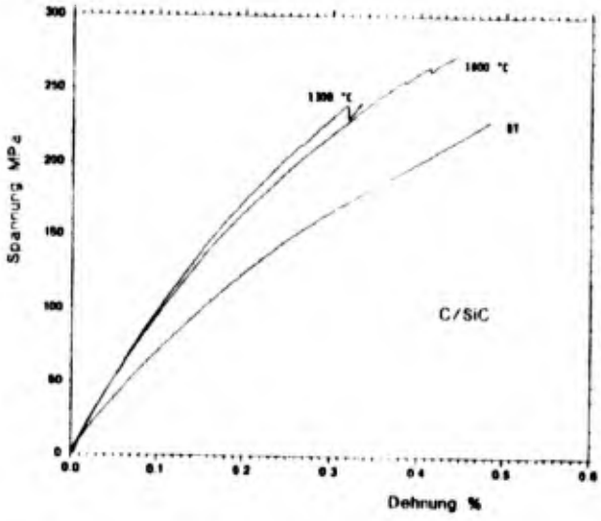

Figure 13: Comparison of tensile test results at different temperature levels

However, both C/SiC and SiC/SiC are sensitive to oxidation at elevated temperatures above 550°C and need, therefore, protective coatings for high temperature applications in oxidising environment. What has been developed is a coating consisting of a thermoviscous glassy phase and refractory second phase for mechanical stabilization against shear loads induced in high gas flows.

Test results obtained with coated C/SiC samples in cyclic oxidation tests at 550 and 1200°C are shown in Figure 14. The measured mass losses and, correspondingly, the strength losses were very low. As can be seen, the protection is more critical in the lower temperature regime because the crack sealing efficiency of the glassy phase is limited owing to the high viscosity. Thus, it must be seen that the protectivity of the coating can only be temporary and the useful life time of a part depends on the coating durability under particular service conditions.

In the next test series coated C/SiC and SiC/SiC samples were exposed to the supersonic flame of a high speed flame spraying gun. After ten cycles of three minutes duration each with intermediate cooling down

to room temperature, the residual tensile strength was determined. For C/SiC a strength reduction of 65 - 70 % and for SiC/SiC of 50 - 60 % was found.

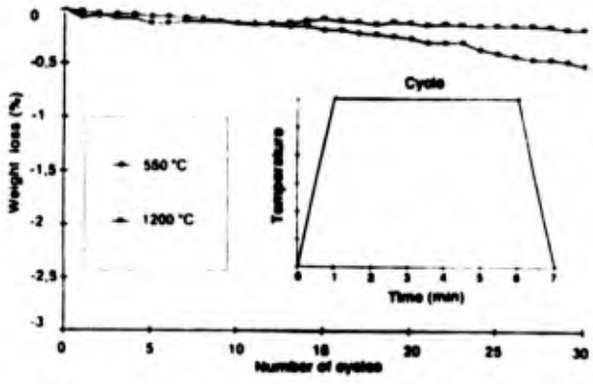

Figure 14: Mass loss of C/SiC with protective coating in cyclic oxidation tests

For application where temperatures above 1000°C are encountered C/SiC is the better choice because of the appreciably superior temperature resistance of the carbon fibres over the SiC fibres. In Figure 15 the tensile strength of C/SiC retained after exposure to temperatures up to 1600 °C in vacuum is represented. The strength maximum at 1400 °C is due to the relief of mismatch stresses from the manufacture.

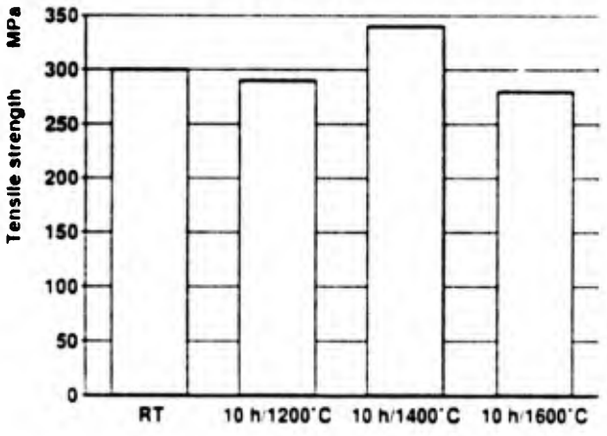

Figure 15: Tensile strength of C/SiC at different temperature levels after 10 h exposure in vacuum

The suitability of the gradient-CVI CMCs for dynamically loaded components has been underscored by the results of low cycle fatigue tests. These tests have been performed as cyclic strain-controlled push-pull tests with predetermined stress amplitudes, [9]. Figure 16 depicts a set of curves obtained in such a test at different cycles. The curves are artificially offset to make the differences in the material behaviour with increasing number of cycles better visible. Due to the matrix cracking beyond the linear-eleastic regime the shape of the stress-strain curve of the first load cycle is not found any more in the subsequent cycles. Thus, the material stiffness remains reduced in tension. The results are very good as the specimen broke after $8.6 \cdot 10^6$ cycles.

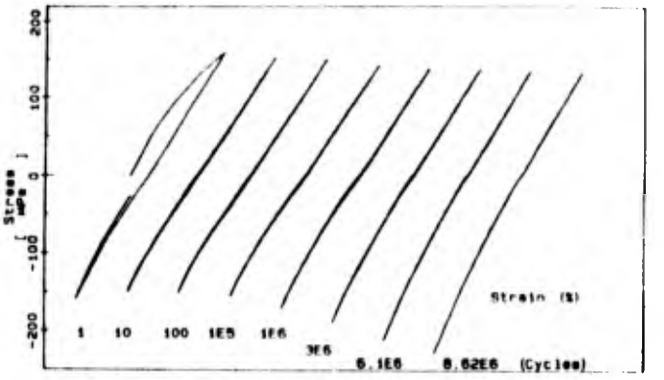

Figure 16: Stress-strain curves from a LCF test with 2D-C/SiC (numbers below denote cycle)

The sample of a SiC/SiC LCF-test, loaded with an initial stress of 310 MPa, was broken after 5.4×10^5 cycles, see Figure 17.

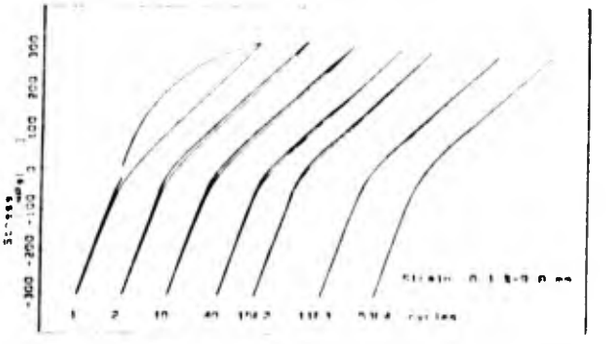

Figure 17: Stress-strain curves from a LCF test with 2D-SiC/SiC (numbers below denote cycle)

5.2 Component tests

For an hypersonic spaceplane with a maximum speed of 5.6 Mach a flexible C/SiC intake ramp for the engine duct up to 1200°C was developped. The design approach uses relative simple design elements to built up the component (see Figure 18).

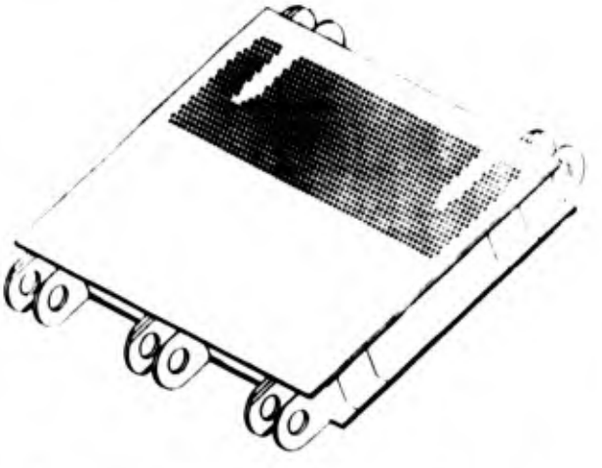

Figure 18: C/SiC intake ramp for a hypersonic airplane

The most critical elements in the intake ramp are the bearing lugs, where the load is introduced. Figure 19 shows the test conditions of a cutted lug and the obtained results. The mechanical loads of the component led to maximum force of about 5 kN at the lug, neglecting the additional temperature gradient induced loading. The measured rupture load is about 23 kN, which is considerably higher than the design load and less reduced by the significant stress concentration in the lug. As consequence the thickness of the lug can be reduced to save weight.

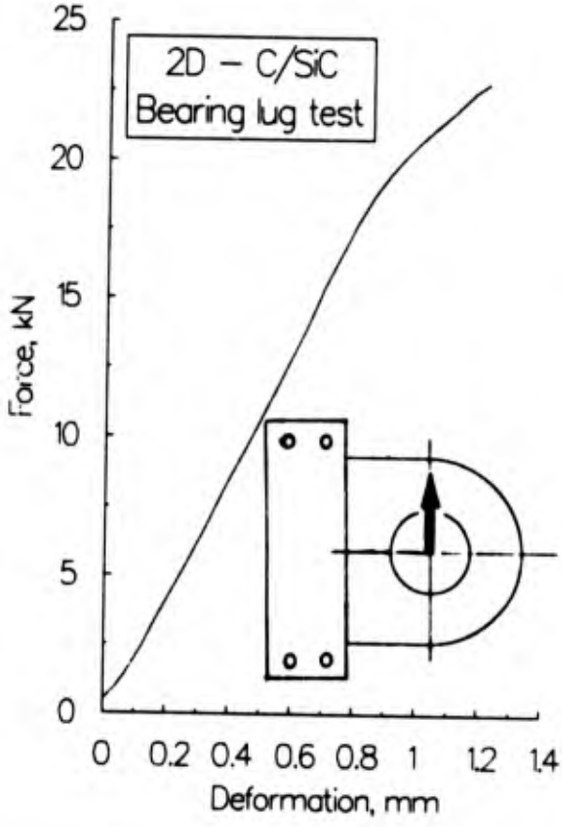

Figure 19: Test results of a C/SiC bearing lug

Figure 18 shows the skin of the intake ramp with small holes of 4 mm ∅. As the skin is temperature loaded, compressive stresses develop in this part of the component. The strength of the perforated skin was proven by a compression test in a special frame holder, according to DIN 65561. The test results and the test set-up are presented in Figure 20. The sample failed in shear across the first row of holes. Both the rupture strain as well as the rupture load were far above the computed maximal loads in the skin. Here is also a wall thickness reduction possible to reduce the weight.

According to the design concept, all elements (skin, stringer and angle) are fitted by high temperature fasteners consisting of refractory metal, see Figure 21. Therefore, the reliability of the connection concept was tested, using a single shear specimen test with metallic bolt and supporting frame according Figure 22. Failure occured around the fastener hole with a big amount of defonnation in load direction. The bolt was turned around and the material was damaged locally, pushing a number of layers before rupture occured, (Figure 24). The quasi-plastic deformation of the material led to such a high rupture load (Figure 23), which gives additional safety margins for the structure.

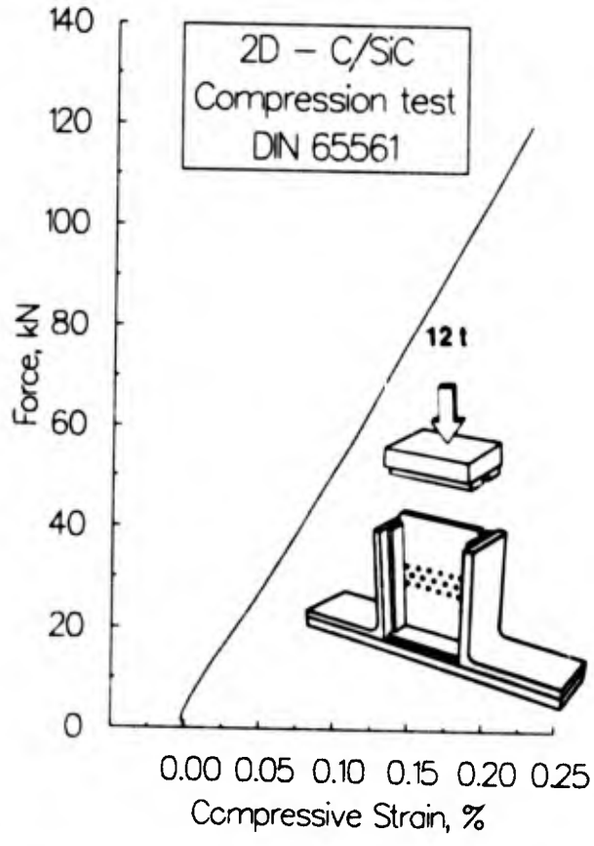

Figure 20: Compression test results of a perforated C/SiC plate

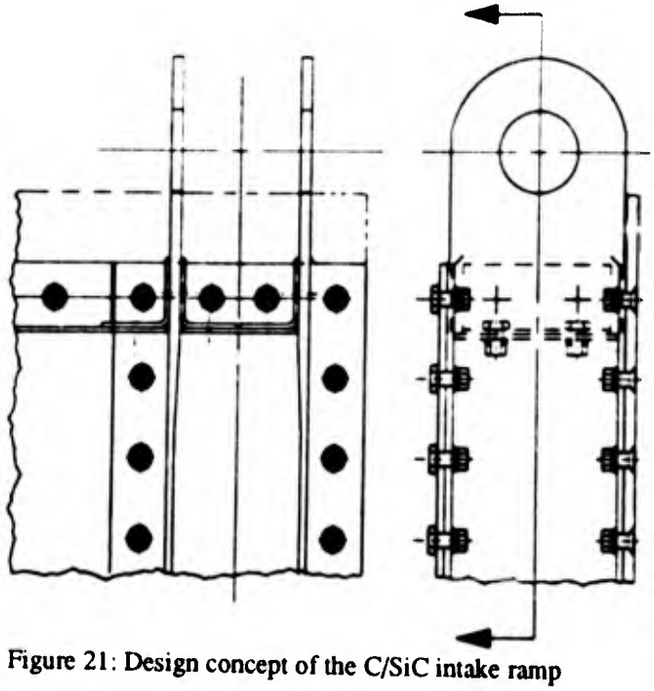

Figure 21: Design concept of the C/SiC intake ramp

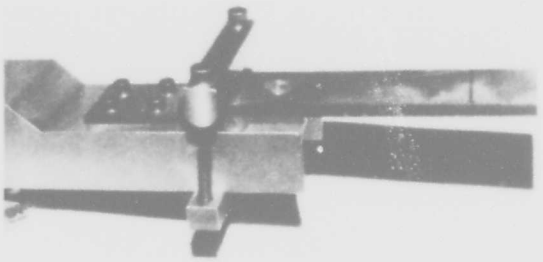

Figure 22: Single shear specimen with supporting frame and refractory bolt.

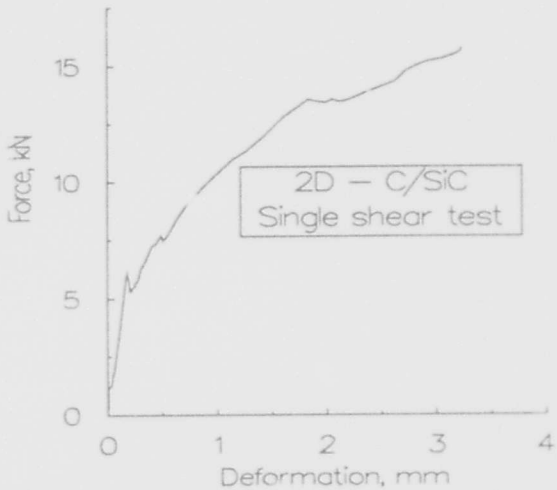

Figure 23: Results of the single shear test with refractory bolt and C/SiC specimen

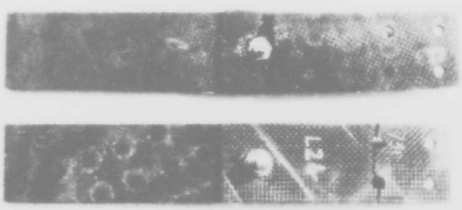

Figure 24: Single shear specimens with refractory bolt after rupture.

6. CONCLUSIONS

The gradient-CVI process has been shown to provide ceramic composition with SiC matrix which possess the required properties for application in high performance components, e.g. high strength and strain to fracture and high temperature resistance. The favourable shear and compressive strengths are useful for joining with bolts.

The gradient-CVI process itself was affirmed to offer the advantage of short infiltration periods what makes this process cost-effective and allows short development cycles for CMC products. Its applicability for the manufacture of parts could successfully be demonstrated. The particularities of the process favour regularly shaped parts. A design principle has therefore been developped for the assembly of standardized parts to complex components.

Further development efforts require, however, to improve oxidation protection and perform the long time endurance (> 1000 hours) testing at high temperatures in oxidising environment with protected CMCs based on SiC matrix. Major demands to be fulfilled in this respect are improved SiC fibres, oxidation resistent fibre coatings and external seal-coats with increased performance.

7. ACKNOWLEDGEMENT

Some results were obtained within the German Hypersonic Technology Project, which is supported by the Federal Ministry for Research and Technology, (BMFT). Part of the tests were performed at IABG with contribution from DASA.

8. REFERENCES

[1] D. Sygulla and P. Agatonovic: "Analysis and Testing of Ceramic Matrix Composites in Diesel Engines", 4th International Symposium on Ceramic Materials & Components for Engines, Goeteborg, Sweden 1991

[2] M. Leuchs: "Ceramic Composite Applications in Diesel Engines - Experiences and Chances", 4th International Symposium on Ceramic Materials & Components for Engine, Goeteborg, Sweden 1991

[3] H. Zechmeister, M. Leuchs and A. Mühlratzer: "Properties and Possibilities For Application of CMC In Mechanical Engineering", Ceramic Transactions, Vol. 19, The American Ceramic Society, 1991, pp 1095-1105

[4] F. E. Papalegis and R.G. Bourdeau, AFML Technical Documentary Report ML-TDR-64-201, July 1964; referenced in: "Chemistry and Physics of Carbon", Vol. 9, P.L. Walker, Jr. u. P.A. Thrower, Marcel Dekker Incl, New York 1973

[5] D. P. Stinton, A.J. Caputo and R.A. Lowden: "Synthesis of Fiber-Reinforced SiC Composites by Chemical Vapor Infiltration", J. Amer. Ceram. Soc. Bull. 65, 2 (1986), pp 347-350

[6] L. N. McCartney: "Mechanics of Matrix Cracking in Brittle-Matrix Fibre-Reinforced Composites", Proc R. Soc. London A 409, (1987), pp. 329-350

[7] D. B. Marshal and A. G. Evans: "Application of Fracture Mechanics to Fibre Composites", 9th Conf. Composites & Advanced Ceramics, 1985

[8] E. Minford and K.M. Prewo: "Fatigue Behaviour of Silicon Carbide Fiber Reinforced Lithium-Alumino-Silicate Glass-Ceramic", pp. 561-570.

[9] P. Agatonovic, and R. Grunmann: "Fatigue Life Tests on Composite Ceramic", 7th Europ. Conf. on Fracture, Budapest, 19-24 Sept. 1988

ULTRASONIC NONDESTRUCTIVE EVALUATION AS A TOOL FOR THE DEVELOPMENT OF AEROSPACE STRUCTURAL CERAMIC COMPOSITES*

by

Theodore E. Matikas
National Research Council Associate, WL/MLLP
Materials Directorate, Wright Laboratory
Wright Patterson Air Force Base, Ohio 45433-7178
United States

and

Prasanna Karpur
Research Institute, University of Dayton
300 College Park Avenue
Dayton, Ohio 45469-0127
United States

SUMMARY

Insertion of ceramic materials into structural composites for aerospace applications requires a good characterization and evaluation of nascent composite systems in research and developmental stages as well as during eventual production and use. During research and developmental stages of the composite, it is critical to evaluate the compatibility of different types of matrix materials with different types of fibers, and the effect of material processing conditions. Also, the suitability of the overall mechanical properties and material behavior of the composite for the intended application will have to be evaluated. On the other hand, after the composite has been designed and developed, it is imperative to assure that the designed properties are being achieved during production and retained during use.

Many destructive and nondestructive methods are being used to evaluate the composite during its evolution process. Some of the destructive tests in use are fiber push-out, fiber pull-out, thermal and mechanical fatigue, etc. Nondestructive methods in use include x-rays, laser, ultrasound, etc. Ultrasonic NDE techniques have an excellent potential for use during all phases of the life cycle of the composite systems.

This paper outlines new concepts for the utilization of various ultrasonic techniques for the evaluation of different aspects of development and use of ceramic matrix composites. We introduce a novel mechanical parameter called the interfacial shear stiffness coefficient which can be measured using ultrasonic shear wave reflectivity technique to characterize and quantify the fiber-matrix interface. This newly proposed parameter is promising as a common basis of composite evaluation among the composites developing, composites mechanics modeling and composites testing groups. The paper will also discuss other ultrasonic NDE techniques such as ultrasonic microscopy which can provide comprehensive evaluation of the composite system during all phases of development and use.

* This work was supported by and performed on-site in the Materials Directorate, Wright Laboratory, Wright Patterson Air Force Base, Ohio 45433. Contract No. F33615-89-C-5612 (P. Karpur).

INTRODUCTION

Ceramic materials are well suited for use in structural composites for aerospace applications because of their high temperature properties. Also, the ceramic materials in the composites facilitate sub-critical matrix cracking, interface debonding and fiber sliding. Due to these microscopic damage mechanisms, the ceramic matrix composites (CMCs) can achieve the elastic-plastic strain hardening similar to metals although the CMCs are made of brittle constituents. However, the insertion of ceramics into structural composites for aerospace applications requires a good characterization and evaluation of nascent composite systems in research and developmental stages. Such a need for the characterization requires a concurrent development approach involving several fields of expertise as shown in Figure 1. In order to verify that the designed properties are being achieved, the interactions among various fields of expertise during research and developmental stages of the composite are essential. Such multi-disciplinary interactions make it possible to evaluate (a) the compatibility of different types of matrix materials with different types of fibers including the effect of different types of fiber coating on the load transfer between the matrix and the fiber, (b) the effect of processing conditions such as temperature, pressure, environmental gases used during fabrication, duration of processing, etc., (c) the suitability of the overall mechanical properties for the intended application, and (d) the material behavior and life prediction studies to evaluate failure modes and life expectancy under use conditions.

The development of a new CMC system should be done using a 'Pyramid' approach as shown in Figure 2. In order to design a composite with suitable properties for the intended application, the development of the composite system should progress from a global sense to a microscopic approach through the macroscopic control. For example, during the initial stage of design, materials will have to be selected for optimum chemical compatibility to avoid global problems such as warping, corrosion, etc. In the next stage of design, the composite system will have to be evaluated for macroscopic anomalies such as porosity, lack of consolidation, fiber swimming, etc. Thus, in this stage of development, there is a

Presented at an AGARD Workshop entitled 'Introduction of Ceramics into Aerospace Structural Composites', April, 1993.

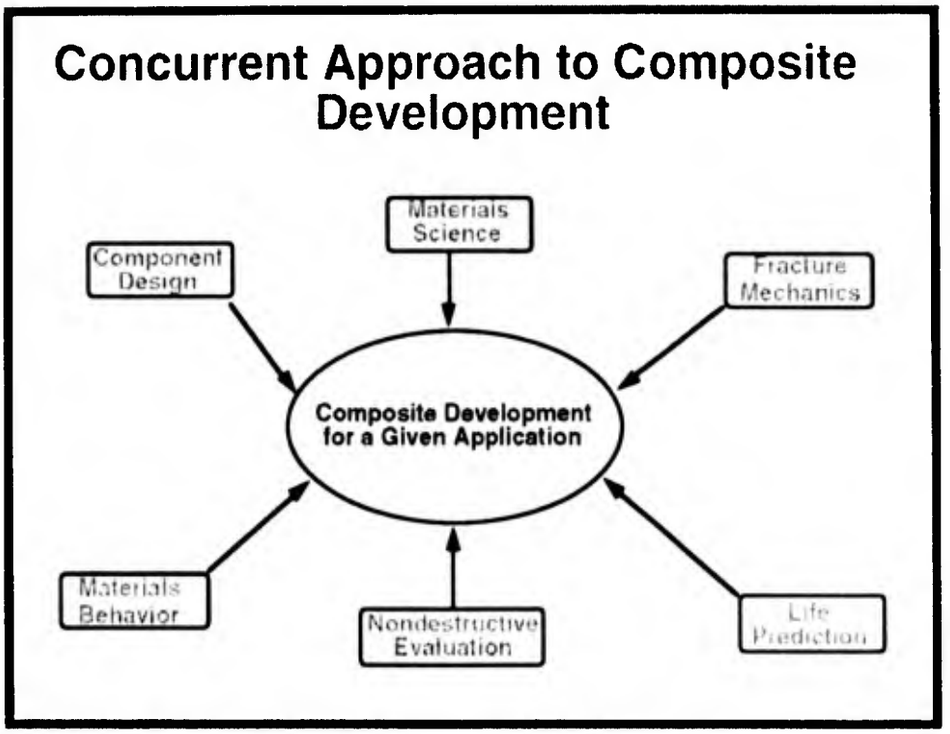

Fig. 1 Concurrent engineering approach to the development of a new structural ceramic composite syste

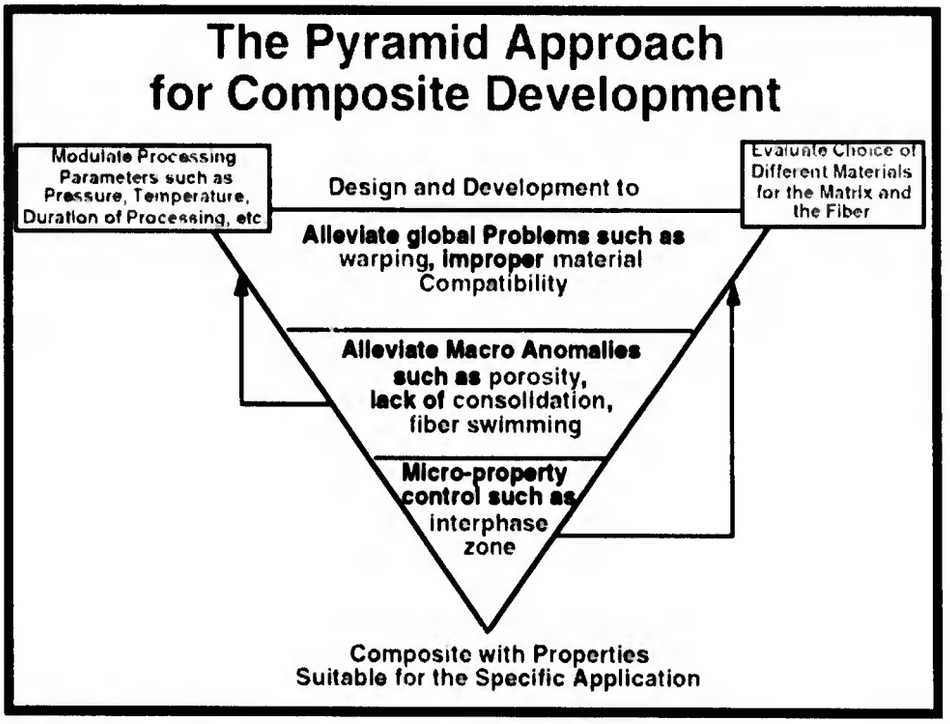

Fig. 2 A pyramid approach to composite development.

need for optimization of the material processing parameters. However, since the changes in the processing parameters could introduce global problems of warping, etc., there is a need for iterative material selection and processing parameter modulation until the global and macroscopic design is achieved to satisfaction. The third and the final step (with the necessary feed back as shown in Figure 2) of composite development would be the micro-control of the properties such as the chemically formed interphase region between the fiber and the matrix materials.

The objective of this paper is to describe the role of ultrasonic nondestructive evaluation in materials development so that the composite being designed can be evaluated through various stages of development such as material selection, life prediction, material behavior, fracture mechanics, etc. The nondestructive methods developed during the initial stages of the design of the composite system can also be used after the development in order to: (a) assure that the composite panel is free of defects while the designed properties are being achieved during production, and (b) detect the degradation of initial properties because of use.

ROLE OF ULTRASONIC NDE IN MATERIAL DEVELOPMENT

Ceramic matrix composites are designed and developed as structural materials for use at elevated temperatures made with two components: a matrix material and embedded fibers. There are various aspects of the composite developmental procedure that can benefit from the use of ultrasonic NDE. For example, improper consolidation of the matrix at the interfacial region can be easily detected [1] using ultrasound as shown in Figure 3. Such a capability to nondestructively detect consolidation problems will help to eliminate the use of samples in further tests such as fiber push-in for interfacial strength estimation as discussed next.

Figure 4 shows the result of fiber push-in tests on a SCS-6/Glass sample where a section of the sample was intentionally selected in a region shown to have some areas of consolidation problems while other areas were properly consolidated. In the figure, the inset shows the section of the sample used for fiber push-in tests. The ultrasonic image shows that the consolidation is good from fiber 1 to 5 while it is progressively poor going from fiber 6 to 12. The peak loads that were required to push-in the fibers in the sample clearly show a correlation with the ultrasonic evaluation of the interfacial consolidation. Thus, if the ultrasonic scan is properly used to sort out the samples with improper consolidation, the validity of tests such as fiber push-in can be enhanced because the push-out results will now reflect only the interfacial strength rather than the scatter due to manufacturing problems. Further details of this experiment can be obtained from the literature [2].

Ultrasonic NDE can also be effectively used to evaluate and study the elastic behavior of the interphase region [3, 4] between the fiber and the matrix materials. Such an evaluation is important because the overall properties of the composite are largely dominated by the behavior of the interface. The interface provides the load transfer between the matrix and the fiber. At the same time, the interface acts as a mechanical fuse and provides crack resistance to the composite and prevents catastrophic failure. As a result, the characterization of the interface between different types of fibers and matrix materials is of great interest to the researchers who are developing the composite materials. The objective of the evaluation of the interface would be to estim-

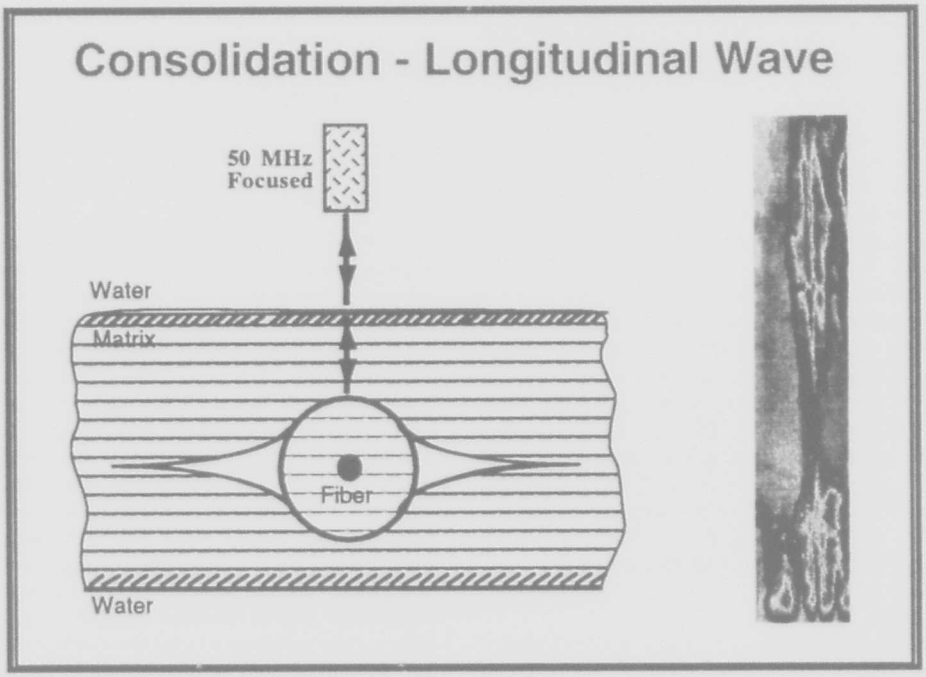

Fig. 3 Detection of improper consolidation using ultrasound.

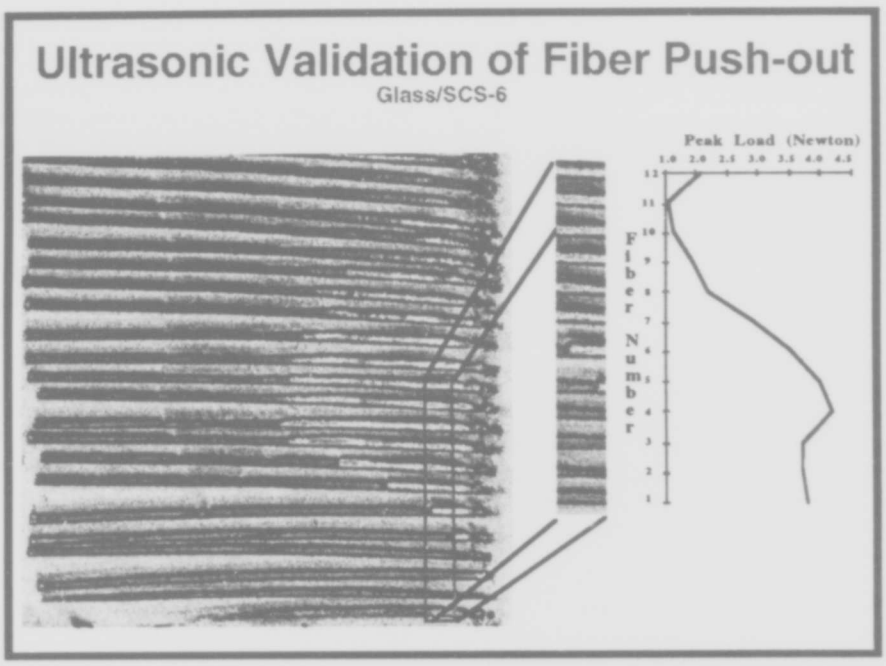

Fig. 4 Ultrasonic corroboration of fiber push-out tests.

ate the achieved interfacial load transfer behavior between the fiber and the matrix in order to obtain a composite with suitable fracture behavior. Since the destructive tests of interfacial evaluation render the sample unusable, there is a need to develop an ultrasonic nondestructive tool for the characterization of the interface to study the fiber-matrix interface in at least the outermost layers of a real, multi-fiber composite system.

An ultrasonic back-reflectivity technique has been developed to complement other existing techniques for the characterization of the interfacial behavior in fiber reinforced composites. The ultrasonic characterization of the interface is achieved by the analysis of the back-reflected signal from the fiber-matrix interface. The advantages of the ultrasonic back-reflectivity technique are several: (1) the method is completely nondestructive and facilitates the use of the same sample for the tests (fatigue and creep) other than the interface analysis, (2) the technique can provide the distribution and variation of the interfacial properties along the length of the fibers thereby facilitating better process control, and (3) the interface can be monitored for degradation and changes during fatigue tests for life prediction. The configuration of the model is shown in Figure 5a, the boundary conditions used are shown in Figure 5b, the analytical expression obtained is shown in Figure 5c, and an example of the result obtained from the model is shown in Figure 5d. Further details of the modeling analysis can be obtained from the literature [3]. An extensive physical reasoning behind the modeling [3] has been described in the literature [4].

CONCLUSION

Ultrasonic NDE is an excellent complementary methodology to be used in concert with the development of a new structural material such as ceramic matrix composite. Ultrasonic NDE facilitates interrupted tests during fatigue experiments by ensuring that the sample is available for further tests of interest. Also, ultrasonic NDE is effective to characterize the fiber-matrix interface in ceramic composites and provides a tool to help the developers of new composite systems to (1) determine the compatibility between the matrix and the fiber of choice, (2) establish the processing parameters such as pressure and temperature, (3) evaluate the interface for degradation and debonding during temperature and mechanical fatigue tests, (4) obtain an accurate measurement of the fiber debonded length produced by push-in tests and also by fiber fracture thereby providing a common basis for the stress analysis and fracture mechanics groups, (5) monitor fiber breaks, crack initiation [5], and growth in ceramic composites during fatigue tests, (6) validate and reduce data scatter for interface evaluation tests such as fiber push-in, push-out, fiber fragmentation, etc.

The design and development of a new CMC needs a pyramid approach where first global, then macro and finally micro properties are iteratively designed with extensive feedback and interaction. Concurrent engineering approach is essential for the design and development of CMCs wherein there are extensive interactions and involvements by groups working in material science, fracture mechanics, nondestructive evaluation, component design, etc. It is critical to view the CMC development process from 'out side' the existing conventions, and formalities. Design procedures and manufacturing methodologies will have to be evaluated concurrently to obtain the best possible benefit from the composites for a given application. Common 'scientific language' (definitions, terminology, etc.) need to be established for groups from different fields to be able to interact. Other NDE techniques such as laser induced ultrasound need to be cultivated to evaluate the interface at elevated temperatures. However, improvements in signal-to-noise ratio, sensitivity, etc., are to be achieved before effective use.

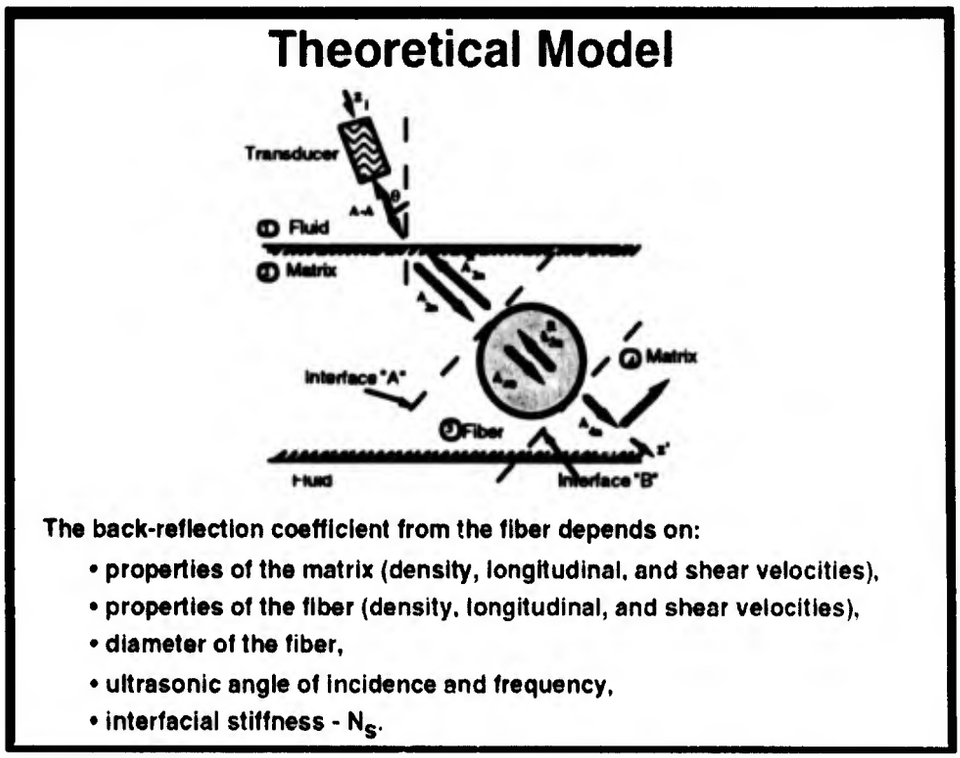

Fig. 5a Configuration for the theoretical model of ultrasonic interfacial characterization.

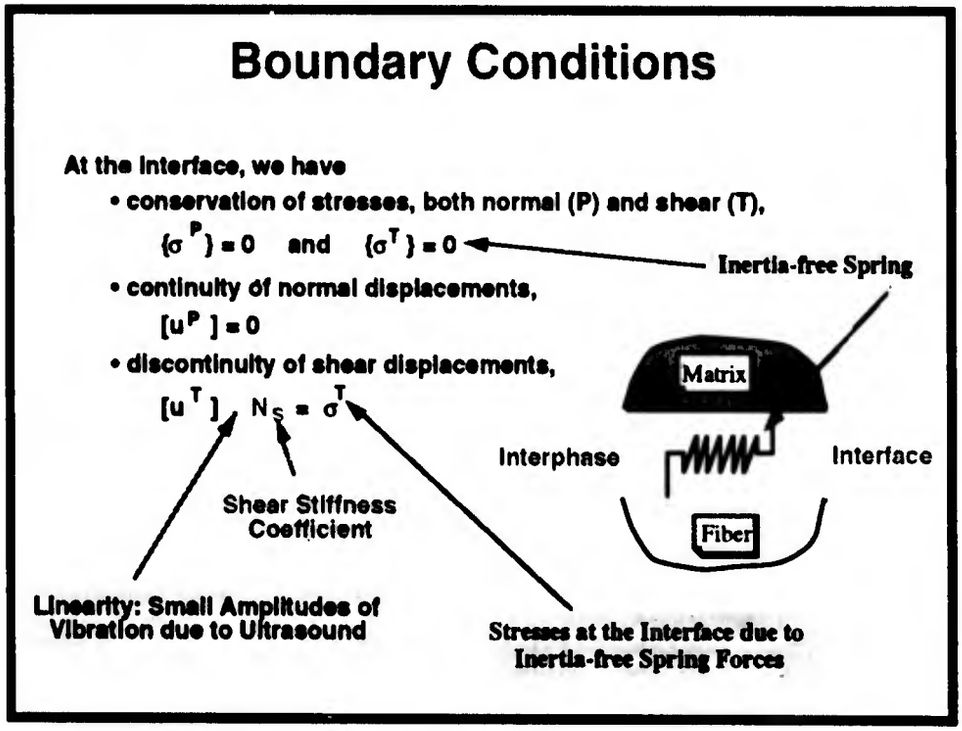

Fig. 5b Boundary conditions used for the theoretical model in figure 5a.

The Final Expression

$$|R| = |TS| \cdot |WS| \cdot |T|$$

$$TS = -\frac{2\left(\frac{c_{2S}}{c_{2L}}\right)^2 \sin 2\theta_{2L}}{\left(\frac{c_{2S}}{c_{2L}}\right)^2 \sin 2\theta_L \sin 2\theta_S + \cos^2 2\theta_S + \frac{\rho_1 c_1}{\rho_2 c_2}\frac{\cos\theta_L}{\cos\theta}}$$

$$T = \frac{2\frac{\rho_1 c_1}{\rho_2 c_{2L}}\frac{\cos\theta_L \cos 2\theta_S}{\cos\theta}}{\left(\frac{c_{2S}}{c_{2L}}\right)^2 \sin 2\theta_L \sin 2\theta_S + \cos^2 2\theta_S + \frac{\rho_1 c_1}{\rho_2 c_2}\frac{\cos\theta_L}{\cos\theta}}$$

$$WS = \frac{A^2B^2(e'-1) + N_S\bar{N}_S(A^2-B^2)(1-e') - iAB[\bar{N}_S(A(1+e') + B(1-e') + N_S(A(1+e') - B(1-e'))]}{A^2B^2(e-1) + N_S\bar{N}_S[(A^2+B^2)(1-e) + 2AB(1+e')] - iAB[\bar{N}_S(A(1+e') + B(1-e) + N_S(A(1+e) + B(1-e'))]}$$

where $e' = e^{ik_{3S}2d}$ $\quad A = Z_{2S}c_{2S}k_{2S}$ $\quad B = Z_{3S}c_{3S}k_{3S}$

and d = Fiber diameter
A, B = Functions of the properties (Moduli, Density, Poisson's ratio) of the matrix and the fiber respectively.

Fig. 5c The final expression obtained from the model in figure 5a for reflection coefficient analysis.

Reflectivity vs. Stiffness Coefficient

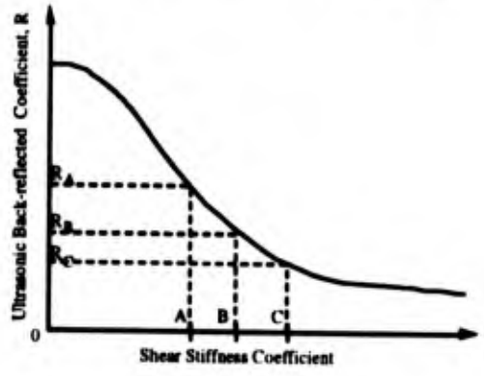

R_A = Ultrasonic reflection coefficient in the presence of tensile residual stresses
R_B = Ultrasonic reflection coefficient when residual stresses are absent
R_C = Ultrasonic reflection coefficient in the presence of compressive residual stresses

A = Effective stiffness coefficient, N_e, corresponding to R_A
B = Effective stiffness coefficient, N_e, corresponding to R_B.
($N_e = N_S$ when residual stresses are zero).
C = Effective stiffness coefficient, N_e, corresponding to R_C

Fig. 5d Result obtained from the model in figure 5a showing ultrasonic reflectivity as a function of interfacial shear stiffness coefficient.

REFERENCES

1. Krishnamurthy S, Matikas TE, Karpur P and Miracle DB *Evaluation of the Processing of Fiber-Reinforced Metal Matrix Composites Using Ultrasonic Methods*, submitted for publication in Journal of Composites Science and Technology, 1993.

2. Kent R, Matikas TE and Karpur P *Ultrasonic Analysis of Interfacial Debond in Ceramic Matrix Composites*, to be presented in the Sixth International Symposium on Nondestructive Characterization of Materials, Oahu, Hawaii, June 1993.

3. Matikas TE and Karpur P *Ultrasonic Reflectivity Technique for the Characterization of Fiber-Matrix Interface in Metal Matrix Composites*, to be published in Journal of Applied Physics, 1993.

4. Karpur P, Matikas TE and Krishnamurthy S *A novel Parameter to Characterize the Fiber-Matrix Interphase/Interface for Mechanics of Continuous Fiber Reinforced Metal Matrix and Ceramic Matrix Composites*, submitted for publication in Journal of Composites Science and Technology, 1993.

5. Karpur P, Matikas TE, Blodgett MP, Blatt D and Jira J *Nondestructive Crack Size and Interfacial Degradation Evaluation in Metal Matrix Composites Using High Frequency Ultrasonic Microscopy*, to be presented in ASTM Symposium on Special Applications and Advanced Techniques for Crack Size Determination, Atlanta, May 1993.

REPORT DOCUMENTATION PAGE

1. Recipient's Reference	2. Originator's Reference	3. Further Reference	4. Security Classification of Document
	AGARD-R-795	ISBN 92-835-0728-2	UNCLASSIFIED/ UNLIMITED

5. Originator Advisory Group for Aerospace Research and Development
North Atlantic Treaty Organization
7 Rue Ancelle, 92200 Neuilly sur Seine, France

6. Title
INTRODUCTION OF CERAMICS INTO AEROSPACE STRUCTURAL COMPOSITES

7. Presented at a Workshop held by the AGARD Structures and Materials Panel, in Antalya, Turkey, 21st—22nd April 1993.

8. Author(s)/Editor(s)	9. Date
Various	November 1993
10. Author's/Editor's Address	**11. Pages**
Various	160

12. Distribution Statement There are no restrictions on the distribution of this document. Information about the availability of this and other AGARD unclassified publications is given on the back cover.

13. Keywords/Descriptors

Ceramics	Missiles
Ceramic composites	Fiber laminates
Glass matrix composites	Crack propagation
Structural components	Fracture mechanics
Aircraft engines	Fatigue — materials
Aerospace engineering	Creep properties

14. Abstract

Ceramics have been considered over the last two decades as a possible alternative to refractory metals and alloys to be used as structural materials for aeronautical use. The main disadvantage of these materials is their brittleness and the very low value of the critical size of defects leading to fracture.

The concept of ceramic matrix composites has been recognized as one of the ways to escape this difficulty.

Extensive work has been performed to identify the mechanisms of crack propagation and general fracture for unidirectional composites, laminates or other fabrics, including the understanding of their long term response: creep and fatigue effects or environmental degradation.

The Workshop which has been held by AGARD SMP at Antalya (Turkey), April 1993, aimed at reviewing the present knowledge on all these aspects.

AGARD Report 795
Advisory Group for Aerospace Research and Development, NATO
INTRODUCTION OF CERAMICS INTO AEROSPACE STRUCTURAL COMPONENTS
Published November 1993
160 pages

Ceramics have been considered over the last two decades as a possible alternative to refractory metals and alloys to be used as structural materials for aeronautical use. The main disadvantage of these materials is their brittleness and the very low value of the critical size of defects leading to fracture.

The concept of ceramic matrix composites has been recognized as one of the ways to escape this difficulty.

P.T.O.

AGARD-R-795

Ceramics
Ceramic composites
Glass matrix composites
Structural components
Aircraft engines
Aerospace engineering
Missiles
Fiber laminates
Crack propagation
Fracture mechanics
Fatigue – materials
Creep Properties

AGARD Report 795
Advisory Group for Aerospace Research and Development, NATO
INTRODUCTION OF CERAMICS INTO AEROSPACE STRUCTURAL COMPONENTS
Published November 1993
160 pages

Ceramics have been considered over the last two decades as a possible alternative to refractory metals and alloys to be used as structural materials for aeronautical use. The main disadvantage of these materials is their brittleness and the very low value of the critical size of defects leading to fracture.

The concept of ceramic matrix composites has been recognized as one of the ways to escape this difficulty.

P.T.O.

AGARD-R-795

Ceramics
Ceramic composites
Glass matrix composites
Structural components
Aircraft engines
Aerospace engineering
Missiles
Fiber laminates
Crack propagation
Fracture mechanics
Fatigue – materials
Creep Properties

AGARD Report 795
Advisory Group for Aerospace Research and Development, NATO
INTRODUCTION OF CERAMICS INTO AEROSPACE STRUCTURAL COMPONENTS
Published November 1993
160 pages

Ceramics have been considered over the last two decades as a possible alternative to refractory metals and alloys to be used as structural materials for aeronautical use. The main disadvantage of these materials is their brittleness and the very low value of the critical size of defects leading to fracture.

The concept of ceramic matrix composites has been recognized as one of the ways to escape this difficulty.

P.T.O.

AGARD-R-795

Ceramics
Ceramic composites
Glass matrix composites
Structural components
Aircraft engines
Aerospace engineering
Missiles
Fiber laminates
Crack propagation
Fracture mechanics
Fatigue – materials
Creep Properties

Extensive work has been performed to identify the mechanisms of crack propagation and general fracture for unidirectional composites, laminates or other fabrics, including the understanding of their long term response: creep and fatigue effects or environmental degradation.

The Workshop which has been held by AGARD SMP at Antalya (Turkey), April 1993, aimed at reviewing the present knowledge on all these aspects.

ISBN 92-835-0728-2

Extensive work has been performed to identify the mechanisms of crack propagation and general fracture for unidirectional composites, laminates or other fabrics, including the understanding of their long term response: creep and fatigue effects or environmental degradation.

The Workshop which has been held by AGARD SMP at Antalya (Turkey), April 1993, aimed at reviewing the present knowledge on all these aspects.

ISBN 92-835-0728-2

Extensive work has been performed to identify the mechanisms of crack propagation and general fracture for unidirectional composites, laminates or other fabrics, including the understanding of their long term response: creep and fatigue effects or environmental degradation.

The Workshop which has been held by AGARD SMP at Antalya (Turkey), April 1993, aimed at reviewing the present knowledge on all these aspects.

ISBN 92-835-0728-2

Extensive work has been performed to identify the mechanisms of crack propagation and general fracture for unidirectional composites, laminates or other fabrics, including the understanding of their long term response: creep and fatigue effects or environmental degradation.

The Workshop which has been held by AGARD SMP at Antalya (Turkey), April 1993, aimed at reviewing the present knowledge on all these aspects.

ISBN 92-835-0728-2

AGARD

NATO OTAN

7 RUE ANCELLE · 92200 NEUILLY-SUR-SEINE

FRANCE

Télécopie (1)47.38.57.99 · Télex 610 176

DIFFUSION DES PUBLICATIONS
AGARD NON CLASSIFIEES

Aucun stock de publications n'a existé à AGARD. A partir de 1993, AGARD détiendra un stock limité des publications associées aux cycles de conférences et cours spéciaux ainsi que les AGARDographies et les rapports des groupes de travail, organisés et publiés à partir de 1993 inclus. Les demandes de renseignements doivent être adressées à AGARD par lettre ou par fax à l'adresse indiquée ci-dessus. *Veuillez ne pas téléphoner.* La diffusion initiale de toutes les publications de l'AGARD est effectuée auprès des pays membres de l'OTAN par l'intermédiaire des centres de distribution nationaux indiqués ci-dessous. Des exemplaires supplémentaires peuvent parfois être obtenus auprès de ces centres (à l'exception des Etats-Unis). Si vous souhaitez recevoir toutes les publications de l'AGARD, ou simplement celles qui concernent certains Panels, vous pouvez demander à être inclu sur la liste d'envoi de l'un de ces centres. Les publications de l'AGARD sont en vente auprès des agences indiquées ci-dessous, sous forme de photocopie ou de microfiche.

CENTRES DE DIFFUSION NATIONAUX

ALLEMAGNE
Fachinformationszentrum,
Karlsruhe
D-7514 Eggenstein-Leopoldshafen 2

BELGIQUE
Coordonnateur AGARD-VSL
Etat-Major de la Force Aérienne
Quartier Reine Elisabeth
Rue d'Evere, 1140 Bruxelles

CANADA
Directeur du Service des Renseignements Scientifiques
Ministère de la Défense Nationale
Ottawa, Ontario K1A 0K2

DANEMARK
Danish Defence Research Establishment
Ryvangs Allé 1
P.O. Box 2715
DK-2100 Copenhagen Ø

ESPAGNE
INTA (AGARD Publications)
Pintor Rosales 34
28008 Madrid

ETATS-UNIS
National Aeronautics and Space Administration
Langley Research Center
M/S 180
Hampton, Virginia 23665

FRANCE
O.N.E.R.A. (Direction)
29, Avenue de la Division Leclerc
92322 Châtillon Cedex

GRECE
Hellenic Air Force
Air War College
Scientific and Technical Library
Dekelia Air Force Base
Dekelia, Athens TGA 1010

ISLANDE
Director of Aviation
c/o Flugrad
Reykjavik

ITALIE
Aeronautica Militare
Ufficio del Delegato Nazionale all'AGARD
Aeroporto Pratica di Mare
00040 Pomezia (Roma)

LUXEMBOURG
Voir Belgique

NORVEGE
Norwegian Defence Research Establishment
Attn: Biblioteket
P.O. Box 25
N-2007 Kjeller

PAYS-BAS
Netherlands Delegation to AGARD
National Aerospace Laboratory NLR
P.O. Box 90502
1006 BM Amsterdam

PORTUGAL
Força Aérea Portuguesa
Centro de Documentação e Informação
Alfragide
2700 Amadora

ROYAUME UNI
Defence Research Information Centre
Kentigern House
65 Brown Street
Glasgow G2 8EX

TURQUIE
Millî Savunma Başkanlığı (MSB)
ARGE Daire Başkanlığı (ARGE)
Ankara

Le centre de distribution national des Etats-Unis (NASA/Langley) ne détient PAS de stocks des publications de l'AGARD. D'éventuelles demandes de photocopies doivent être formulées directement auprès du NASA Center for Aerospace Information (CASI) à l'adresse suivante:

AGENCES DE VENTE

NASA Center for
Aerospace Information (CASI)
800 Elkridge Landing Road
Linthicum Heights, MD 21090-2934
United States

ESA/Information Retrieval Service
European Space Agency
10, rue Mario Nikis
75015 Paris
France

The British Library
Document Supply Division
Boston Spa, Wetherby
West Yorkshire LS23 7BQ
Royaume Uni

Les demandes de microfiches ou de photocopies de documents AGARD (y compris les demandes faites auprès du CASI) doivent comporter la dénomination AGARD, ainsi que le numéro de série d'AGARD (par exemple AGARD-AG-315). Des informations analogues, telles que le titre et la date de publication sont souhaitables. Veuiller noter qu'il y a lieu de spécifier AGARD-R-nnn et AGARD-AR-nnn lors de la commande des rapports AGARD et des rapports consultatifs AGARD respectivement. Des références bibliographiques complètes ainsi que des résumés des publications AGARD figurent dans les journaux suivants:

Scientifique and Technical Aerospace Reports (STAR)
publié par la NASA Scientific and Technical
Information Program
NASA Headquarters (JTT)
Washington D.C. 20546
Etats-Unis

Government Reports Announcements and Index (GRA&I)
publié par le National Technical Information Service
Springfield
Virginia 22161
Etats-Unis

(accessible également en mode interactif dans la base de données bibliographiques en ligne du NTIS, et sur CD-ROM)

Imprimé par Specialised Printing Services Limited
40 Chigwell Lane, Loughton, Essex IG10 3TZ

AGARD

NATO OTAN

7 RUE ANCELLE · 92200 NEUILLY-SUR-SEINE

FRANCE

Telefax (1)47.38.57.99 · Telex 610 176

DISTRIBUTION OF UNCLASSIFIED AGARD PUBLICATIONS

AGARD holds limited quantities of the publications that accompanied Lecture Series and Special Courses held in 1993 or later, and of AGARDographs and Working Group reports published from 1993 onward. For details, write or send a telefax to the address given above. *Please do not telephone.*

AGARD does not hold stocks of publications that accompanied earlier Lecture Series or Courses or of any other publications. Initial distribution of all AGARD publications is made to NATO nations through the National Distribution Centres listed below. Further copies are sometimes available from these centres (except in the United States). If you have a need to receive all AGARD publications, or just those relating to one or more specific AGARD Panels, they may be willing to include you (or your organisation) on their distribution list. AGARD publications may be purchased from the Sales Agencies listed below, in photocopy or microfiche form.

NATIONAL DISTRIBUTION CENTRES

BELGIUM
Coordonnateur AGARD — VSL
Etat-Major de la Force Aérienne
Quartier Reine Elisabeth
Rue d'Evere, 1140 Bruxelles

CANADA
Director Scientific Information Services
Dept of National Defence
Ottawa, Ontario K1A 0K2

DENMARK
Danish Defence Research Establishment
Ryvangs Allé 1
P.O. Box 2715
DK-2100 Copenhagen Ø

FRANCE
O.N.E.R.A. (Direction)
29 Avenue de la Division Leclerc
92322 Châtillon Cedex

GERMANY
Fachinformationszentrum
Karlsruhe
D-7514 Eggenstein-Leopoldshafen 2

GREECE
Hellenic Air Force
Air War College
Scientific and Technical Library
Dekelia Air Force Base
Dekelia, Athens TGA 1010

ICELAND
Director of Aviation
c/o Flugrad
Reykjavik

ITALY
Aeronautica Militare
Ufficio del Delegato Nazionale all'AGARD
Aeroporto Pratica di Mare
00040 Pomezia (Roma)

LUXEMBOURG
See Belgium

NETHERLANDS
Netherlands Delegation to AGARD
National Aerospace Laboratory, NLR
P.O. Box 90502
1006 BM Amsterdam

NORWAY
Norwegian Defence Research Establishment
Attn: Biblioteket
P.O. Box 25
N-2007 Kjeller

PORTUGAL
Força Aérea Portuguesa
Centro de Documentação e Informação
Alfragide
2700 Amadora

SPAIN
INTA (AGARD Publications)
Pintor Rosales 34
28008 Madrid

TURKEY
Milli Savunma Başkanlığı (MSB)
ARGE Daire Başkanlığı (ARGE)
Ankara

UNITED KINGDOM
Defence Research Information Centre
Kentigern House
65 Brown Street
Glasgow G2 8EX

UNITED STATES
National Aeronautics and Space Administration (NASA)
Langley Research Center
M/S 180
Hampton, Virginia 23665

The United States National Distribution Centre (NASA/Langley) does NOT hold stocks of AGARD publications.
Applications for copies should be made direct to the NASA Center for Aerospace Information (CASI) at the address below.

SALES AGENCIES

NASA Center for
Aerospace Information (CASI)
800 Elkridge Landing Road
Linthicum Heights, MD 21090-2934
United States

ESA/Information Retrieval Service
European Space Agency
10, rue Mario Nikis
75015 Paris
France

The British Library
Document Supply Centre
Boston Spa, Wetherby
West Yorkshire LS23 7BQ
United Kingdom

Requests for microfiches or photocopies of AGARD documents (including requests to CASI) should include the word 'AGARD' and the AGARD serial number (for example AGARD-AG-315). Collateral information such as title and publication date is desirable. Note that AGARD Reports and Advisory Reports should be specified as AGARD-R-nnn and AGARD-AR-nnn, respectively. Full bibliographical references and abstracts of AGARD publications are given in the following journals:

Scientific and Technical Aerospace Reports (STAR)
published by NASA Scientific and Technical
Information Program
NASA Headquarters (JTT)
Washington D.C. 20546
United States

Government Reports Announcements and Index (GRA&I)
published by the National Technical Information Service
Springfield
Virginia 22161
United States
(also available online in the NTIS Bibliographic
Database or on CD-ROM)

Printed by Specialised Printing Services Limited
40 Chigwell Lane, Loughton, Essex IG10 3TZ

ISBN 92-835-0728-2